

**Facies Analysis and Sandbody Geometry of the Paleogene Battfjellet
Formation, Central Western Nordenskiöld Land, Spitsbergen**

Master of Science Thesis in Petroleum Geology

By

Helge Kollsete Gjelberg

22.11.2010



Department of Earth Science, University of Bergen, and
Department of Arctic Geology, University Centre in Svalbard

Abstract

New sedimentological data from the central part of Nordenskiöld Land, Spitsbergen, contributes to the understanding of the depositional processes and sandbody geometry of the Battfjellet Formation (Eocene). A detailed study, with focus on internal facies distribution and local parasequence stacking pattern, has been carried out in an approximately 70km² study area. A total of twelve aggrading and forwards stepping parasequences of a fluvio-wave dominated deltaic origin are recognized.

Local variations and complex geometry of the parasequences in the formation are best explained by autogenic mechanisms and accompanied delta lobe switching, characteristic of a delta with a fluvial dominated morphology (Helland-Hansen, 2010). In contrast, facies analysis of the formation reveals a predominance of wave generated structures. However, the parasequences locally show a characteristic development of alternating plane parallel laminated sandstone units (5-30 cm set thickness) and symmetrical small scale ripples. These units reflect deposition in front of, or close to, an active river mouth bar system, strongly influenced by hyperpycnal flow processes during flood events and accompanying wave reworking during waning flood and fair weather aggradation. The local variations of this facies makes it possible to recognize and map the position of the most fluvial influenced shoreface/delta front successions and their spatial distribution as a consequence of auto-cyclic lobe change processes.

In contrast to the well studied western, more proximal positioned, reaches of the basin, there are no developed clinothems or basin floor fan systems in the study area. This has been interpreted to be a consequence of the progressive shallowing of the basin through time.

Acknowledgments:

This thesis is a part of a master's degree in petroleum geology at the Department of Earth Science at the University of Bergen.

I would like to thank my supervisor Professor William Helland-Hansen for suggesting the field area, outline of the thesis and for discussions and help with the interpretation and writing process.

I also want to thank my fellow students for discussions during long coffee breaks. Special thanks to Jan Helge Aalbu for practical help and patient assistance during long days in the field during the 2009 field season. Thanks also to Eivind Patrick Hanevik for the company during field reconnaissance and for help with transport of supply for the 2010 field season.

In addition I would like to thank my parents for practical help during the final compilation of the theses, and my dad, John Gjelberg, for discussions and scientific quarreling.

I would like to thank Statoil ASA for economical support, making it possible to carry out the field work in a remote area on Svalbard. I would also like to thank the logistics department at UNIS for help with the practicalities related to the field work.

Finally, but not least I want to thank my dear Eva Marie Skulstad for patient help and support during the compilation of the thesis and valuable assistance in the field during the 2010 field season.

Table of content:

TABLE OF CONTENT:	7
1. INTRODUCTION	9
1.1 PURPOSE OF STUDY	9
1.2 PREVIOUS WORK.....	9
1.3 STUDY AREA.....	11
2. METHODS	13
2.1 FIELD WORK	13
2.2 POST – FIELD WORK.....	13
3. GEOLOGICAL FRAMEWORK	15
3.1 INTRODUCTION	15
3.2 PRE-CENOZOIC	17
3.2.1 Pre-Caledonian	17
3.2.2 Devonian – old red.....	17
3.2.3 Latest Devonian to middle Permian	18
3.2.4 Late Permian – Early Triassic.....	19
3.2.5 Late Triassic – Middle Jurassic.....	20
3.2.6 Late Jurassic and Cretaceous.....	20
3.3 CENOZOIC:	22
3.3.1 Introduction:.....	22
3.3.2 Tectonic history:	23
3.3.3 The Central Tertiary Basin:	27
3.3.4 Van Mijenfjorden Group:.....	29
4. LITHOFACIES AND FACIES ASSOCIATIONS:	36
4.1 INTRODUCTION:.....	36
4.2 FACIES ASSOCIATIONS:.....	38
4.2.1 FA1: Offshore/shelf.....	38
4.2.2 FA2: Offshore/transition.....	41
4.2.3 FA3: Lower shoreface	46
4.2.4 FA4: Middle shoreface:.....	55
4.2.5 FA5: Upper shoreface:	58
4.2.6: FA6: Foreshore.....	62
4.2.7: FA7: Continental deposits.....	63
5. PALEOCURRENT DATA	69
5.1 INTRODUCTION:.....	69
5.2 GEOSTATISTIC ANALYSIS:	70
Results:	71
Interpretation:	75
6. SANDBODY GEOMETRY	77
6.1 INTRODUCTION.....	77
6.2 METHODS AND PRINCIPLES FOR CORRELATION:	77
6.3 PARASEQUENCE STACKING PATTERN	80
6.4 CORRELATION PANELS.....	83
6.4.1 The Sandsteinsfjellet-Mefjellet transect.....	84

6.4.2 The Tillbergsfjellet – Ringdalsfjellet – Mefjellet transect.....	87
6.4.3 The Tillbergsfjellet transect	89
6.5 SOURCES OF ERROR	91
6.5.1 Eastern Ringdalsfjellet	91
6.5.2 Eastern Mefjellet	95
6.5.3 Southern Sandsteinsfjellet	98
CHAPTER 7: DEPOSITIONAL ENVIRONMENT AND PALEOGEOGRAPHY.....	99
7.1 DEPOSITIONAL ENVIRONMENT:	99
7.2 FORMATION BOUNDARIES:.....	103
7.3 SEQUENCE STRATIGRAPHY:	104
7.4 DELTA TYPE:	110
7.4.1 Modern analogues.....	110
7.4.2 Delta size	113
7.5 BASIN GEOMETRY.....	113
8. SUMMARY AND CONCLUSIONS	118
SUGGESTIONS FOR FURTHER WORK	119
9. REFERENCES :	120
APPENDIX 1: LITHOSTRATIGRAPHICAL LOGS	126
APPENDIX 2: PALEOCURRENT DATA.....	168
APPENDIX 3: THE MOUNTAINS OF THE STUDY AREA.....	171

1. Introduction

1.1 Purpose of study

For the last few decades most of the work on the Battfjellet Formation in the Central Tertiary Basin has been concentrated in the western part of the basin along the Van Keulenfjorden where spectacular clinoforms and related basin floor fan deposits are exposed (Kellogg, 1975; Steel, 1977; Dalland, 1979; Helland-Hansen, 1985, 1990, 1992; Plink-Bjørklund et al., 2001; Mellere et al., 2002; Deibert et al., 2003; Plink-Bjørklund and Steel, 2004; Crabaugh and Seel, 2004; Johannesen and Steel, 2005; Løseth et al., 2006; Petter and Steel, 2006; Clark and Steel, 2006; Uroza and Steel, 2008; Helland-Hansen, 2010). The Battfjellet Formation in the central part of the Nordenskiöld Land, where sand prone clinoforms and basin floor fans are not well developed, has not been that well studied. The purpose of this study is to, through detailed sedimentological studies, facies analysis and sequence stratigraphic concepts, to generate a model for the sand body geometries in the study area (70 square km) in the Ringdalen - Medalen area in the central part of the basin. This model is further applied to generate local and regional paleo-geomorphic models, and explain differences between the central and western part of the basin with respect to clinoform and basin floor fan development.

1.2 Previous work

The sandstone of the Battfjellet Formation forms a significant contrast to the underlying shales of the Frysjaodden Formation and overlying mixed sandstone and fine grained continental deposits of the Aspelintoppen Formation, as it is a cliff forming succession, easily recognized in the field. For this reason it has been recognized as a stratigraphic unit since the earliest geological work was carried out on the Cenozoic succession on Spitsbergen at the beginning of the 20th century (Nathorst, 1910; Ljutkevic, 1937; Orvin, 1940). The Battfjellet Formation was named after the mountain Battfjellet in central Nordenskiöld Land, and the name was first used by Major and Nagy (1964). The current stratigraphic definition of the Battfjellet Formation was established by the same authors in 1972. Initially, the bulk of the geological field work carried out on Svalbard was devoted to units of economic interest; hence the Battfjellet Formation was given little interest in that respect since it has no commercial value.

Later regional stratigraphic and structural studies carried out in the Central Spitsbergen also incorporated the Battfjellet Formation (Major and Nagy, 1964, 1972; Kellogg, 1975; Steel, 1977; Dalland, 1979). During the last decades the formation has been subject to thorough sedimentological studies with particular focus on the clinofolds and associated basin floor fan development. Through the extensive studies by Helland-Hansen (1985), a paleogeographic and paleoenvironmental understanding of the Battfjellet Formation was established. Several papers by Steel and coworkers presents the development of the clinofolds in the Van Keulenfjorden area and the development of these with respect to sediment by-pass across the shelf edge and development of shelf edge deltas (e.g. Steel, 1977; Plink-Bjørklund and Steel, 2004; Crabaugh and Steel, 2004; Johannesen and Steel, 2005; Petter and Steel, 2006; Clark and Steel, 2006; Uroza and Steel, 2008). Because of the excellent outcrops, the Battfjellet Formation represents an excellent opportunity to study parasequence stacking patterns, as well as the transition from shallow to deep marine deposits of a deltaic system. The exposures are of seismic scale and hence of interest to the oil industry. This has motivated studies with focus on sequence stratigraphy, shoreline trajectory development and sandbody geometries in the formation in recent years (Helland-Hansen et al., 1994; Plink-Bjørklund et al., 2001; Mellere et al., 2002; Deibert et al., 2003; Plink-Bjørklund and Steel, 2004; Crabaugh and Steel, 2004; Johannesen and Steel, 2005; Løseth et al., 2006; Petter and Steel, 2006; Clark and Steel, 2006; Uroza and Steel, 2008; Olsen, 2008); Stene, 2009; Skarpeid, 2010; Helland-Hansen, 2010). No detailed sedimentological work of the study area of this thesis has been carried out before, but several studies of the formation in adjacent areas have been carried out (Helland-Hansen, 1985; Helland-Hansen, 1990; Plink-Bjørklund et al., 2001, Skarpeid, 2010; Helland-Hansen, 2010).

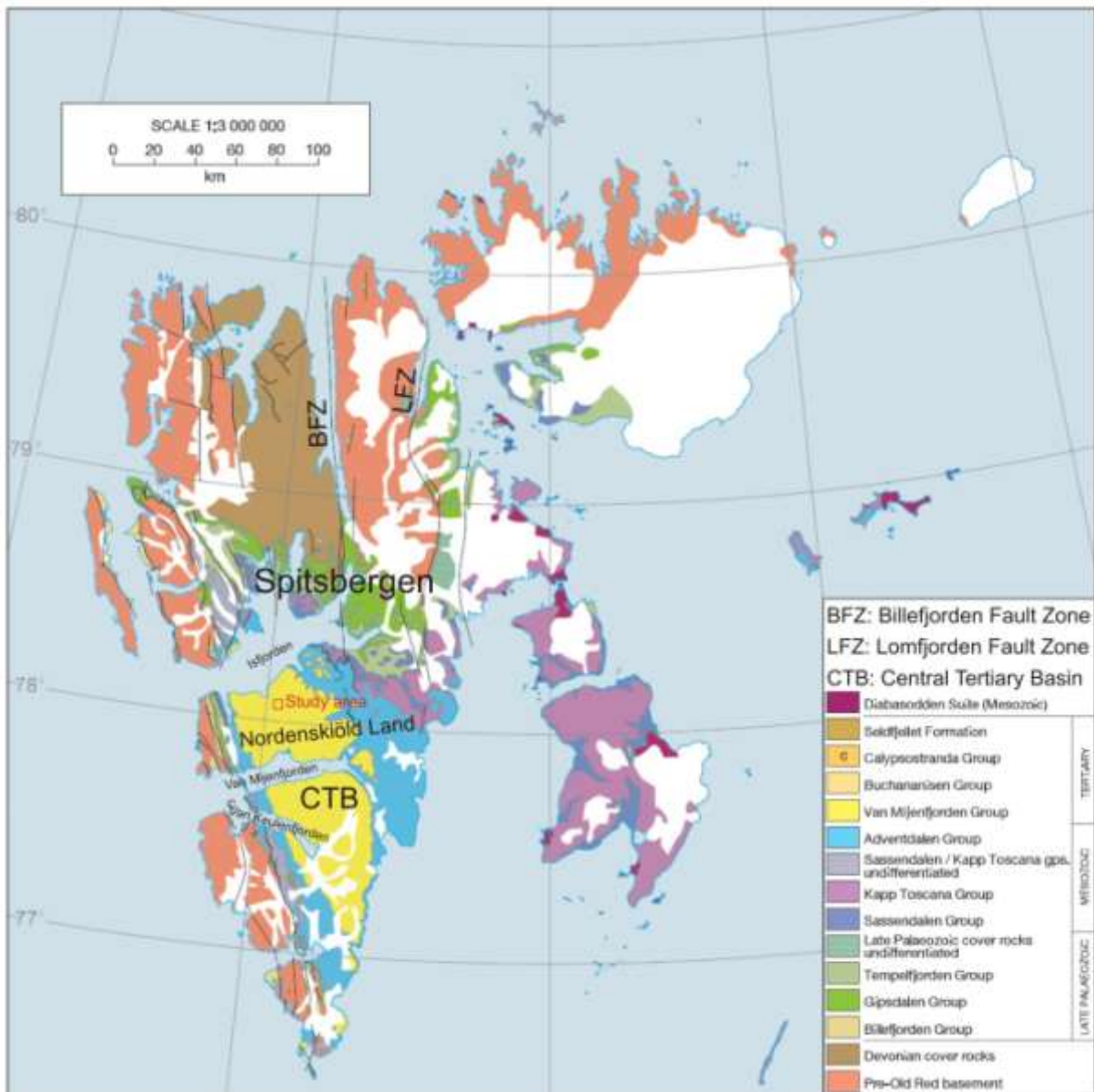


Figure 1.1: Geological map of Svalbard indicating the position of the study area on Nordenskiöld Land (modified from Dallmann et al., 1999)

1.3 Study area

The Central Tertiary Basin is located on the south-central parts of Spitsbergen, which is the largest island of the Svalbard Archipelago of the north-western Barents Sea (Figure 1.1). The study area is located in the north-central part of the basin, in the central part of the Nordenskiöld Land. The field work was carried out over a five week period during the summer 2009, and one week during the summer 2010. The field camp was located in the eastern reaches of Colsedalen and 22 lithostratigraphic profiles were logged on the surrounding mountains of Tillbergfjellet, Ringdalsfjellet, Sandsteinsfjellet and Mefjellet (Figure 1.2). Pictures of the four mountains in the study area are provided in Appendix 3. The locations of the different profiles are scattered over an area covering 10 km in an N-S

direction, and 7 km in a W-E direction. Most of the outcrops of the Battfjellet Formation in the study area are located at various altitudes within the range of 450m and 750m. The only way to get to the outcrops was by foot, and a more than three hour hike was necessary to reach the most distant outcrops.

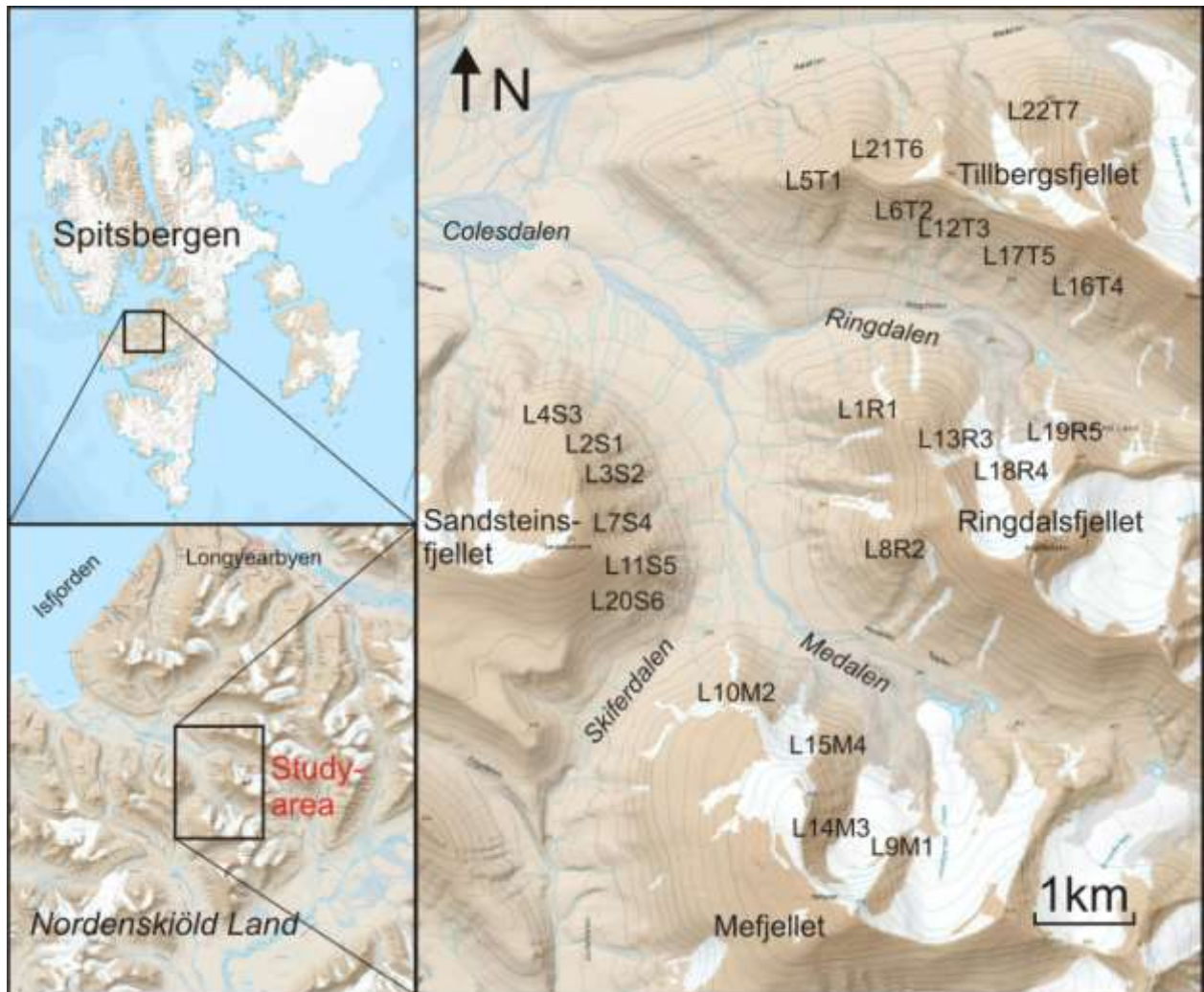


Figure 1.2: Overview map of the study area marking the location of the different logged sections on Sandsteinsfjellet, Mefjellet, Ringdalsfjellet and Tillbergfjellet (map: Norsk Polarinstitutt).

The names of the lithostratigraphic logs are based on the chronological order they were logged, and the second letter in the annotation indicates the mountain it was logged (eg. L1R1= Log 1, Ringdalsfjellet 1).

2. Methods

2.1 Field work

The observations and results presented in this thesis are obtained from sedimentological field work. The main method used in the field was lithostratigraphic logging, where features like sedimentary structures, bed thickness, colour, boundary types, texture, and mineralogical composition is observed and described. Large scale geometrical features of the sandstone bodies were observed at a distance. Paleocurrent measurements were obtained by the use of a geological compass. GPS and altimeters were used to record the altitude of studied outcrops. These instruments are based on the atmospheric pressure, and daily calibration to a point of known altitude was conducted. There are some uncertainties related to the use of altimeters as it may be strongly biased by local variations in atmospheric pressure. Other equipment used during field work include a geological hammer, grain size identification sheet, measuring stick, hand lens, binoculars, camera and graph paper with all necessary writing equipment. The sites of the logs in the study area were thoroughly picked to reflect a representative section of the rock unit. The logs were conducted vertically along the outcrop, but lateral shifts were sometimes necessary in order to include all of the exposed beds. The logs performed in the field were in a 1:20 scale.

The means of transportation to the study area was by helicopter for the first field season (summer 2009), and by hiking for the second season (summer 2010).

2.2 Post - field work

Post-field work processing of the data includes digital redrawing of the logs in a 1:50 scale by the use of CorelDraw X4 software. Correlation of the logs along various 2D transects were also conducted by the use of CorelDraw X4. Additionally, simplistic correlation of the sand bodies in 3D was conducted by the use of Google SketchUp 7 (*Figure 2.1*) where a DEM (digital elevation model) of the study area was extracted from Google Earth. Rose diagrams of the paleocurrent data was created by the use of the software Rozeta 2.0, and later edited in CorelDraw X3. Geostatistical analysis of the rose diagrams was carried out by the use of the Microsoft Excel based software Ez-Rose 1.0 by Baas (2000).

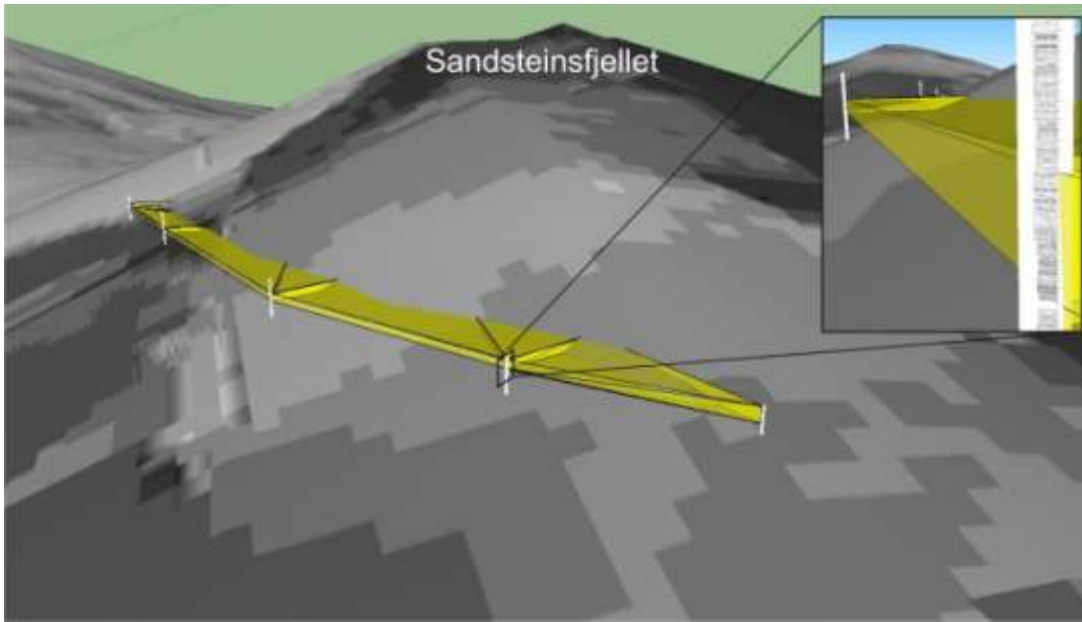


Figure 2.1: Snapshot from Google SketchUp 7 showing the correlation of P3 (Chapter 6) on Sandsteinsfjellet.

3. Geological framework

3.1 Introduction

Svalbard is an archipelago situated in the north-western Barents Sea, and comprises the islands located between the latitudes of 74° and 81° N and longitudes between 10° to 35° E. The archipelago represents an uplifted part of the Barents Sea, and reveals a comprehensive geological history as it contains a near complete stratigraphic succession ranging in age from Precambrium to Oligocene. Since the initiation of systematic geological survey on Svalbard by pioneers like A. E. Nordenskiöld, A.G. Nathorst and G. de Geer at the end of the 19th and the beginning of the 20th century (Dallman, 1999 and references therein), Svalbard has been subject to extensive geological investigations. The stratigraphic record of Svalbard (*Figure 3.1*) is highly variable and comprises igneous, metamorphic and sedimentary rocks. The sedimentary succession represents a large range of depositional environments from different climatic conditions, reflecting the progressive northward movement of Svalbard from an equatorial position in Carboniferous to the present day arctic position (Worsley, 2008; Worsley and Aga, 1986). Tectonic events of different ages have influenced the rocks on Svalbard. Of those, the most significant tectonic events are the Grenvillian (Precambrium), Caledonian (Ordovician-Silurian), and West Spitsbergen (Paleogene) orogenies (Dallmann et al., 1999). N-S to NW-SE oriented structural lineaments dominates the tectonic imprint on Svalbard and reflects inversion and reactivation during different tectonic phases (Steel and Worsley, 1984). The most prominent of these lineaments are the Billefjorden Fault Zone (BFZ) and the Lomfjorden/Agardhbukta Fault Zone (LFZ) (*Figure 1.1*). This chapter gives an overview of the geological history of Svalbard with a brief introduction to the Pre-Cenozoic (Chapter 3.2) and a more thorough description of the Cenozoic (Chapter 3.3).

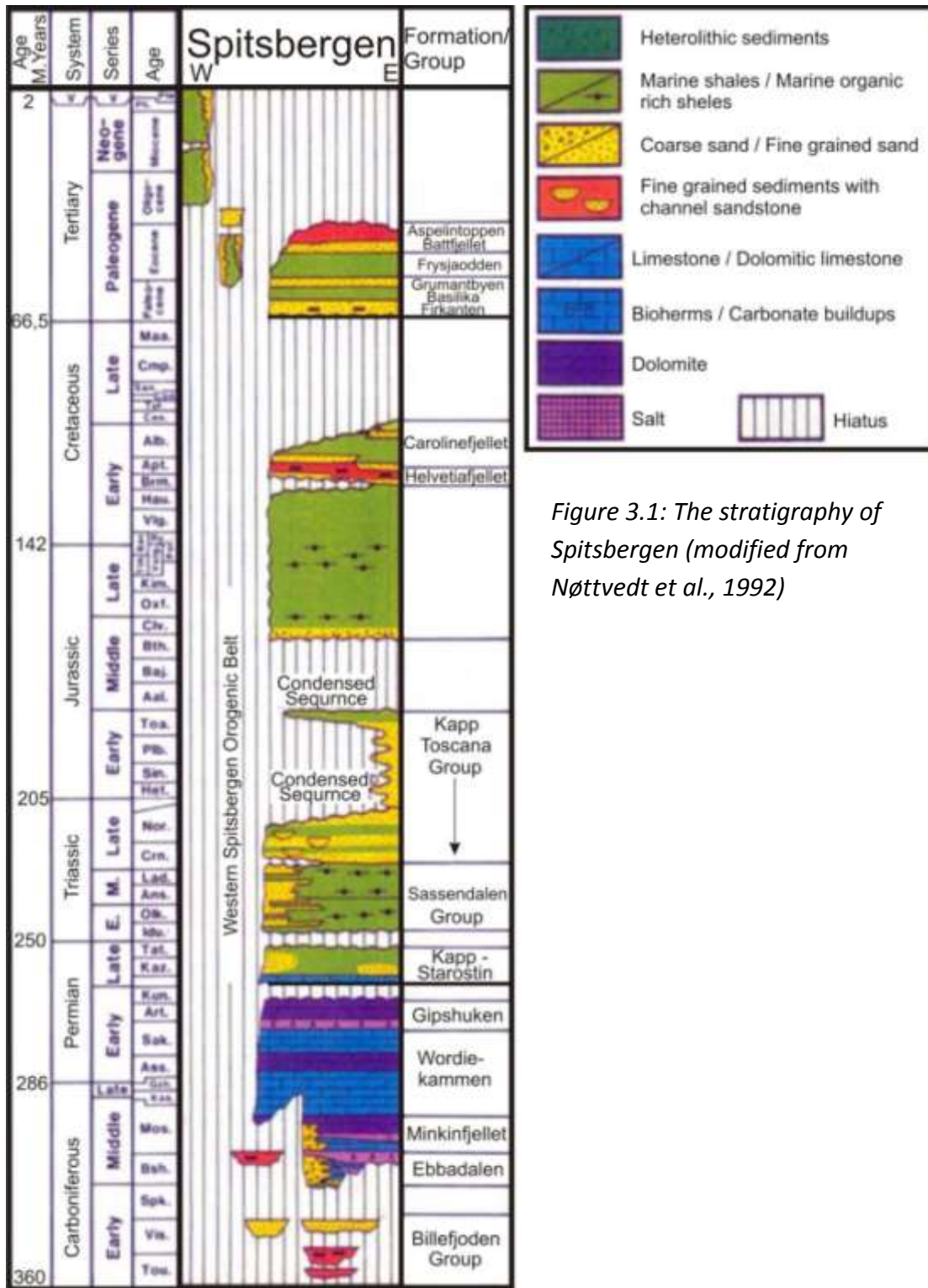


Figure 3.1: The stratigraphy of Spitsbergen (modified from Nøttvedt et al., 1992)

3.2 Pre-Cenozoic

3.2.1 Pre-Caledonian

The pre-Caledonian rocks on Svalbard, traditionally called the Hecla Hoek succession, comprise rocks of different lithologies, spanning in age from Precambrium to Early Silurian. Deformation from several orogenic events have influenced the pre-Caledonian rocks; in addition to the two main tectonic phases of the Caledonian Orogeny (Finnmarkian and Scandian), deformation from the Baikalian/Timanide orogeny (600-650Ma), and the Grenvillian orogeny has been recorded in the pre-Caledonian succession on Svalbard (Dallmann et al., 1999). The main Caledonian tectonic event on Svalbard, called the Ny Friesland orogenic phase, is of Middle to Late Silurian age and is regarded as the equivalent to the Scandian orogenic phase of the Caledonides on mainland Norway (Harland; 1997; Dallmann et al., 1999). There are some disputes regarding the age of this orogenic phase; e.g. a Late Ordovician/Early Silurian age was suggested by Birkenmajer (1975) and Worsley (1986). The pre-Caledonian rocks are commonly sub-grouped into three different terranes; a northwestern, southwestern and an eastern (Gee and Teben`kov, 2004; Harland, 1985). The Hecla-Hoek succession contains metasedimentary, metamorphic and igneous rocks of 20 different lithostratigraphic groups with a combined maximum stratigraphic thickness of approximately 20km (Worsley, 2008).

3.2.2 Devonian – old red

Late Silurian/Devonian deposits on Svalbard in large part represent post-orogenic molasse deposit following the mid-Silurian Ny-Freisland Orogen. The bulk of these deposits are located in a major down-faulted graben structure in Andrée Land in the northern part of Svalbard. The lowermost part of the Devonian succession consists of the Red Bay Group (earliest Devonian), constituting coarse grained clastic fluvial deposits above a prominent angular unconformity. This succession is overlain by the Andrée Land Group which consists of clastic fluvial red-beds with some coarse-grained (conglomeratic) intervals in the upper part (Friend and Moody-Stuart 1972). A major unconformity separates the Andrée Land Group from the overlying Billefjorden Group which spans the Devonian – Carboniferous Boundary. This unconformity developed during the Svalbardian tectonic phase (Harland, 1997).

3.2.3 Latest Devonian to middle Permian

Post Caledonian extension with the formation of half-grabens along the major N-S/NW-SE verging lineament zones is the dominating tectonic setting during Carboniferous on Svalbard. Two main stratigraphical groups were deposited during Carboniferous to middle Permian on Svalbard; the Famennian to Visean Billefjorden Group, and the Bashkirian to Sakmarian Gipsdalen Group (Steel and Worsley, 1984; Worsley, 2008).

3.2.3.1 Latest Devonian to middle Carboniferous

The Billefjorden Group consists of siliciclastic sediments of mainly delta plain, lacustrine and fluvial origin (Worsley, 2008; Gjelberg and Steel, 1981). The sediment fill of the Billefjorden Group was deposited in half grabens with differential subsidence (Nøttvedt et al., 1992). Coal seams of economic quantities occur within the Billefjorden Group on Svalbard, and have previously been mined at Pyramiden. The deposits of the Billefjorden Group represent a humid and tropical continental depositional environment that occurred along the northern margins of the supercontinent Pangea (Worsley, 2008; Worsley and Aga, 1984).

3.2.3.2 Middle Carboniferous-Middle Permian

The Gipsdalen Group consists of shallow marine/shelf carbonates and evaporites of a sabkha environment and minor amounts of siliciclastic sediments. The transition of the Billefjorden Group to the Gipsdalen Group is marked with the change from gray to red continental siliciclastic beds (Worsley, 2008; Gjelberg and Steel, 1981). The continued transgression into the marine carbonates that dominates the Gipsdalen Group is believed to reflect a long term regional sea level rise (Gjelberg and Steel, 1981). The Gipsdalen Group comprises three syn-rift half-graben restricted sub-groups and the overlying, post-rift Dickson Land subgroup (Dallmann et al., 1999). The transition from tropical continental deposits of The Billefjorden Group and arid deposits, indicated by the red beds and carbonate deposits, of the Gipsdalen Group mark a change in climatic conditions between the two groups. The ongoing northwards movement of Laurasia results in deposits influenced from climatic conditions of gradually higher latitudes. The abrupt change in climate is believed to be the combined effects of the northwards movement of the plate and the climatic effects of the convergence

of Laurasia and Gondwanaland, with closure of the Hercynian Ocean, resulting in more arid conditions.

3.2.4 Late Permian – Early Triassic

In Late Permian there was a significant change in lithofacies from evaporites and carbonates of the upper part of the Gipsdalen Group to a cherty succession dominated by siliciclastic sediments of the Tempelfjorden Group (Steel and Worsley, 1984). There is a significant hiatus separating the two groups (Worsley, 2008). The Kapp Starostin Formation is the main stratigraphic unit of the Tempelfjorden Group (Harland, 1997). The Kapp Starostin Formation is a transgressive unit, evolving from shallow marine brachiopod rich deposits of the Vøringen Member to spiculite rich deep marine shales of the Svenskeega and Hovtinden Members (Dallmann et al., 1999). The cold-water spiculite rich deposits of the Tempelfjorden Group mark a rapid climatic transition from the warm water carbonate dominated deposits of the Gispdalen Group. This is believed to be the combined results of the ongoing northwards movement of the Laurasian plate and the formation of the Uralides, inhibiting the connection with the warm Tethys Ocean (Worsley, 2008).

The transition from the silica rich shales of the Late Permian succession to the Early Triassic non-siliceous shales is an important unconformity (Worsley, 2008), and it also coincides with the Late Permian mass extinction event.

The Early to Middle Triassic succession consists of siliciclastic dominated deposits of the Sassendalen Group (Steel and Worsley, 1984). From a regional perspective, including the entire Barents Sea, the most important sediment source area for the Sassendalen Group was the hinterland created by the Uralides (Riis, 2008). However, the source area for the Triassic deposits on Spitsbergen up to the beginning of the Carnian stage was mainly to the west. The Sassendalen Group consists of transgressive-regressive cycles of marine shales to shoreface/delta front sandstones with rare carbonate intercalations (Steel and Worsley, 1984). Middle Triassic deep organic rich shales of the Bravaisberget (west Spitsbergen) and Botneheia (east Spitsbergen) formations are potential hydrocarbon source rocks and are roughly time-equivalent to the proven source rock of the Steinkobbe Formation of the Barents Sea (Riis, 2008).

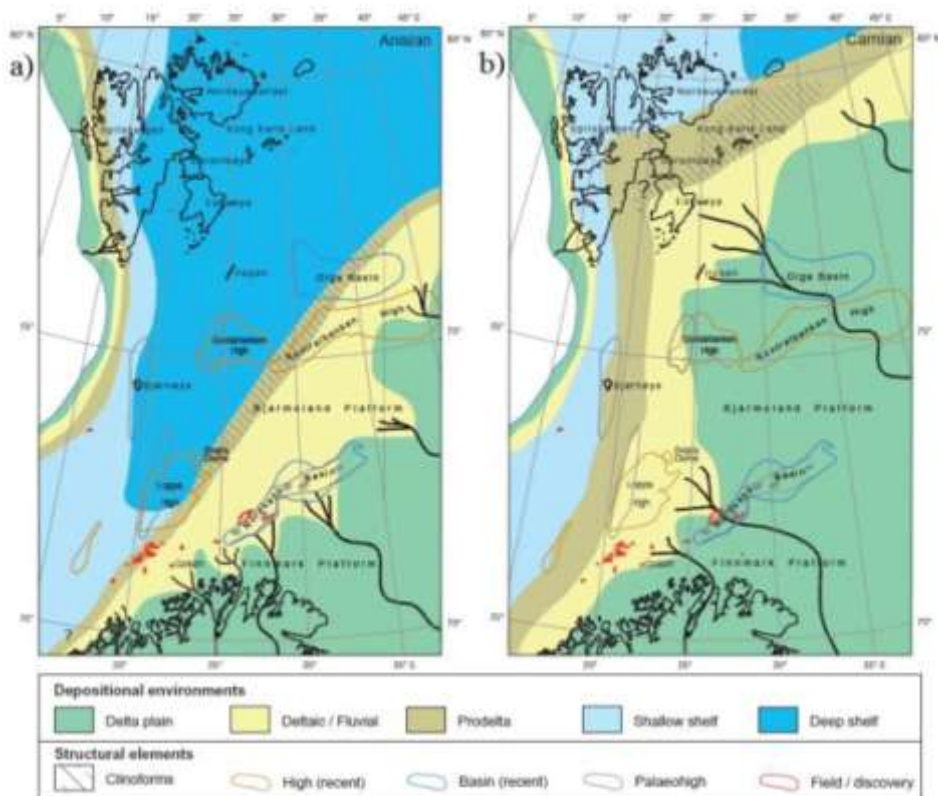


Figure 3.2:

Figure from Riis (2008) showing the overall westward progradation of the Triassic deltaic system from Anisian to Carnian. Dark blue colour indicates the position of the HC-source rock of the Steinkobbe Formation.

3.2.5 Late Triassic – Middle Jurassic

The Storfjorden Subgroup of the Kapp Toscana Group of Late Triassic to Middle Jurassic age is, as the underlying Sassendalen Group, an overall progradational siliciclastic deltaic system and may be regarded as a natural continuation of the underlying group (Steel and Worsley, 1984; Riis, 2008). The westward progradational deltaic system, sourced by the Uralides, formed a continuous paralic shelf environment over the Barents Sea and Svalbard in Carnian (Riis, 2008). The De Geerdalen Formation of the eastern Spitsbergen is thus believed to be the diachronous equivalent to the Snadd Formation of the Barents Sea (Riis, 2008).

3.2.6 Late Jurassic and Cretaceous

The strongly condensed Jurassic succession in the western part of Spitsbergen reflects several episodes of erosion and non-deposition, probably in a shallow, sediment starved shelf (Steel and Worsley, 1984). However, well defined coarsening upwards sequences that developed within the eastern part of Spitsbergen indicate delta progradation from the east. An important unconformity subdivides the Lower Jurassic from the Upper Jurassic. The

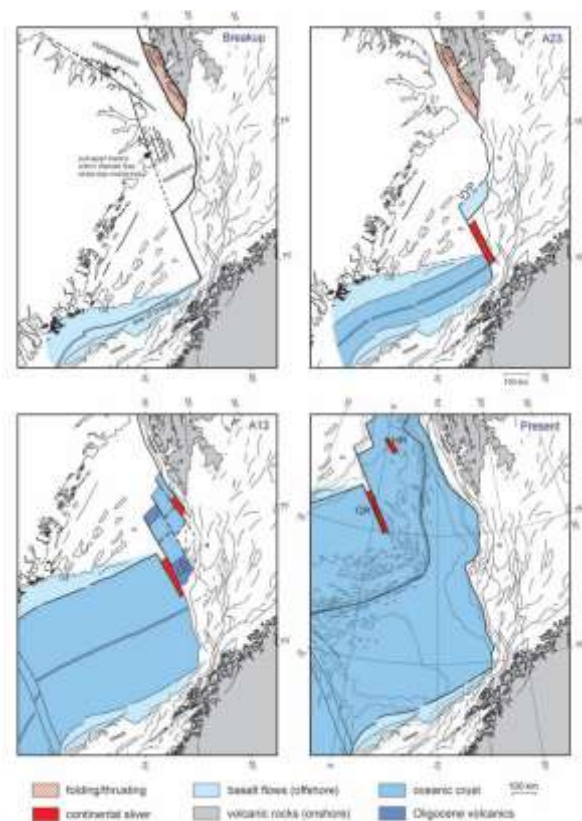
Brentskarhaugen bed occurs immediately above this unconformity. During Late Jurassic times thick homogeneous shale was deposited all over Spitsbergen, known as the Agardhfjellet Formation. This succession was first defined as a member of the Janusfjellet Formation (Parker, 1967) but is currently defined as a formation of the Janusfjellet Subgroup (Dypvik et al., 1991). The lowermost Cretaceous succession consists of shales of the Agardhfjellet Formation (Mørk et al. 1982, Dypvik et al. 1991). A major sequence stratigraphic boundary is present at the Hauterivian/Barremian boundary, overlain by the overall transgressive Helvetiafjellet Formation (Parker, 1967; Gjelberg and Steel, 1995; Midtkandal and Nystuen, 2009). The formation represents fluvial and deltaic deposits overlain by shelfal sandstones and shales of the Carolinefjellet Formation. A significant stratigraphic break separates the Cretaceous Succession from the Cenozoic succession. All of the Upper Cretaceous is missing below this unconformity. The Cenozoic succession above this unconformity starts with a basal conglomerate (the Grønfjorden Bed).

3.3 Cenozoic:

3.3.1 Introduction:

The dominating tectonic event during Cenozoic on Svalbard is the formation of the West Spitsbergen Orogen as a result of transpression related to dextral shear along the De Geer Fault Zone during the opening of the Norwegian-Greenland Sea (*Figure 3.3*). The Central Tertiary basin is a foreland basin that developed adjacent to the West Spitsbergen Orogenic Belt in Paleogene time. The sedimentary succession of the basin makes out the Van Mijenfjorden Group, which is further subdivided into seven formations (Harland 1997; Harland 1969). The basin consists of cyclic infills of mixed continental and marine sediments, reflecting deposition during episodic transgressive and regressive cycles as well as different tectonic regimes. The basin has a thickness of 1,5km in the northeast and 2.5km in the southwest (Harland 1997). Post-orogenic isostatic uplift resulted in erosion of 1,7 – 3 km of the succession. The youngest rocks exposed in the basin are of Late Eocene/Earliest Oligocene age (Peach, 1999). This chapter describes the formation of the West Spitsbergen Orogen (Chapter 3.3.2) and the formation of the Central Tertiary Basin (Chapter 3.3.3), as well as the stratigraphy and basin fill of the Central Tertiary Basin (Chapter 3.3.4)

Figure 3.3: Plate tectonic setting during the opening of the Atlantic Ocean (Faleide, 2008).



3.3.2 Tectonic history:

As previously mentioned, the West Spitsbergen Orogen formed as a result of dextral transpression between Greenland and Svalbard during the opening of the Norwegian-Greenland Sea in Late Cretaceous to Eocene times. The West Spitsbergen Orogen forms a 100-200km long prism that thins eastwards. The Orogen can be sub-divided into four main strike parallel zones (*Figure 3.5*); a basement dominated hinterland, a western basement-involved fold and thrust complex, a central fold and thrust belt, and an eastern foreland zone (Bergh et al., 1997; Braathen et al., 1999). The three latter zones represents the fold and thrust belt portion of the orogen.

The basement outcropping on the west coast of Spitsbergen represents the hinterland area of the orogen. Indicative of the absence of cover strata, this zone has experienced the deepest erosion along the transect, and represents the thickest portion of the accretionary prism (Braathen et al., 1999). Post-orogenic extensional grabens, including the Forlandsundet Graben (Harlan and Horsfield, 1974; Steel et al., 1985), are located in this section of the orogen.

The western basement-involved zone is dominated by stacked thrusts and macro-scale folding (chevron-style monoclines, synclines and anticlines) with a wave length of 5km (Bergh et al., 1997, Braathen et al., 1999). A distinctive feature of this zone of the orogen is the presence of basement rooted (thick skinned) thrusts (Bergh et al., 1997, Braathen et al., 1999).

The central fold and thrust belt represents a thin-skinned thrust system with a regional decollement in Permian evaporites of the Gipshuken Formation, with additional detachment surfaces in shales of the Mid-Triassic Bravaisberget Formation and the Jurassic Janusfjellet Subgroup (Bergh et al., 1997, Braathen et al., 1999). Thrust associated fault propagation folds on a macro-scale are a common feature of this zone (*Figure 3.4*). The transition to the eastern foreland province is marked with a major thrust ramp front (Braathen et al., 1999). A notable feature of this zone is the presence of out of sequence thrusts that cuts through pre-existing thrusts.

The eastern zone of the orogen is that of a foreland tectonic regime, represented with sub-parallel cover strata with internal deformation in the form of fault propagation and fault

bend folds associated with décollement rooted thrust faults (Bergh et al., 1997, Braathen et al., 1999). Another feature of this zone is the presence of inversion structures related to reactivation of pre-existing normal faults such as in the Billefjorden Faults Zone and the Lomfjorden Fault zone (Braathen and Bergh, 1995, Braathen et al., 1999). Locally, out-of-sequence thrusts can be observed (Braathen et al., 1999).



Figure 3.4: Stacked thrust nappes of the Permian and Triassic succession at Mediumfjellet displaying large fault propagation folds.

Bergh et al. (1997) and Braathen et al. (1999) have applied a five-stage kinematic evolution of the West Spitsbergen Orogen that encompasses the entire evolution from the initiation of shortening in Late Cretaceous/Early Paleocene to the Late Eocene/Oligocene extensional collapse of the orogen. Braathen et al. (1999) applied a critical taper model to explain the tectonic evolution of the orogen in terms of wedge geometry of the accretionary prism. The critical taper model is based on the assumption that the wedge geometry of the orogen forms a subcritical, critical or supercritical taper angle that controls the structural evolution of the orogen. The taper angle is the combined angle of the basal décollement angle and the angle of the surface slope and is controlled by factors like the compression rate, basal friction, rock strength, erosion rate at the surface and gravity (Braathen et al., 1999). A

condition of a supercritical taper can result in hinterland extensional collapse, and foreland propagation with out-of-sequence thrusting with a magnitude depending on degree of supercritical taper angle. A summary of the five tectonic stages from Bergh et al. (1997) and Braathen et al. (1999) is provided below:

- Stage 1: NNE/SSW directed bedding parallel shortening. Folds and detachment thrusts are of a pre-uplift stage. Observed structures of this stage is limited to the basement-involved fold-thrust complex zone of the orogen. The shortening of this stage is believed to represent the initiation of the West Spitsbergen Orogen in Late Cretaceous/Early Eocene times.
- Stage 2: ENE/WSW directed shortening. Formation of the Svartfjella-Eidembukta-Daudmannsodden lineament (SEDL) in the western hinterland zone. Thick skinned thrusting and rotation of pre-existing (stage 1) thrusts in the basement-involved fold-thrust complex zone of the orogen. In-sequence thin skinned piggy-back thrusting in the central fold-thrust belt zone, and layer parallel shortening and décollement thrusting in the eastern foreland province. The stage 2 deformation of the orogen is believed to be of Early- to Middle Paleocene age.
- Stage 3: Continued ENE/WSW shortening. Sinistral strike-slip overprint of the SEDL in the western hinterland. Thick skinned thrusting and further rotation of pre-existing faults (stage 1 and stage 2) in the basement-involved fold-thrust complex zone. Continued in sequence thrusting in the central zone and layer parallel shortening and décollement thrusting in the eastern foreland province. During stage 2 and stage 3, the crustal thickening of the hinterland is believed to have created an unstable supercritical wedge, resulting in increased eastwards thrusting in the central zone to create a stable taper.
- Stage 4: NE/SW shortening. Dextral strike-slip movement along SEDL in the western hinterland. Conjugate strike slip faults with predominant dextral movement in the basement involved fold-thrust belt zone. Out of sequence thrusting with NE-directed truncation of pre-existing faults in the central zone. In the eastern foreland province, pre-existing fault zones experienced reverse reactivation with resulting overlying inversion structures

(monoclines). Towards the end of stage 3 and during stage 4, the taper angle is believed to have been adjusted to a critical angle, by the combined effects of transcurrent faulting, erosion, and extensional faulting. The wedge is then believed to have reached a new critical taper angle following renewed shortening of the hinterland, with resulting out-of-sequence faulting in the central fold-thrust zone.

- Stage 5: E-W to ENE-WSW extension. Local extension and graben formation in the western hinterland. Continued out of sequence thrusting in the central and eastern foreland province with truncation of inversion monoclines. With the cessation of the shortening and the local extension of the hinterland, the wedge reached a critical taper angle during stage 5 of the tectonic evolution of the orogen.

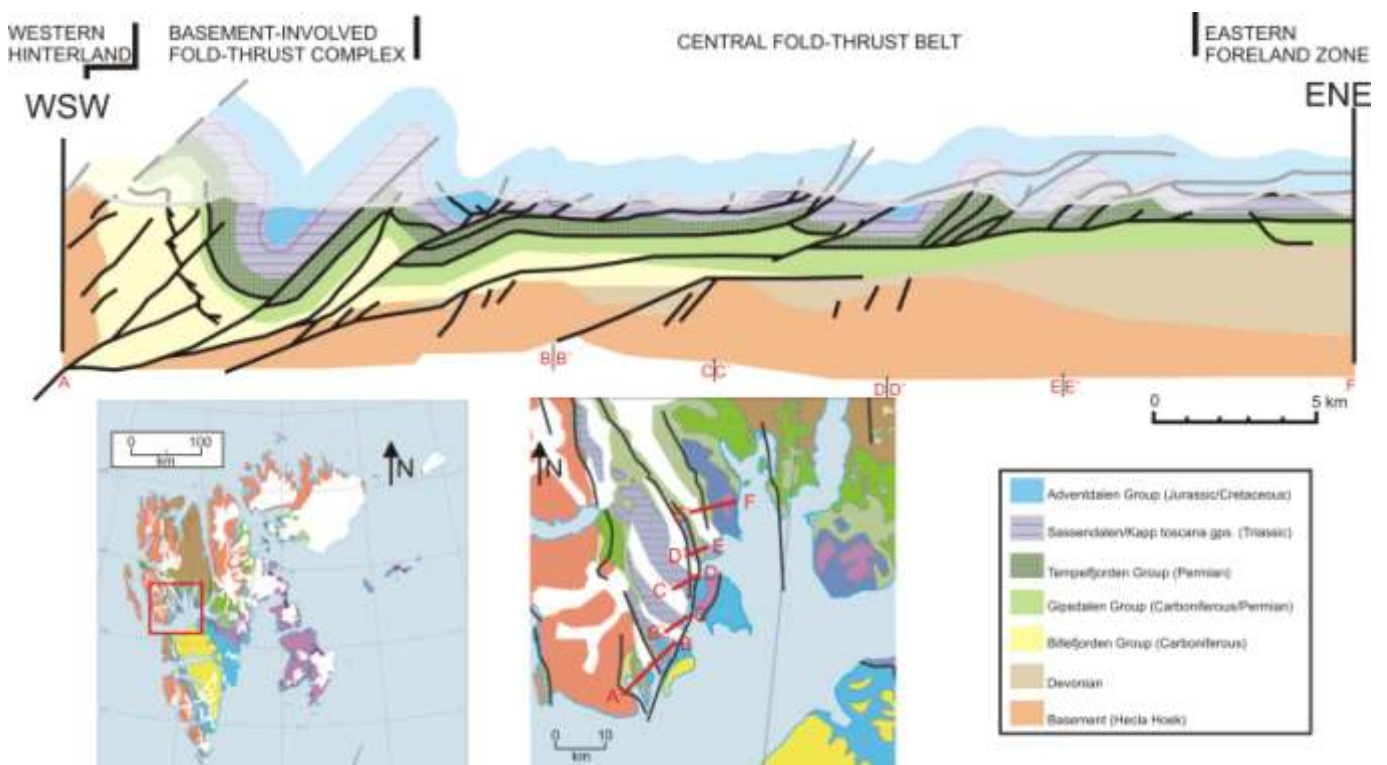


Figure 3.5: Cross section from Oscar II Land, showing the different deformation zones of the West Spitsbergen Orogen (redrawn from Braathen et al., 1999, geologic map modified from Dallmann et al., 1999)

3.3.3 The Central Tertiary Basin:

The Central Tertiary Basin has been classified as a foreland basin by Steel et al. (1985), Helland-Hansen (1990) and Bruhn and Steel (2003). The main arguments for a foreland basin setting as presented by Helland-Hansen (1990) is the adjacent location to a fold and thrust belt, the asymmetric transverse profile of the basin with thicker successions closer to the hinterland, and syn-depositional tilting and deformational incorporation of the deposits in the proximal areas of the basin. However, applying typical foreland basin models for the entire Paleogene basin succession is not straight forward. The sedimentary succession of the basin does not show a consistent hinterland derived sediment input from the west throughout the entire evolution of the basin; there is a significant shift in source area in Late Paleocene/Eocene (Steel et al., 1985; Bruhn and Steel, 2003). In addition, the flanking fold and thrust belt is, as previously mentioned, of transpressional origin rather than purely compressional origin, which is an unusual setting for a foreland basin.

Two main models of the tectonic evolution of the Central Tertiary Basin exist to account for the sediment infill evolution of the basin from Early Paleocene to Late Eocene/Early Oligocene.

A two stage tectonic evolution was proposed by Steel et al. (1981) and Steel et al. (1985). This interpretation states that the basin evolved over two main distinct tectonic settings; from an extensional/transensional setting, with a series of sub-basins, for the lower succession of Early Paleocene to late Paleocene age, to a transpressive setting for the Late Paleocene to Late Eocene/Oligocene deposits. The main arguments for this interpretation is the contrast between the mainly easterly derived, mainly transgressive, Paleocene succession, and the regressive, westerly derived, Eocene succession, as well as the presence of minor E-W verging strike-slip faults, that might be indicative of an extensional setting (Steel et al., 1985, Bruhn and Steel, 2003). In addition, the record of the sea-floor spreading between Greenland and Eurasia at the time is not supportive of compression before the Paleocene/Eocene transition (chron 24-25) (Bruhn and Steel, 2003).

The model proposed by Bruhn and Steel (2003) is that of a compressional (transpressional?) flexural foreland basin throughout the entire tectonic evolutionary history of the basin. The, at least partially, eastern provenance of the Paleocene deposits of the Central Tertiary Basin

is, in this model, explained to be derived from an eastwards migrating peripheral bulge. The main arguments for this model is the better concordance with existing tectonic models of the West Spitsbergen Orogen proposed by Bergh et al. (1997), Braathen et al. (1995), and Braathen et al. (1999), an apparently better fitting model to the basin fill, as well as the lack of evidence for an originally transtensional setting of the basin.

There is a broad consensus of a foreland basin setting associated with flexure as a result of thrust nappes of the West Spitsbergen Orogen for the basin fill of the Late Paleocene to Eocene/Early Oligocene deposits (Frysjaodden, Battfjellett, and Aspelintoppen formations). This succession has a prominent provenance from a western hinterland. In addition, there is an eastwards migration of the depocenter of the basin fill, which likely is coupled with the eastwards growth of the fold and thrust belt (Helland-Hansen, 1990, Steel et al., 2003). The drainage reversal to a western provenance and the texturally more immature sediments with an increased content of metamorphic grains is argued to be the result of a major change in the tectonic setting of the basin by Steel et al. (1985).

Nichols and Lüthje (2008) proposed that the basin formed as a result of compressional flexure rather than flexure as a result of loading related to thrust nappes. They argued that long wavelength asymmetric folding of the crust, related to the Hornsund fault zone, could create a similar basin setting.

A simple coupling of the basin fill and the tectonic model proposed by Bergh et al. (1997) and Braathen et al. (1999), with a subdivision of the orogen into 4 distinct provinces and with a five-stage tectonic evolution, was conducted in Braathen et al. (1999). In this model, the Paleocene Firkanten, Basilika and Grumantbyen formations corresponds to tectonic stage 2, with deposition in the eastern foreland and central fold and thrust belt provinces of the orogen. The western shift of the source area is coupled with the main contractional uplift of tectonic stage 3 with deposition of the Frysjaodden, Battfjellet, and Aspelintoppen formations throughout stage 3 and 4 in the central fold and thrust belt and eastern foreland provinces. At some time during stage 3 and 4, thin skinned thrust sheets emerged on the eastern side of the basin, giving the basin the characteristics of a piggyback basin (Helland-Hansen, 1990; Braathen et al., 1999).

3.3.4 Van Mijenfjorden Group:

The Van Mijenfjorden Group consists of seven formations; the Firkanten, Basilika, Grumantbyen, Frysjaodden, Hollenderdalen, Battfjellet and Aspelintoppen formations (Figure 3.6). According to Steel et al. (1985), the deposits of the Van Mijenfjorden Group include three main depositional cycles. The lower two are intermediate-scale transgressive-regressive cycles; the lower one from the Firkanten Formation to the lower Basilika Formation, and the second from the Basilika Formation to the Grumantbyen Formation (Bruhn and Steel, 2003). The third depositional cycle is an ascending regressive megasequence deposited during the main deformational stage of the West Spitsbergen Orogen and includes the Frysjaodden, Battfjellet and Aspelintoppen formations.

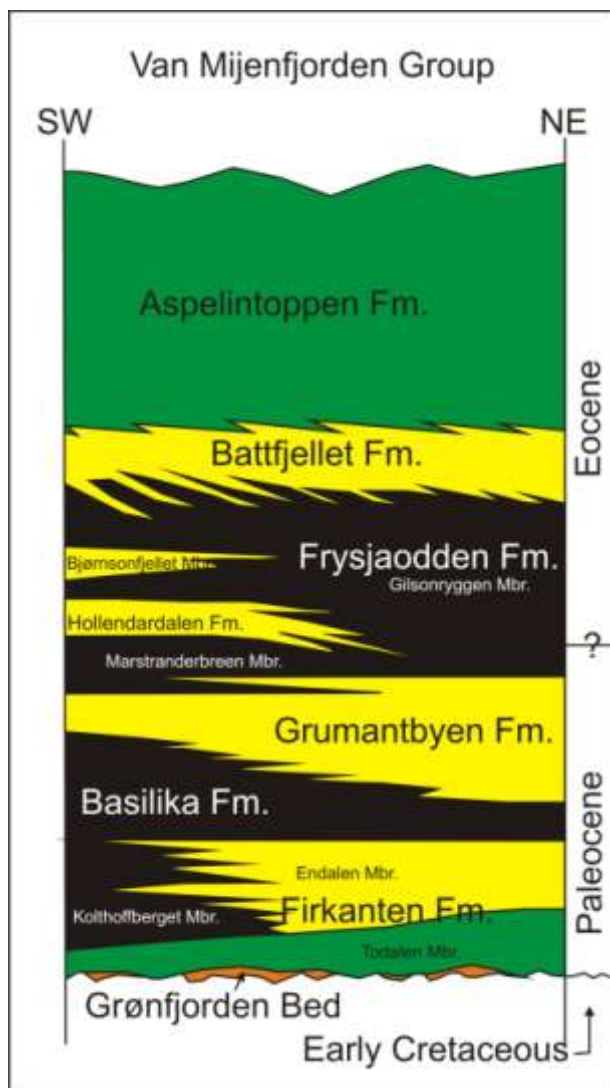


Figure 3.6: The Stratigraphic formations of the Central Tertiary Basin (modified from Steel et al., 1985)

3.3.4.1 Firkanten Formation

The Firkanten Formation is the basal succession of the Van Mijenfjorden Group of the Central Tertiary Basin. It is made up of the Grønfjorden, Todalen, Endalen and Kalthoffberget members, and was deposited during the early stages of the Central Tertiary Basin within either a transtensional setting, or an early stage transpressive foreland setting with peripheral bulge sourced sediments, depending on the assigned model as previously discussed. The main source of sediments derived from the east and northeast.

The basal bed of mainly sandstone with conglomerates at some locations is called the Grønfjorden Member (Harland, 1997). The Grønfjorden Member lies uncoformably on Lower Cretaceous marine shales (Bruhn and Steel 2003). There is a hiatus of approximately 32 My between the Lower Cretaceous sediments and the Paleocene sediments of the Firkanten Formation (Harland 1997). The conglomerates of the Grønfjorden member are concentrated in the western and northwestern regions of the basin and are absent south of Van Mijenfjorden (Kellogg, 1975). The conglomerate, with well rounded chert and quartzite pebbles, is believed to be braided river deposits derived from the eastern part of the basin (Bruhn and Steel, 2003).

Overlying the Grønfjorden Member is the Todalen Member with fluvial-tide dominated deltaic sediments (Harland, 1997). The sedimentary sequence of the Todalen Member is made up of alternating coals, shales and sandstones. The Todalen Member changes facies laterally from a tide and fluvial dominated system in the northeast to a more uniform lower plain succession in the southwest (Harland, 1997). The shale/sand ratio increases towards the west, and the source of the Todalen Member was likely at the northeastern rim of the basin. Towards the west, the Todalen Member interfingers with the overlying Endalen Member.

The Endalen Member consists of quartz-arenitic sandstones deposited in a wave dominated delta-front and barrier bar environment (Harland, 1997; Steel and Worsley 1984). The Endalen Member interfingers with its fine grained deep water equivalent in the west; the prodelta to delta-front sediments of the Kalthoffberget Member (Bruhn and Steel 2003).

The overall stratigraphic evolution of the Firkanten Formation is of a transgressive nature, developing from non marine fluvial facies in the Grønfjorden and Todalen members to

marine facies in most of the Endalen Member. Although there is an overall transgressive development of the Firkanten Formation, it is made up of multiple minor regressive sequences. The Firkanten Formation is completed with a more prominent regressive development as the Endalen Member evolves from shallow marine to continental fluvial deposits at the uppermost part of the member (Bruhn and Steel 2003).

The Firkanten Formation is of lower to mid Paleocene age. Based on foraminifera analysis taken from the Kalthoffberget Member in the Basilikaelva, Nagy et al. (2000) established a Selandian age for the deposits while analysis of fission tracks in apatite grains from the Endalen and Todalen Members gives a slightly younger age (Danian) (Blythe and Kleinsphen, 1998; Bruhn and Steel, 2003). Of the exposed section of the Tertiary Central Basin, the Firkanten Formation is thickest (>200m) between Isfjorden and Van Mijenfjorden, but the original depocenter is believed to have been located west of the present western margin of the basin (Kellogg, 1975; Bruhn and Steel 2003).

3.3.4.2 Basilika Formation

The sediments of the Basilika Formation are mostly deep marine and shelf deposits consisting of dark gray, black or greenish shales and siltstones of a Late Paleocene age (Harland, 1997). The distal characteristics of these sediments conform to a continuation to the transgressive evolution of the underlying Firkanten Formation. The Basilika Formation is thickest in the south and southwest, where it has a thickness of 300-350m. Towards the north and northeast it is gradually thinning out to a thickness of approximately 20m (Harland, 1997). Interbeds of sandstones and siltstones with a thickness of 50-150 cm are present in the basal 45m of the formation in the western part of the basin (Kellogg, 1975).

A zone of deep water shales in the basal part of the Basilika Formation marks the maximum transgressive surface, above which there is an increase in grain size upwards in the formation (Bruhn and Steel, 2003). This marks a change in depositional style from the transgressive succession of the lower Paleocene sediments to a regressive succession as evidenced by the upper part of the Basilika Formation and the Grumantbyen Formation (Kellogg, 1975). The Basilika Formation interfingers with sandstones of the regressive

Grumantbyen Formation, originating from a prograding inner shelf environment in the northeast.

As with the Firkanten Formation, the sediment input to the lower transgressive part of the Basilika Formation was from the east, west and north, whereas the sediments of the upper regressive part of the formation was mostly derived from the north and northeast (Helland-Hansen 1990).

3.3.4.3 Grumantbyen Formation

The Late Paleocene Grumantbyen Formation overlies the Basilika Formation, and interfingers with the Basilika Formation in the southwest. The Grumantbyen Formation was interpreted as deposits of a “shallow offshore bar complex” by Harland, (1997). It consists of five major sheets of greenish, highly bioturbated sandstones, representing smaller scale sequences within the formation (Bruhn and Steel, 2003). Tempestites and trace fossils of the Cruziana, Zoophycus and Nerites ichnofacies have been recognized at the lower two sandstone sheets, indicating a distal shelf depositional environment (Bruhn and Steel, 2003). As a contrast, the three upper sandstone sheets have sedimentary structures including hummocky cross-stratification, planar lamination and wave ripples, which indicate influence of storm generated waves at a more proximal shelf setting (Bruhn and Steel, 2003). The lower boundary to the Basilika Formation is gradational, and defined by the first appearance of the greenish, highly bioturbated sandstone (Dallmann et al., 1999). The Grumantbyen formation is thinning westwards from a thickness of approximately 450m in the eastern/north-eastern area of the basin to a thickness of approximately 200m in the western/south-western area of the basin (Dallmann et al., 1999).

3.3.4.4 Frysjaodden Formation

The Frysjaodden Formation is a uniform olive- to dark-gray shale succession situated between the uppermost sandstone sheet of the Grumantbyen Formation and the lowermost sandstone body of the overlying Battfjellet Formation (Kellogg, 1975). A few turbiditic interbeds of siltstone and sandstone and scattered chert pebbles are present in the formation (Steel et al. 1980). There is an increase in thickness of the Frysjaodden Formation

west- and southwards; the thickness is increasing from 200m in the northern Nordenskiöld Land to approximately 400m south of the Van Mijenfjorden (Steel et al. 1980). The Frysjaodden Formation was originally named the Gilsonryggen Formation but was given its present name to include the Marstranderbreen Member, located below the Hollendardalen Formation (Harland, 1997).

The deposition of the Frysjaodden Formation is believed to have taken place simultaneously with the Late Paleocene/Early Eocene overthrusting of the West Spitsbergen Fold belt. As a result of the overthrusting and associated regional uplift of the area, the sediment input for the formation was from the west, marking a change in dominating sediment input-direction from the underlying formations (Helland-Hansen, 1990; Dallmann et al., 1999). The Frysjaodden Formation is believed to have a deltaic source west of the present day western margin of the basin which has been succumbed by the eastward prograding west Spitsbergen thrust and fold belt (Harland, 1997).

3.3.4.5 Hollendardalen Formation

The Hollendardalen Formation is a sandstone unit of a tidal dominated deltaic origin located above the Marstranderbreen Member and below the Gilsonryggen Member of the Frysjaodden Formation. It is 150m thick in the south-westernmost region of the basin and is thinning out towards the east until it ultimately pinches out in the Frysjaodden Formation (Steel et al. 1985). The deltaic system is prograding eastwards with the sediment source in the west (Steel et al 1985).

3.3.4.6 Battfjellet Formation

The Battfjellet formation consists of shallow marine wave influenced deltaic sandstones and siltstones. The formation is a part of an upwards coarsening megasequence and is not separated from the underlying Frysjaodden Formation by a distinct surface, rather the base of the Battfjellet Formation can be established where the proportion of sandstone exceeds the proportion of shale (Helland-Hansen, 1990). The Frysjaodden Formation, Battfjellet Formation and the overlying Aspelintoppen Formation forms the third depositional cycle of the Central Tertiary Basin which is a strongly ascending regression with sedimentation

strongly exceeding accommodation (Helland-Hansen, 1990). The Battfjellet Formation is at least partly of Early Eocene age and is believed to have formed contemporaneous to the ongoing development of the West Spitsbergen Ocean as a result of transpressive plate movement between the Eurasian and Greenland plates (Deibert et al. 2003). The resultant foreland basin setting with a high supply of sediment from the west and an eastward progradation of the sediment produced several large scale clinothems in the western part of the basin (Helland-Hansen, 1990; Deibert et al. 2003). The clinothems have an easterly dip and wedge out in the Frysjaodden shales in a basinward direction (Helland-Hansen, 1992). The clinothems of the Battfjellet Formation are well exposed at some locations, and the sediments from different facies can be traced laterally, from coastal plain to deltaic and shallow marine, to the more distal shelf and basin floor facies (Steel, 1977; Helland-Hansen, 1985; Helland-Hansen, 1990; Deibert et al. 2003). Steel et al. (2000) classified the clinoforms into four main groups on the basis of aggradation/progradation styles, degree of channel incision at the shelf edge, and the sand distribution along the clinoform (*Figure 3.7*).

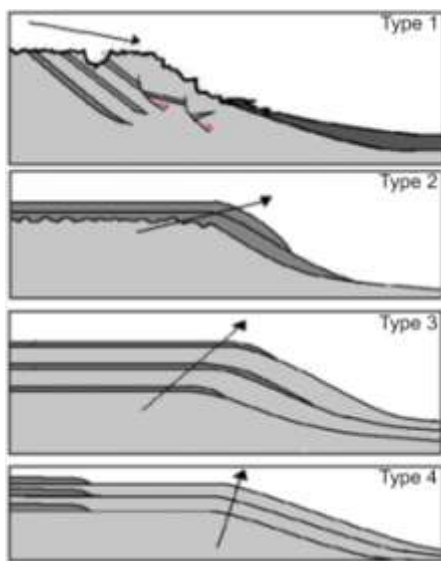


Figure 3.7: The four main types of clinoforms after Steel (2000):

Type 1: Descending progradation; erosion from incised fluvial channels from shelf edge deltas. Aggradation of basin floor due to sediment transport beyond shelf edge.

Type 2: Highly progradational; sediment delivery from shelf edge deltas with little degree of channel incision. Sand delivery to shelf edge and slope but little to the basin floor.

Type 3: Ascending progradational; sand sheets deposited from shelf transiting wave dominated deltas/shoreline. Little sand delivery beyond shelf edge.

Type 4: Aggradational; wave generated sand from stationary deltas/shoreline. Sand confined to inner shelf.

Both in the eastern and the western part of the basin, the shallow marine section of the Battfjellet Formation consists of stacked, upward coarsening parasequences (c.f. Van Wagoner et al., 1990), varying in numbers at different locations with no obvious preferred trend (Helland-Hansen, 1990, Helland-Hansen, 2010).

The sandstones of the Battfjellet Formation are texturally immature, mostly being composed of lithic greywacke, reflecting short transportation from the source area (Helland-Hansen, 1990; Helland-Hansen, 2010). The grains of the sandstones are a mixture of polycrystalline metamorphic quartz grains and sedimentary derived siliclastics and carbonate fragments (Helland-Hansen, 1990). The Battfjellet Formation has a thickness of less than 60m in the north-eastern reaches of the basin and a thickness of more than 300m in the south-western part of the basin, indicating a pronounced eastward thinning of the formation (Dallmann et al. 1999).

3.3.4.7 Aspelintoppen Formation:

The Aspelintoppen Formation consists of delta-plain deposits of alternating sandstones, siltstones, shales, and thin coals (<30cm) (Steel et al. 1985). The formation is a part of the third depositional cycle, the regressive megacycle including the underlying Battfjellet and Frysjaodden formations. The lower boundary of the Aspelintoppen Formation is defined by the first occurrence of coal or the first thick interval of terrestrial mudstone above the sandstones of the Battfjellet Formation (Dallmann et al., 1999). The Aspelintoppen Formation has a thickness of more than 1000m at some locations; it is the youngest of the formations in the Central Tertiary Basin and constitutes the upper reaches of the hill tops.

4. Lithofacies and facies associations:

4.1 Introduction:

The sedimentary rocks of the studied succession have been grouped into lithofacies based on lithologic features like sedimentary textures, sedimentary structures, colour, bioturbation and boundary types. The lithofacies are subsequently grouped into facies associations consisting of one or several lithofacies. These facies associations constitute the basis for the interpretation of the depositional environments. Thus, spatially and genetically related lithofacies, deposited by different processes within the same gross depositional environment are grouped into the same facies association. The studied section is subdivided into 16 lithofacies (Table 4.1) and 7 facies associations (Table 4.2). A brief description and interpretation of the lithofacies is provided in Table 4.1, and a more thorough description and interpretation are provided for the lithofacies in the context of their respective facies associations. In the text, lithofacies are referred to as FX, and facies associations FAX (where X represents the number of the lithofacies/facies association). The facies associations are arranged in ascending order from the most distal to the most proximal.

The emphasis of this study has been on the shallow marine succession of the Battfjellet Formation, which has been devoted a more thorough study and discussion than the continental deposits of Aspelintoppen Formation.

Table 4.1: Lithofacies:

Lithofacies	Grain size:	Description:	Interpretation:
F1	Clay-/ siltstone	Frissile/flakey shales. Varying in colour from light gray to dark gray/purpleish to light brown/reddish (iron content)	Deposits settled from suspension in a tranquil environment
F2	Mudstone	Mixture of clay, silt and sand grains (vf). Irregular lamination, commonly gray to dark gray/purpleish to light brown/reddish colour.	Low density turbidite deposits/basin floor fan fringe deposits.
F3	Clay-/siltstone and very fine grained sandstone	Load casts/ball and pillow structures: Spherical and hemispherical sandstone structures enclosed, or partially enclosed, in fine grained sediment. Varying proportions of fine grained sediment and sandstone.	Deformed sandstone as a result of rapid deposition of sand over partially consolidated mud.
F4	Very fine grained sandstone	Mainly isotropic convex hummocky cross-stratification structures with approximately 1 cm spacing between stratification surfaces. Varying wave length. Small scale symmetrical ripples with straight to slightly sinuous crest are often superimposed on the bed.	Distal tempestite deposits from episodes of high oscillatory currents.
F5	Very fine to fine grained sandstone	Swaley cross-stratification with a few cm spacing between stratification surfaces. Varying wave length.	Proximal tempestite deposits from episodes of high oscillatory currents.
F6	Very fine grained sandstone	Regular undulations in very fine grained sandstone where absence of internal lamina and exposed ripple crests inhibit further classification.	Deposits of relatively low velocity currents, where either the unidirectional or oscillational is the prevailing.
F7	Very fine to fine grained sandstone	Small scale asymmetrical ripples	Deposits of from a current where the unidirectional component (although relatively small) is the prevailing.
F8	Very fine to fine grained sandstone	Small scale symmetrical to combined flow ripples with 2D to 3D ripple crest geometry.	Deposits of oscillational and combined flows of relatively low velocity current velocities.
F9	Very fine to fine grained sandstone	Plane parallel lamination/stratification with approximately 1 cm spacing between lamina.	Hyperpycnal flow deposits
F10	Very fine to medium grained sandstone	Large scale 2D to 3D symmetrical to asymmetrical ripples. Bioturbation and trace fossils of skolithos and ophiomorpha.	Deposits of oscillational/combined flow dunes
F11	Fine to medium grained sandstone	Trough cross-stratification. Bed set with internal lamina terminating against a curved/trough shaped lower set surface.	Deposition from migration of dunes.
F12	Fine to medium grained sandstone	Tabular cross stratification with predominantly tangential foresets, with some rare examples of nontangential and sigmoidal foresets. Great variation in paleocurrent direction and may be characterized as herringbone cross-stratification at some locations	Deposition from migration of dunes.
F13	Fine to medium grained sandstone	Low-inclined sub-parallel stratification with a variable spacing between strata.	Wave-swash/beach deposits
F14	Very fine to medium grained sandstone	Normal graded sandstone beds with predominantly a massive appearance. Bed thickness of 0,5 to 1,5m.	Minor distributary channel/crevasse channel
F15	Very fine to medium grained sandstone	Normal graded sandstone beds with predominantly a massive appearance. Bed thickness of 3,5 to 4,5m.	Major distributary channel
F16	Shaley coal	Coal with a high content of shale, dull appearance.	Coal

4.2 Facies Associations:

Table 4.2: Facies Associations:

Facies association:	Sub-group:	Lithofacies:	Depositional environment:
FA1	-	F1,F2	Offshore/shelf
FA2	-	F1,F2,F3,F4	Offshore/transition
FA3:	FA3 A: FA3 B:	F4, F5 (F7),F8,F9	Lower shoreface
FA4:	-	F5,(F7),F8,F9,F10,F11	Middle shoreface
FA5:	-	F5,(F7),(F8),(F9),F10,F11	Upper shoreface
FA6:	-	F13	Foreshore
FA7:	FA7 A: FA7 B: FA7 C:	F1,F2,F7,F8,F3,F6 F7,F6,F16 F14,F15	Continental

4.2.1 FA1: Offshore/shelf

The section stretching from the top of the Hollendardalen Formation to the first occurrence of sandstone of the Battfjellet Formation consists of shales and mudstones of the Frysjaodden Formation, and makes up the lowermost facies association of the studied section. The measured thickness of the formation in the study area generally exceeds 300m. The facies association is mostly covered by scree, thus the description is based on sparse outcrops and weathered debris of the scree.

Observations:

The facies association consists mainly of light gray to dark gray/purplish laminated silty claystones and clayey siltstones (F1), but also contains interbedded mudstones containing grains varying in size from clay to very fine grained sandstone (F2). As observed from the scree cover, the proportion of silt- and sand grains relative to clay increases upwards in the facies association. Outcrops in the uppermost reaches, towards the overlying offshore/transition facies association (FA2), often have heterolithic appearance with alternations of F1 and F2 on a cm-scale. The mudstone beds with a high content of sand grains have no visible current influenced depositional structures, nor do they have erosive based bedding surfaces. Well rounded phosphate nodules with a diameter of a few centimeters are present in the weathered debris. At an interval between approximately 340-360 meters above sea level, distinctive horizons stand out in the northeast facing slope of Sandsteinsfjellet (*Figure 3.1*). The deposits along these horizons crops out at some locations,

and reveals a heterolithic appearance of alternating shales (F1) and mudstones (F2) of an overall coarser nature than that of the shale in the over- and underlying scree. These horizons are located approximately 150 meters below the outcrops of Battfjellet Formation, and are traceable from the northeastern ridge on Sandsteinsfjellet, to the northern ridge on Mefjellet. There is a coarsening upwards trend within these distinct intervals as the proportion of silt and sand is higher towards the top.

Interpretation:

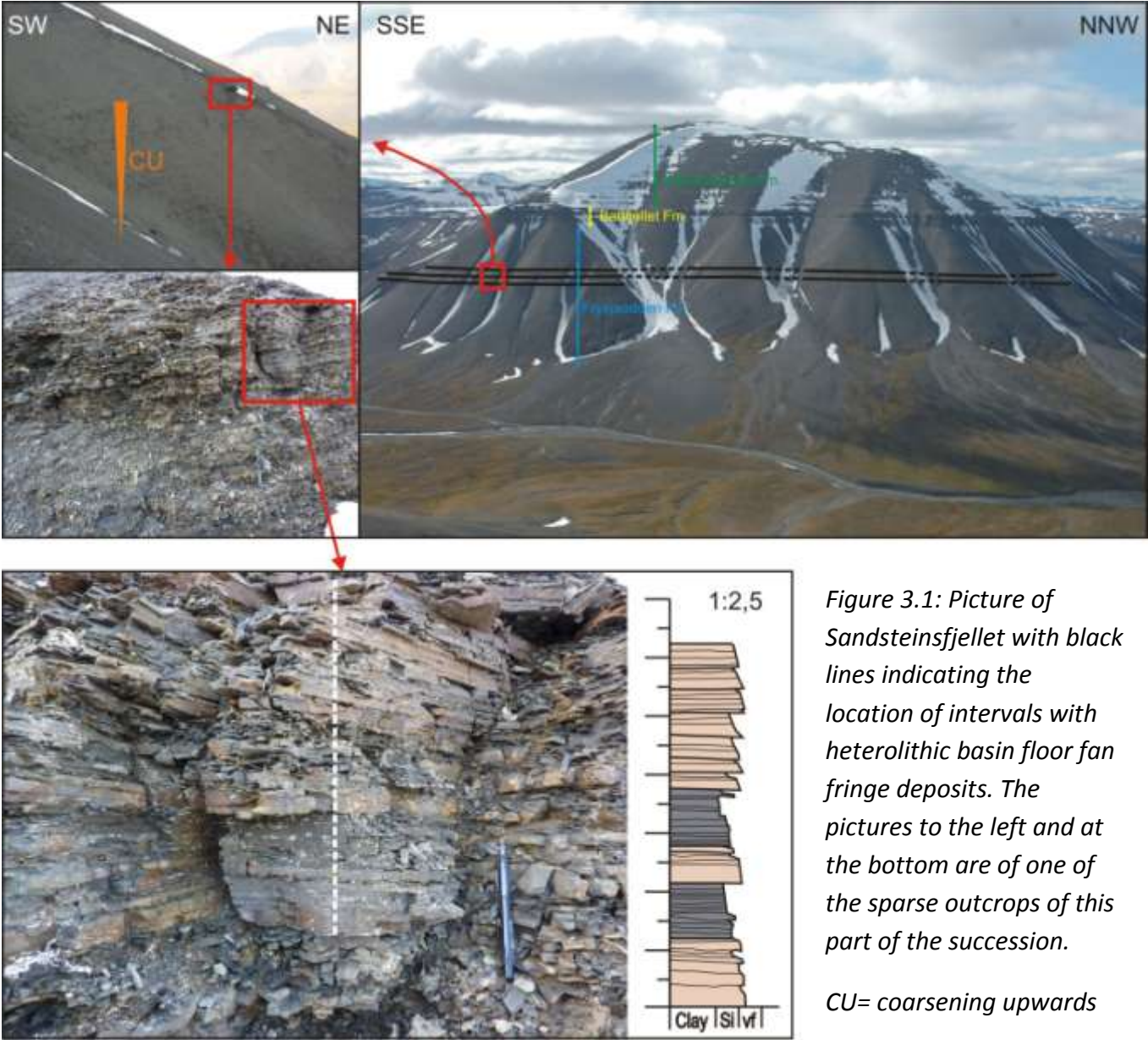


Figure 3.1: Picture of Sandsteinsfjellet with black lines indicating the location of intervals with heterolithic basin floor fan fringe deposits. The pictures to the left and at the bottom are of one of the sparse outcrops of this part of the succession.

CU= coarsening upwards

It is suggested that this facies was deposited from suspension in a tranquil environment below storm weather wave base. This interpretation is based on the fine grained nature of the sediments and the absence of erosional bedding surfaces and absence of depositional structures reflecting oscillatory and combined flow current movement that would be expected in an environment subject to storm processes. As clay fragments are more easily kept in suspension than silt fragments, the higher silt content towards the top of the facies association reflect suspension in shallower waters. The sand prone mudstones in the proximal reaches of the facies association may represent events of increased seaward transport, and are interpreted to be distal low density hyperpycnal flow deposits (see further discussion below).

The coarser grained horizons observed approximately 150m under the shoreface sandstones of Battfjellet Formation in the southwestern part of the study area represents deposition from a higher energy regime than the surrounding shale. By studies carried out on Semmelryggen, approximately 5 km southwest of the northeastern slope of Sandsteinsfjellet, Plink-Björklund et al. (2001) observed a series clinothems (their clinothem complex 5) with a progradational and retrogradation stacking patterns, delivering sand to the basin floor. The lower slope and basin floor deposits observed in these studies consisted of sandstones from “sheet like turbidites” pinching out on the basin floor over a distance of 5km (Plink-Björklund et al., 2001). The coarser grained interval in the Frysjaodden Formation in the present study is interpreted to be basin floor fan fringe deposits (distal sheet turbidite deposits) of this clinothem complex. The heterolithic deposits on Sandsteinsfjellet of the present study has a position corresponding to an outer rim position of the clinothem complex on Semmelryggen (*Figure 3.2*), as it is positioned at a distance of approximately 5km, the same as the observed pinch-out distance of the clinothem complex in discussion (Plink-Björklund et al., 2001). Similar fine grained heterolithic facies were observed by Plink-Björklund and Steel (2003) in a distal position from the classical sand dominated basin floor fan deposits.

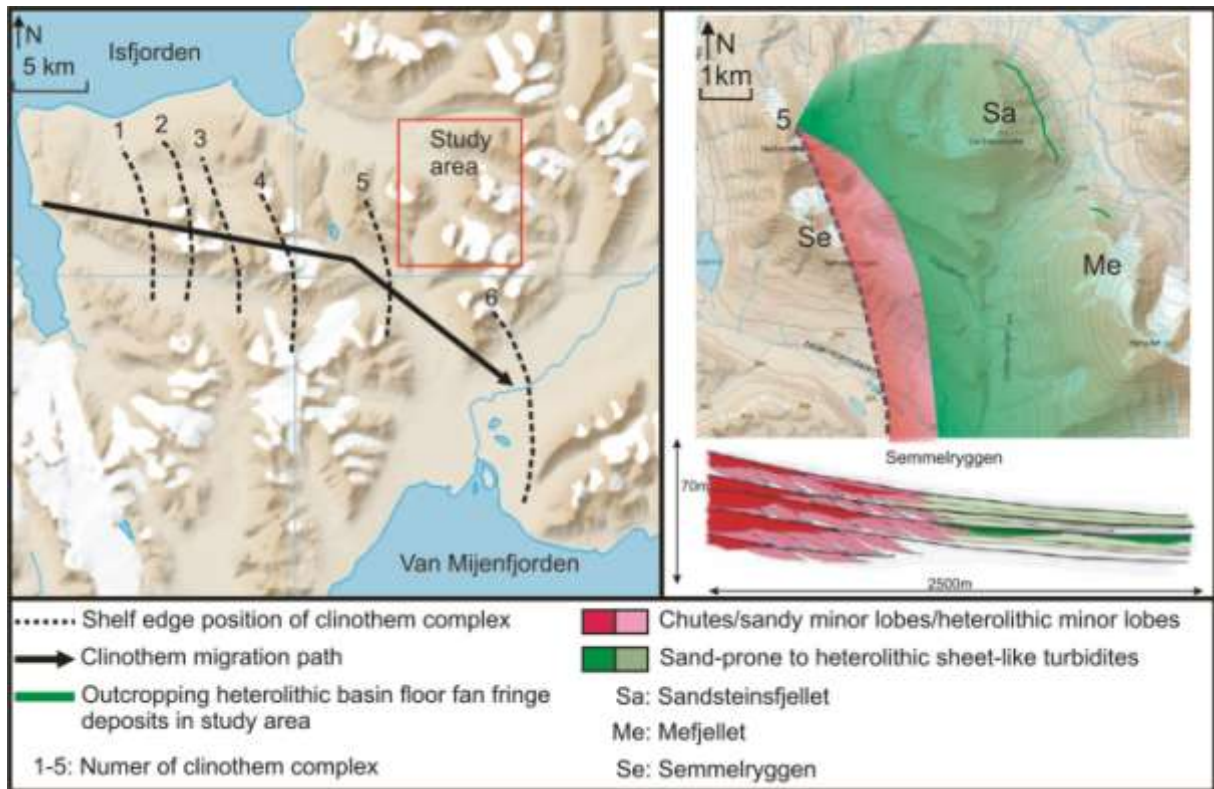


Figure 3.2: The picture to the left is an overview map showing the clinothem complexes described in (Plink-Björklund et al., 2001). The picture to the right shows the possible lateral extent of clinothem complex 5 on Semmelryggen, and indicates the position of the described heterolithic section on Sandsteinsfjellet and Mefjellet.

4.2.2 FA2: Offshore/transition

Observations:

FA2 consists of fine grained sediments varying in grain size from clay to silt, and with interbedded layers of very fine and fine grained sandstone (Figure 3.3 D; E). The facies association is generally confined to the lowermost parasequences of the individual logged sections and represents the transition from the offshore shales of the Frysjaodden Formation to the sandstones of the Battfjellet Formation. The first occurrence of a sandstone bed, commonly containing hummocky cross stratification, marks the lower boundary of the facies association. The registered thickness of the facies association varies from a few meters to approximately 15 meters. However, there is an uncertainty both in identifying the base of the facies association and its thickness as the base of the facies association may be covered in scree. The facies association constitutes a coarsening upwards sequence as the proportion of sandstone beds increases upwards relative to the fine grained

sediments. The individual sandstone beds of this facies have a thickness ranging from approximately 10 to 40cm, with an average thickness around 25cm.

The sandstones are light gray, texturally immature, and consist of quartz grains and lithic fragments. There is little variation in the textural characteristics of the sandstones laterally, nor are there major differences between the different facies. This has also been observed by Helland-Hansen (2010) in nearby studies of the same formation. By the use of petrographic thin-section analysis and X-ray diffraction identification and quantification, Helland-Hansen (2010) classified the sandstones as litharenites according to Folks (1974) classification scheme, and as lithic greywackes according to Dott's (1964) classification scheme, when taking the fine grained matrix into account. As there are little compositional differences, and the same mineralogical classification can be applied to the other facies associations, the mineralogy of the other facies associations will not be further discussed.

The most prominent depositional structure of this facies association is hummocky cross-stratification (HCS) (F4). The thickness of sections containing HCS of this facies association range from approximately 10cm to a few meters; thick layers are more common in the upper reaches of the facies association where several beds of HCS are amalgamated. The spacing between lamina is typically 1 cm, but may be as much as 5cm as it varies within and between HCS beds. The lamina have a convex up shape, with overlying on-lapping low angle lamina. The hummocky cross-stratification structures are isotropic in three dimensions, giving no evidence of a decisive unidirectional current movement. Some HCS beds are normal graded, grading from very fine to fine grained sandstone at the base, to very fine grained sandstone at the top. Symmetrical small ripples superimposed on the HCS beds are common. These symmetrical ripples have straight to slightly sinuous crests with a predominance of north/south orientation (Chapter 5).

At some locations, heterolithic intervals of alternating very fine grained sandstone and fine grained (silty and muddy) sediments with bed thicknesses in the range of 1-7cm occur in this facies association (*Figure 3.3 C*). The thin sandstone beds predominantly consist of both combined flow and symmetrical small ripples. The sandstone beds locally exhibit soft sediment deformational structures.

In general, soft sediment deformational structures and load cast structures (F3) are common in this facies association. These structures represent different degrees of deformation influencing both sandstones and fine grained sediments. The size and shape of these structures varies with varying sand to mud ratio, and varying degree of deformation. A low proportion of sandstone typically forms 5-10 cm big ball and pillow structures, with ellipsoid or spherical shapes, enclosed in fine grained sediments in the upper part of a mud layer. A higher proportion of sandstone results in connected and bigger ball and pillow structures, with a diameter up to 2 meters, where the internal stratification, although deformed, is preserved. The shape of these big ball and pillow structures are typically half ellipsoid, where the top of the structure is truncated by an overlying sandstone bed (*Figure 3.3 A*). The sandstone in these deformational structures has, as with the remainder of the sandstones in this facies, a grain size of very fine and fine sand. These deformational structures have a higher concentration in the lower part of the facies association.

The fine grained sediments (F1 and F2) of this facies association are mostly covered by scree, but may crop out where the interval between sandstone layers is thin. Dark gray/purplish clayey siltstone with flaky, irregular laminations on a mm-scale is the most common lithology of the fine grained sediments in this facies association, but reddish weathering siderite-mud layers, and lighter gray silty claystone layers also occur. Carbonaceous plant fragments are common in this facies association.

Bioturbation is rare in this facies association. Examples of trace fossils of *Helminthopsis* have been observed at some of the HCS bedding planes (*Figure 3.3*).

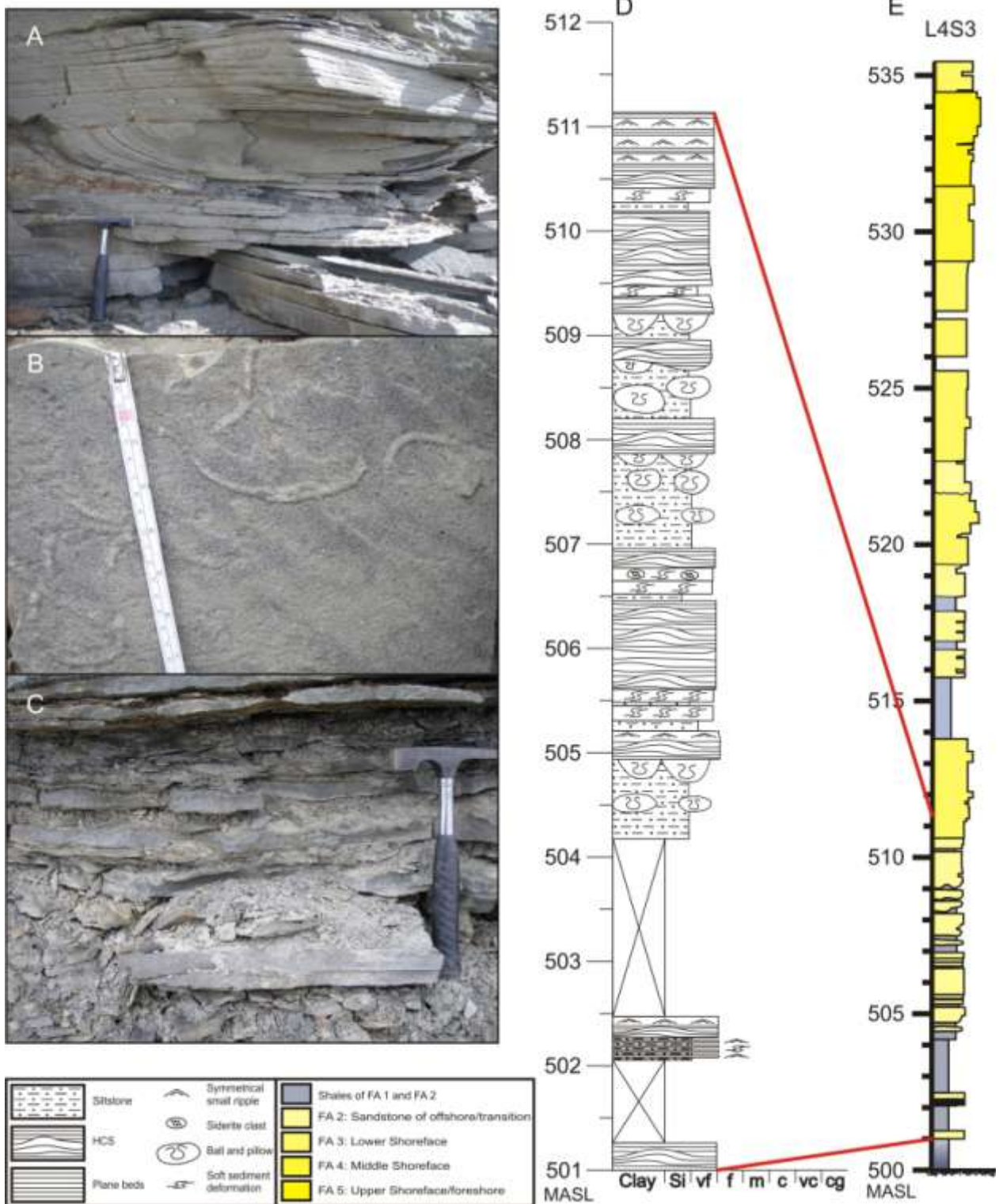


Figure 3.3:

A: Truncated ball and pillow structure with hummocky cross stratified very fine grained sandstone superimposed (L1R1 on Ringdalsfjellet).

B: Horizontal burrows of *Helminthopsis* at the bedding plane of a HCS-bed (L12T3 on Tillbergsfjellet)

C: Heterolithic alternation of symmetrical rippled very fine grained sandstone and siltstone (L18R4 on Ringdalsfjellet).

D: Example of a logged section of FA2: Offshore/transition from L4S3 (Sandsteinsfjellet)

E: L4S3 with different colours for the different facies associations. Red lines highlights the section of the log presented in Figure 3.3D

Interpretation:

The interbedding of fine grained sediments (silt and mudstone) and sandstone beds indicate variations in depositional energy for the sediments. The fine grained sediments are believed to be low-energetic deposits below fair-weather wave base, whereas the HCS beds are believed to be high energetic storm generated tempestites. The sediment source for the storm deposits are believed to be eroded material from shallow shoreface and foreshore areas. This is in concordance with the beach-cycle model (Reading, 1996; Sonu & Van Beek, 1971), which states that there is an aggradation of shoreface and foreshore deposits during fair weather conditions, and erosion, with resulting seaward transport of sediment, during storms.

Hummocky cross stratified structures are believed to have developed mainly under large orbital oscillatory waves, with the symmetrical small ripples forming in the waning stages of the storm. The triggering mechanism for the ball and pillow structures is believed to be the rapid deposition of sand, over poorly consolidated mud during storms. This is evident in the case where truncated ball and pillow structures are overlain by fine grained hummocky cross-stratified sandstones containing rip-up mud clasts.

The assumption that the source of the sediment of the HCS beds is eroded material from more proximal shoreface areas implies a unidirectional paleocurrent component in a paleoseaward direction. However, the effect of a unidirectional current influence on these deposits is hard to deduce; a unidirectional signature of the beds is negligible as the structures appear to be isotropic in three dimensions. The case of a strong unidirectional influence on fairly isotropic HCS and SCS deposits have been proposed in other field based publications (Nøttvedt and Kreisa, 1987; Allen and Underhill, 1989). Recent laboratory studies have contributed to new knowledge on the effect of combinations of oscillatory (U_o) and unidirectional (U_u) current movements, and its resulting depositional structures under different current regimes (Dumas et al. 2004; Dumas and Arnott, 2006; Lacy et al., 2007; Cataño-Lopera et al., 2009; Cummings et al., 2009; Pedocchi and Garcia, 2009). Dumas and Arnott (2006) proposed that isotropic HCS-structures in very fine sand are a result of U_o -values higher than 50cm/s and U_u -values lower than 5cm/s. Despite the fact that synthetic aggradation were created by stacking of "sidewall bed profiles" in the wave tunnel experiments of Dumas and Arnott (2006), one might question if the full effect of the rapid

sediment influx during the deposition of these structures can be accounted for in enclosed laboratory experiments. Even though the unidirectional component might be higher than 5cm/s, a combined flow regime with the oscillatory component being prevailing is proposed for the studied deposits. This interpretation is further emphasized by the dominating symmetrical signature on the small scale ripples superimposed on the HCS-beds.

An offshore transition zone depositional environment is proposed for the sediments of this facies association. The presence of storm generated sandstone beds gives evidence for deposition above storm wave-base. The deposits of this facies association represents a transition from the offshore deposits of the Frysjaodden Formation to the shallow marine sandstones of the Battfjellet Formation, and although the transition to the overlying lower shoreface facies association is gradational, the boundary is put at the top of the uppermost interlayer of mudstone. Ideally, the offshore transition zone represents the area between storm wave base (SWB) and fair weather wave base (FWWB) (Reading, 1996). However, there are uncertainties in pinpointing the location of the fair weather wave base, as fine grained sediments may be deposited above FWWB, and thick amalgamated HCS-beds may form below (Clifton, 2006).

4.2.3 FA3: Lower shoreface

The main features of the facies association are beds of very fine to fine grained sandstone with amalgamated hummocky and swaley cross-stratification (F4 and F5), and beds with alternating planar parallel laminations (F9) and small scale symmetrical ripples (F8). Although these facies may interfinger throughout the facies association, the latter dominates the lower reaches, while the former dominates the upper reaches. On this basis, and because of variations in facies occurrence between logs, the facies association is subdivided into FA3-A: *Amalgamated hummocky and swaley cross-stratification* and FA3-B: *Alternations of plane parallel laminations and symmetrical small ripples*. The thickness of the facies association varies from a few meters to some rare examples up to 10 meters. The thickness distribution of the two sub-groups of the facies association varies, but FA3-B typically constitutes the thickest portion.

FA3-A: Amalgamated hummocky and swaley cross-stratification:

Observations:

FA3-A consists of stacked beds of very fine to fine grained sandstone with amalgamated HCS and SCS, similar to those described in FA2 (*Figure 3.4*). As opposed to the underlying facies association, the amalgamated HCS beds of FA3-A are not separated by mudstones. Another distinct feature is the appearance of SCS. These are concave up shaped sets of laminated very fine to fine grained sandstone with low angle truncational surfaces. The SCS beds of this facies association are genetically linked to the HCS beds, and have similar amplitudes and wavelengths.



Figure 3.4:

Hummocky cross stratification beds of FA3-A from L19R5 at Ringdalsfjellet.

Symmetrical small ripples superimposed on the HCS beds are not common for this facies association because of the amalgamated stacking of the beds. If present, the ripples are often truncated by overlying hummocky cross stratified beds. Carbonaceous plant debris and siderite mud clasts are common in the strata of the HCS beds in this facies association as well.

Interpretation:

The deposits of this formation are interpreted to be lower shoreface deposits. FA3-A is interpreted to be shoreface storm deposits above fair weather wave base. This is based on the absence of mudstone and presence of swaley cross-stratification. Swaley cross-stratification is commonly regarded as a shallower equivalent of hummocky cross-stratification, characteristic of shoreface storm deposits (Reading, 1996). The source of the

sandstone of the storm deposits are believed to be eroded material from shallower shoreface and foreshore areas. Since FA3-A consists of amalgamated storm deposits without structures indicating fair weather conditions, it is reasonable to assume a high frequency of storms and a high sedimentation rate. This assumption is further emphasized by the relatively low degree of bioturbation; a high degree of bioturbation would be expected if the storm deposits were “undisturbed” on the seabed over a considerable time period.

FA3-B: Alternations of plane parallel lamination and symmetrical small ripples:

There are some uncertainties when it comes to the interpretation of the active processes during the deposition of the bed sets of alternating plane parallel lamination (F9) and symmetrical small ripples (F8) in the literature. For this reason, and the possible implications of the active depositional setting (discussed below), a thorough discussion of this facies association is presented below.

Observations:

Typically, there is no significant grain size difference between the plane parallel lamination and symmetrical small ripple sets; they both appear in very fine to fine grained sandstone (*Figure 3.5 B*). However, at some locations the plane parallel laminated beds are normal graded, grading from fine grained sandstone at the base to silty sandstone at the top. Where grading of the beds is observed, the spacing between the lamina decreases upwards in the bed. Although the visible spacing between the lamina of the beds characterized as F9: *Plane parallel lamination* most commonly is around 1cm, the beds locally have a massive appearance of up to 10cm thick intervals, and locally have lamination on a mm-scale (*Figure 3.7*). Beds of symmetrical small ripples typically have a thickness varying from 2-20 cm, with an average around 6 cm. Beds of plane parallel laminations have a more variable thickness, they form the thickest sections of the two, ranging from 3-30 cm, and averaging around 12cm. The thickness of the plane parallel lamination beds have a tendency to increase upwards in the succession (*Figure 3.5 D*). The symmetrical small ripples are often truncated by the overlying bed of planar parallel lamination; hence preserved ripple crests are uncommon. Of the symmetrical ripple crests exposed, straight to sinuous geometries as well as disconnected 3D crests were observed. While the former two were observed in FA3-A as well, the latter was not. A weak degree of bioturbation including *Skolithos* and *Ophiomorpha*

trace fossils can be found at some locations within FA3-B, most typically within the rippled sections. Isolated large scaled symmetrical ripples are present in the upper reaches of FA3-B at some locations. At the base of the sub-facies association (at the transition from the underlying FA3-A), interbedding of hummocky and swaley cross-stratified sandstone is common. The thickness of FA3-B in the different logged outcrops in the study area is highly variable; in some logs FA3-B is absent, while the thickness in a single parasequence may be as much as 5-6m in other localities (Chapter 6). Sometimes poorly developed striations can be observed at the base of the bedding planes of the plane parallel laminated beds.

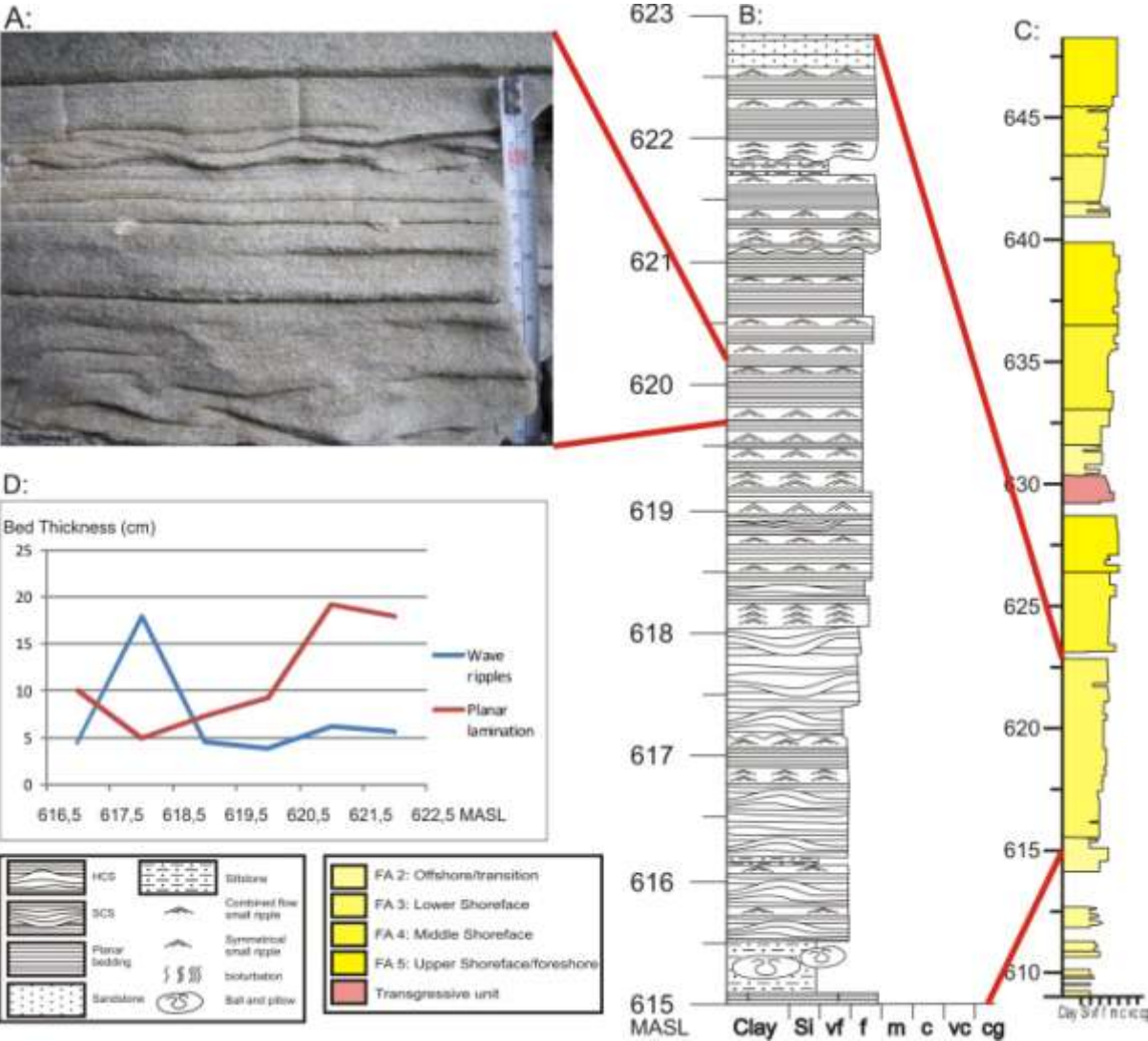


Figure 3.5:
A: Alternating plane parallel laminated beds and symmetrical small ripples from L1R1.
B: Example of FA3 from L1R1. Deposits of FA3-A covers the section from 615,5 to 618 MASL, while the rest of log contains deposits of FA3-B.
C: Log L1R1 with the different facies associations presented with different colours.
D: Graph showing the thickness of the alternating beds of FA3-B (y-axis) with height in the log (x-axis). Note the increase in thickness of the plane parallel laminate beds (n=2x18).

Interpretation:

Wave period, grain size, and unidirectional/oscillatory current velocities are controlling factors in terms of the signature of the depositional structures of the sands in the shoreface (Dumas et al. 2004; Dumas and Arnott 2006; Hill et al. 2003; Cummings et al. 2009). Stability field diagrams for different depositional structures based on these criteria have been made by Myrow and Southard (1991), Dumas et al. (2004) and Cummings et al. (2009). Based on wave tunnel experiments, Dumas et al. (2004) calculated the stability field of symmetrical small ripples in very fine grained sand (0,14mm). For wave periods of 8,0s, this stability field is in a current regime of that over the sediment movement threshold, and below that of $U_o \sim 40\text{cm/s}$ and $U_u \sim 10\text{cm/s}$ (U_o = oscillation current velocity, U_u = unidirectional current velocity)). From the same studies, the stability field of planar beds in very fine grained sandstone is in a current regime of $U_o > 85\text{cm/s}$ for purely oscillatory currents, but may also form at lower U_o with higher U_u (for $U_u > 20\text{cm/s}$, plane beds may form at U_o as low as 60cm/s) (Dumas et al, 2004). This imply that small ripples are generated from the sediment movement threshold up to $U_o = 40\text{cm/s}$, whereas plane parallel lamination develop at current velocities between 85 and 60 cm/s, depending on the unidirectional current component (*Figure 3.6*). The values presented in these stability field diagrams are derived from laboratory studies and should thus be applied with some caution. However, they do give a rough perception of the active current velocities during deposition of the different structures.

A striking feature of FA3-B is the absence of an intermediate step of cross stratification/HCS (large scale ripples following the nomenclature of Dumas et al., 2004), as would be expected for a gradually waning flow from upper flow plane beds to small symmetrical ripples. The terminology used for oscillation and combined flow generated structures in the stability field diagrams of Dumas et al. (2004)(*Figure 3.6*) follows the definition by Hanes et al. (2001) where the term “ripple” is applied for all topographic bed forms. The term small ripples is applied to structures with a wavelength below 30cm, while the term large ripples is applied to structures with a wavelength above 30cm. The corresponding terminology following more established definitions (Campbell, 1967; McKee and Weir, 1953) is ripple laminae for wavelengths above one feet (30,48cm), and cross-stratification for bed forms with higher wavelengths.

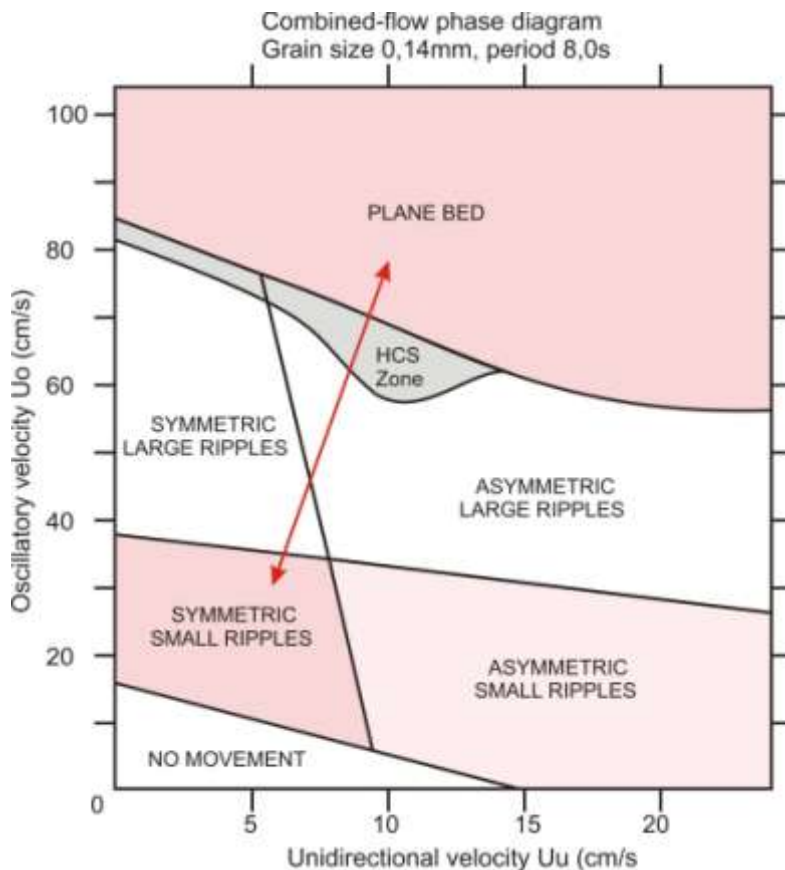


Figure 3.6: Stability field diagram for combined flow depositional structures of very fine grained sand at a wave period of 8,0s (modified from Dumas et al., 2004). The positions of the respective beds of FA3-B (plane bed and small ripples) are highlighted in pink.

Similar couplets of plane beds and symmetrical small ripples have been observed in other wave dominated shoreface deposits (Roep et al. 1979, Hill et al. 2003). Hill et al. (2003) measured the active current velocities (U_o and U_u) at a 10 m depth over the shoreface of a present day wave dominated delta (the Grande-rivière-de-la-Baleine Delta) during fair weather-, moderate storm- and major storm-conditions. The measured fair weather current velocities of these studies plot within the stability field of small scale ripples (c.f. Dumas et al., 2004). The current velocities of moderate storms gave readings within the stability field of HCS/large scale ripples, but also reached the stability field of plane beds, up to 20cm/s for the unidirectional currents (U_u) and 60cm/s for oscillatory currents (U_o). For major storms, the highest current velocity values was that of $U_u \sim 40$ cm/s and $U_o > 100$ cm/s, well within the stability field of plane beds. Hill et al. (2003) argued that the lack of preserved intermediate deposits between that of small scale ripples and plane beds is caused by a too rapid transition of current velocities between the two stability fields for any intermediate deposits to reach depositional equilibration. As such, the presence of HCS/SCS in more distal shoreface deposits could be explained by assuming that the waning flow spends more time within the stability field of HCS, allowing its deposition. For such a setting, the plane beds

would be contemporaneous proximal equivalents to the distal tempestites consisting of HCS and SCS. An interpretation of the plane beds as more proximal storm deposits than that of the HCS beds provokes problems, as the vertical thickness of the plane beds in general are less than that of the HCS-beds. In addition the HCS beds show more profound erosion and truncations than that of the plane beds, which have planar lower bedding surfaces and less profound truncations.

Since the transition between the different deposits of FA3-B cannot be explained with fair weather alternations or fair weather-storm alternations (c.f. Dumas et al., 2004), and since an interpretation of a high energetic storm origin for the plane beds does not correlate well with the more distal storm deposits, alternative explanations than those limited to the stability field diagrams should be addressed.

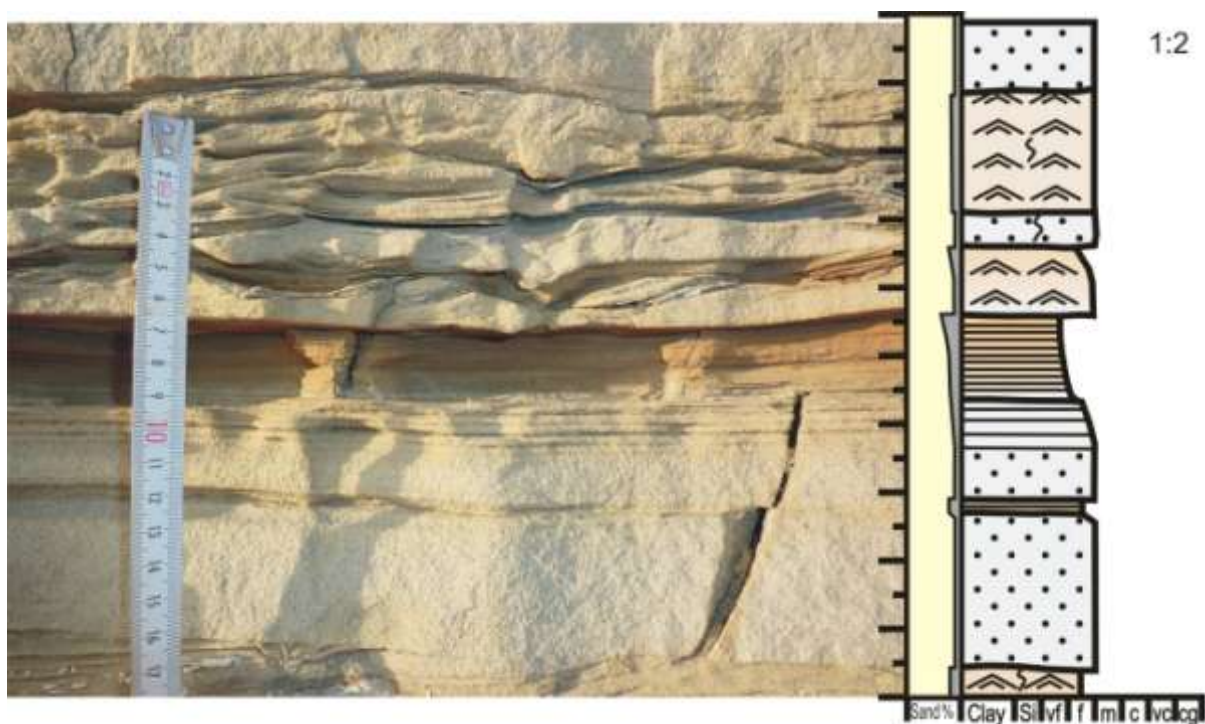


Figure 3.7: Example of a normal graded bed of the parallel laminated sandstone, grading from fine grained sandstone at the base, to silty sandstone at the top. The spacing between the lamina gets progressively thinner upwards in the bed, from a massive appearance at the base to lamination on a mm-scale at the top. The features of these beds might resemble that of Bouma T_{ab} and T_{abc} turbidite deposits.

Similar beds, consisting of alternating massive to parallel laminated beds and rippled beds, were observed in delta front deposits by Olariu et al. (2010) on studies carried out on the Panther Tongue Delta, Book Cliffs. Their interpretation of these beds was that of high energy and high concentration river fed gravity (hyperpycnal) underflows with variable flow intensity. The main arguments for the interpretation of a hyperpycnal origin of the beds provided by Olariu et al. (2010), were the similarity to Bouma-division T_{abc}, the waxing and waning type of the flow, that supposedly are more characteristic of hyperpycnal flows (cf. Mulder et al., 2003), and the concordance of river induced hyperpycnites with the established regional geomorphological models.

Traditionally, the formation of hyperpycnal flows were believed to be uncommon in marine settings, but studies over the last decade have revealed that many marine deltas can accommodate hyperpycnal conditions (Bhattacharya and Maceachern, 2009 and references therein). Hyperpycnal flow deposits have been recognized in Battfjellet Formation in the western reaches of the basin where well developed clinothems are present (Plink-Björklund et al., 2001, Mellere et al., 2002, Plink-Björklund and Steel, 2004 and Peter and Steel, 2006). These studies have focused on hyperpycnal deposits on the slope, and the role of hyperpycnal flow generated channels as conduits for turbidite currents to the basin floor. Since the Central Tertiary Basin of Spitsbergen was a restricted basin with high fluvial influx it is therefore tentatively suggested that it periodically experienced strongly brackish waters, which may increase the potential for generating hyperpycnal flows.

The delta front slope gradient of the Battfjellet Formation delta system in the area is relatively low. Deltas with a steep gradient ($>0,70^\circ$) have the capacity to generate hyperpycnal flows directly from river channels, whereas low angle systems ($<0,3^\circ$) requires additional turbulence caused either by tidal or wave processes (Bhattacharya and Maceachern, 2009). The predominance of wave generated structures in the delta front deposits of Battfjellet Formation, and the symmetrical signature on the ripples superimposed on the parallel laminated bed, may suggest that storm processes play an important role in the generation of the hyperpycnal flows. Oscillational current movement during storms may add to the turbulence at the seabed and thus contribute to the motion of the hyperpycnal flows (c.f. Bhattacharya and Maceachern, 2009). Depending on the duration of high density fluvial discharge input from the river, hyperpycnal flows can be

sustained over a low gradient slope for a long period, the traveling distance for a hyperpycnal flow is in large part dependent on the duration of the flood (Zavala et al., 2006). The deposits of FA3-B are thin and generally confined to the middle- and lower shoreface area, and may thus represent that of relatively short lived flood events. The slope gradient difference from the shoreface to the offshore/transition might further delimit the down-dip transport of the hyperpycnal flows.

The thickening of the parallel laminated beds upwards in the succession implies that the bed has its greatest thickness in a proximal position and pinches out distally. In contrast, no profound thickness variations were found for the rippled interval of the facies association (*Figure 3.5*). The expected fair weather current regime of the lower shoreface depositional environment for the Battfjellet Formation is tentatively suggested to be roughly the same as those observed at a 10m water depth at the Grande-rivière-de-la-Baleine Delta by Hill et al. (2003); within the stability field of symmetrical small ripples (c.f. Dumas et al, 2004). The rippled interval may thus represent fair weather aggradation between that of cyclic (annual?) hyperpycnal generating flood events.

The deposits of FA3 B are suggested to represent flood and wave aided low duration hyperpycnal flow deposits. This interpretation is based on the following assumptions:

- The geomorphological setting and depositional environment supports the formation of hyperpycnal flows.
- An explanation of the deposits being formed as a result of wave/storm action is not plausible.
- The deposits show a striking similarity to other deposits interpreted to be by hyperpycnal flows in a delta front depositional environment (c.f. Olariu et al., 2010)

The thickness of FA3-B intervals varies locally along depositional strike internally in a parasequence. It is suggested that the thickness of this facies association reflects the relative distance to a distributary channel system at the delta front (Chapter 7).

4.2.4 FA4: Middle shoreface:

Observations:

This facies association consists of dark gray/brownish sandstone with grain sizes ranging from very fine/fine, to fine grained sand (*Figure 3.9 A; B*). The main depositional structures of the facies association are trough cross-stratification and large scale swaley cross-beds, but small scale symmetrical ripples are also common in the association. The lithofacies making up this facies association are F5-F11.

A prominent feature of this facies association is the presence of isolated or stacked troughs with set length typically in the range of 8-100cm (average around 25cm), and set thickness in the range of 2-8cm (average around 5cm). The troughs have a predominance of symmetrical and sub-parallel internal lamination (*Figure 3.8 A*), but combined flow signatures in the form of foresets terminating at the base of the troughs can be observed locally (*Figure 3.8 B*). The symmetrical nature of the structures makes it hard to deduce a preferred direction of flow for the deposits of this facies association. The bed sets show an amalgamated stacking pattern and the beds are typically bounded by irregular, curved erosional surfaces at the base.

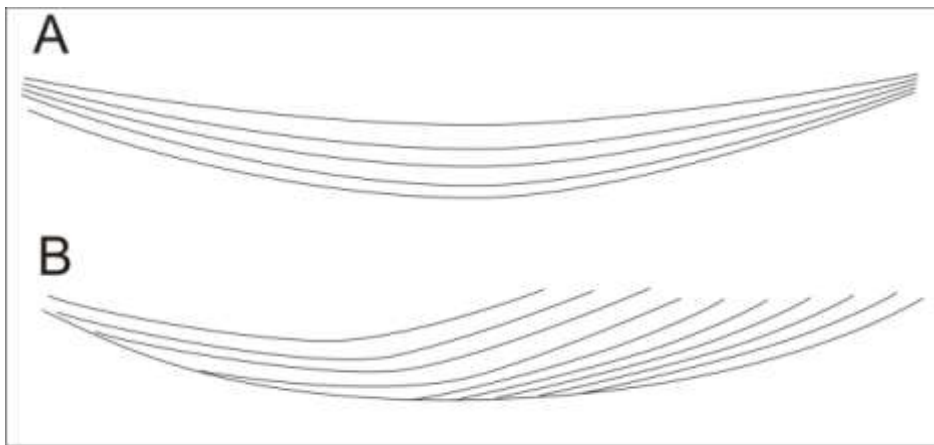


Figure 3.8: Typical trough infill geometry in Facies Association 4 (FA 4).

A: Parallel to sub-parallel infill of the trough.

B: Tangential down-lapping stratification developing into more parallel to sub-parallel stratification laterally. The orientation of the trough axis with respect to the exposed surface is very important with respect to the internal lamination shown. The upper example may represent a section perpendicular to the trough axis, whereas the lower section may be sub-parallel to the trough axis.

Beds with alternating planar parallel lamination and symmetrical ripples are locally present in this facies association. These beds share most of the characteristics of the beds described for FA3-B. However, the grain size of the beds tends to be slightly coarser and the symmetrical ripples tend to have higher amplitude. Symmetrical ripples independent of plane laminated beds are also common within this facies association. The geometry of the exposed ripple crests varies from straight to a disconnected 3D geometry.

The degree of bioturbation within the facies association varies from 0 (no bioturbation) to 5 (intense bioturbation), following the classification scheme of Reineck (1963) and Taylor and Golding (1993). The highest degree of bioturbation is found in beds associated with trough cross stratification. Locally the stratification is completely disturbed as a result of intense bioturbation. *Skolithos* (Figure 3.9 D), *Ophiomorpha* (Figure 3.9 C), *Cylindrichnus*, *Teichichnus* and *Glyphichnus* (figure 3.9 D) trace fossils were recorded in this facies association.

Interpretation:

The larger scale of the symmetrical ripples compared to the underlying facies association, and the disconnected 3D ripple crest geometries testify to deposition from higher velocity oscillation current velocities. Isolated and irregularly developed troughs defined by curved basal erosional surfaces are believed to represent scour and fill structures. The more regular stacked and amalgamated troughs with a well defined sub-parallel lamination are believed to be trough cross-stratification formed as a result of migration of dunes. These deposits are believed to represent an intricate stacking of deposits from direct wave action under fair weather aggradation, migration of dunes from longshore and rip currents, and erosion and fill from periods of higher energy (storm). Based on these criteria, a middle shoreface depositional environment is proposed for this facies association. Similar deposits of the formation elsewhere have been given the same interpretation by Helland-Hansen (2010). Trace fossils of *Skolithos*, *Ophiomorpha* and *Glyphichnus* are all characteristic of shallow marine deposits, but no further subdivision can be based on the presence of these trace fossils as they are not restricted to a middle-shoreface depositional environment.

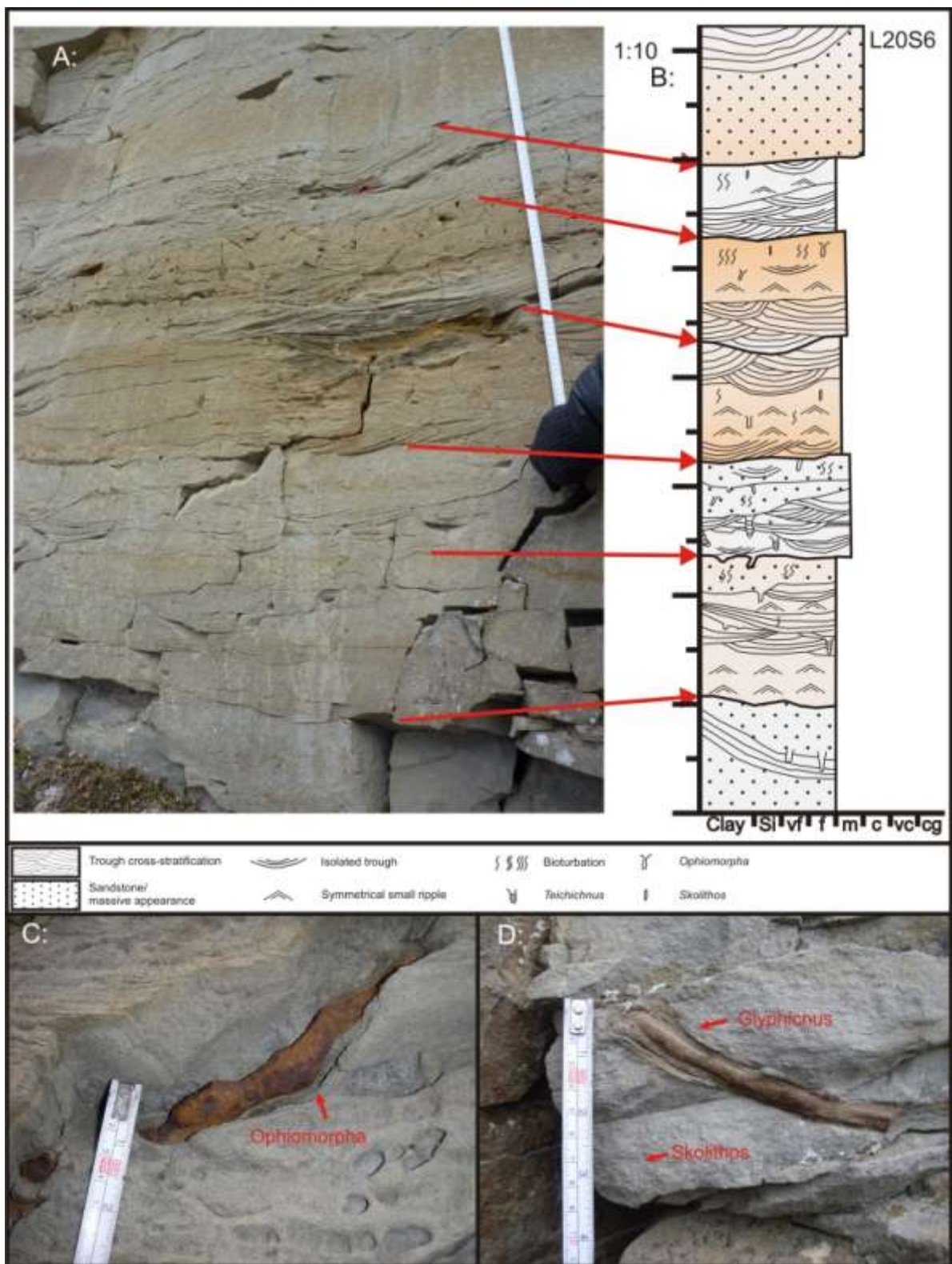


Figure 3.9:
 A: Picture of an outcropping section of middle shoreface deposits at L20S6 (Sandsteinsfjellet).
 B: Lithostratigraphic log of the same section. Scale 1:10
 C: Ophiomorpha trace fossils with pellets along the wall of the burrow at L6T2 (Tillbergsfjellet).
 D: Glyphicnus and Skolithos trace fossils at L6T2 (Tillbergsfjellet).

4.2.5 FA5: Upper shoreface:

Observations:

This facies association consists of fine to medium grained light to dark gray/brownish sandstone with tabular cross-stratification and low angle stratification. The thickness of the facies association varies from 2-3 meters.

The cross strata of this facies association consists predominantly of tangential foresets within sets with sub-parallel boundaries (*Figure 3.12 E*). Such cross sets may be categorized as tabular cross stratification (F12) following McKee and Weirs (1953) identification scheme (see also Boggs, 2006). Although tangential foresets dominates, rare examples of non-tangential and sigmoidal foresets also occur. There is a great variation in the bed thickness of the tabular cross sets. The measured thickness ranges from 4cm to 63 cm, but most lie within the range of 8-25cm. The spacing between visible individual lamina tends to increase with increasing thickness of the tabular cross sets, a spacing between the lamina in the range of 0.5-1cm is common for small scale sets with a thickness less than 5cm, while a spacing of 2-4cm is common for large scale sets with a thickness up to 20cm. There is a great variation in paleocurrent direction for the cross sets of this facies association, both from different outcrops and locally. Locally, co-sets of tabular cross stratification show bidirectional paleocurrent directions, and may be characterized as herringbone cross-stratifications (*Figure 3.10; 3.12 D*). Rare examples of double mud drapes in the foresets of the herringbone cross-stratifications were also observed. A special structure within this facies association that also may be present within the middle shoreface facies association (see below) is gigantic troughs up to 6 meter wide and 1 meter deep (*Figure 3.11*). The troughs consist of fine to medium grained sandstone with internal stratification that is parallel with, or downlapping the curved concave basal surface.

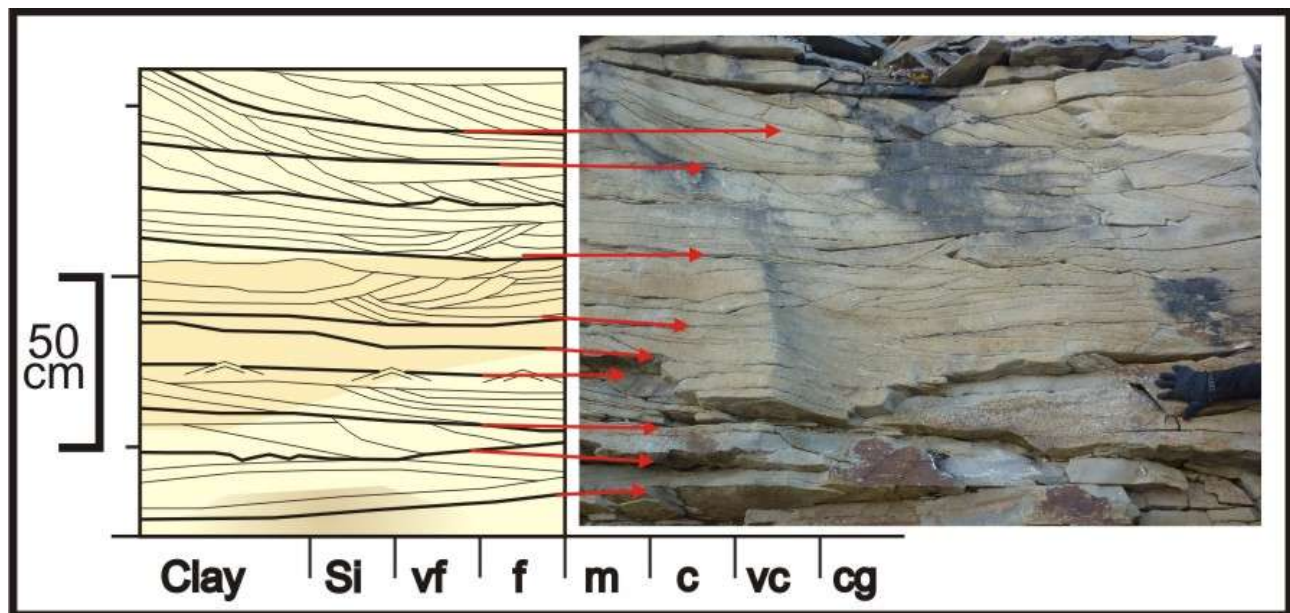


Figure 3.10: Example of bidirectional tabular cross-stratification co-sets from L21R6 on Ringdalsfjellet.

Interpretation:

The sediments of this facies association have, together with the overlying foreshore facies association, a very low degree of bioturbation, and demonstrate the coarsest grain size of the studied succession. The tabular cross sets represent migrating dunes at the seabed. The cross sets show a wide range of paleocurrent directions (Chapter 5). Such a wide range of paleocurrent measurements have been recorded in numerous other studies of similar deposits (Helland-Hansen, 2010; Roux & Elgueta, 1996; Davies, 1978). The dunes forming the cross sets are believed to have been formed as a result of longshore- and possibly rip-currents in a wave dominated upper shoreface depositional environment. This interpretation is in concordance with models for wave dominated clastic shoreline systems where the upper shoreface has been described as the most energetic part of the system where dunes are formed as a result of such processes (Clifton, 2006). The deposits of this facies association are believed to be remnants of upper shoreface fair weather aggradation of a dissipative shoreline. The opposing paleocurrent directions of the herringbone cross stratifications is likely a result of tidal influence, and deposition during ebb and flood generated currents. The tidally influenced deposits are locally restricted, and may be related to processes within or associated with tidal inlets, in areas connecting interdistributary bays with the open sea. The origin and the morphology of the giant troughs (Figure 3.11) are not well understood, and it is uncertain if they represent bed forms of giant migrating dunes or large cut and fill structures. The morphology and the very local occurrences may suggest that

they represent very shallow aggrading channels. Due to great variety of possible channel generating processes in an upper shoreface depositional environment, no further speculation about the origin of the structures will be given here, but they may be related to rip currents, sub-tidal channels, or “chute channels” that could be conduits for hyperpycnal flows.

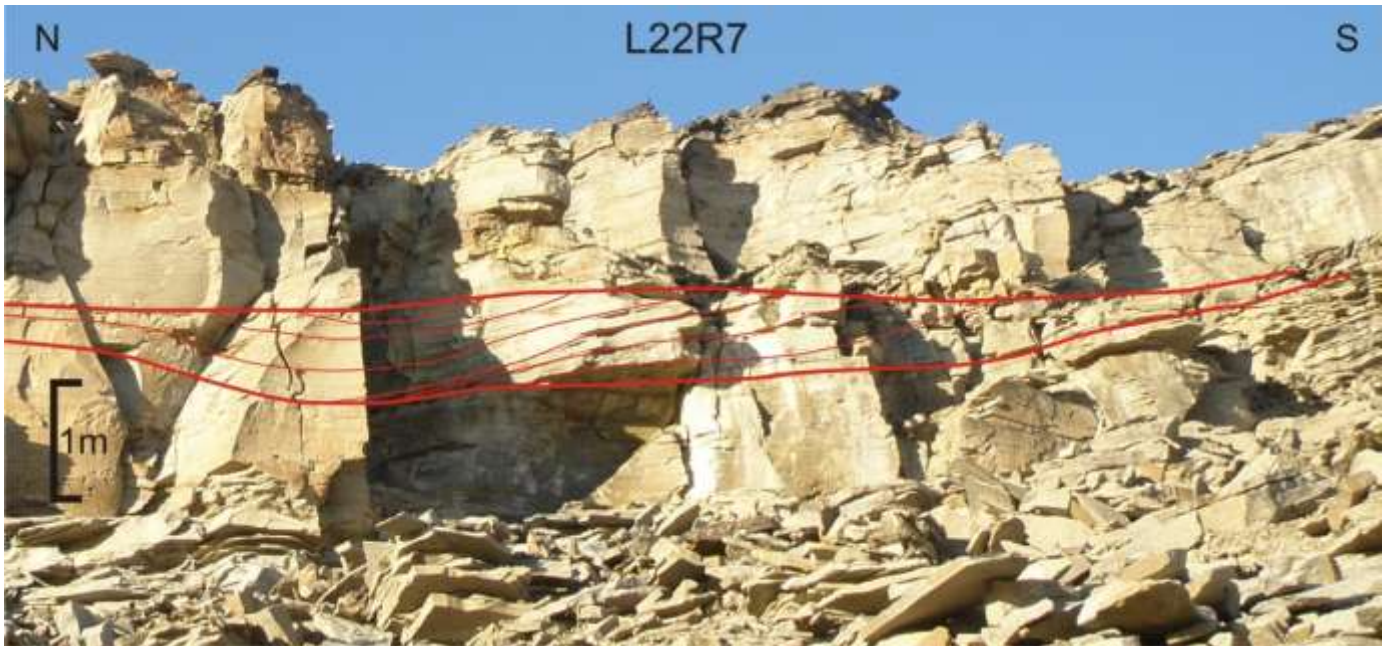


Figure 3.11: Large trough shaped structure on Tillbergsfjellet at L22T7.

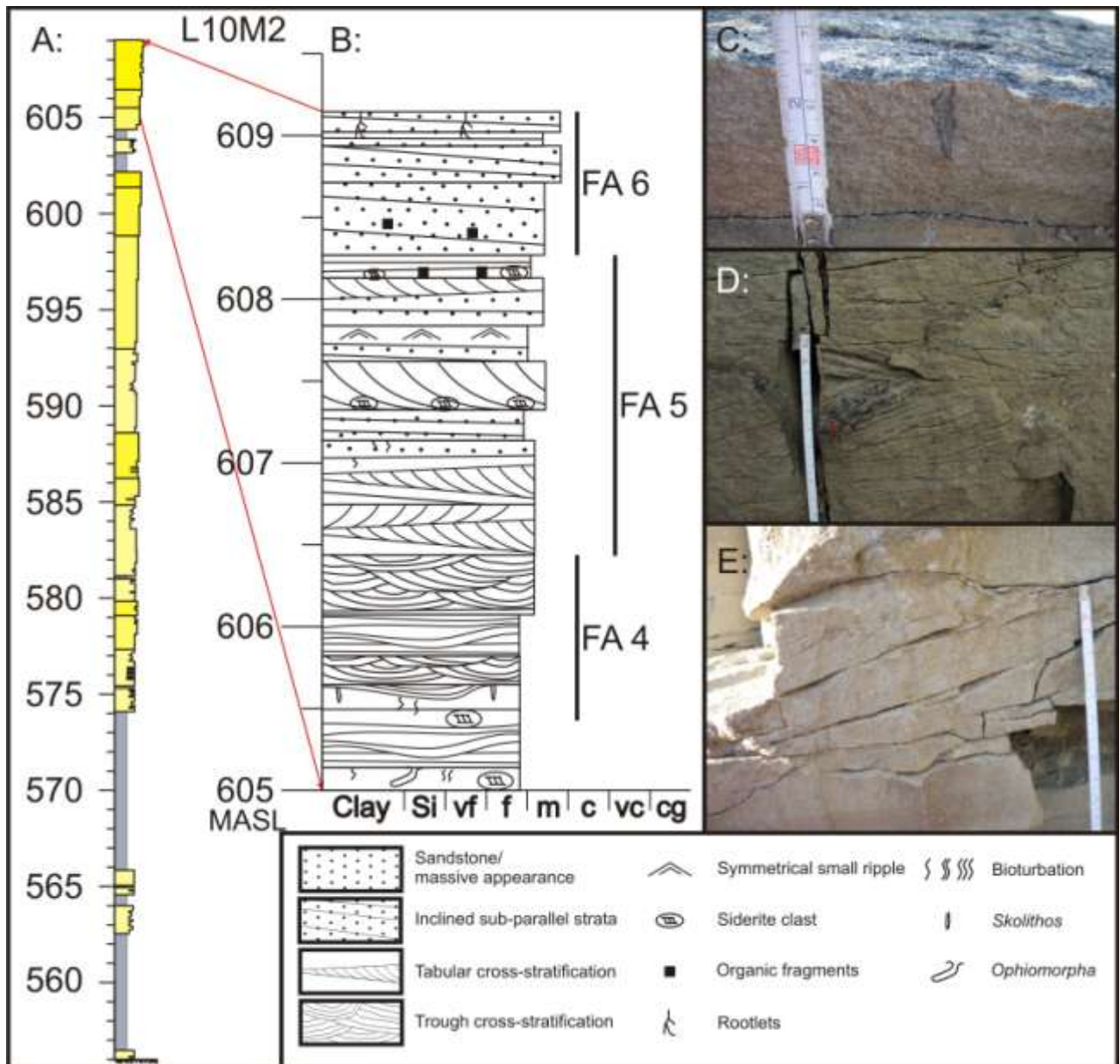


Figure 3.12:

A: L10M2 with different colours indicating different facies associations.

B: Examples of FA5: Upper shoreface and FA6: Foreshore deposits from L10M2.

C: Picture of carbonaceous rootlet protruding down in medium grained sandstone of the FA6 at L5T1 (Tillbergfjellet).

D: Co-sets of tabular cross stratification with opposing paleocurrent directions (Herringbone cross-stratification), L10M2 on Meffjellet.

E: Tabular cross-stratification with tangential foresets (L9M1 on Meffjellet).

4.2.6: FA6: Foreshore

Observations:

The foreshore facies association consists of fine to medium grained sandstone with a gray/brownish colour. The dominating features of this facies association are inclined surfaces (or lamination) forming low angle, and irregular non-parallel stratification (F13) (Figure 3.13). The spacing between the strata is highly variable, ranging from a few centimeters to several decimeters. This facies association is typically located at the top of the exposed cliffs, and is thus strongly exposed for weathering. As a result the sandstone of this facies association often has a massive appearance with exfoliation joints. This facies association has only been observed in the uppermost parasequences for the individual logged sections in the study area. Fossilized plant root fragments with a vertical thickness up to 5 cm can be seen at the top of the rocks of this facies association at some locations (Figure 3.12 C). The registered thickness of the facies association ranges from 0.7 m to approximately 3 m.



Figure 3.13: Low angle stratification of FA6 at L9M1 on Mejjellet.

Interpretation:

The sediments of this facies association are interpreted to be foreshore deposits. The low angle strata are believed to be a result of wave swash and back-wash processes on the beach. This interpretation is enhanced by the presence of plant roots at the top of the facies association indicating partially subaerial exposure. The presence of continental deposits immediately above the deposits of this facies association further strengthens the interpretation of a foreshore depositional environment. The preservation potential for this facies association is low as a consequence of erosion and wave reworking during minor transgressions related to abandonment, probably as a consequence of autocyclic lobe change in an otherwise rapidly subsiding basin (Chapter 7).

4.2.7: FA7: Continental deposits

This facies association comprises the continental deposits of the Aspelintoppen Formation and constitutes the uppermost section of the logs, above that of the shallow marine deposits of Battfjellet Formation. The sediments of this facies association consist of deposits from a lower delta plain environment, and associated sub-environments. The facies association has been observed and logged with variable thickness in ten of the logged sections, but due to sparse outcrops, no continuous sections have been measured through the facies association. The facies association has been subdivided into three sub-groups;

- FA7-A Interdistributary bay,
- FA7-B Subaerial Lower delta plain (interchannel area).
- FA7-C Distributary channel.

The facies association is collectively classified as continental deposits

FA7-A: Interdistributary bay

Observations:

FA7-A consists of silt dominated mudstones to very fine grained sandstone, typically forming upwards coarsening sequences with a thickness usually between 0,5m to 2m. Heterolithic intervals of alternating mudstone and very fine grained sandstone on a cm-scale (thickness of sandstone beds increase towards the top of an individual sequence) are common throughout the sequences. Ripple cross-laminations are the dominating depositional

structures observed in this facies association. The lack of visible internal lamina and ripple crest geometries in most cases inhibits further classification of the ripples, and they are thus termed “undifferentiated ripples” (F6). However, at some locations, both symmetrical small scale ripples (F8), and asymmetric (current) ripples (F7) are recognized in the sandstone beds of the succession. Soft sediment deformation, convolute bedding and minor ball and pillow structures (F3) of a diameter of approximately 5cm are locally observed in this facies association. Fossilized plant fragments are observed in FA7-A, however in less quantities than in FA7-B (see below). Rare burrows also occur, and trace fossils of *Arenicolites* and *Skolithos* were recognized. FA7-A is the dominating facies association in the continental section immediately above the marine deposits of Battfjellet Formation.

Interpretation:

The presence of mudstone at the base of this facies association indicates a protected depositional environment where fine grained sediments were allowed to settle from suspension. The presence of symmetrical ripples gives evidence of wave reworking of the sediments, in an environment probably open to marine water. Asymmetric ripples give evidence of, at least episodic, influence from unidirectional currents, and are likely flood induced overbank deposits. The coarsening upwards trends is believed to represent deposition during progressive higher energies as may take place when a bay is filled with sediments, and gradually become shallower. FA7-A is thus interpreted to be interdistributary bay deposits. Although not diagnostic of the environment, the presence of *Skolithos* and *Arenicolites* are common trace fossils in an interdistributary bay environment, and thus support the interpretation (c.f. Buatois et al., 2005).

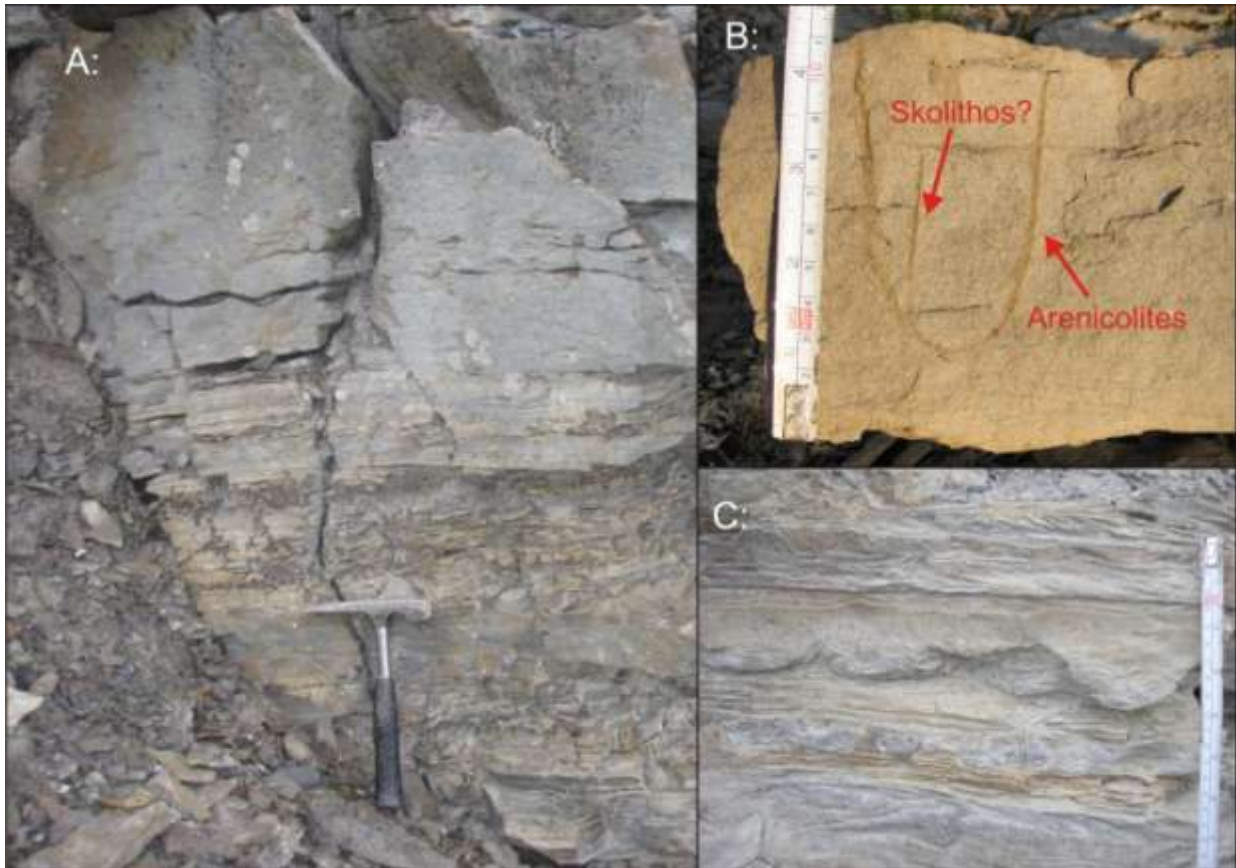


Figure 3.14:

A: Interdistributary bay deposits (FA7-A) showing the typical upwards coarsening trend of these deposits from mudstone to sandstone. Symmetrical small ripples are visible in the sandstone prone upper reaches of the section.

B: Arenicolites and Skolithos trace fossils in interdistributary deposited sandstone at L9M1 on Meffjellet

C: Small scale load casts and asymmetric (current) ripples at L15M4 (Meffjellet)

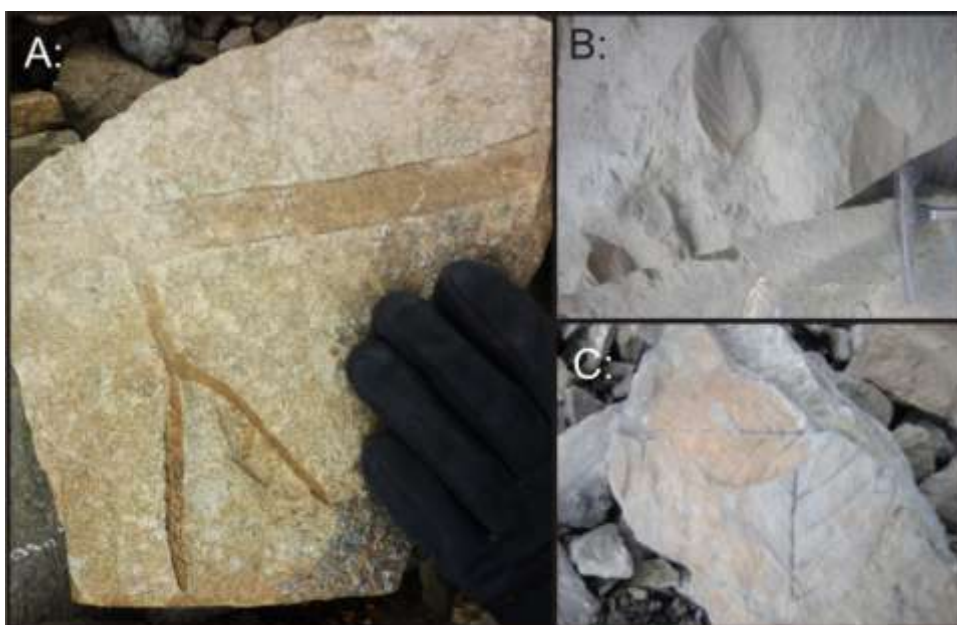


Figure 3.15:

A: Fossilized plant, displaying leaves, a branch and the stalk (near L22T7, Tillbergsfjellet).

B: Fossilized leaf in a fluvial channel (L8R2, Ringdalsfjellet)

C: Leaves in debris near L22T7 (Tillbergsfjellet)

FA7-B: Floodplain

Observations:

FA7-B consists of predominantly of a heterolithic alternation of mudstone and very fine grained sandstone with bed thicknesses typically varying in the range of a few centimeters to a few decimeters. The main depositional structures are undifferentiated ripples (F6), but asymmetric ripples (F7) are recognized locally. Soft sediment deformation and a high abundance of plant fragments, rootlets, and carbonaceous fragments are common in this facies association. Locally, up to 10cm thick coal seams and horizons of coaly shale (F16)(up to 10cm thick)are present. No profound coarsening and fining upwards trends were recorded within this facies association.

Interpretation:

FA7-B is interpreted to be subaerial overbank deposits in a lower delta plain depositional environment. The absence of marine indicators in the form of trace fossils and symmetrical ripples differentiates it from FA7-A. In addition, the content of fossilized plant fragments (*Figure 3.15*) and rootlets is significantly higher in this facies association. The thin sandstone beds with asymmetrical ripples are believed to be overbank levee deposits, with deposition from unidirectional flows dispersed from distributary channels during flood events. The undifferentiated ripples are interpreted to be deposits of the same process, although this is speculative since no evidence of the active current regime during deposition can be deduced from the structures. The grain size and thickness of the beds are believed to roughly reflect the distance from the distributary channel at time of deposition in the sense that thin and fine grained beds are distal levee deposits, while thicker and coarser grained beds represent more proximal levee/crevasse splay deposits.

FA7-C: Distributary channel

Observations:

This facies association consists of upwards fining sandstone successions with grain sizes in the range from very fine to medium. On the basis of the thickness and grain size of these sandstone bodies they can be subdivided into two main groups. The first (FA7-C1), consists of very fine to fine grained sandstone beds with a thickness between 0,5 to 1,5m (F14). The base of these sandstone bodies is erosive, whereas large scale parallel strata are the most

common internal feature. Tabular cross-stratification has been observed in one of the outcrops. FA7-C1 has been observed in 5 of the logged sections.

The second type of sandstone within this facies association (sub-group FA7-C2) consists of 3,5 to 4,5m thick very fine to medium grained sandstone bodies (F15). As with the first group, the dominating internal feature of the sandstone of FA7-C2 is large scale parallel strata above an erosive base. At one location, large scale (one meter thick) tabular cross-stratification with tangential low-angle foresets is observed.

The sandstone bodies of both subgroups have a limited lateral extent. Sparse plant fragments are observed in this facies association.

Artic weathering processes and associated exfoliation make it often difficult to recognize internal sedimentary structures of these sandstones.

Interpretation:

These characteristic upwards fining sandstone bodies with erosive bases and a limited lateral extent, located within a lower delta plain environment have been interpreted as distributary channel deposits. Because of the general lack of visible internal depositional structures, an interpretation of internal flow strength and processes, as well as paleocurrent measurements were hard to deduce from the deposits. The tabular cross-stratification observed in one of the units may have been generated from a migrating transverse bar. The large scale tabular, low angle cross-stratification (one meter thick) observed in one of the channel sandbodies may represent lateral accretion surfaces with a migration direction perpendicular to or oblique to the mainflow direction.. However, this is difficult to confirm because of the lack of paleocurrent measurements from the deposits. As no other potential lateral accretion structures were observed, it is tentatively suggested that the channels are of low sinuosity ribbon-like distributaries (c.f. Dreyer et al., 1990). The two different thickness ranges of the sandstones in this facies association is believed to reflect a hierarchy of distributary channels; the sandstones of a thickness between 3,5m to 4,5m are major distributary channels, while the sandstones of 0,5m to 1,5m thickness are minor distributary channels or crevasse channels.

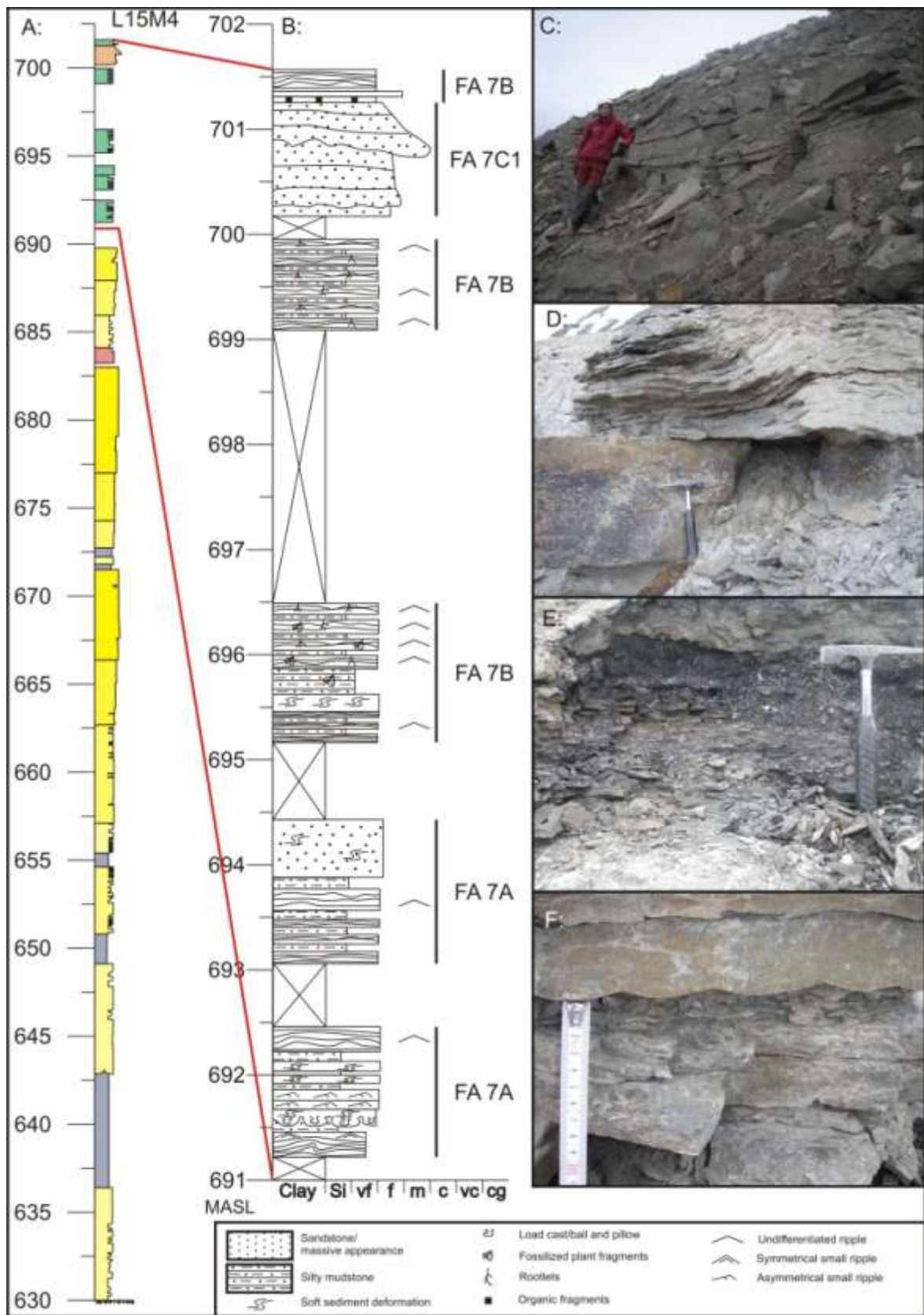


Figure 3.16: A: Lithostratigraphic log L15M4 (Mefjellet). B: The uppermost section of the log, displaying deposits of FA7. C: Fluvial channel at L8R2 (Ringdalsfjellet) with large scale cross-stratification possible formed as a result of lateral migration of a point bar. D: Deposits of FA7-B superimposed on deposits of FA6 (foreshore) at L3S2 on Sandsteinsfjellet. E: Thin shaly coal layer at L3S2 (Sandsteinsfjellet). F: Interdistributary bay deposits with symmetrical small ripples (L9M1, Mefjellet).

5. Paleocurrent data

5.1 Introduction:

This chapter gives an overview of the paleocurrent measurements in the study area. The data is presented in rose diagrams, illustrating the distribution of vectors ranging from 1° to 360°. Frequency of paleocurrent values within 10 degree intervals are grouped to individual columns in the rose diagram. The **rose diagrams** (Figure 5.1; 5.3; 5.4; 5.5) are constructed for illustrational purposes with the length of the column being proportional to the number of measurements within each 10° sector at a linear relationship. This is in contrast to the properties of a **circular histogram** (Figure 5.2) where the frequency of the individual columns should be proportional to the *area* of the column (Nemec, 1988). As such, geostatistical evaluations of the data cannot be deduced from the *rose diagrams*. Furthermore, the columns of the presented rose diagrams does not reflect a given percentage of the total sample population, but reflect relative proportions, with the column of highest frequency extended to the rim of the diagram. The software used for making the rose diagrams is Rozeta 2.0. Geostatistical analysis of the data has been conducted independently of the rose diagrams using the software EZ-Rose 1.0 by Baas (2000), and includes the non-parametric Kuiper and Watson tests and the parametric Rayleigh test.

Two main groups of paleocurrent data are presented;

- circular (1° to 360°) point vectors of paleocurrent measurements of cross-stratification and asymmetric ripples
- Semi-circular (1° to 180°) lineament vectors of symmetrical ripple crests.

The former will henceforth be referred to as "*paleocurrent directions*" and the latter as "*symmetrical ripple crest orientations*". "Paleocurrent data" is used as a collective term. A complete list of the paleocurrent data, with a further sub-division of the data into facies association and individual logs, is included in Appendix 2. The sample population of the *paleocurrent directions* is n=97, and n=88 for the *symmetrical ripple crest orientations*.

The symmetrical ripple crest orientations were measured on bedding planes with exposed straight or slightly sinuous crests (Figure 5.1). Measurements of symmetrical ripple crests are recorded from all shoreface facies associations, but the bulk is confined to FA2-FA4. As the symmetrical ripple crest orientations are lineament vectors rather than point vectors, two

values exists for each measurement; the measured direction and the opposing direction at $\pm 180^\circ$. Both of these are plotted in the rose diagrams. Paleocurrent directions were collected measuring the strike and dip direction of foresets in tabular/planar cross-strata (Figure 5.1) and on asymmetrical ripples.

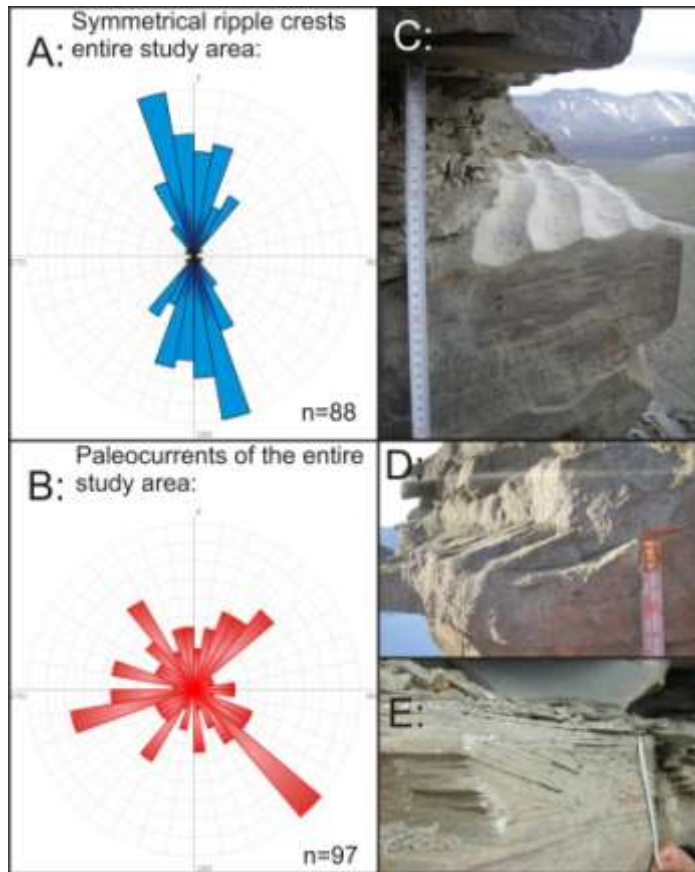


Figure 5.1

A: Rose diagram of all symmetrical ripple crests

B: Rose diagram of all paleocurrent directions.

C: Exposed symmetrical ripple crests.

D and E: Measurable foresets of tabular cross-stratification sets.

5.2 Geostatistic analysis:

The geostatistical analysis of the paleocurrent values are conducted to test if the samples have preferred orientations and to test the validity of the mean values. This is done with the Kuiper, Watson and Rayleigh tests in EZ-Rose where the following hypothesis are tested (Baas, 2000):

H_0 : The vectorial population sampled has a uniform (non-preferential) distribution

H_1 : The vectorial population sampled has a non-uniform (preferential) distribution

Thus, if H_0 is accepted the sample is chaotic and has a useless mean value, while the mean value of the measurements indicates of the preferred direction if H_0 is rejected. The confidence sector of the sample is automatically calculated in Ez-rose using the following equation:

$$\text{Eq.1} \quad d^\circ = \frac{m_\alpha}{\sqrt{nRK}}$$

For Eq.1, d° is the confidence sector of the mean, n is the number of samples in the population, R is the vector length of the mean, and K is the concentration of vector data (strength of the vector mean) (Baas, 2000). The value of m_α is depending of the confidence level of the test, which in this case are $\alpha=0.05$ and $\alpha=0.01$ ($m_\alpha = 112$ and $m_\alpha = 148$ respectively). For a detailed explanation and formulas of the three different tests, see Baas (2000). In addition to the geostatistical analysis carried out on the total measurements collected, the sample population has been analyzed based on locality, and the facies association from which it was measured.

Results:

The results of the geostatistical analysis along with rose diagrams are presented in *Figure 5.2* and *Figure 5.3*. The results reveal that there is a very consistent orientation for the symmetrical ripple crests. H_0 was rejected at a confidence level (α) of 0.01 for all of the tests. The mean value obtained is $179,56^\circ$, with a confidence sector of $5,77^\circ$ (at $\alpha=0.01$). This means that there is a 99% probability that the mean of the population is between $173,79^\circ$ and $185,33^\circ$. For the paleocurrent directions of the entire study area, H_0 was accepted at both confidence levels for all three tests. The distribution of the paleocurrent directions is thus chaotic, and no preferred direction can be deduced from the data.

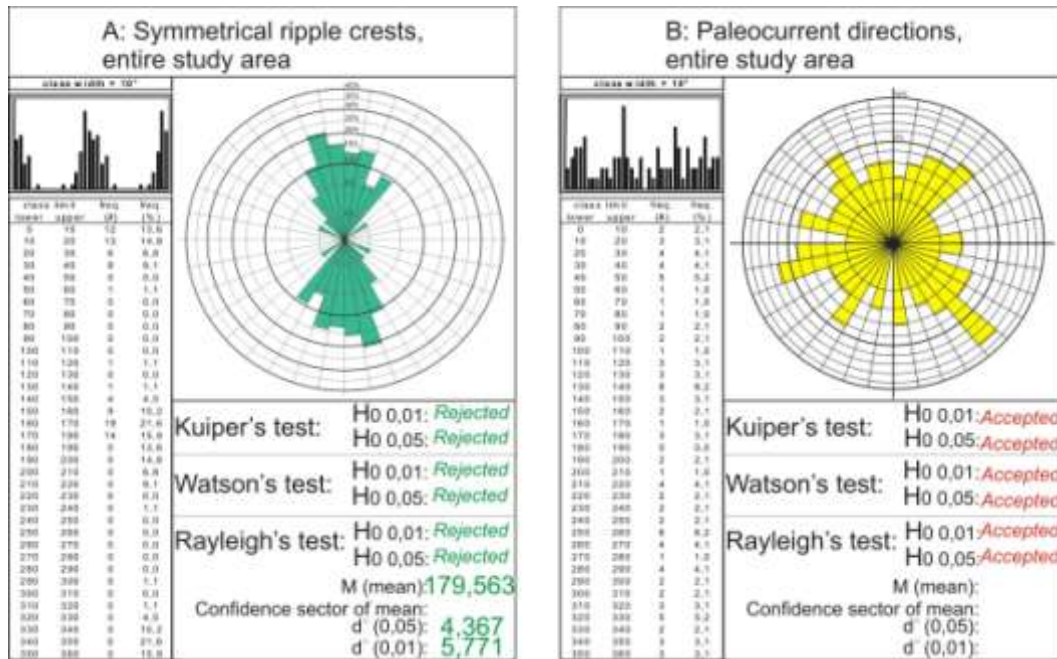


Figure 5.2: Circular histograms of symmetrical ripple crests (A) and paleocurrent directions (B), and the results of Kuiper's, Watson's and Rayleigh's tests.

The results of the symmetrical ripple crest orientations at the different localities reveal similar results as that of the results of the entire study area (Figure 5.3; Figure 5.5). H₀ is rejected at both confidence levels for all three tests at all locations, and the mean values roughly have a N-S orientation (ranging from 171,2° to 182,2°). Since the sample population at the different locations is less than that of the entire study area, the confidence sector is higher (ranging from 8,9° to 14,9° at a confidence level of 0,01).

The results for the paleocurrent directions at the various locations are much more variable (Figure 5.3; Figure 5.5). H₀ is accepted for both confidence levels for all three tests at Tillbergsfjellet and Ringdalsfjellet. However, H₀ is rejected for all the three tests at the two different confidence levels for Mefjellet. The mean for the paleocurrent directions on Mefjellet is 308,6° with a confidence sector of 32,8° at a confidence level of 0,05 and 43,35° for a confidence level of 0,01. The tests from Sandsteinsfjellet was accepted at a confidence level of 0,01, but rejected at a confidence level of 0,05 for all tests. The mean vale is 94,5° with a confidence sector of 41,4° at a confidence level of 0,05.

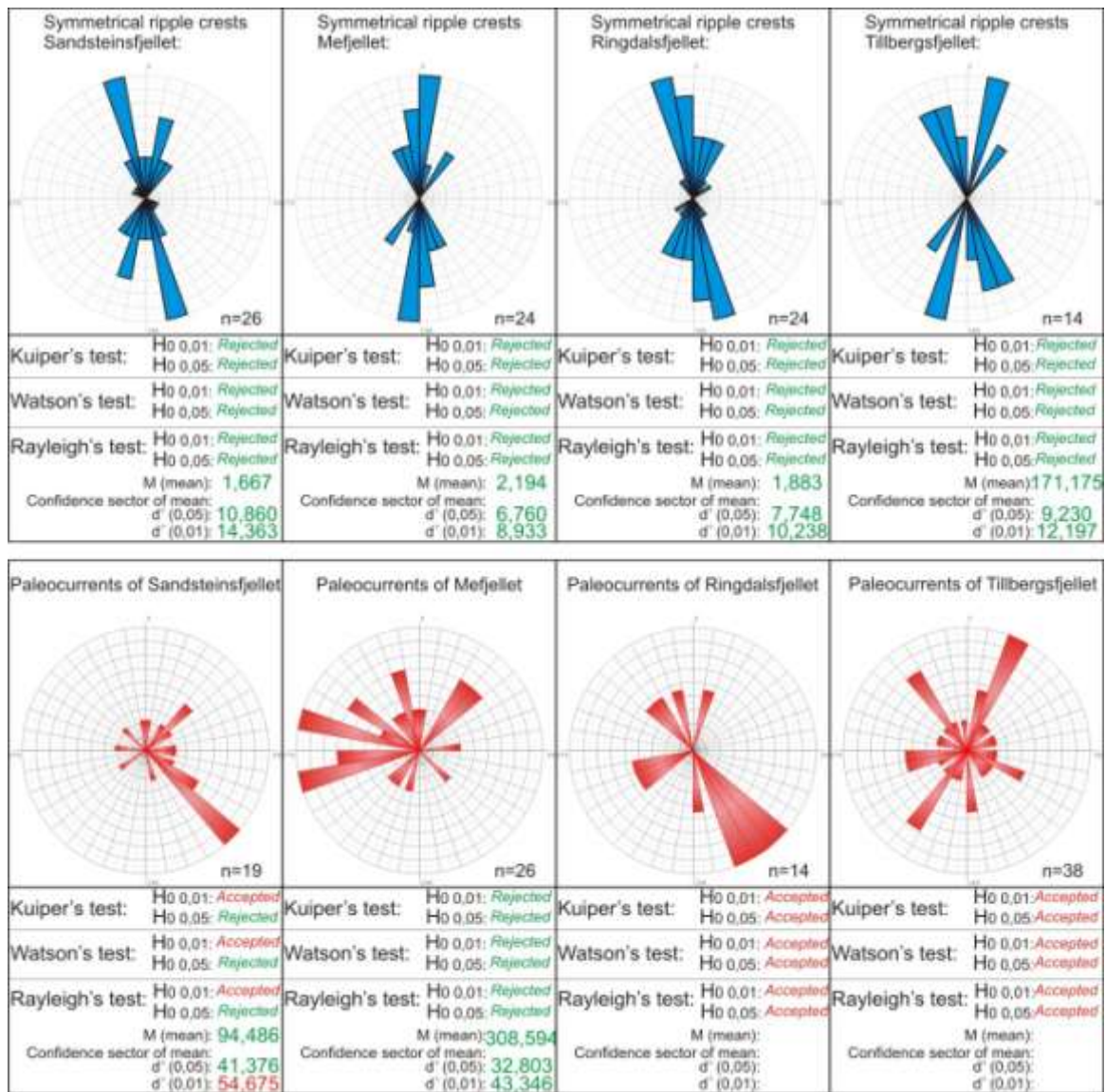


Figure 5.3: Rose diagrams and the results of the geostatistical analysis for different areas in the study area.

There is little variation between the different facies associations with respect to the orientations of the *symmetrical ripple crests*, with exception of FA5 (upper shoreface) where the Rayleigh test was accepted because of too few samples (n=11), all of the tests performed on the different facies associations were rejected for both confidence levels. The mean values of the symmetrical crest ripples of FA2 and FA4 are 1,9° and 175,6° respectively. The N-S orientation observed from these facies association conforms to the mean value of all symmetrical ripple crest orientations measured. However, a small shift to the east compared to the other values is registered for the mean value for FA3 (lower shoreface)

which has a mean value of $10,5^\circ$. On the other hand, the difference is minor and the confidence sector intervals of the means for the different facies associations overlap.

The *paleocurrent directions* of FA5 (which holds the bulk of the measurements) are accepted for all the tests at both confidence levels, and thus shows no preferred direction. Kuiper's and Watson's tests are rejected at both confidence levels for FA2 and FA3 (combined). However, H_0 is rejected by the Rayleigh test because of too few samples.

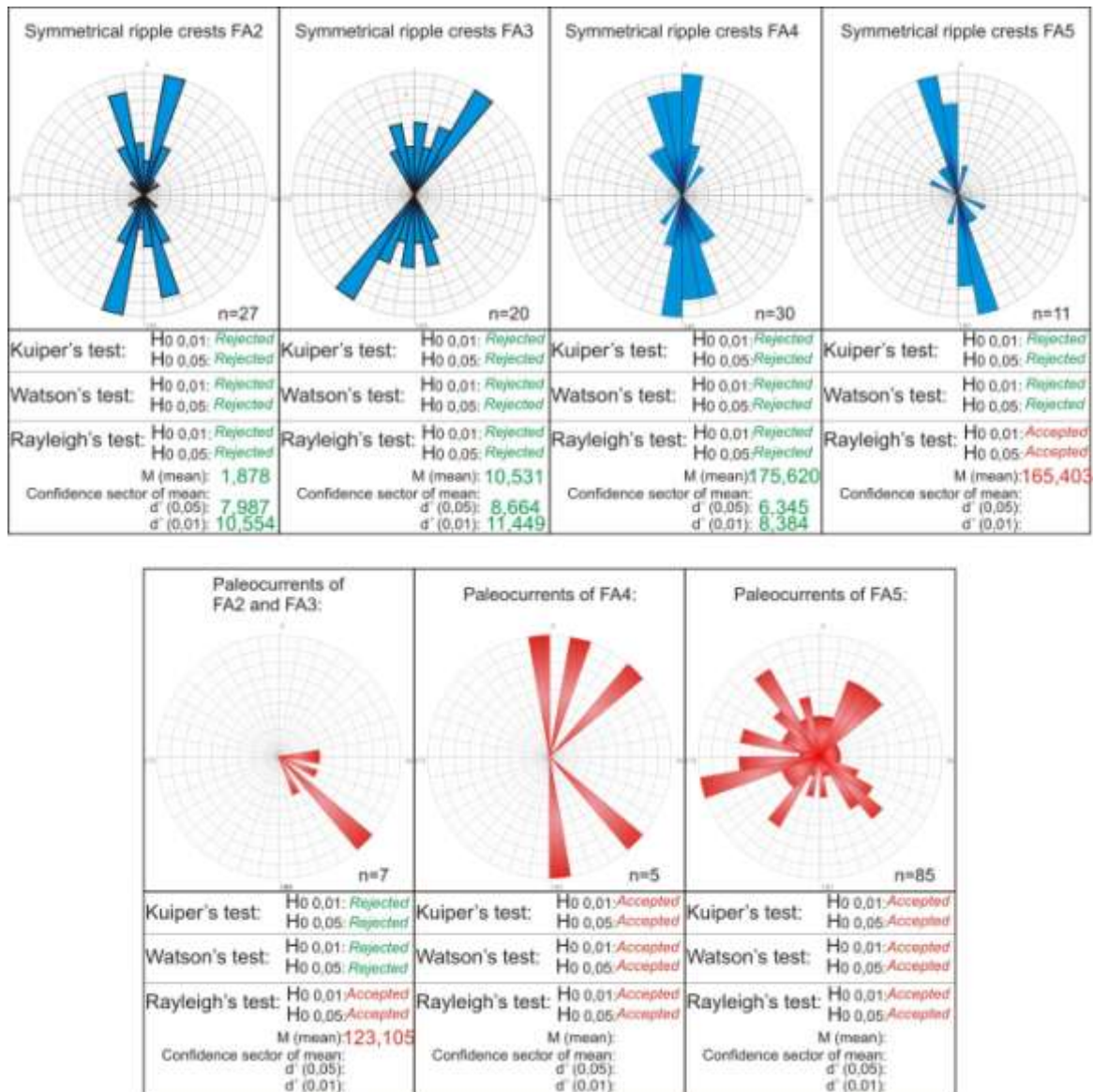


Figure 5.4: Rose diagrams and the results of the geostatistical analysis of the different facies associations.

Interpretation:

The strongly preferred N-S orientation of the *symmetrical ripple* crests, as testified by the small confidence sector of the mean value of $179,56^\circ$ at a confidence level of 0,01, is the result of stable wave influence both in time and space. This assumption is enhanced by the small variations observed in ripple crest orientations in the different facies associations and at different localities. N-S directed orientations of symmetrical ripple crests have been registered throughout the formations by various studies (Steel, 1977; Helland-Hansen, 1985; Helland-Hansen, 1990; Johannesen and Steel, 2005; Olsen, 2008; Stene, 2009; Helland-Hansen, 2010). These measurements conform to the established depositional model of the Battfjellet Formation, with an overall approximately N-S orientation of the paleo-coastline, and progradation of the deltaic system towards the east. The combined *paleocurrent directions* have a chaotic distribution, with no preferred directions. This is believed to reflect the complexity of currents in the upper shoreface depositional environment, which is the facies association where most of the paleocurrent measurements originate from. The weak preferred directions observed at Sandsteinsfjellet have roughly a perpendicular direction to the orientations of the symmetrical ripple crest. If the assumption that the orientation of the symmetrical ripple crests roughly represents the strike direction of the paleo-coastline is made, then the preferred direction in a perpendicular seaward direction might be a result of rip currents. In contrast, the paleocurrent directions on Mefjellet have a weak preference in an oblique direction between a landward direction and a direction normal to the strike of the coast line. This is more likely to be the result of longshore currents. Although the registered preferred directions might reflect local variations in dominating current, the confidence sector of the mean is very high, and as such, there are uncertainties to the obtained means. The paleocurrent directions of FA2-FA4 have a too small sample size to validate if they have a preferred direction. However, it is worth noting that of the total 12 paleocurrent directions of the distal facies associations, none have a landward (westerly) direction.

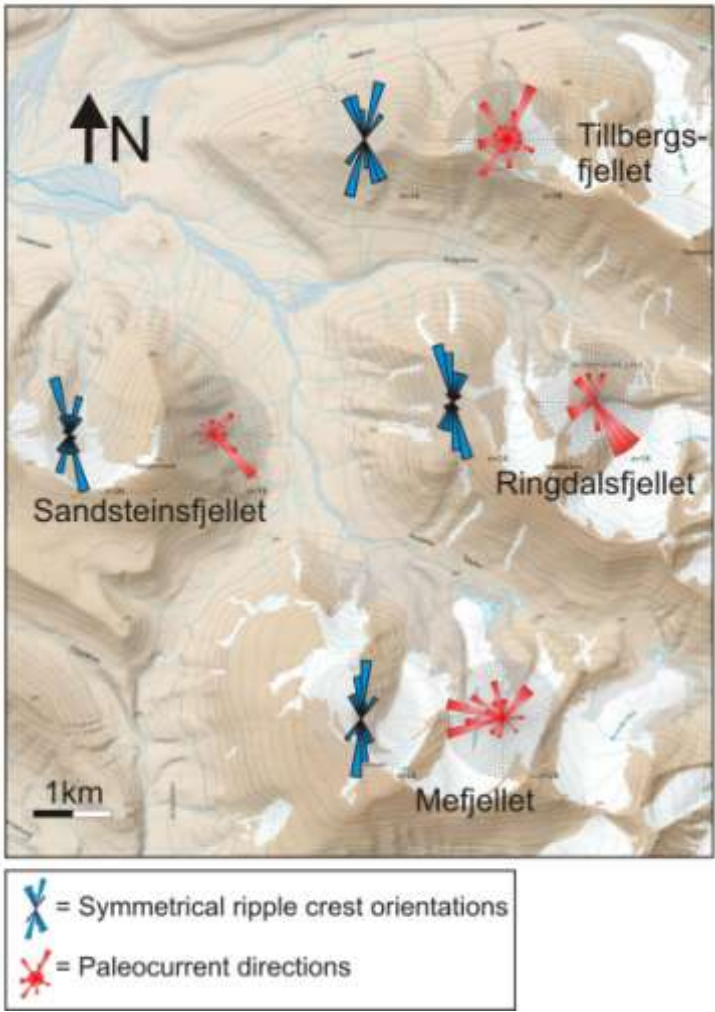


Figure 5.5: Overview map with rose diagrams from the different mountains.

6. Sandbody Geometry

6.1 Introduction

The data obtained from the logged sections, along with other observations from the study area has been compiled into a model of the sandbody geometries. The aim of this chapter is to present the stacking of parasequences in the study area as a whole, and to present a more detailed description of local parasequence stacking patterns, and internal distribution of facies associations both along strike and dip through chosen transects.

6.2 Methods and principles for correlation:

To extract information from each individual log and compile it into a 3D model, a set of sequence stratigraphic concepts must be fulfilled for both the detailed interpretation of each individual log and for the subsequent correlation. The first step of this work is to classify the facies associations and flooding surfaces of each logged section, and then subdivide them into parasequences. The set of facies associations observed vertically (Chapter 4), grading conformably from FA1 to FA7 represents deposits of progressively shallower environments following Walther's law. Following the definition from Van Wagoner et al. (1990), a parasequence is "a succession of relatively conformable and genetically related beds or bedsets bounded by flooding surfaces or their correlative surfaces". Thus violations of Walther's law, in the sense that a facies association is suddenly overlain by a much more distal facies associations mark a flooding surface and the onset of a new parasequence. There are a few localities in the present study of stacked sandstone units that have been assigned to different parasequences, although the facies association assemblage of the two bodies does not reflect a violation of Walther's law. This has been done when the correlative surface of a more proximally expressed flooding surface is traceable along the outcrop. The correlative surfaces identified in the present studies are all within the FA2 (offshore/transition) succession of the logs. Because of the lack of consistent outcrops within the delta plain deposits of Aspelintoppen Formation, and the absence of continental deposits towards the top of parasequences (discussed below), no correlative surfaces have been identified within the continental deposits in the study area.

As outlined in Chapter 5, the progradational direction of the system is towards east. A parasequence is thus expected to grade from delta plain deposits through the

foreshore/backshore and shoreface facies associations and eventually pinch out in the offshore shale of the Frysjaodden Formation along dip from west to east.

Preservation of transgressive deposits between parasequences are rare, in most cases the transition between parasequences is marked with a flooding surface where distal deposits are superimposed directly on more proximal deposits. No sandy turbidite units or basin floor fans have been observed in the study area. Neither have sandy clinothems, where sand has been transported past the shelf edge/prodelta slope been identified. However, the parasequences have a clinoform shape in the sense that the relative inclination in the dip direction increase from the low inclinational delta plain and foreshore/backshore deposits to a higher inclination of the shoreface deposits, before it again returns to a lower inclination in the offshore/transition succession, giving a characteristic lensoid shape. The thickness of a parasequence is thus expected to increase before it thins and eventually pinches out in a dip direction. This has been partially observed at various locations in the study area (*Figure 6.7*), and is partially conceptual, based on the thickness variations of sandbodies observed between the logs. The flooding surfaces are correlated as isochronous lines while facies association boundaries are correlated as diachronous lines.

The sandstones of the Battfjellet Formation are cliff forming because of its higher resistivity to weathering than the underlying shales of the Frysjaodden Formation. Parasequences are to some extent recognizable along the cliff exposures of the Battfjellet Formation (*Figure 6.1*). The reason for this is that each parasequence usually starts with a shaley/silty horizon that weathers more easily than the sandstone and hence develops a thin marker horizon that can be traced along the exposures. However, visible correlation along mountain slopes is in many cases limited because of cover by scree and glaciers. Correlation of parasequences *between* mountains is problematic because of the significant lateral variations along strike and dip, even over relatively short distances. Even though the same number of parasequences is observed on two different mountains separated by a valley, they are not necessarily the same parasequences. Thus, correlation is in large part based on sequence stratigraphic concepts.

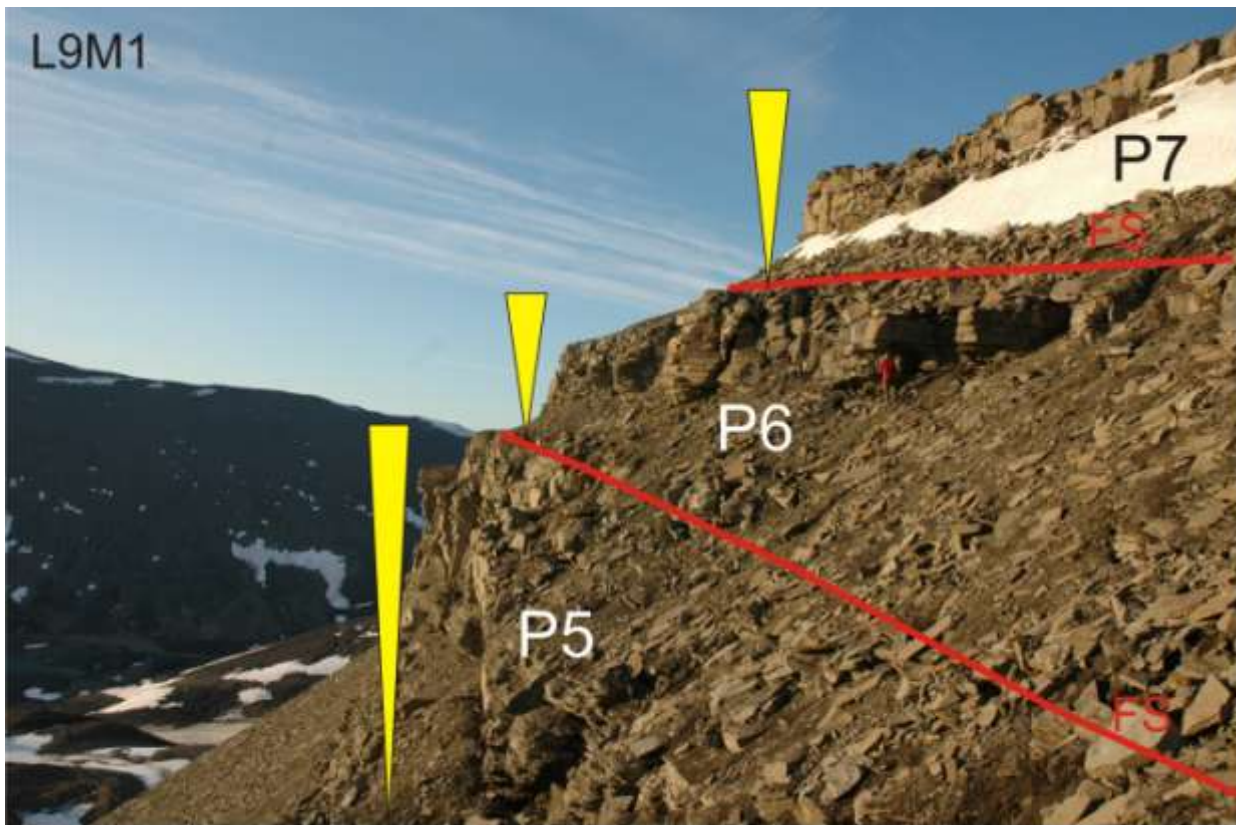


Figure 6.1 Example from L9M1 showing the recognizable cliff forming tendency of individual parasequences. Coarsening upward trends is marked with yellow, and flooding surfaces are marked with red lines.

6.3 Parasequence stacking pattern

A total of twelve different parasequences are recognized in the study area, but the number of parasequences present for each individual logged section varies between three and five (Table 6.1). The twelve recorded parasequences are given named based on its position relative to hinterland, thus P1 (lower most parasequence at the western edge of the study area) is the oldest, while P12 (top most parasequence at the eastern edge of the study area) is the youngest (figure 6.2).

	Log nr:	P1	P2	P3	P4	P5	P6	P7	P8	P9	P10	P11	P12	Σ
Sandsteinsfjellet	L4S3	X	X	X	X	-	-	-	-	-	-	-	-	4
	L2S1	X	X	X	X	-	-	-	-	-	-	-	-	4
	L3S2	X	X	X	X	-	-	-	-	-	-	-	-	4
	L7S4	X	X	X	X	-	-	-	-	-	-	-	-	4
	L11S5	X	X	X	X	-	-	-	-	-	-	-	-	4
	L20S6	-	-	-	-	-	-	-	-	-	-	-	-	-
Mefjellet	L10M2	-	X	X	X	X	X	-	-	-	-	-	-	5
	L15M4	-	-	-	X	X	X	X	-	-	-	-	-	4
	L14M3	-	-	-	X	X	X	-	-	-	-	-	-	3
	L9M1	-	-	-	X	X	X	X	-	-	-	-	-	4
Ringdalsfjellet	L1R1	-	-	-	-	-	X	X	X	-	-	-	-	3
	L8R2	-	-	-	-	-	X	X	X	-	-	-	-	3
	L13R3	-	-	-	-	-	X	X	X	-	-	-	-	3
	L18R4	-	-	-	-	-	-	X	X	X	X	-	-	4
	L19R5	-	-	-	-	-	-	-	-	X	X	X	-	3
Tillbergfjellet	L5T1	-	-	-	-	X	X	X	-	-	-	-	-	3
	L21T6	-	-	-	-	-	X	X	X	-	-	-	-	3
	L6T2	-	-	-	-	-	X	X	X	X	-	-	-	4
	L12T3	-	-	-	-	-	X	X	X	X	X	-	-	5
	L17T4	-	-	-	-	-	-	-	X	X	X	X	-	4
	L22T7	-	-	-	-	-	-	-	-	X	X	X	X	4
	L16T5	-	-	-	-	-	-	-	-	X	X	X	X	4

Table 6.1: Listing the presence of parasequences (P1 – P12) at the different logs, and the total parasequences present at a given log.

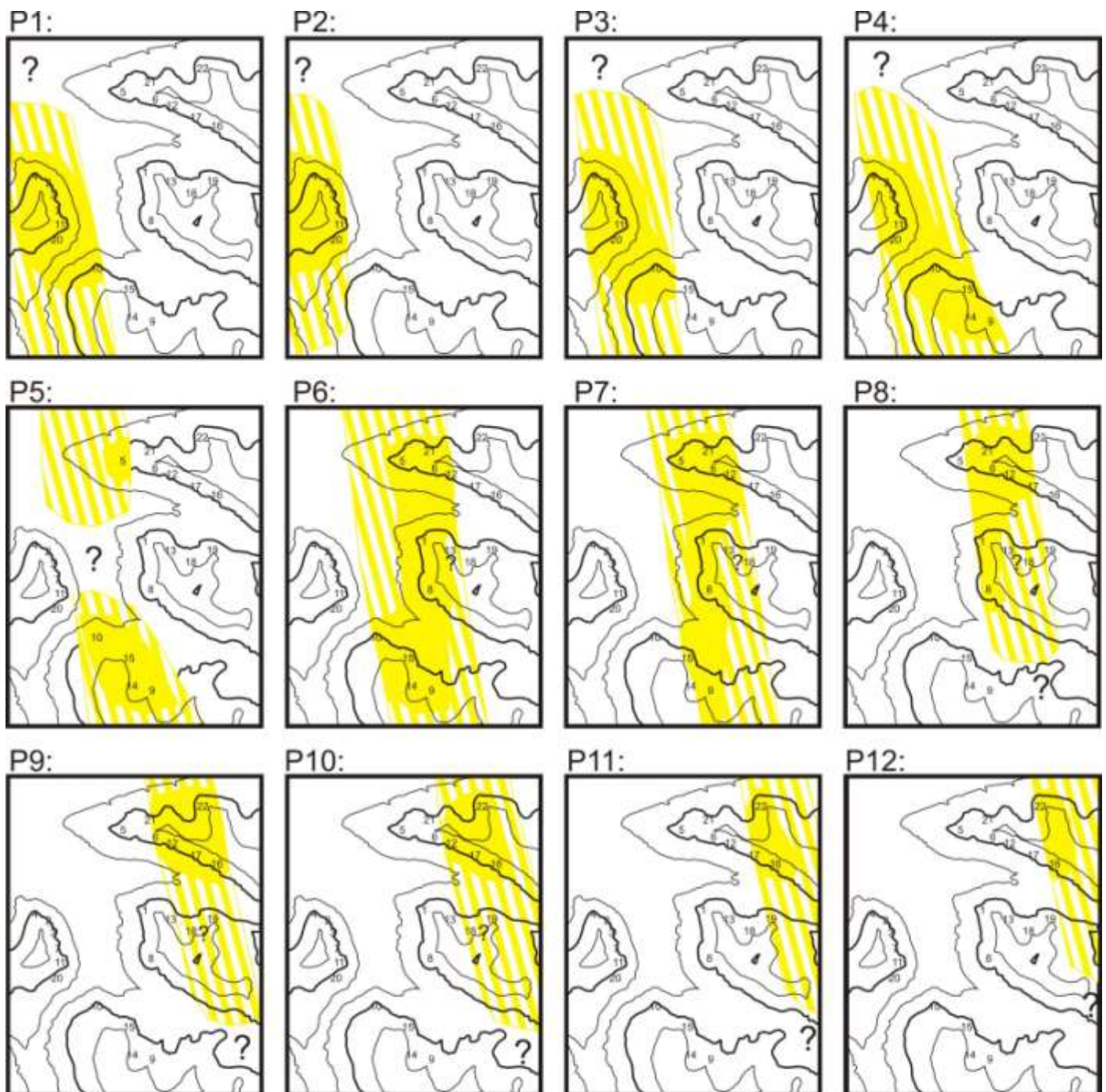
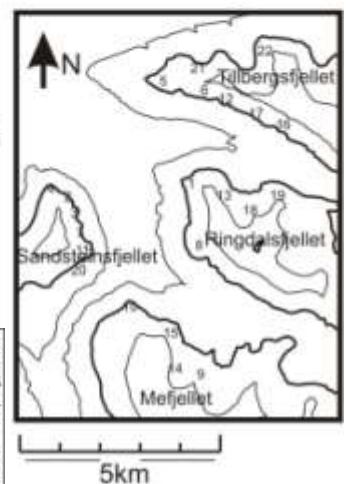


Figure 6.2: Overview maps showing the distribution of individual parasequences, indicating their observed lateral extent both along strike and dip. The locations of the logged sections are marked with numbers. Yellow colour indicates the presence of a parasequence at, and close to a logged section where it has been demonstrated, while dashed yellow colour indicates the expected position of a parasequence where it is not observed. Due to uncertainties related to extensive local deformation (discussed below), the logged sections in the eastern area of Ringdalsfjellet are marked with a dashed yellow colour.

- Contour lines 250/750 MASL
- Contour line 500 MASL
- Presence of parasequence at, and in proximity to logged section
- Expected presence of parasequence

Note: Due to the small scale of the maps, only the chronological number of the logs are given, and not the full annotation.

1: L1R1	12: L12T3
2: L2S1	13: L13R3
3: L3S2	14: L14M3
4: L4S3	15: L15M4
5: L5T1	16: L16T4
6: L6T2	17: L17T5
7: L7S4	18: L18R4
8: L8R2	19: L19R5
9: L9M1	20: L20S6
10: L10M2	21: L21T6
11: L11S5	22: L22T7



Because of the expected lensoid shape of the parasequences, there are thickness variations along strike and dip of each individual parasequence. The lowermost parasequence typically is the thickest one (most commonly in the range between 7-20m). The reason for the lowermost parasequence being the thickest was explained by Helland-Hansen (2010) to be a result of progradation into deeper waters. The onset of a renewed progradation following a transgression will prograde above a previously developed parasequence and therefore have less accommodation space to fill. For the same reason, the uppermost parasequence in many cases is the thinnest (4-15m thickness). The thickness of a parasequence rarely exceeds 20m. The recorded depositional dip length of the shoreface part of the parasequences, from FA6 to FA2, is between 2 and 4km. The onset and termination of P8 is visibly traceable along the southern mountain slope of Tillbergsfjellet, and pinches out over a distance of 2,5km. There are more uncertainties in estimating the length of the parasequences in strike direction. P6 and P7 have been correlated from the northern to the southern rim of the study area, and the length of these parasequences thus exceeds 10km in strike direction. There are however uncertainties to these correlations as there are two wide valleys within the correlated distance.

Extensive studies by Helland-Hansen (2010) and additional contributions by Skarpeid (2010) are the basis of a map indicating the number of parasequences present at different locations throughout Nordenskiöld Land. This map, together with the number of parasequences observed at the various locations of the present study is presented in Figure 6.3:

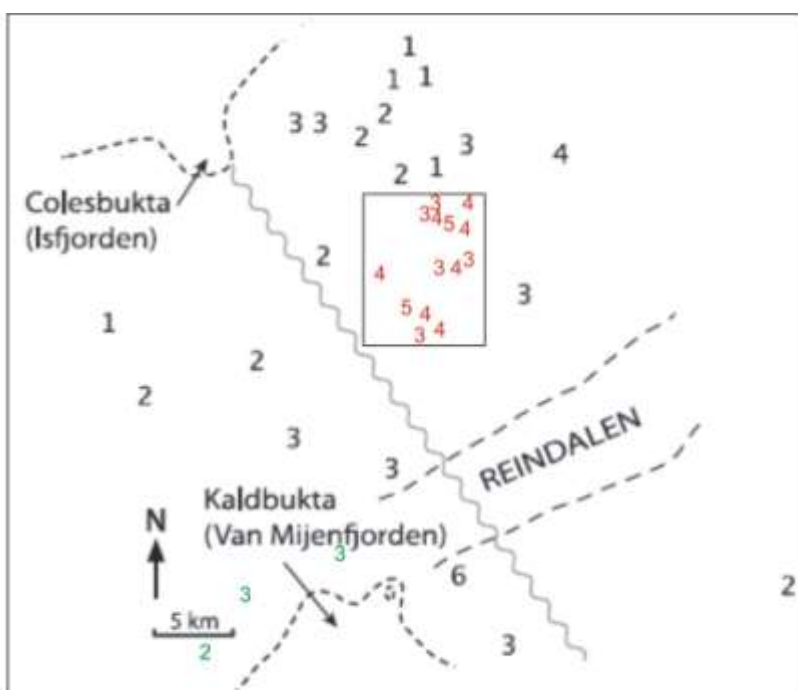


Figure 6.3: Overview map of Nordenskiöld Land indicating the position and number of parasequences at various locations as established by Helland-Hansen (2010). Green colour indicates the additional contributions to this map by Skarpeid (2010), while red colour indicates the number and position of parasequences in the study area of the present study.

6.4 Correlation panels

Three correlation panels along different transects of the study area is presented in this chapter in order to address different aspects of the local sandbody geometry (Figure 6.4). A transect through Sandsteinsfjellet and Mefjellet is presented to address internal facies association variations, both along strike and dip. A roughly N-S oriented transect through logged sections on Mefjellet, Ringdalsfjellet, and Tillbergsfjellet is presented to address parasequence variations along strike, and a WNW – ESE oriented transect along the southern slope of Tillbergsfjellet is presented to address parasequence variations along dip.

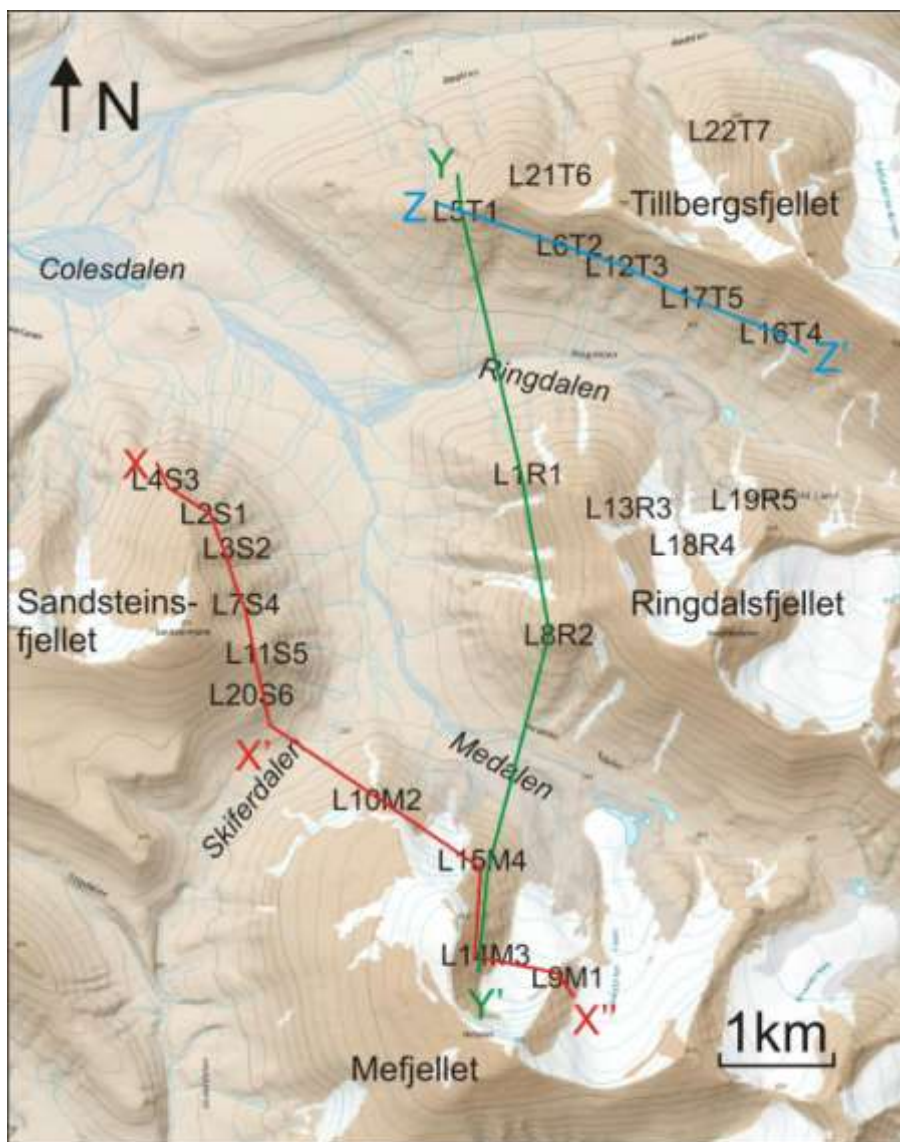


Figure 6.4:
Overview map of
the study area
indicating the
location of the
transects presented
in this chapter.

6.4.1 The Sandsteinsfjellet-Mefjellet transect

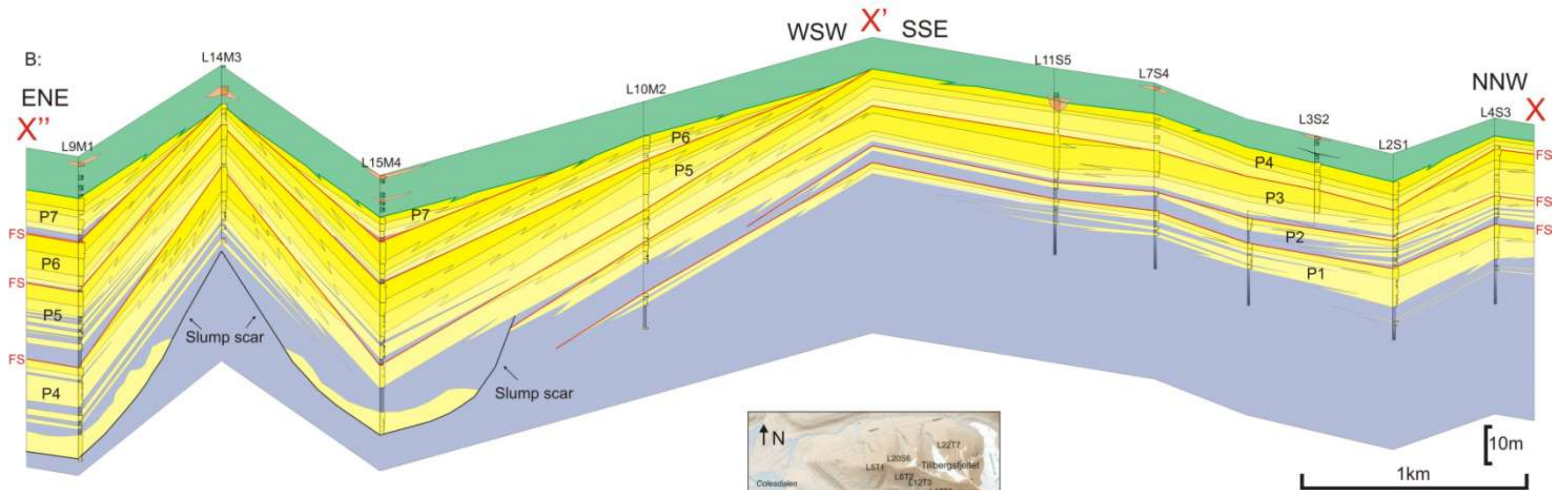
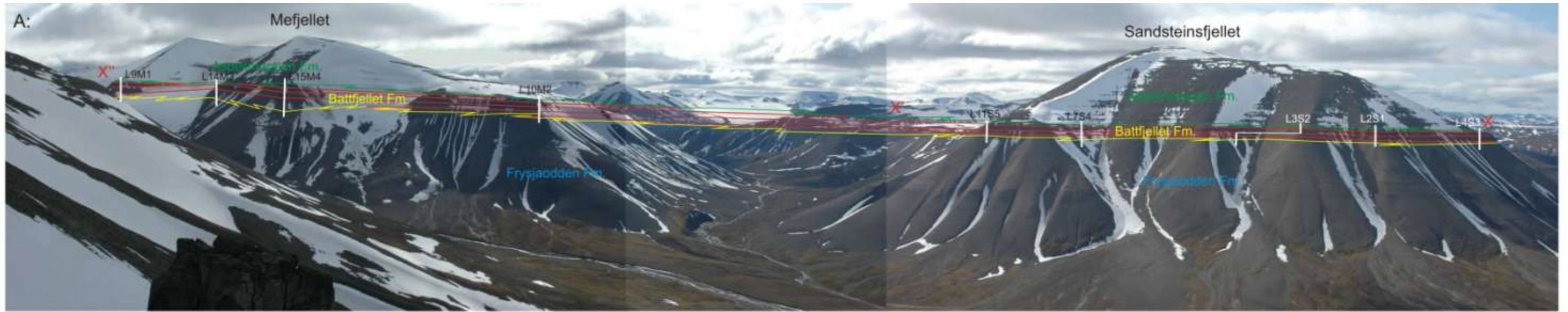
The Sandsteinsfjellet-Mefjellet transect includes 5 logged sections on Sandsteinsfjellet with a slightly oblique orientation relative to strike, and 4 logged sections on Mefjellet, that have a more scattered position relative to strike and dip. L20S6 on Sandsteinsfjellet is not included as it is not in an *in situ* position (will be discussed below). In order to illustrate the internal facies association development of the seven parasequences (P1-P7) recorded along the transect, the transition from the shallow marine Battfjellet Formation to the continental Aspelintoppen Formation is plotted as a horizontal line, and the vertical thickness of the correlation panel is exaggerated (*Figure 6.5 B*).

There are no onset or terminations of parasequences along the transect at Sandsteinsfjellet; all five logged section consists of the same four stacked parasequences (P1-P4). However, a marked thinning from NNW to SSW is registered for the two lower parasequences. The second parasequence (P2) is thinner and has a more distal internal facies association distribution than that of the underlying parasequence (P1). For this reason, and for the better fitting with the spatial distribution of the sandbodies, P1 and P3 are correlated to the two lowermost parasequences on Mefjellet (*Figure 6.5 B*), while P2 is pinching out between the two parasequences. P4 is the only parasequence that can be correlated between all logs in the transect. It represents the uppermost parasequence at Sandsteinsfjellet, and the lowermost parasequence at the three south-easternmost logged sections on Mefjellet. Of the latter three, L14M3 has a more proximal internal facies distribution than L9M1 and L15M4, which consists of thick sections of offshore/transition deposits. P5 and P6 can be correlated between the four logged sections on Mefjellet, while P7 is only present at L9M1 and L15M4.

Interpretation:

The small variations observed between the logged sections on Sandsteinsfjellet are believed to reflect their roughly parallel/slightly oblique position relative to strike. The small contrasts between the NNW/SSE oriented transect in discussion, and the expected N-S orientation of the strike of the paleo-coastline, is evident by the thinning of the two lowermost parasequences towards SSE. As P2 has a more distal internal facies association distribution, and are thinner than P1, it is interpreted to reflect a retrogradational parasequence stacking pattern. This is only observed between P1 and P2; the other parasequences show a

progradational stacking pattern. The position of the logs on Mefjellet in a dip direction relative to the logs on Sandsteinsfjellet is evident from the onset of two superimposed parasequences (P5 and P6) on L10M2. The close resemblance between L9M1 and L154, and their contrast to L14M3, reflect the more proximal position of the latter. Because of the relative position between the three logs in discussion, this observation implies that the strike of the paleo-coastline locally had a NNW-SSE orientation. Such local variations of the paleo-coastline are expected following the depositional model of Battfjellet formation (Chapter 7.) The reason for the thick offshore/transition deposits at L9M1 and L15M4 is believed to be caused by slumping (discussed below).



- | | |
|---------------------------------------|--------------------------------|
| FA 1: Offshore/shelf (Frysaodden Fm.) | Flooding surface (isochronous) |
| FA 2: Offshore/Transition | FA-boundary (diachronous) |
| FA 3: Lower shoreface | Parasequence number |
| FA 4: Middle shoreface | Flooding surface |
| FA 5/FA 6: Upper shoreface/foreshore | |
| FA 7: Continental (Aspelintoppen Fm.) | |
| Transgressive deposits | |

Mefjellet

Sandsteinsfjellet

Figure 6.5 (Previous page)

A: Panorama picture of Sandsteinsfjellet and Mefjellet. Correlated flooding surfaces are marked with red straight (isochronous) lines, and the upper and lower formation boundaries of the Battfjellet Formation with green and yellow ragged (diachronous) lines.

B: Correlation of logs on Sandsteinsfjellet and Mefjellet. The boundary between the Battfjellet Formation and Aspelintoppen Formation has been used as datum. Facies association boundaries are marked with diachronous lines, while flooding surfaces is marked with isochronous lines.

6.4.2 The Tillbergsfjellet – Ringdalsfjellet – Mefjellet transect.

A roughly N-S oriented correlation panel was made along a transect incorporating two logs on Mefjellet, two logs on Ringdalsfjellet, and one log on Tillbergsfjellet (*Figure 6.6*). The main emphasis of this correlation is to address variations along strike for the parasequences, and address problems related to correlation across valleys. Five different parasequences are recorded in the correlation, and individual logs consist of three or four parasequences. A distinctive feature in this correlation is that all the logs (excluding L14M3) has a 0,5 to 1,5m thick succession of transgressive deposits superimposed on a transgressive surface.

Interpretation:

From correlation along dip from L5T1 and L15M4 to their nearest neighboring down-dip log (L6T2 and L9M1, respectively), transgressive deposits are registered above the same transgressive surface. Beside this, there are no transgressive deposits in the study area. The transgressive unit is thus believed to be a marker bed, and a correlative horizon at a close to isochronous level. From the recorded parasequences in the study area, the transgressive unit is located between parasequence P6 and P7. As illustrated in *Figure 6.5*, the onset of P7 is inferred to occur between L14M3 and L15M4, and as the topmost parasequence at L14M3 is P6, the transgressive unit is not possible to detect here, as it would be located with the Aspelintoppen Formation. For L15M4 and L5T1, the transgressive unit is located at the base of the topmost parasequence, while there are two parasequences above the unit at the logs on Ringdalsfjellet. As the logs on the Ringdalsfjellet are located slightly more to the east than the other logs along the transect, the additional parasequence present above the transgressive unit at that location is inferred to be the onset of a new, more basinward located, parasequence (P8) in dip direction. For the same reason, the additional parasequences present below the transgressive unit at L5T1 and L15M4 are pinching out in a basinward direction, and are thus not present at the logs on Ringdalsfjellet. The lowermost

parasequence at L5T1 has been assigned to P5 based on its position relative to the other parasequences and the transgressive unit. However, it might not be correlative with P5 on Mefjellet; there are uncertainties related to the great distance between the two logs. Thick sandbodies assigned to P4 and P5 on L15M4 pinch out over a relatively short distance to L8R2 on Ringdalsfjellet. A possible explanation for the thick sandstone units pinching out over relatively short distances may be that the basal part of these sandstones are slump deposits with a limited lateral extent, while the overlying succession was deposited by shoreline aggradation (discussed below). In addition, the slight NE-SW direction of the paleo-coastline of the area adds to the distance along dip between the two logs from what is perceived if the paleo-coastline had a straight N-S orientation.

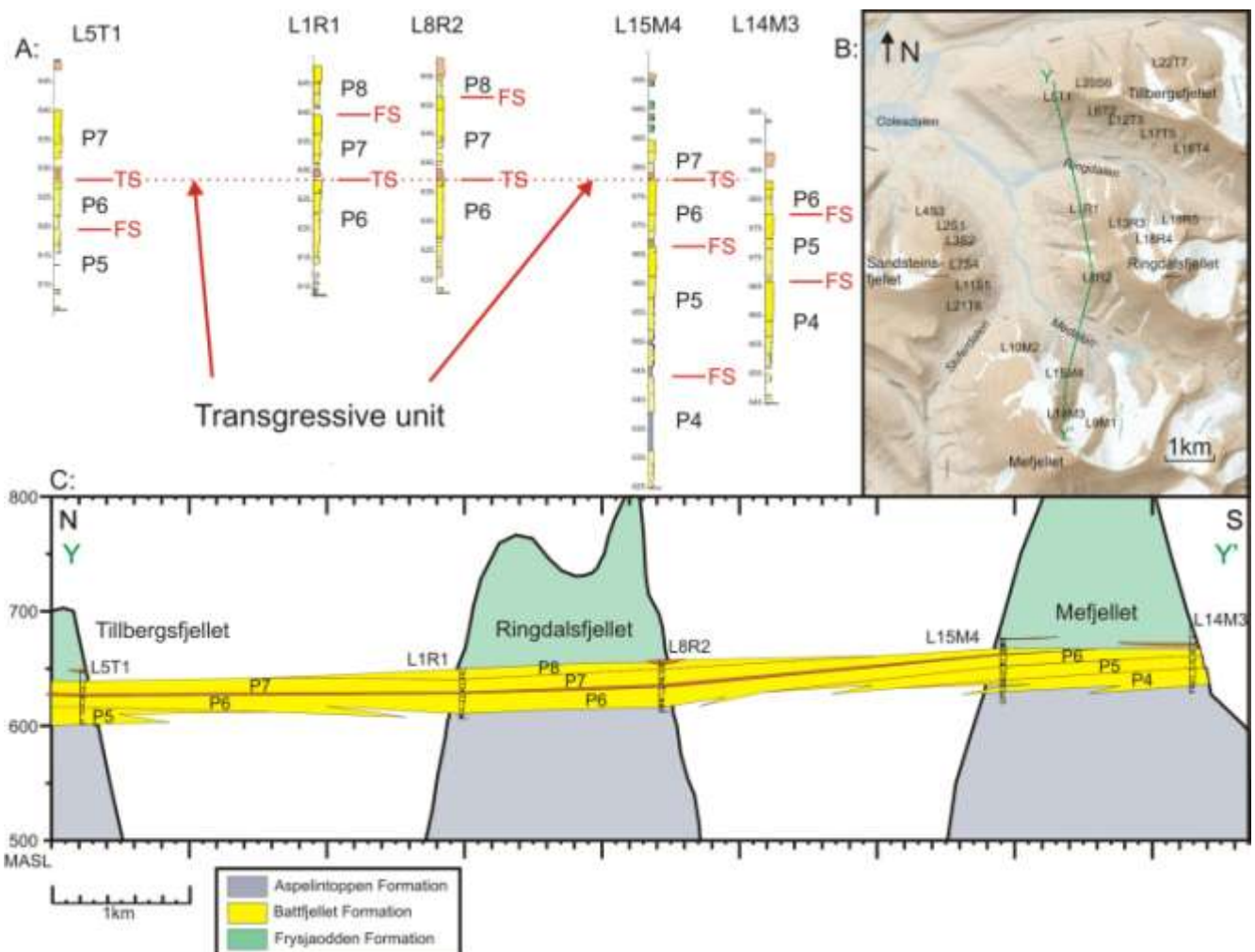


Figure 6.6

A: The logs of the NS oriented correlation panel, positioned with their relative distance from each other and aligned with the transgressive unit as datum.

B: Overview map indicating the position of the transect.

C: Correlation panel between logs on Tillbergsfjellet, Ringdalsfjellet and Mefjellet. The vertical axis is exaggerated.

6.4.3 The Tillbergfjellet transect

The correlation panel from Tillbergfjellet presents the stacking pattern of P5 to P12 at an orientation roughly along dip (*Figure 6.7*). The correlation panel consists of 5 logs, spread over a distance of 4km. Thicknesses of the parasequences containing shoreface deposits range from 5 to 20m. The characteristic lensoid shape of the parasequences, with a thickening – thinning trend along depositional dip, is to some degree observed along this transect.

The stacking pattern of P5 to P9 in the western area of the transect (between L5T1 and L12T3) reveals a shoreline trajectory with a high aggradational component. This is evident by the high number of vertically stacked parasequences (5 at L12T3) and the thickness of each individual parasequence. In contrast, a stronger progradational component for the shoreline trajectory of P10 to P12 in the eastern section of the transect (between L12T3 and L16T4) is evident by the relatively thin parasequences.

Interpretation:

The correlation panel in discussion is believed to represent a roughly depositional dip parallel transect. The observations made, with the onset and termination of parasequences over relatively short distances conforms to this assumption. Sediment input and subsidence rate are believed to be the controlling factors of the variations of the shoreline trajectories observed along the transect. The thick parasequences in the western part of the transect might reflect a high subsidence rate with increased accommodation and a resulting relatively high aggradation rate. In contrast, the thin parasequences in the eastern part of the transect might reflect a slower subsidence rate and a relatively high sediment input, resulting in a strong progradation. Shoreline trajectories, and its controlling factors will be further discussed in Chapter 7.

L17T5 has a lower position on the mountain slope than the outcrops of the other logs. This is believed to be a result of modern landslide, resulting in a displacement of 20-30m. This has been corrected for in the correlation panel, but inevitable there are some uncertainties related to this. Modern landslides as a possible source of error when conducting correlations will be discussed below.

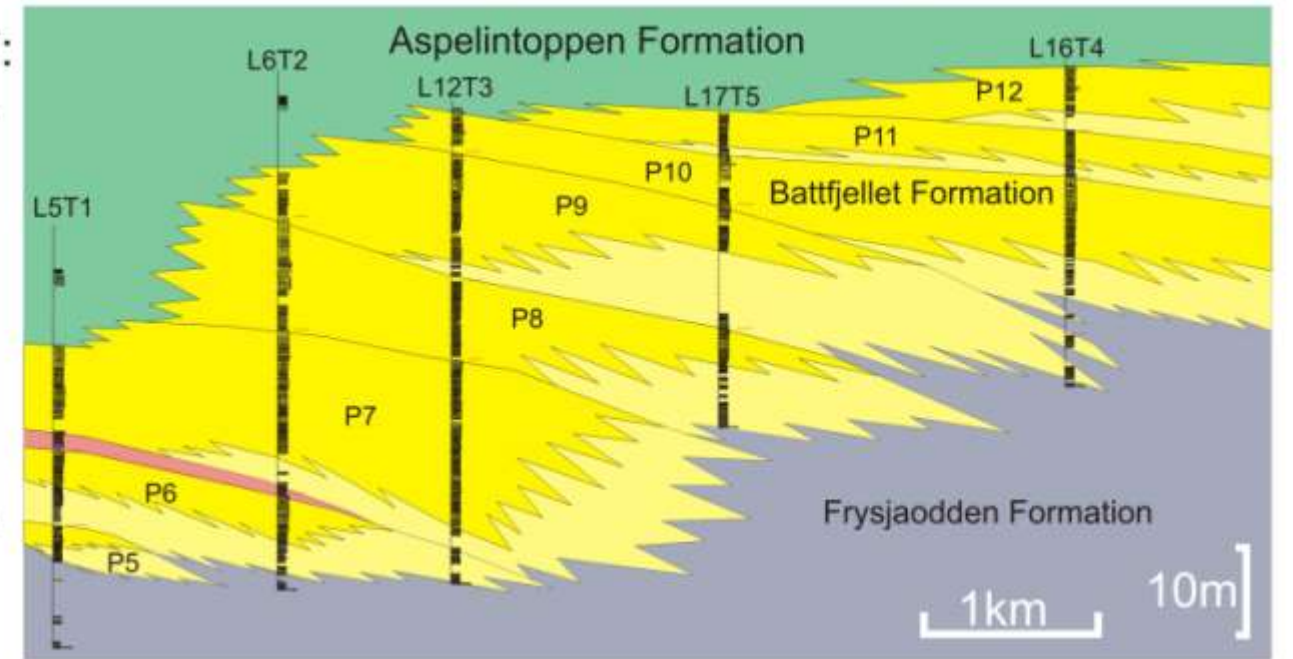
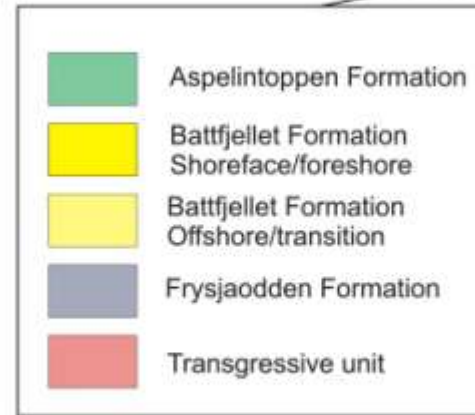
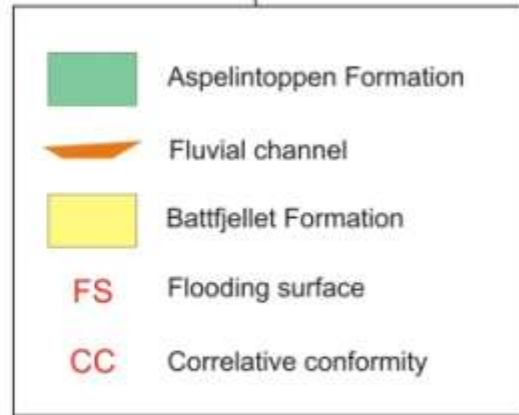
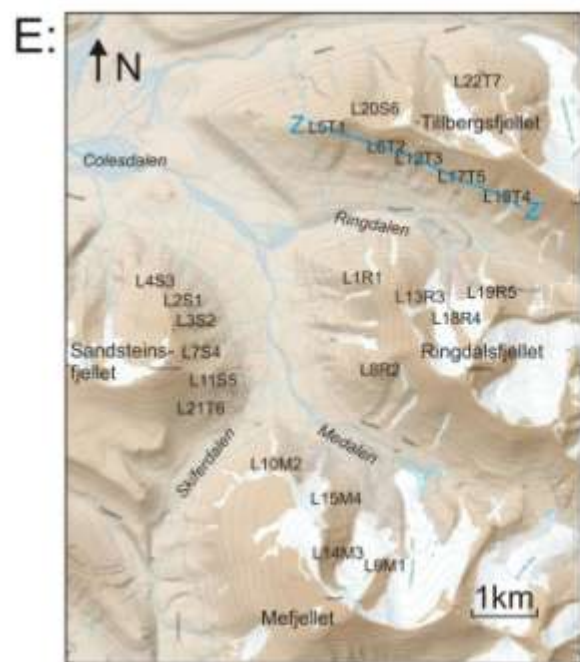
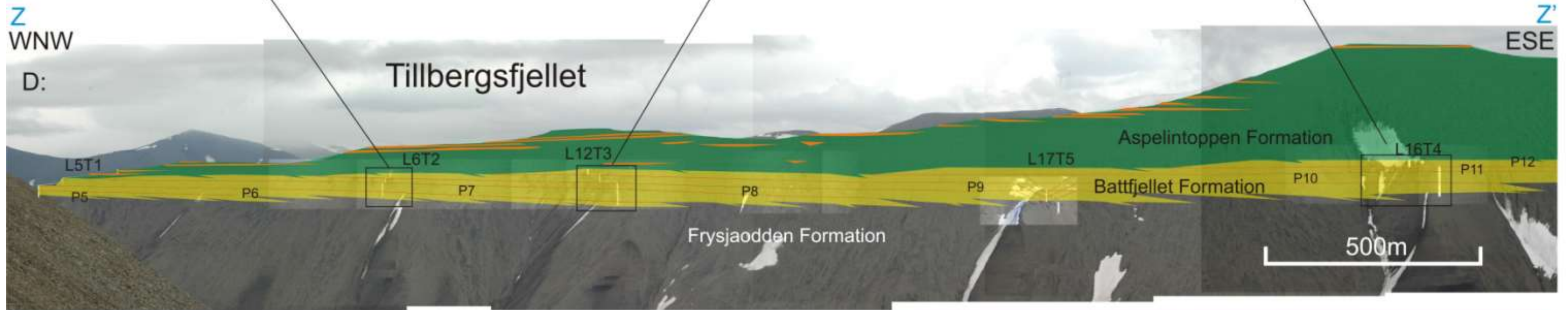
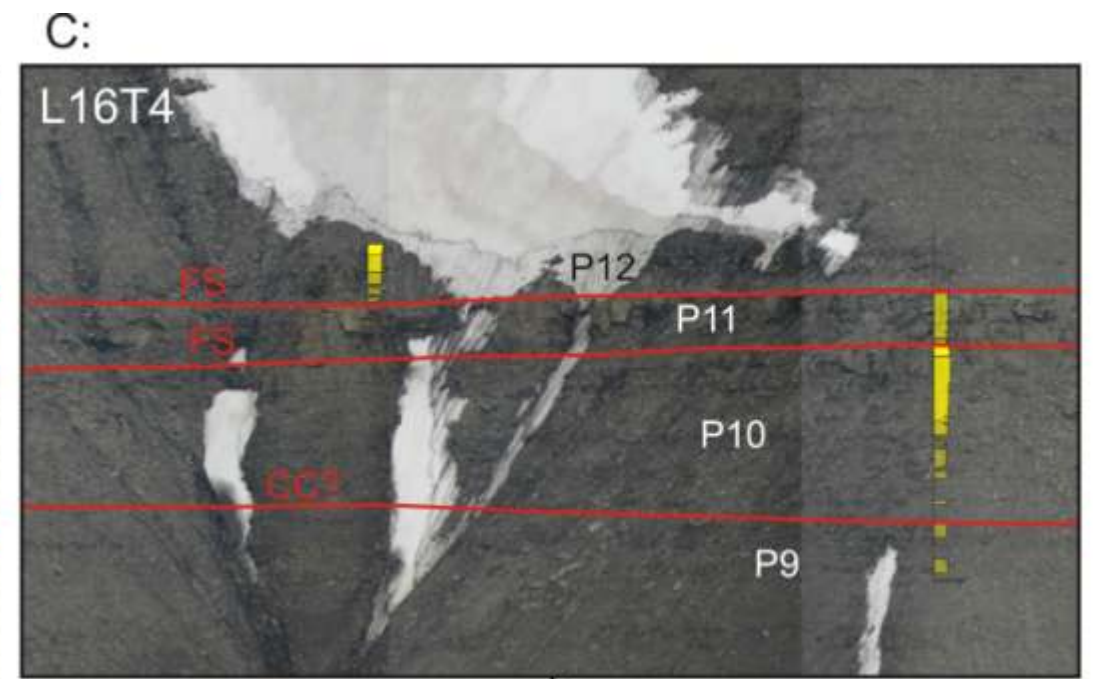
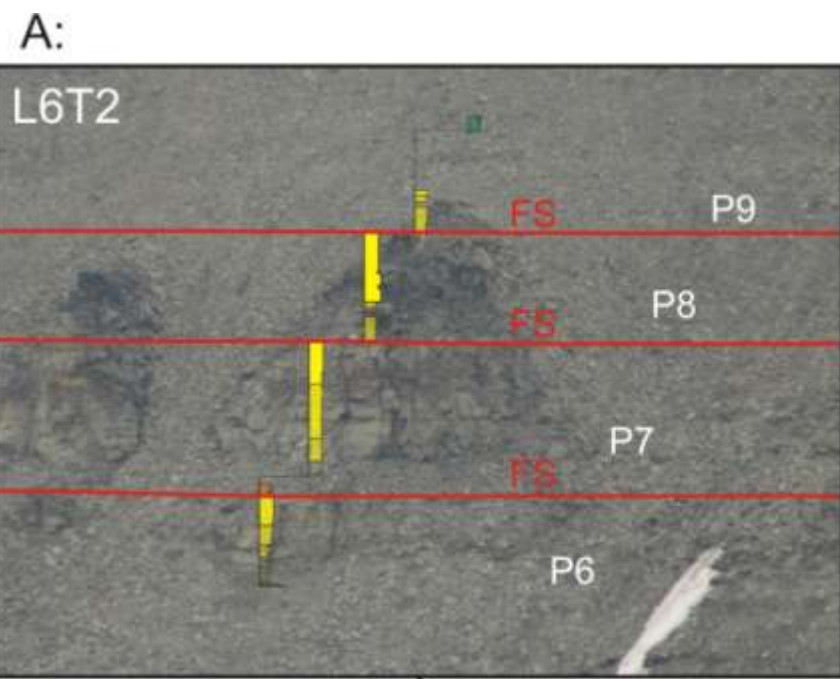


Figure 6.7 (Previous page):

A-C: Pictures of the outcrops where L6T2, L12T3 and L16T4 were logged. Flooding surfaces are marked with red lines.

D: Correlation panel along the mountain slope of Tillbergsfjellet showing the parasequence stacking pattern roughly along depositional dip.

E: Overview map indicating the position of the transect.

F: Correlation panel of the same transect with exaggerated vertical axis.

6.5 Sources of error

The model for the sandbody geometry is a “best fit model” from the data available. As previously described, there are uncertainties related to cover by scree and glaciers as well as uncertainties related to correlation across wide valleys. In addition, the data could be erroneously collected due to errors caused by instruments (eg. altimeter error due to local variations in atmospheric pressure), or sand bodies that are not in an *in situ* position could erroneously be incorporated in the model. The latter was given special interest when conducting the field work. In the following section, three different sand bodies, interpreted to not be in an *in situ* position are discussed.

6.5.1 Eastern Ringdalsfjellet

At the eastern part of Ringdalsfjellet (at L13R3, L18R4 and partially at L19R5), there is a zone of extensive deformation, marked with the presence of deformed and homogenized sandstones, local thrusting and isoclinal folding.

There are two different clusters of sandstone bodies in the area, where the lower cluster is located 20-50m below the upper. The upper cluster consists of typical shoreface deposits of the Battfjellet Formation, although locally deformed and folded. The lower cluster is more deformed than the upper, and is characterized by strongly deformed/homogenized intervals associated with a local thrust plane.

The lower cluster consist predominantly of deformed sandstone with a mixture between mud and very fine grained sandstone. However, less deformed intervals with preserved sedimentary structures, such as HCS-stratification and alternating plane parallel lamina and symmetrical

small ripples also occur. The beds in the sandstone of the lower cluster are slightly inclined with a dip direction towards the southwest (*Figure 6.8 A*). A minor thrust fault with a displacement of approximately 20 cm was observed at one location in the lower cluster, adjacent to L13R3 (*Figure 6.8 D*). The strike and dip of the fault plane is 172/23, indicating a propagation direction of the fault towards east-northeast (082°).

Deformed and homogenized sandstone intervals were also observed in the upper sandstone cluster, albeit with a slightly coarser grain size (very fine to medium grained sandstone) than the deformed sandstone in the lower sandstone cluster. An isoclinal fold with the hinge dipping towards northeast was observed at one of the outcrops of the upper sandstone cluster (*Figure 6.8 B; 6.8 C*). The contrast between the northeastern limb of the isoclinal fold and the dip of the adjacent sandstone beds tentatively suggests the presence of a fault (*Figure 6.8 B*). This fault can be correlated to the next ridge, where similar contrast in dip is observed. The strike of the fault plane, as inferred from correlating the fault between the two ridges is roughly 320°. Slickensides, with secondary growth of quartz crystals, were observed in both the lower and upper cluster. Direction measurements of the striations in the slickensides reveal a consistent direction roughly towards northeast (*Figure 6.8 G*).

Interpretation:

The Battfjellet Formation consists of syntectonic deposits in a foreland basin adjacent to an ongoing fold and thrust building orogen. The presence of thrust faults and isoclinal folding in the study area are indicative of compression. As such it is natural to look for explanations related to the compressive tectonic regime. The thick succession of shale in the Frysjaodden Formation is susceptible to form a detachment and decollement zones for thrust fault propagation. The isoclinal folding observed in the area of discussion, could then be explained as a result of folding related to fault propagation. However, there are no other indications testifying to the presence of a major thrust in the study area. Furthermore, no major thrust faults have been recorded in the Cenozoic succession on Svalbard, and evidentially neither has

Frysjødden Formation been recognized as a major detachment/decollement zone, although small detachments do occur (Helland-Hansen, 2010, personal communication).

The presence of shoreface deposits in the lower sandstone cluster indicates that these deposits probably were part of the delta front depositional system of the Battfjellet Formation. Although thrusting of the overlying sandstone unit could account for the displacement between the two units, listric downfaulting of the underlying unit is more likely. The strike of the measured fault planes and the directions of the slickensides are parallel to the strike and dip of the paleo-coastline, respectively. These directions conform to the expected directions of a listric fault system in the depositional model of the Battfjellet Formation.

The presence of homogenized/deformed sandstone (soft sediment deformation) as well as brittle and ductile deformational structures indicates that the sediment was partially consolidated at the time of deformation. Displacement of delta front sandstone bodies on the mountain slopes at other locations in the study area been interpreted to be a result of modern landslides (discussed below). The presence of homogenized sandstone and ductile deformational structures renders such an interpretation for the location in discussion less likely.

Although a given number of parasequences have been recognized in the logged section of the area in discussion, there are uncertainties to correlating them to the other parasequences of the study area due to the extensive deformation.

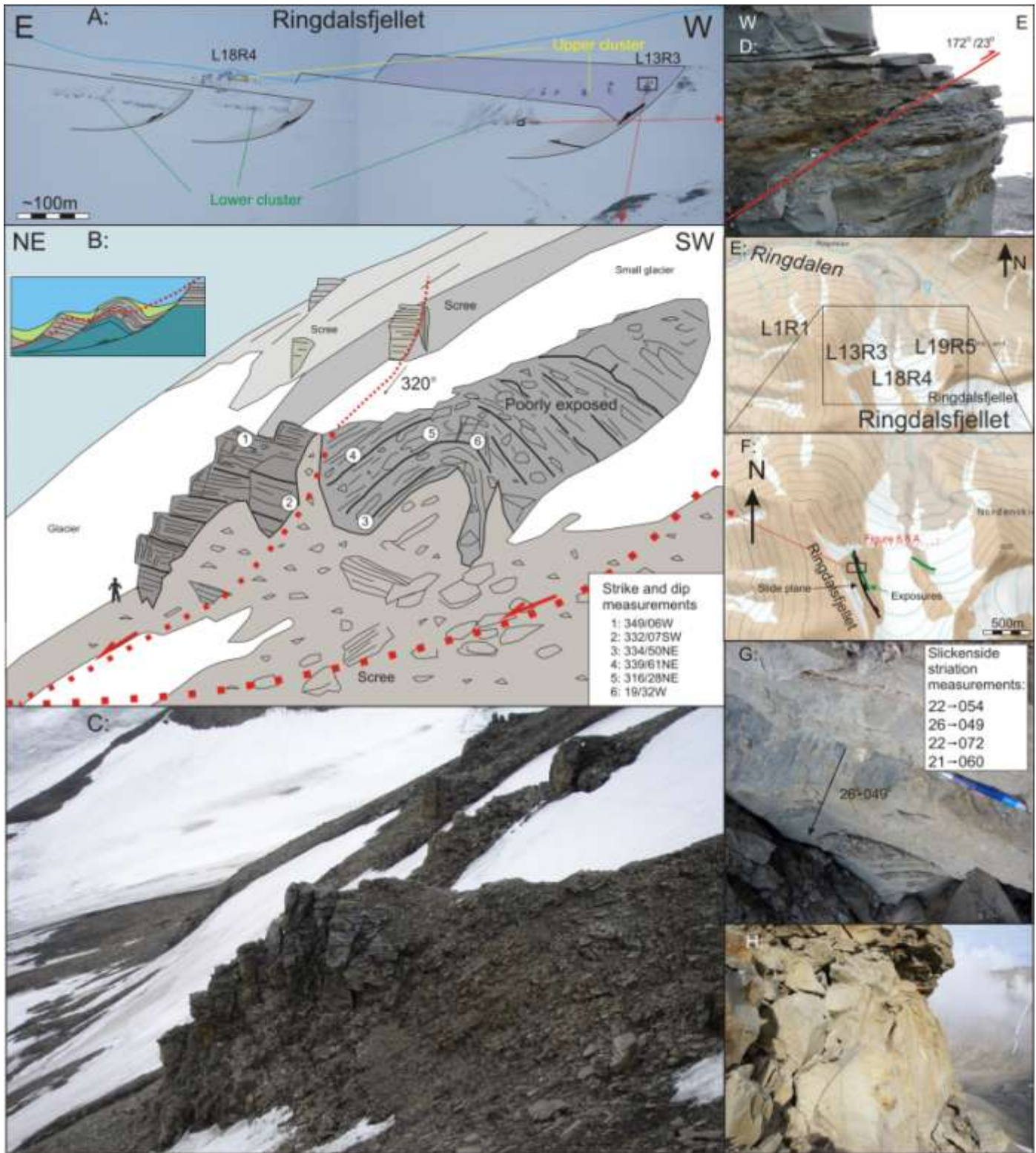


Figure 6.8 (Previous page):

A: Overview picture of the area of extensive deformation on the east side of Ringdalsfjellet. Several listric faults with relative shallow detachment planes displace the Battfjellet Formation both laterally and vertically. The throws of the individual faults are small. It is difficult to distinguish such faults from modern landslides, but the soft sediment deformation and folding suggests early movements with unconsolidated sediments.

B: Field sketch from L13R3 showing the listric faulting and isoclinal folding in the upper sandstone cluster.

C: Picture from the same area as Figure 6.8 B

D: Thrust fault in the lower sandstone cluster at L13R3.

E: Overview map showing the position of the logged sections in the eastern part of Ringdalsfjellet.

F: Overview map showing the position of the fault plane observed at L13R3, and the location of the exposures in the area.

G: Example of slickensides and a list of the slickenside striation measurements.

H: Deformed homogenized sandstone in the upper sandstone cluster.

6.5.2 Eastern Mefjellet

At profile L9M1, in the south-eastern edge of the study area, a 5m thick section of a deformed chaotic mixture of very fine and fine grained sandstone and mudstone was observed at the base of the outcropping Battfjellet Formation. Although sparse remnants of hummocky cross stratification was observed, the overall expression of the section is chaotic, partially homogenous and structureless with no profound grading. Overlying the deformed section is a 30m thick succession with deposits mainly of FA2 (offshore/transition). Such a thickness is unusually thick for this facies association, and it also contains the most abundant occurrence of soft sediment deformation (e.g. ball and pillow structures) in the study area.

The same trend, but with a somewhat lesser thickness, was observed at profile L15M5. Here, the section of deformed homogenous sandstone is much thinner (approximately 2m). The unit appears to be slightly less deformed than the equivalent unit at L9M1 and has a higher abundance of visible hummocky cross-stratification structures.

Interpretation:

The chaotic, partially homogenous, deformed sandstone body is interpreted to be slump deposits following delta front slope failure. Remolding and liquefaction of the internal stratification during slumping may result in a chaotic and deformed sandstone body as seen at

L9M1 (Reading, 1996). No evident shear plane of the slump structure was observed at the profile as most of the basal part of the unit is covered by scree and ice. *In situ* post burial remobilization is an alternative explanation for the deformation of the sandstone to a chaotic and partially homogenous state. However, the lack of indications of fluidization in the form of injection structures, fluid escape structures and mud lumps renders this possibility less likely. In addition, *in situ* remobilization does not explain the abnormally thick interval of sandstones present at this interval of the profile. In contrast, paleoseaward transport of sand as a result of slumping explains the thick section of deformed sandstone. In addition, slumping may explain the thick section of the offshore/transition deposits overlying the deformed sandstone unit. A slump structure of this magnitude is likely to have created a significant change in the local shoreface slope geometry, with increased accommodation space in the slump scar. The increased accommodation space likely decelerated the rate of progradation, and caused the sediment to aggrade with a near vertical shoreline trajectory (*Figure 6.9 A*). As the slump scar is healed and an equilibrium delta front slope profile is acquired, the system goes back to a normal progradational setting. The thick offshore/transition succession of L9M1 and L15M4 is correlative to parasequence P4, which can be correlated over the profiles at Mefjellet and Sandsteinsfjellet. The slumping is thus believed to have happened prior to, or at an initial stage of the development of P4. Profile L14M3 is located between, but with a more proximal position with respect to the hinterland than L9M1 and L15M4. The thickness of the offshore/transition facies for P4 at L14M3 is not thicker than normal. However, the thickness of middle shoreface and upper shoreface succession in P4 at L14M3 has a combined thickness of approximately 20m, which is thicker than the average thickness of the middle and upper shoreface successions in the study area, and is considerably thicker than for the other parasequences of the profile. It is thus reasonable to assume that middle and upper shoreface deposits of P4 at L14M3 are part of the same progradational system with increased thickness due to increased accommodation at the collapse scar. No clear aggradational trend for P4 can be observed at the profiles at Sandsteinsfjellet, nor at the northwestern ridge at Mefjellet. The oversteepening of the profile, and the resulting slumping, may be a result of proximity to a distributary channel at the time of deposition. This interpretation is based on the assumption that to the area in front of a

distributary channel would have a high sediment input, and thus be more prone to oversteepening and resulting slope failure. In addition, the concentration of interpreted hyperpycnal flow deposits is higher in the logged sections close to where the slump deposits are observed for P4 than at the other locations (Sandsteinsfjellet and north-eastern ridge on Mefjellet).

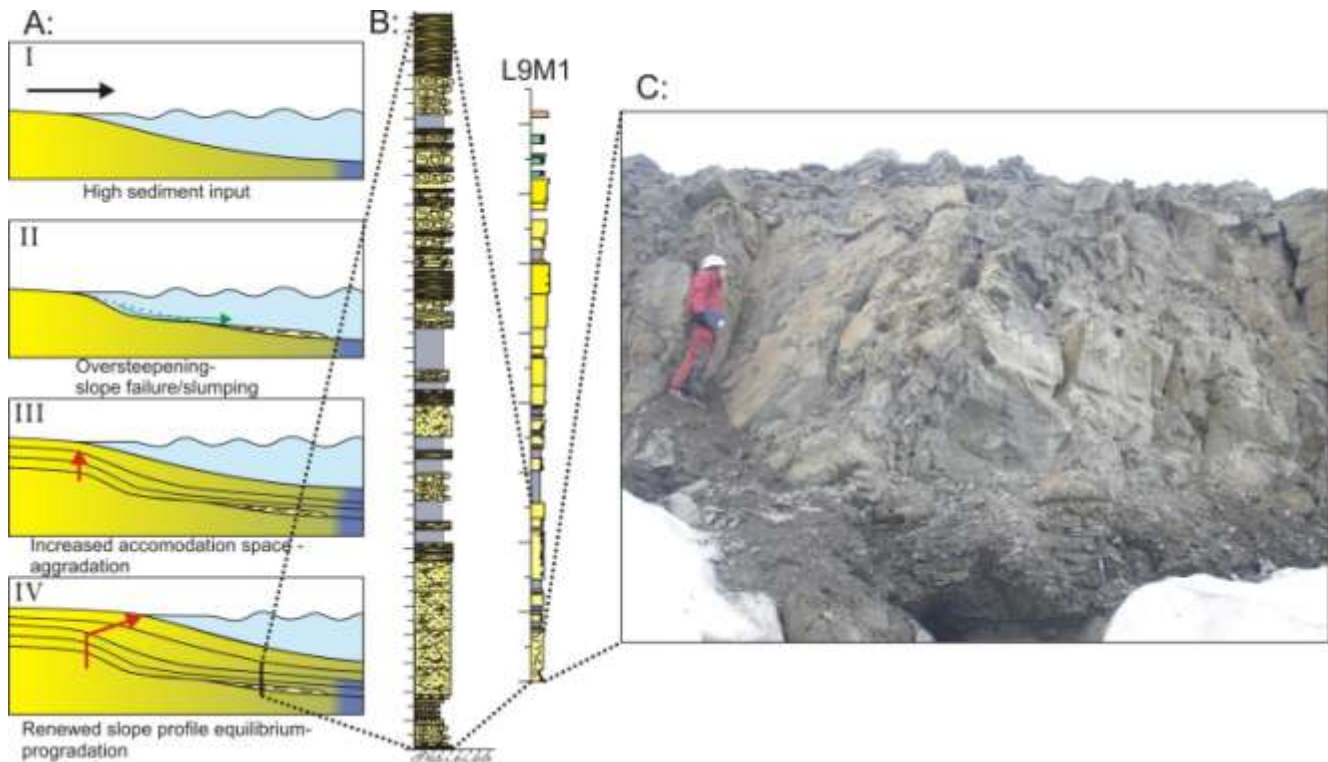


Figure 6.9:

A: Schematic illustrations showing the interpreted evolution of the delta front slope with oversteepening and slumping (II), and resultant aggradation as a result of the increased accommodation (III).

B: Lower part of the logged section at L9M1

C: Deformed homogenized very fine grained sandstone interpreted to be slump deposits at the base of L9M1.

6.5.3 Southern Sandsteinsfjellet

A problem in performing geological mapping in the field and the subsequent correlation is the possibility of outcrops being allocthonous due to displacement as a result of modern landslides. Displacement as a result of modern landslide has been recorded at two of the logged sections (L17T5 and L20S6). They show little internal signs of deformation, but the displaced body at L20S6 is slightly rotated, which is evident from the inclination of the bedding with a dip towards the mountain slope (*Figure 6.10 B*). The small degree internal deformation is a possible pitfall for subsequent correlation. L20S6 (*Figure 6.10*) is located more than 100m below the *in situ* shallow marine sandstone bodies at the other logged sections on Sandsteinsfjellet and is not incorporated in the correlation. L17T5 is believed to only be displaced by 20-30m and is included in the correlation with constrain.

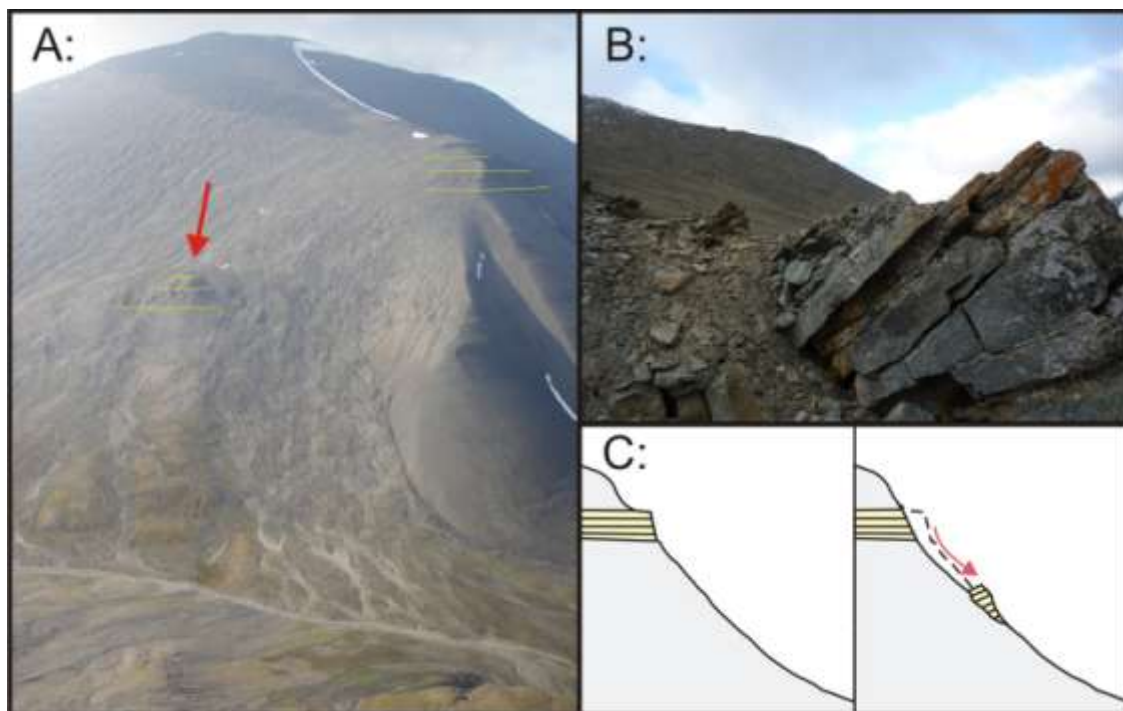


Figure 6.10:

A: Picture of the southeastern slope of Sandsteinsfjellet displaying the displaced sandstone body at L20S6.

B: Uppermost section of the sandstone body, illustrating the dip of the strata towards the mountain slope.

C: Simplistic and schematic illustration of a modern landslide.

Chapter 7: Depositional environment and paleogeography

7.1 Depositional environment:

The facies associations and their respective depositional environments were described in Chapter 4. The facies associations were ordered from the most distal to the most proximal with increasing serial numbers. The shoreface succession (FA3-FA5) shows a predominance of wave generated structures. The high abundance of tempestites in the offshore/transition (FA2) and lower shoreface (FA3) testify to a depositional environment subject to frequent storms. The fair weather aggradation deposits of the proximal shoreface successions indicate increasing oscillation current velocities with decreasing depth of deposition. The upper shoreface (FA5) is dominated by deposits laid down from longshore and rip currents (Chapter 5). Tidal influenced deposits are observed locally, probably related to tidal inlets, connecting embayments along the coastline with the open sea. A schematic figure illustrating the different depositional environment along the coastline is provided in Figure 7.1. Because of the local variations in potential hyperpycnal flow deposits (FA3-B), two dip parallel transects are provided.

A rough estimate of the water depth of the different facies associations can be obtained by measuring the thickness from the top of the uppermost parasequence (where the transition from shallow marine to continental facies is well documented) down to the respective facies associations. These measurements is believed to give a rough estimate of the water depth based on the assumptions that the effect of compaction (decreasing thickness) and subsidence (increasing thickness due to aggradational component) roughly level each other out, and that the system progrades at a low shoreline trajectory (Helland-Hansen, 2010). From these assumptions, the following approximate range of water depths were calculated; FA6 (foreshore): 0-2m, FA5 (upper shoreface): 1-6,5m, FA4 (middle shoreface): 3-8m, FA3 (lower shoreface): 4,5-12,5m. The lower extent of FA2 is commonly not present in the uppermost parasequence, and the range of FA2 is thus not obtained, although it has not been observed at shallower thicknesses than 7m.

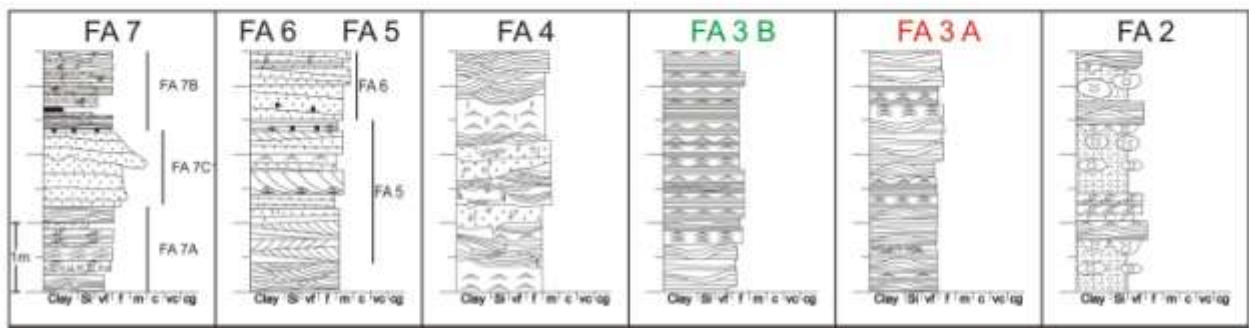
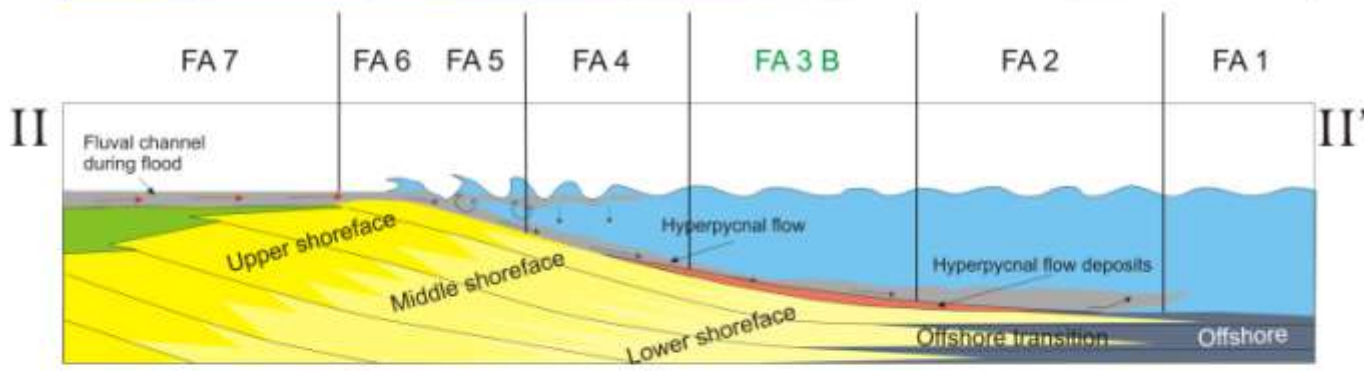
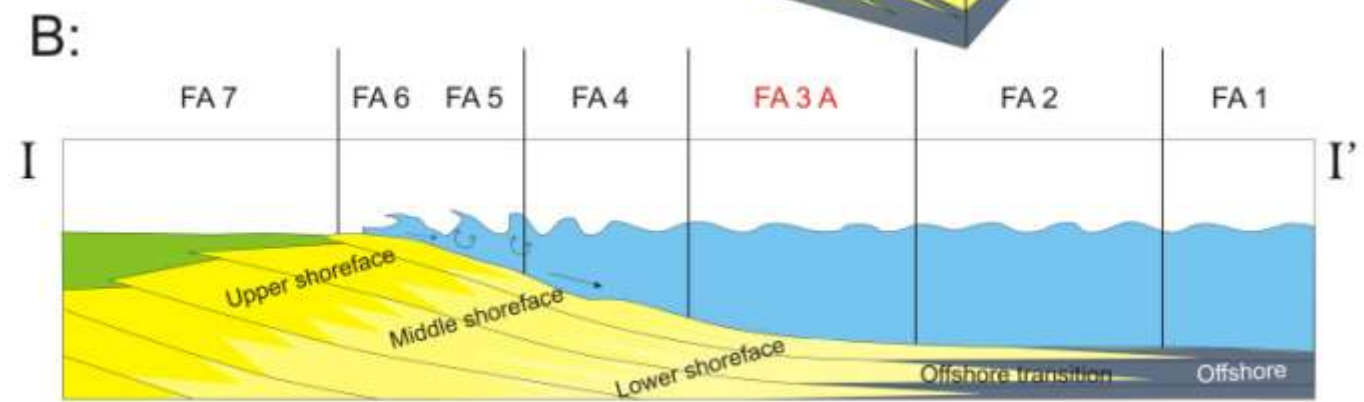
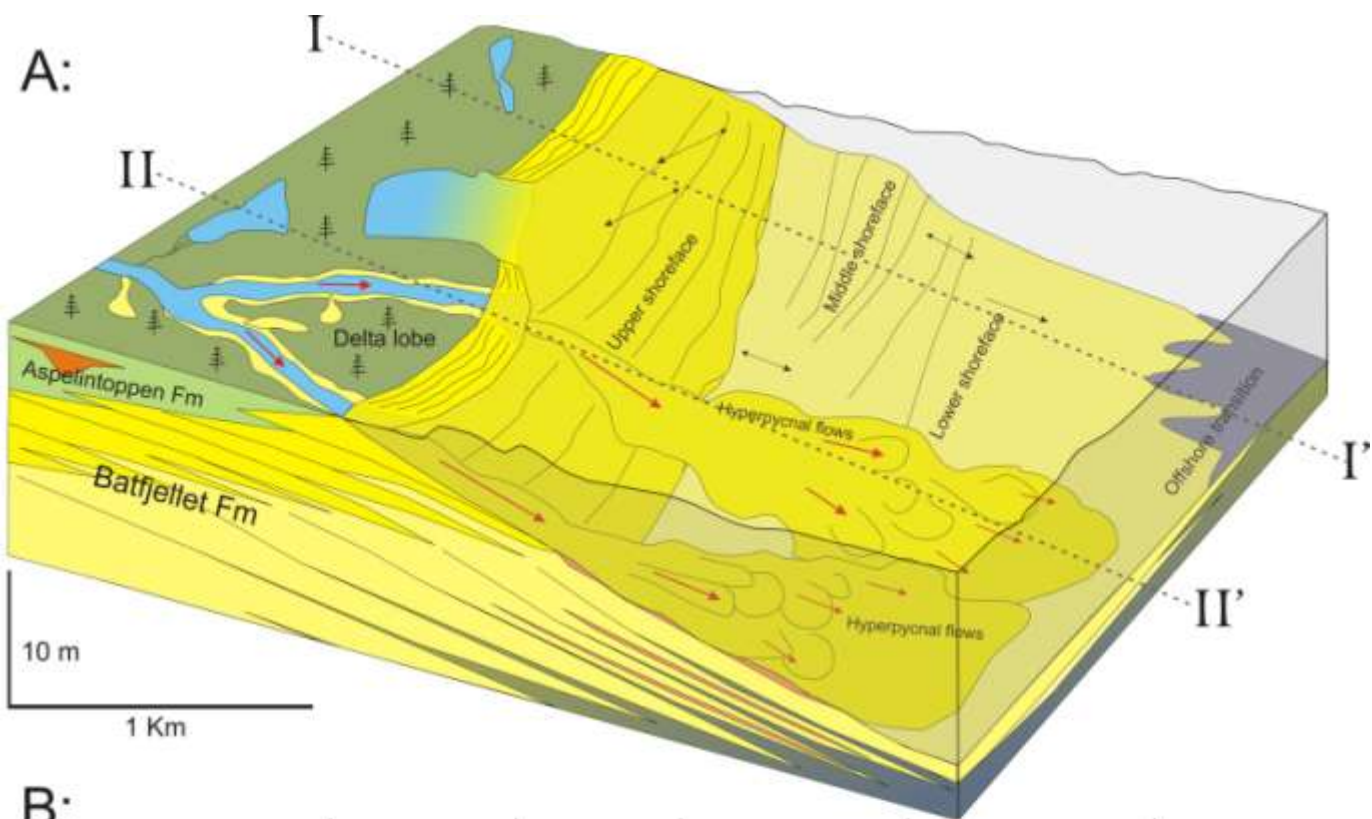


Figure 7.1 (Previous page):

A: Schematic block diagram illustrating the various depositional environments of the facies associations recognized in the study area. The delta front is strongly influenced by wave processes but in front of the fluvial channel mouths hyperpycnal under-flows may develop. The dashed lines illustrate the position of the respective dip parallel transects presented in Figure 7.1 B.

B: Two delta front transects where the upper one represents a delta front depositional environment dominated by wave processes. The lower one shows a more fluvial influenced delta front with hyperpycnal flow development.

As described in chapter 3, the concentration of hyperpycnal flow deposits in the lower/middle shoreface is expected to be higher for successions being deposited in front of the river mouth. The total concentration of hyperpycnal flow deposits (hyperpycnite thickness in relation to the total shoreface thickness) is plotted in Figure 7.2 to illustrate the variability of the facies association in the study area. It is worth noting that the eastern Ringdalsfjellet and southeastern Mefjellet, which are areas interpreted to have experienced slope failure as a result of a high local sediment supply (Chapter 6), both have a fairly high concentration of hyperpycnal flow deposits.

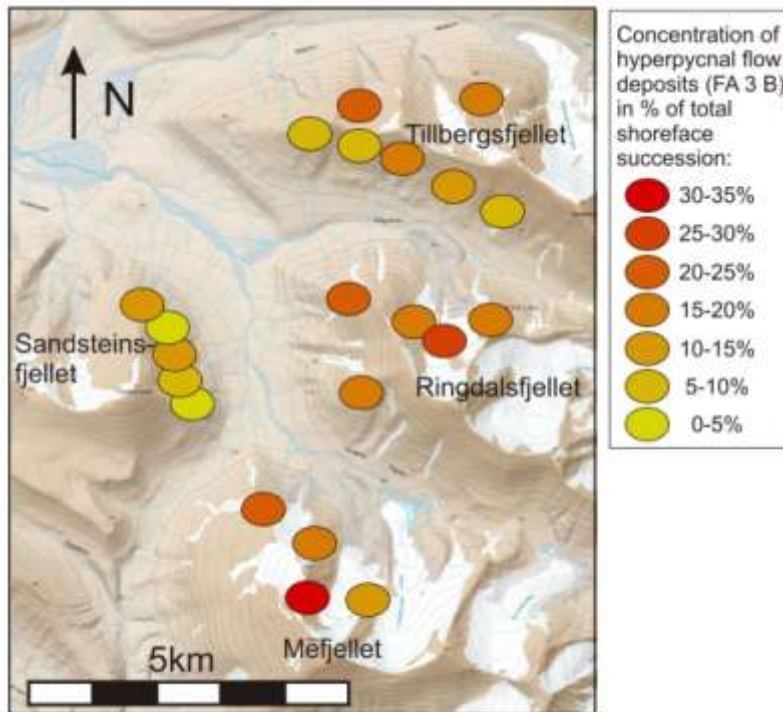


Figure 7.2:
Concentration of hyperpycnites (% of total shoreface thickness) illustrated in colours ranging from yellow (low concentration) to red (high concentration). See Figure 1.2 for names of the logged sections.

By plotting the thickness of the hyperpycnal flow deposits for individual parasequences (Chapter 6), a clear trend in the spatial distribution of the facies association (FA3-B) was observed. For any given parasequence, the logged sections containing thick sections of hyperpycnal flow deposits tend to be clustered in specific areas. It is tentatively suggested that the position of these clusters indicate a position in front of a terminal distributary channel. This trend is most evident for the parasequences stretching the entire N-S oriented width of the study area (P5-P7), where a shift in the clusters is registered between the different parasequences (*Figure 7.3*). The shifts imply a lateral shift in the order of 3,4-5km, which is in concordance with the estimated lateral distribution of the parasequences.

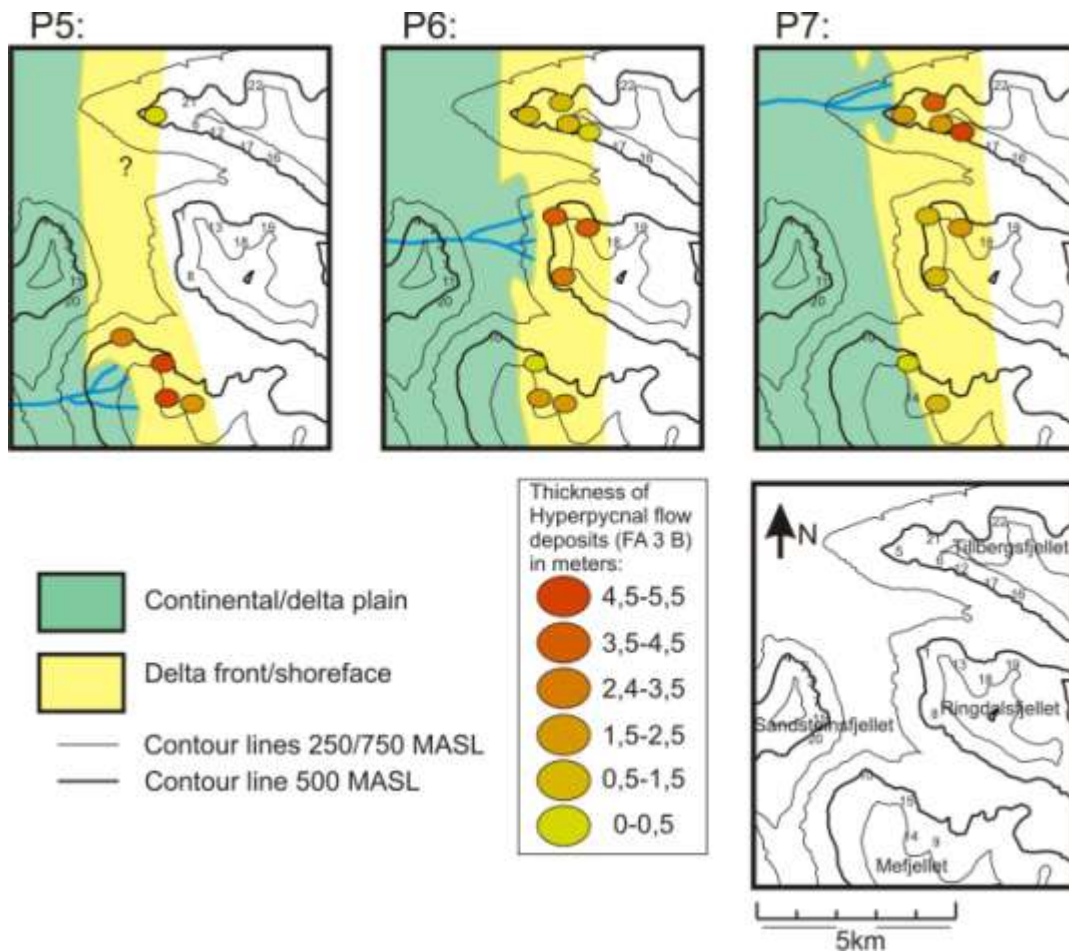


Figure 7.3: Overview maps of the study area showing the distribution and thickness of hyperpycnites of the different logged sections at P5, P6 and P7. The thickness of hyperpycnites at the various logged sections is marked with colours ranging from yellow (thin) to red (thick). Simplistic illustration of the inferred position of the delta lobe for the different parasequences is provided. See Figure 6.2 for parasequence distributions.

7.2 Formation boundaries:

The Frysjaodden, Battfjellet and Aspelintoppen formations represent different depositional environments of the same overall progradational deltaic system. Segments of each of the formations occurred simultaneously, thus the boundaries are diachronous; no major sequence stratigraphic surfaces/hiatus separate the formations.

The transition between the underlying offshore/shelf deposits of the Frysjaodden Formation to the shoreface succession of the Battfjellet Formation is put at the base of the first occurrence of an interpreted tempestite bed of FA2 (Chapter 3).

The transition between the Battfjellet Formation and the overlying Aspelintoppen Formation is complicated and usually not well exposed. Only at one single locality (L3S2 on Sandsteinsfjellet) has the contact between the two formations been observed (excluding locations where fluvial channels cut into shoreface deposits) (Figure 7.4). At this particular location there is a sharp transition between foreshore (FA6) deposits of the Battfjellet Formation and floodplain (FA7-B) of the Aspelintoppen Formation. Outcrops of floodplain deposits immediately above the Battfjellet formation are rare; interdistributary bay deposits (FA7-A) are most commonly the first occurring exposed deposits of the Aspelintoppen Formation.

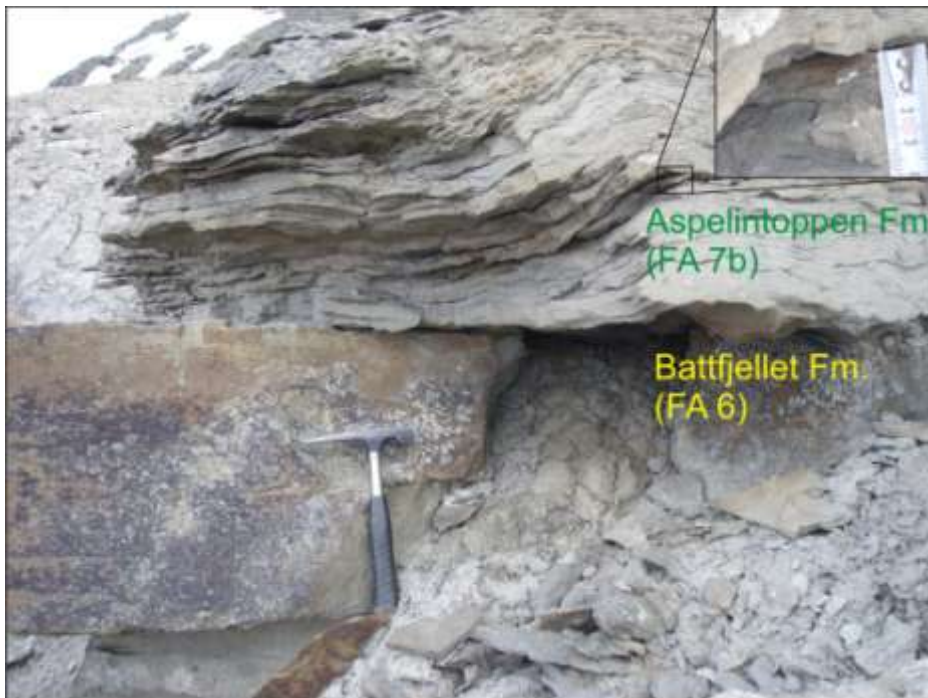


Figure 7.4:
The boundary between foreshore (FA6) deposits of the Battfjellet Formation and floodplain deposits (FA7b) of the aspelintoppen Formation at L3S2. The picture in the upper right corner is of an in situ fossilized leaf.

Pinpointing the boundary between the two formations is often difficult because of the lack of exposures. The boundary is put at the top of the exposed Battfjellet Formation if the uppermost section consists of foreshore deposits (FA6). In cases where the uppermost section of the formation is missing, and deposits of more distal facies associations makes out the topmost exposures, the boundary is conceptually placed, based on expected thicknesses observed at other logged sections. The boundary between the two formations seems to be relatively sharp all over the area with no observed interfingering pattern. The lack of profound interfingering between the two formations is likely to be a result of the limited transgressions between the parasequences caused by autogenic delta lobe switching (see discussion below).

7.3 Sequence stratigraphy:

The limited extent of the study area and the overall progradation of the Battfjellet delta system make it difficult to apply traditional sequence stratigraphic concepts (e.g. Haq et al., 1987; Galloway, 1989; Van Wagoner et al., 1990; Embry and Johannesen, 1992) in the stratigraphic interpretation. The apparent absence of deposition during relative sea level fall together with the absence of major flooding events makes a subdivision into system tracts inapplicable. For this reason, a model independent approach on the basis of ascending and descending regressive and transgressive shoreline trajectories (c.f. Helland-Hansen and Gjelberg, 1994; Helland-Hansen and Martinsen, 1996; Helland-Hansen and Hampson, 2009) will be applied.

The shoreline trajectory is dependent on factors like sediment supply, basin topography, eustasy and subsidence (Helland-Hansen and Martinsen, 1996; Helland-Hansen and Hampson, 2009). The Battfjellet deltaic system is part of a regressive megasequence, incorporating Frysjaodden and Aspelintoppen formations. As a result of its position in a foreland basin, adjacent to an ongoing orogen, the deltaic system was laid down concomitant with high sedimentation and high subsidence conditions.

The overall progradational pattern for the Battfjellet Formation is well known and has been documented by many workers (e.g. Kellogg, 1975; Steel, 1977; Helland-Hansen, 1990). The formation shows a general progradational and aggradational pattern with parasequences

generally stepping basinward with a shoreline trajectory at a relatively low ascending angle, although local variations of the trajectory occur. Descending shoreline trajectories (forced regressions) are not commonly recorded in the Battfjellet Formation but a few exceptions have been documented (eg. at Høgsynta; Plink-Bjørklund and Steel, 2002). Descending regressions observed in the formation are in large part restricted to the western clinothem forming area of the basin, and no descending regressions have been observed in area of the present study.

Fluvial channels cutting into shoreface deposits have been observed at two of the logged sections (L11S5 and L8R2). Although often indicative of a descending regression (RSFE), these channel erosions are not interpreted to be so as there are no other indications of a descending regression along the same parasequences, and since fluvial channels have the capacity to erode below sea level (c.f. Bhattacharya, 2006).

Interpreting the key factors controlling the shoreline trajectory at different segments of the overall progradation is often speculative. A relatively strong aggradational component with a more strongly ascending trajectory, as observed between P6 and P10 along the Tillbergsfjellet transect (Chapter 6; *Figure 6.7*), can be a result of different factors. Aggradational shoreline trajectories could take place in abandonment areas, marginal to active sediment supply systems where the local sediment supply is relatively low. In addition, a high subsidence rate generating increased accommodation space could result in a strongly ascending trajectory, even in front of an active sediment supply system. Similarly, a strong progradational low angle ascending shoreline trajectory could be a result of high sediment supply or low subsidence rate. It is tentatively suggested that sediment supply is the driving mechanism of these factors, as switching of delta lobes easily explains the variations both along strike and dip of the coastline.

Relative sea level variations as a consequence of the combined effect of eustasy and tectonically driven subsidence may be an important factor influencing the progradational pattern. High frequent large scale eustatic sea level fluctuations are not documented for the Eocene Epoch and no glaciations have been reported from the literature. However, eustatic sea level fluctuations due to other processes might have taken place. It is tentatively suggested that the absence of descending regressions, as may be an expected response to eustatic sea level

falls, is a result of the high subsidence rate of the basin (*Figure 7.5*). If the subsidence rate is sufficiently high, the effect of eustatic sea level fall might only result in a still stand or reduced rate of the relative sea level rise. This would result in a more rapid progradation and basinward forward stepping of the parasequences.

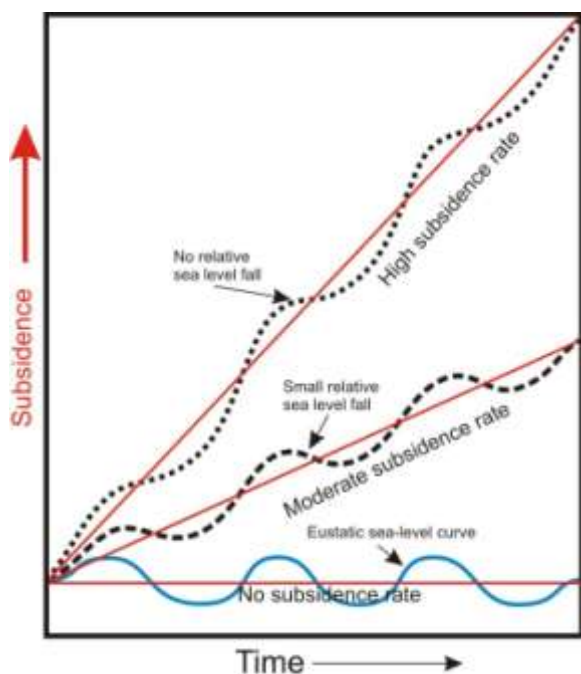


Figure 7.5:
The figure shows how a rhythmic relative sea-level curve will be influenced by different basin floor subsidence rates. A fall in eustatic sea level fall may not result in relative sea level fall if the subsidence rate is high enough.

In most locations the parasequences show a progradational vertical stacking pattern, with a more proximal internal facies distribution in stratigraphically higher parasequences. However, locally retrogradational stacking patterns are present, such as on P2 on Sandsteinsfjellet (Chapter 6: *Figure 6.5*). Although retrogradational stacking patterns may be observed locally, it is not necessarily diagnostic of an overall retreating shoreline, but may rather reflect a lateral lobe change, with temporarily low sediment supply at the abandonment.

The cause of the non-accretionary transgressions separating the parasequences can be the result of tectonically driven subsidence, eustasy, or simultaneous variations along strike of the coastline due to autogenic processes. Autogenic lobe switching, where the shoreline regress at the delta lobe (high local sediment supply), and simultaneously transgress at the strandplain (low local sediment supply) best explains the limited lateral extent and the complex stacking

pattern of the parasequences as described in Chapter 6 (Figure 7.6). The negligible amount of transgressive deposits supports this notion, as a transgression caused by allogenic processes (eustasy or tectonically driven subsidence) is more likely to transgress over larger area of the low gradient delta plain (Helland-Hansen, 2010). Autogenic process has been recognized as a driving mechanism for generating low order sequence stratigraphic surfaces, and the vast majority of the studies conducted on Battfjellet Formation has recognized delta lobe switching as the driving mechanism in generating the transgressions separating the parasequences (e.g. Helland-Hansen, 1990; Olsen, 2008; Stene, 2009; Helland-Hansen, 2010; Skarpeid, 2010).

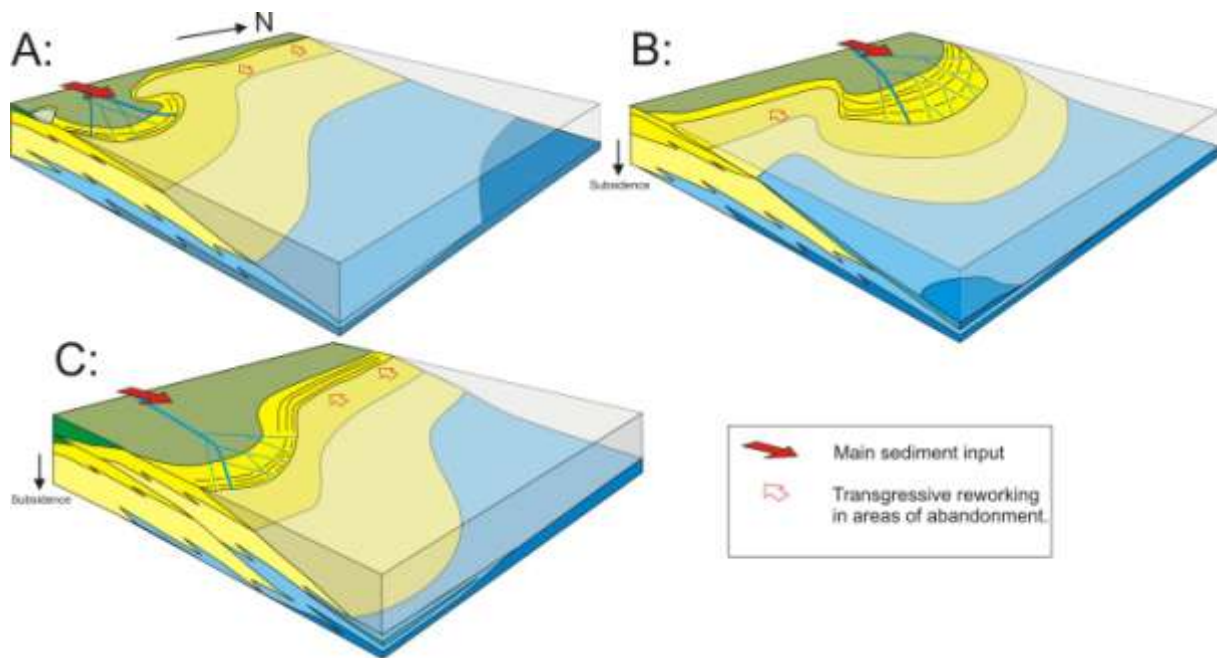


Figure 7.6: Schematic illustrations showing the generation of parasequences as a result of autogenic lobe switching. The delta front progrades at the front of the delta lobe as a result of high sediment supply, and simultaneously transgress at the abandonment areas where the sediment supply is cut off.

The transgressive unit observed between P6 and P7, that stretches the entire N-S oriented width of the study area, is unusual. It is tentatively suggested that this transgression represent a more dramatic lobe switch (see discussion below). It may also be related to allogenic processes such as tectonically driven subsidence or a rise in sea level caused by eustasy. As described in chapter 6, there are uncertainties in correlating parasequences over vast distances. The correlation of P6 and P7 is in large part based on their position immediately below and

above the transgressive unit. If the mechanism resulting in the formation of the transgressive unit is of a superior order relative to that of the parasequence generating mechanism, the transgressive unit may cap several parasequences along deposition strike. The parasequences correlated as P6 and P7 may thus represent more than one parasequence respectively.

Because of the variable size of the recorded fluvial channels (Chapter 3; FA7-C1 and FA-7C2) and different degrees of avulsion at different sections of the delta plain, it is reasonable to assume that the delta lobe switching mechanism may develop in a hierarchy (*Figure 7.7*). On a speculative level, three such hierarchy levels are proposed:

- Channel switching within a delta lobe
- Delta lobe switching
- Delta switching

The highest frequency cyclicity, which is connected to active channel switching within the delta lobe itself, would probably not cause any bigger influence on the depositional pattern other than that of local variance of fluvial influence within parasequences. The intermediate hierarchy level on the other hand, representing avulsion of channels on the lower delta plain, results in lobe switching, and is responsible for the parasequence distribution pattern (see discussion above). The highest order switching mechanism, that may take place as a consequence of major avulsions or river captures at more proximal sections of the delta plain, could result in a switch in the entire delta. This is not well documented and remains highly speculative. The result of this kind of switching would normally effect the entire study area, and the lack of continuous exposures makes it difficult to document. There is little relevant literature available about this topic, delta lobe switching mechanisms are discussed in various papers (e.g. López-Blanco et al., 2000; Correggiari et al., 2005; Prélat et al., 2009), but a higher order switching of the entire delta is not incorporated in these discussions.

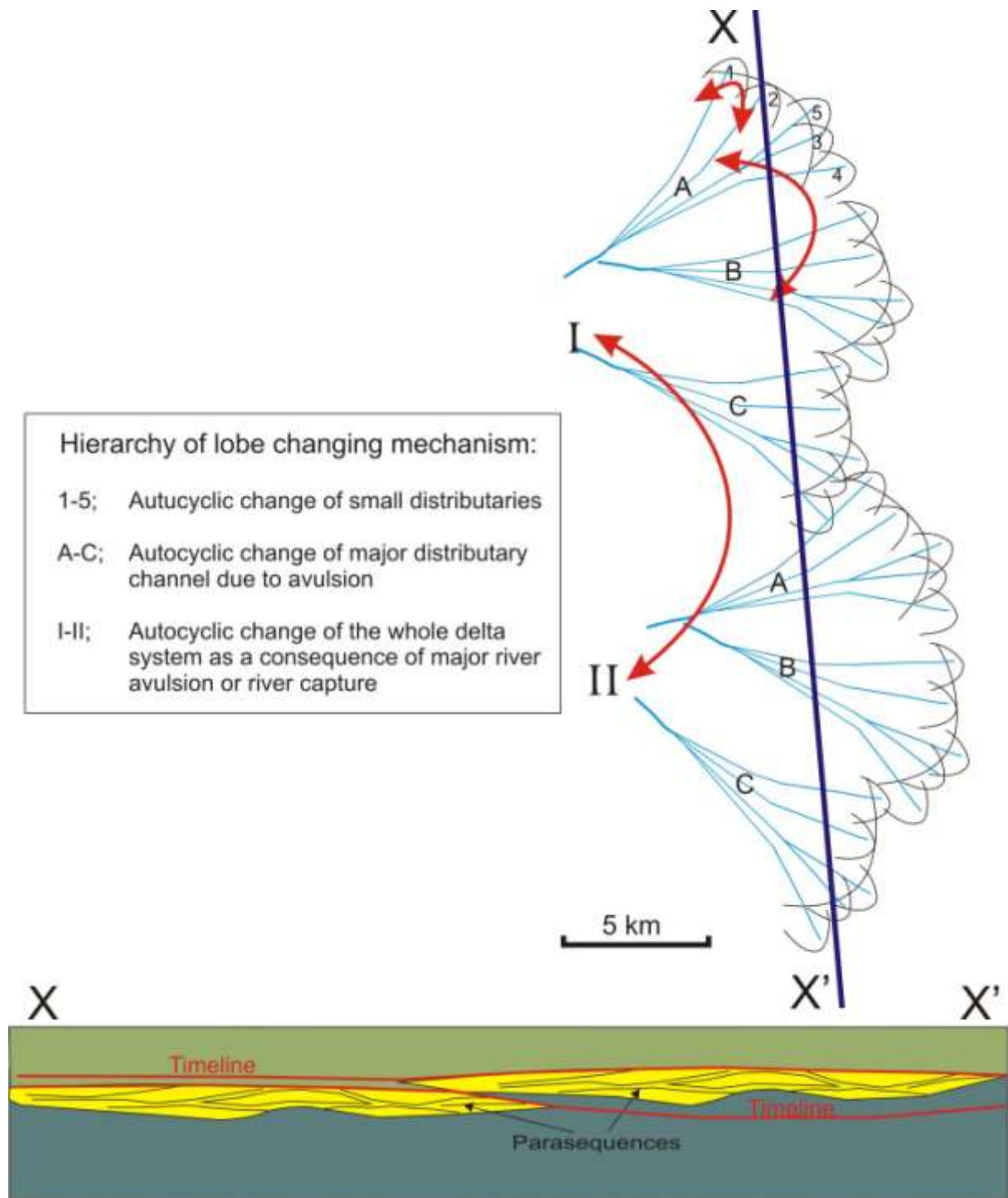


Figure 7.7:
 Figure illustrating the different proposed hierarchy levels of delta lobe switching. 1-5 illustrates channel switching within delta lobes. A-C illustrates switching of delta lobes, while I-II illustrates switching of the entire delta. X-X' is a schematic transect illustrating the possible geometry along depositional strike, with internally stacked parasequence within two different delta systems.

7.4 Delta Type:

A deltaic origin of the succession is evident from the distributary channels cutting into the shoreface deposits, the delta plain depositional environment of the overlying Aspleintoppen Formation, the texturally immature sediments (Helland-Hansen, 2010), and the lobate shoreline morphology, as inferred from the parasequence stacking pattern. The shoreface succession of the Battfjellet formation shows a predominance of structures generated by (wave driven) oscillatory currents (Chapter 3), indicating a wave dominated depositional environment. This is in contrast to the perceived delta lobe morphology of the delta, as delta lobes are a feature associated with fluvial dominated deltas. Problems related to coupling the internal facies architecture of a deltaic depositional system with classification schemes related to the delta morphology has been addressed in recent studies of deltaic systems (Helland-Hansen, 2010 and references therein). Helland-Hansen (2010) classified the Battfjellet delta system as a *fluvio-wave interaction delta*, based on the indicative features of both fluvial and wave action. Helland-Hansen (2010) argued that the abundance of soft sediment deformation structures together with the texturally immature composition of the sandstones testify to a system of high sediment supply. Furthermore, the texturally immature composition reveals that the dispersion of the sediment due to wave action was limited. A texturally mature composition would be expected in a wave dominated delta where wave induced coast parallel currents is the main sediment distributing factor.

The observations made in the present study supports the classification by Helland-Hansen (2010). Additional criteria contributing to this classification, is the recognition of short duration hyperpycnal flow deposits in the delta front succession, which are indicative of fluvial induced sedimentation. In addition, the slope failure structures described in chapter 6 supports the notion that system is of a high sediment supply (see discussion above).

7.4.1 Modern analogues

The Po delta, facing the Adriatic Sea on the northeastern coast of Italy has been brought up as a possible modern analogue to the Battfjellet deltaic system by various workers (Olsen, 2008; Helland-Hansen, 2010; Skarpeid, 2010). As with the Battfjellet deltaic system, The Po delta (*Figure 7.8*) has been classified as a fluvio-wave interaction delta (Helland-Hansen, 2010;

Galloway 1975). Autogenic lobe switching of the delta lobes have been recognized as a parasequence generating mechanism for the Po delta (Correggiari et al., 2005).



*Figure 7.8:
Picture of the Po delta
showing the typical
morphology of a fluvio-
wave interaction delta.
However, the size of the
delta is larger than the
deltas of the Battfjellet
Formation (picture from
Google Earth).*

Another modern delta that may have some similarities with the Battfjellet Formation delta system is the lacustrine Slave Delta in the Great Slave Lake in Arctic Canada. This delta is strongly fluvial dominated but also wave influenced (Smith, 1991). The main difference between this delta and the Battfjellet delta system is the complete lack of tidal processes in the lacustrine Slave Delta. The fresh water conditions of the former delta may also represent a significant difference from the studied marine Battfjellet Formation. On the other hand, it has been tentatively suggested that the Central Tertiary Basin could be strongly fresh water influenced in periods (Chapter 4: FA3-B discussion). The delta is comparable to the Battfjellet Formation both in size and morphology and may also be useful in order to demonstrate the transition between delta plain and delta front environment. This transition is sharp, but may also develop in an oblique aggradational pattern with some interfingering between the continental and marine facies in situations where the shoreline trajectory is aggradational (Figure 7.9).

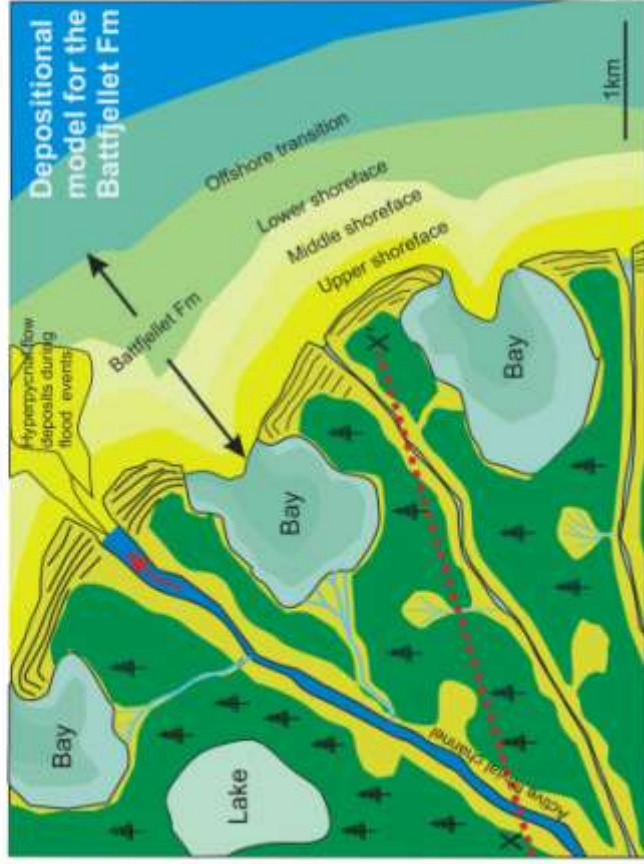
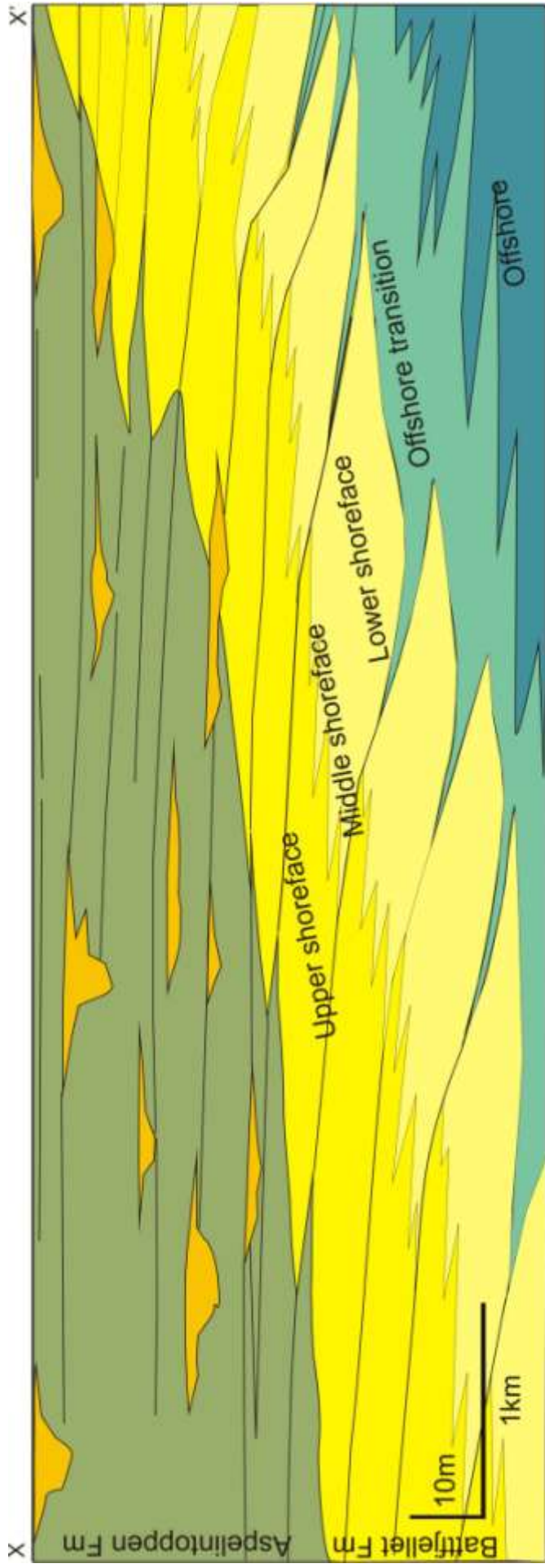


Figure 7.9 (Previous page):

Schematic cross section along dip direction of the Batfjellet Formation, showing the parasequence development and stacking pattern together with the relationship between the Aspelintoppen and Batfjellet Formations. The two figures below show a depositional model of the Batfjellet Aspelintoppen Fms, and a modern analogue represented with the delta of the Slave Delta in the Great Slave Lake.

7.4.2 Delta size

The size of an individual parasequence gives a rough estimate of the size of the individual delta lobes. As pointed out in Chapter 6, there are uncertainties in estimating the length of individual parasequences along strike. Individual parasequences have locally been estimated to exceed the width of the study area of 10km (Chapter 6; P6 and P7). However, the lengths of parasequences, as observed by Helland-Hansen (2010) at other locations on Nordenskiöld Land, was in the range of a few km up to 10km. Helland-Hansen (2010) further argued that the geological setting, with a relatively small basin and a short distance to the catchment area, points to the formation of a relatively small delta. It is thus suggested that the length along strike of an individual parasequence does not exceeds 10km by much, and a range of a few km to approximately 15km is tentatively suggested. The deltaic system is likely to consist of several simultaneously active delta lobes, at variable spatial distributions along the coastline. An estimate of the total delta size will not be conducted in the present studies because of the limited extent of the study area.

7.5 Basin geometry

The general paleogeographic setting and depositional environment for the Eocene succession in the Central Tertiary Basin have been described and well documented by many authors. A foreland basin with an eastward migrating deltaic system is a common perception applied in these models (Chapter 3.3.3). The present studies support these criteria as a framework for the depositional environment. Flexure as a result of tectonic loading related to thrust nappes, is most commonly perceived as the driving mechanism for the subsidence of the Central Tertiary Basin (e.g. Steel et al. 1985; Bruhn and Steel 2003) (Chapter 3.3.3). However, in the recent years an alternative explanation, with the possibility of the subsidence being a result of long wavelength compressional flexure has been debated (Nichols and Lüthje, 2008; Olsen, 2008).

Olsen (2008) argued that loading by thrust nappes as the sole factor controlling the subsidence cannot accommodate for the thick sedimentary succession of the basin, if assuming a purely compressional regime. Olsen (2008) further argued that the strike-slip component of the tectonic regime of the West Spitsbergen Orogen could influence the basin geometry, and that a transpressional regime generates deeper and less wide foreland basins, than that of foreland basins generated by purely compressional regimes. The presence of extensive thrust planes in the western part of Spitsbergen is well known and documented (see Chapter 3.3.2). This suggests that flexure as a result of thrust nappes loading, at least partially, played a role in the subsidence of the basin.

As described in Chapter 3.3.3, there is a marked shift in the basin evolution from the mainly east derived lower succession of the Firkanten, Basilika and Grumantbyen formations (Steel et al. 1985; Bruhn and Steel, 2003), to the upper west derived succession of the Frysjaodden, Hollendardalen, Battfjellet and Aspelintoppen formations. As it exceeds the scope of the present study, no evaluation of whether the lower succession is of a transtensional setting (Steel et al., 1985), a foreland setting with a peripheral forebulge as sediment source (Bruhn and Steel, 2003), or of a compressional flexure generated setting (Nichols and Lüthje, 2008), will be conducted. The upper westerly derived succession of the basin conforms to the main phase of deformation, with substantial uplift of the hinterland in most of these models. This phase of deformation conforms to stage 2 and 3 in the model of the tectonic evolution of the West Spitsbergen Orogen by Bergh et al. (1997), and Braathen et al. (1999). Figure 7.10 illustrates the formation of the upper section of the Central Tertiary Basin in relationship with the tectonic movements of the orogen:

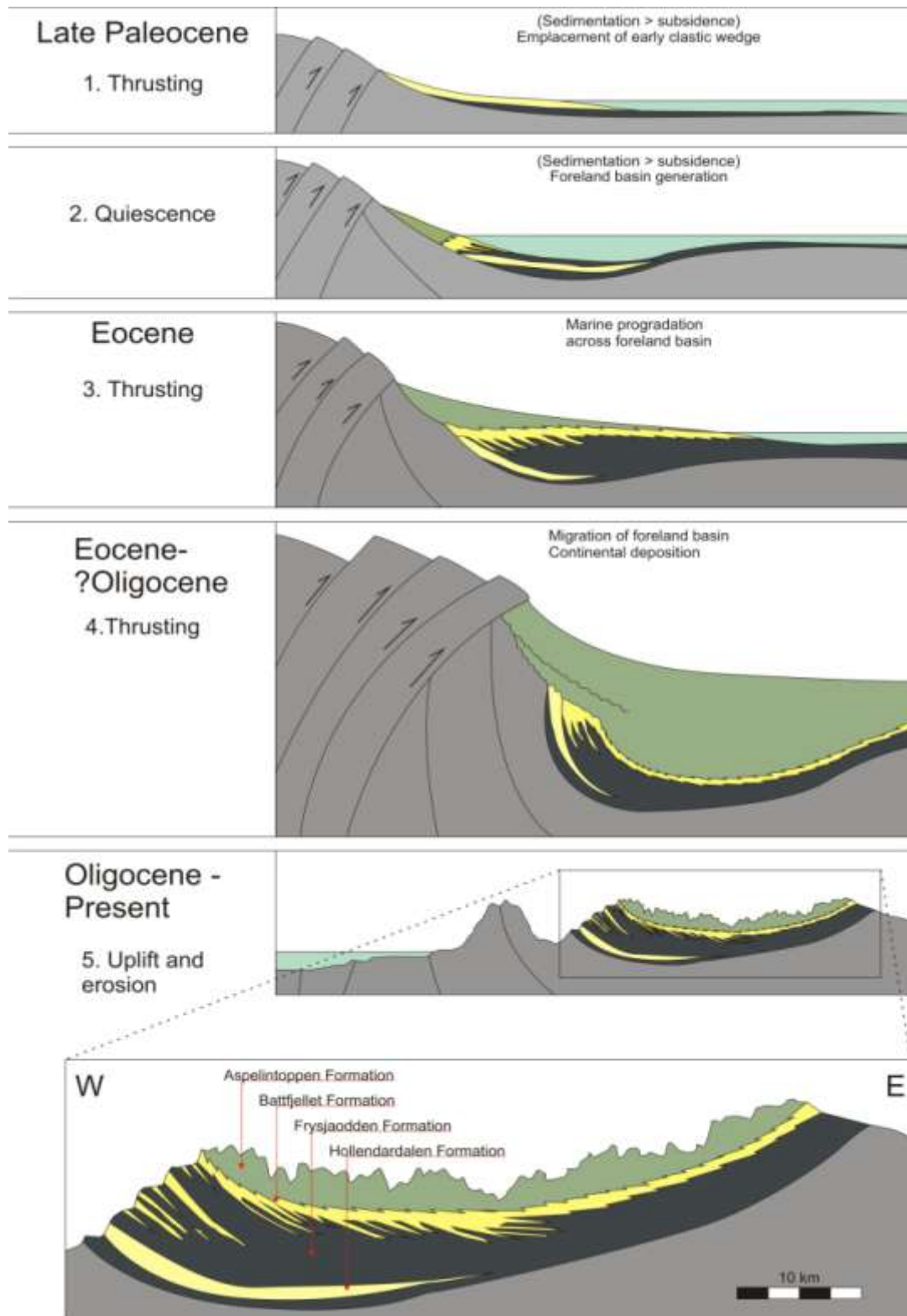


Figure 7.10: Schematic figures illustrating the Late Paleocene to Oligocene basin development of the Central Tertiary Basin. The lowermost figure shows a simplified section of the present day setting of the basin (Redrawn from Helland-Hansen, 1985; Steel et al. 1985).

The lack of basin floor fan deposits in the study area (with the exception of fine grained fringe deposits-Chapter 4), differs from localities in the south and west in the basin where well developed clinofans and basin floor fans are common (eg. Van Keulenfjorden).

Helland-Hansen (2010) explained this to be an effect of shallower waters in the eastern areas of the basin. The eastward shallowing of the basin was explained to be a result of the combined effect of the more distal position in the basin, with less crustal downwarping (less subsidence), and due to infill of the eastern basin from suspension derived mud as the deltaic system prograded in the west. This theory is supported by the observed shallowing eastward trend of the basin floor fans in the basin (Stene, 2009; Olsen, 2008), and the eastward thinning of the Hollendardalen, Frysjaodden and Battfjellet formations towards the east, as derived from isopach maps (*Figure 7.12.*). Figure 7.11 shows conceptual illustrations of the basin setting of the western and eastern area:

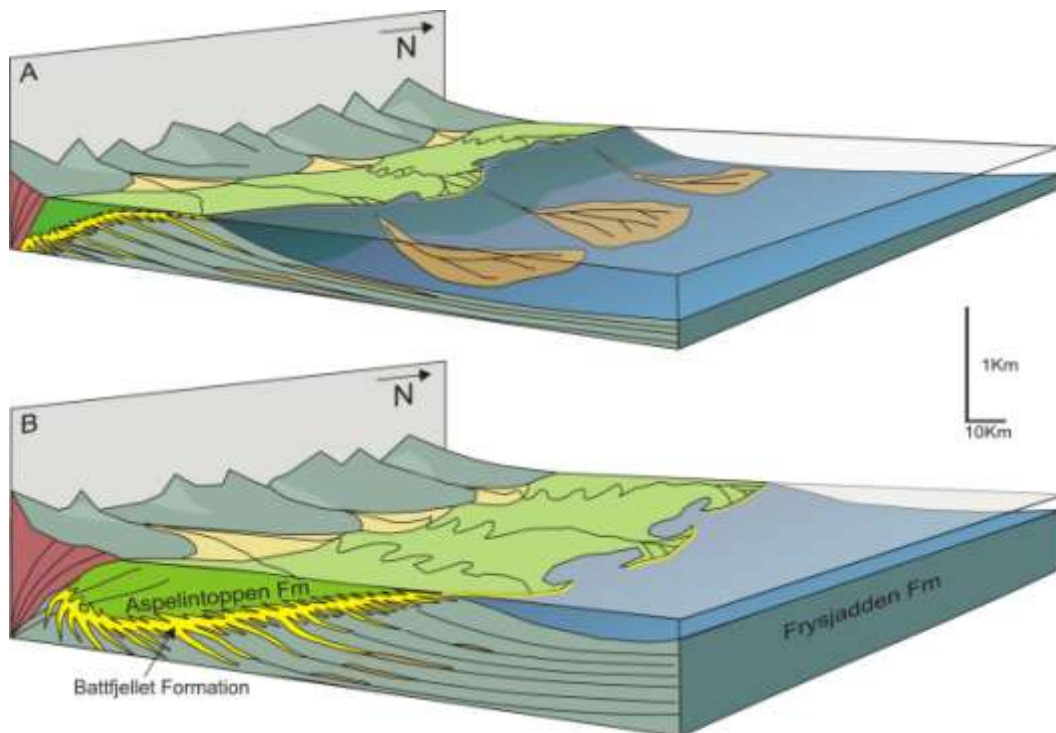


Figure 7.11: Simplified regional paleogeographic model for the Battfjellet Formation showing the development from the West Spitsbergen Orogeny with the eastward progradation and aggradation through time. Basin floor fan deposits developed at a relative early stage when the delta plain/shelf was relative narrow (A). Later when the delta front reached a more easterly position such depositional systems ceased to develop (B).

The asymmetric fill of the basin can be illustrated by plotting the thickness of the westerly derived succession of the basin in an isopach map (Helland-Hansen, 1985; Olsen, 2008; Stene, 2009; Skarpeid, 2010). This includes the Marstranderbreen Member (Frysjaodden Formation), the Hollendardalen Formation, the Gilsonryggen Member (Frysjaodden Formation) and the Battfjellet Formation (*Figure 7.12*). As the Aspelintoppen Formation has no exposed upper boundary, it is not included in the isopach map. Near log L6T1, at Tillbergsjellet north in the study area, the combined thickness of the Gilsonryggen Member and the Battfjellet Formation is 357m. Sætre and Hanevik (2010, personal communication), measured a thickness of 41m for the Marstranderbreen Member and the Hollendardalen Formation at the northwestern part of Ringdalsfjellet. The combined thickness of the Hollendardalen, Frysjaodden and Battfjellet formations in the study area is thus roughly 400m. This value roughly fits within the generalized contours of the isopach map but is slightly less. The NW/SE orientation of the contours is in contrast to the assumed N-S orientation of the paleo-coastline (Chapter 5). This may reflect local variations of the coastline due to variations of the sediment influx pattern. The last basin floor fan complex observed in an eastern direction at various positions in the basins is roughly parallel with the isopach contours, and the termination occur roughly between the 500 and 600 meters contours (*Figure 7.12*).

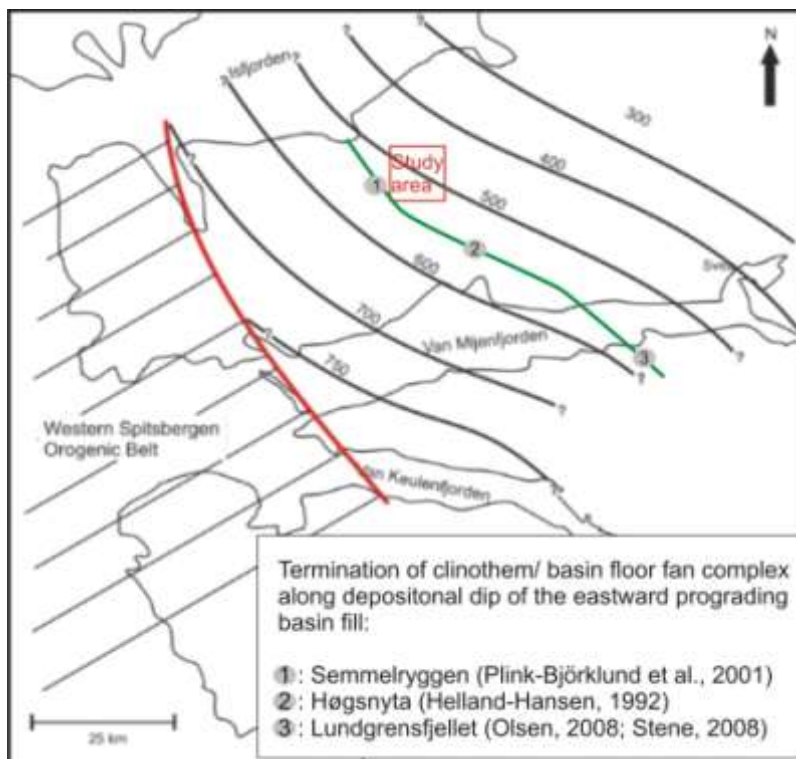


Figure 7.12: Isopach map for the Hollendardalen, Frysjaodden and Battfjellet formations. The green line represents the easternmost extent of the basin floor fan deposits. The grey dots represent areas where such deposits have been recorded (Modified from Helland-Hansen 1985; Olsen, 2008; Stene 2009 and Skarpeid, 2010).

8. Summary and conclusions

The sedimentological development, facies distribution and parasequence geometry and stacking pattern of the Eocene Battfjellet Formation in the central western Nordenskiöld Land is the focus of the present study. A total of twelve aggrading and forward stepping parasequences of a fluvio-wave dominated deltaic origin are recognized.

The Battfjellet Formation constitutes the delta front/shallow marine section of an eastward prograding deltaic system in a foreland basin setting, adjacent to the West Spitsbergen Orogen. The formation has been thoroughly studied for many years, but most of these studies were carried out on localities that are located in a more proximal position with respect to the provenance area, and where both clinothems and basin floor fans are well developed. In the area of the present study, neither clinothems nor well developed basin floor fans are present.

The main conclusions of the study are summarized in the following five paragraphs:

1. The studied successions have been subdivided into facies associations on the basis of depositional environment from a basinal to a landward position. A complete lateral and vertical compilation of these facies association represents the gradual transition from offshore/shelf (FA1), through offshore/transition (FA2), lower shoreface (FA3), middle shoreface (FA4), upper shoreface (FA5), and foreshore (FA6), to the continental deposits of the Aspelintoppen Formation (FA7). Individual parasequences, as observed vertically at the logged sections, consists of a conformable succession of gradually more proximal facies associations, in concordance with Walther's law.
2. The Battfjellet deltaic system has been classified as a fluvio-wave interaction delta. In contrast, the shoreface succession (FA3-FA5) shows a predominance of wave generated structures. The interpretation of direct fluvial influence as reflected by the presence of hyperphycnal flow deposits (FA3-B) is a new way to interpret the parallel laminated beds in alternation with symmetrical small ripples. The distribution of hyperphycnal flow deposits is relevant in order to identify areas where fluvial input has been high and hence the paleo-position of fluvial channels in a landward position.

3. The size, stacking pattern and progradational pattern of parasequences are information that are important in the understanding of the delta building mechanisms, and show that the parasequences develop across a typical distance of 2-3km in the depositional dip direction and over a distance of a few km to 15 km in the depositional strike direction. The parasequences are stepping forwards in a complex manner reflecting the autocyclic switching of delta lobes. A hierarchy of delta lobe switching mechanisms have been suggested, where the highest frequency is related to main distributary channel switching, the second hierarchy to delta lobe switching (with parasequence development) and the third hierarchy (lowest frequency) is related to the entire delta switching.
4. The paleogeographic setting, as inferred from the present study, is consistent with the general understanding of the basinal configuration as established in earlier studies. This is also supported by paleocurrent data, revealing a N-S orientation of the symmetrical ripple crests.
5. The lack of well developed basin floor fan and clinothems in the study area contrasts to the observations in many other localities, such as the Van Keulenfjorden and Western part of the Van Mijenfjorden area where such deposits usually are present. The lack of such deposits is likely to be a consequence of gradually shallower water depths, as the system progrades to the east.

Suggestions for further work

Even though the present study may contribute to the understanding of interacting processes in a fluvio-wave interaction delta, and the understanding of sandbody stacking patterns, there are still many questions to be answered. Further work should focus on parasequence mapping and correlation, combined with further studies on the lobe switching hierarchy. The latter has only briefly been touched in this thesis and needs further elaboration. It may also be useful if the concept of delta front hyperpycnites could be further elaborated and mapped in a more regional setting in order to understand the distribution of the fluvial input spatially. Furthermore, the understanding of the development of the basin and basin fill in response to the tectonic evolution of the West Spitsbergen Orogen should be elaborated.

9. References :

- Allen, P.A. & Underhill, J.R. (1989). Swaley cross-stratification produced by unidirectional flows, Bencliff Grit (Upper Jurassic), Dorset, UK, *Journal of the Geological Society*, April 1989, V. 146, No. 2, pp. 241-252.
- Baas, J.H. (2000). EZ-ROSE: a computer program for equal-area circular histograms and Statistical analysis of two-dimensional vectorial data. *Computer & Geoscience*, V. 26, No. 2, pp. 153-166.
- Bergh, S.G., Braathen, A. & Andresen, A. (1997). Interaction of Basement-Involved and Thin-Skinned Tectonism in the Tertiary Fold-Thrust Belt of Central Spitsbergen, Svalbard. *AAPG Bulletin*, V. 81, No. 4, pp. 637-661.
- Bhattacharya, J.P. (2006). Deltas. *SEPM*, No. 84, pp. 237-292.
- Bhattacharya, J.P. & MacEachern J.A. (2009). Hyperpycnal Rivers and Prodeltaic Shelves in the Cretaceous Seaway of North America. *Journal of Sedimentary Research*, V. 79, No. 4, pp. 184-209.
- Birkenmajer, K. (1975). Caledonides of Svalbard and plate tectonics. *Dan. Geol. Foren.*, V. 24, No. 1-19.
- Blythe, A.E. & Kleinsphen, K.L. (1998). Tectonically versus climatically driven Cenozoic exhumation of the Eurasian plate margin, Svalbard: Fission track analyses. *Tectonics*, V. 17, pp. 621-639.
- Boggs, S. (2006). Principles of sedimentology and stratigraphy, Upper Saddle River, N.J., Pearson Prentice Hall.
- Braathen, A., & Bergh, S.G. (1995). Kinematics of Tertiary deformation in the basement-involved fold-thrust complex, western Nordenskiöld Land, Svalbard: tectonic implications based on fault-slip data analysis. *Tectonophysics*, V. 249, pp. 1-29.
- Braathen, A., Bergh, S.G., & Maher, H.D., Jr (1999). Application of a critical wedge taper model to the Tertiary transpressional fold-thrust belt on Spitsbergen, Svalbard. *Geological Society of America Bulletin*, V. 111, No. 10, pp. 1468-1485.
- Bruhn, R. & Steel, R. (2003). High resolution sequence stratigraphy of a clastic foredeep succession (Paleocene, Spitsbergen): an example of peripheral-bulge-controlled depositional architecture. *Journal of Sedimentary Research*, V. 73, pp. 745-755.
- Buatois, L.A., Gingras, M.K., Maceachern, J., Mángano, M.G., Zonneveld, J-P., Pemberton, S.G. Netto, R.G. & Martin, A. (2005). Colonization of Brackish-Water Systems through Time: Evidence from the Trace-Fossil Record. *Palaios*, V. 20, pp. 321-347.
- Campbell, C.V. (1967). Lamina, lamina set, bed and bed set. *Sedimentology*, V. 8, pp. 7-26.
- Cataño-Lopera, Y.A., Abad, J.D. & García, M.H. (2009). Characterization of bedform Morphology generated under combined flows and currents using wavelet analysis. *Ocean Engineering*, V. 36, No. 9-10, pp. 617-632.
- Clark, B.E. & Steel, R.J. (2006). Eocene Turbidite-Population Statistics from Shelf Edge to Basin Floor, Spitsbergen, Svalbard. *Journal of Sedimentary Research*, V. 76, No. 6, pp. 903-918.
- Clifton, H.E. (2006). A Reexamination of Facies Models for Clastic Shorelines. *Special Publication*, No. 84, pp. 293-337.
- Correggiari, Cattaneo A. & Trincardi, F. (2005). The modern Po Delta system: Lobe witching and asymmetric prodelta growth. *Marine Geology* V. 222-223, pp. 49-74.
- Crabough, J.P. & Steel, R.J. (2004). Basin-floor fans of the Central Tertiary Basin, Spitsbergen: relationship of basin-floor sand-bodies to prograding clinofolds in a structurally active basin. *Geological Society, London. Special Publications*, V. 222, pp. 187-208.
- Cummings, D.I., Dumas, S. & Dalrymple, R. W. (2009) Fine-Grained Versus Coarse-Grained Wave

- Ripples Generated Experimentally Under Large-Scale Oscillatory Flow. *Journal of Sedimentary Research*, February 2009, V. 79, No. 2, pp. 83-93.
- Dalland, A. (1979). Structural geology and petroleum potential of Nordenskiöld Land, Svalbard. *Norsk Petroleumsforening, Norwegian Sea Symposium*, pp. 1-20.
- Dallmann, W.K. (Ed.). (1999). Lithostratigraphic Lexicon of Svalbard. Norwegian Polar Institute, Polar Environmental Centre, 320pp. Review and recommendations for nomenclature use. Upper Paleozoic to Quaternary Bedrock. Tromsø, Norway
- Davis, R.A., Jr. (1978). Beach and nearshore zone. In: R.A. Davis, Jr. (Editor), *Coastal Sedimentary Environments*. Springer-Verlag, New York, pp. 237-285.
- Deibert, J.E., Benda, T., Loseth, T., Schellpeper, M. & Steel, R.J. (2003). Eocene clinoform growth in front of a storm-wave-dominated shelf, Central Basin, Spitsbergen: No significant sand delivery to deepwater areas. *Journal Of Sedimentary Research*, 73(4), 546-558.
- Dott, R.H. (1964). Wacke, graywacke and matrix; what approach to immature sandstone classification? *Journal of Sedimentary Research*; September 1964, V. 34, No. 3, pp. 625-632.
- Dumas, S., & Arnott, R.W.C. (2006). Origin of hummocky and swaley crossstratification-The controlling influence of unidirectional current strength and aggradation rate. *Geology*, V. 34, No. 12, pp. 1073-1076.
- Dumas, S., Arnott, R.W.C. & Southard J.B. (2004). Experiments on oscillatory-flow and combined-flow bed forms: implications for interpreting parts of the shallow-marine sedimentary record. *Journal of Sedimentary Research*, V. 75, No. 3, pp. 501-513.
- Dypvik, H., Nagy, J., Eikeland, T.A., Backer-Owe, K., Andresen, A., Haremo, P., Bjærke, T., Johansen, H. & Elvhøi, A. (1991). The Janusfjellet Subgroup (Bathonian to Hauterivian) on central Spitsbergen: a revised lithostratigraphy. *Polar Research* V. 9, No. 2, pp. 1-43.
- Embry, A., and E. Johannessen, (1992). T-R sequence stratigraphy, facies analysis and reservoir distribution in the uppermost Triassic-Lower Jurassic succession, western Sverdrup Basin. Arctic Canada, in T. Vorren et al., eds., *Arctic geology and petroleum potential: Norwegian Petroleum Society Special Publication 2*. p. 121- 146
- Faleide, J. I., Tsikalas, F., Breivik, A.J, Mjelde, R., Ritzmann, O., Engen, Ø., Wilson, J. & Eldholm, O. (2008). Structure and evolution of the continental margin off Norway and the Barents Sea. *Episodes*, 31, pp. 82-91.
- Folk, R. (1974). *Petrology of Sedimentary Rocks*. Hemphill, Austin, TX.
- Friend, P. F. & Moody-Stuart, M. (1972). Sedimentation of the Wood Bay Formation (Devonian) of Spitsbergen. *Norsk Polarinstitutt Årbok* (1972), pp. 157-237.
- Galloway, W.E. (1975). Process framework for describing the morphologic and stratigraphic evolution of deltaic depositional systems. In: *Deltas, Models for Exploration* (Ed. M.L. Broussard), pp. 87-98. Houston Geological Society, Houston.
- Galloway, W.E. (1989). Genetic stratigraphic sequences in basin analysis, I. Architecture and genesis of flooding-surface bounded depositional units. *American Association of Petroleum Geologists Bulletin* 73, 125-142
- Gee, D.G. & Teben'kov, A.M. (2004). Svalbard: a fragment of the Laurentian margin. *Geological Society, London, Memoirs*, 2004, V. 30, pp. 191-206.
- Gjelberg, J.G. & Steel, R.J. (1981). An outline of Lower-Middle Carboniferous sedimentation on Svalbard: effects of climatic, tectonic and sea level changes in rift basin sequences. *Canadian Society of Petroleum Geologists*, V. 7, pp. 543-561.

- Gjelberg, J.G. & Steel, R.J. (1995). Helvetiafjellet Formation (Barremian-Aptian), Spitsbergen, characteristic of a transgressive succession. In Steel et al. (ed) *Norwegian Petroleum Society*, Special Publication No. 5, pp. 571-593.
- Hanes, D.M., Alymov, V. & Chang, Y.S. (2001). Wave-formed sand ripples at Duck, North Carolina. *Journal of Geophysical Research*, V. 106, No. c10, pp. 22,575–22,592.
- Haq, B.U., Hardenbol, J., Vail, P.R. (1987). Chronology of fluctuating sea levels since the Triassic (250 million years ago to present). *Science* 235, 1156–1166
- Harland, W.B. (1969). Contribution of Spitsbergen to understanding of tectonic evolution of north Atlantic region. In North Atlantic – geology and continental drift. *AAPG Mem.* 12, ed. M. Kay, pp. 817-851.
- Harland, W.B. (1985). Caledonide Svalbard. In Gee, D.G. & Sturt, B.A. (eds) *The Caledonide Orogen-Scandinavia and related areas*, Wiley, Chichester, 999-1016.
- Harland, W.B. (1997). The geology of Svalbard, 17. *Memoirs of the Geological Society London*.
- Harland, W.B. & Horsfield, W.T. (1974). West Spitsbergen Orogen. In: Spencer, A.M. (ed.) *Mesozoic-Cenozoic Orogenic Belts, Data of Orogenic Studies. Special Publications of the Geological Society, London*. 4, pp. 747-755.
- Helland-Hansen, W. (1985). Sedimentology of the Battfjellet Formation (Palaeogene) in *Nordenskiöld Land, Spitsbergen*. University of Bergen, Bergen.
- Helland-Hansen, W. (1990). Sedimentation in Paleogene Foreland Basin, Spitsbergen. *AAPG Bulletin*, V. 74, No. 3, pp. 260-272.
- Helland-Hansen, W. (1992). Geometry and facies of Tertiary clinothems, Spitsbergen. *Sedimentology*, V. 39, pp. 1013-1029.
- Helland-Hansen, W. (2010). Facies and stacking patterns of shelf-deltas within the Paleogene Battfjellet Formation, Nordenskiöld Land, Svalbard: implications for subsurface reservoir prediction. *Sedimentology*, V. 57, No. 1, pp. 190-208.
- Helland-Hansen, W. & Gjelberg, J.G. (1994). Conceptual basis variability in sequence Stratigraphy: a different perspective: *Sedimentary Geology*, V. 92, pp. 31-52.
- Helland-Hansen, W., Helle, H.B. & Sunde, K. (1994). Seismic modeling of Tertiary sandstone clinothems, Spitsbergen. *Basin Research*, V. 6, pp. 181-191.
- Helland-Hansen, W. & Martinesn, O.J. (1996). Shoreline Trajectories and Sequences: Description of Variable Depositional-Dip Scenarios. *Journal of Sedimentary Research*, V. 66, No. 4, pp. 670-688.
- Helland-Hansen, W. & Hampson, G.J. (2009). Trajectory analysis - Concepts and applications. *Basin Research*, 21, pp. 454-483.
- Hill, P.R., Meulé, S. & Longuépée, H. (2003). Combined-Flow Processes and Sedimentary Structures on the Shoreface of the Wave-Dominated Grande-Rivière-De-La-Baleine Delta. *Journal of Sedimentary Research*, V. 73, No. 2, pp. 217-226.
- Johannessen, E.P. & Steel, R.J. (2005). Shelf-margin clinoforms and prediction of deepwater sands. *Basin Research*, V. 17, No. 4, pp. 521-550.
- Kellogg, H.E. (1975). Tertiary Stratigraphy and Tectonism in Svalbard and Continental Drift. *AAPG Bulletin*, V. 59, No. 3, pp. 465-485.
- Lacy, J.R., Rubin, D.M., Ikeda, H., Mokudai, K., Hanes, D.M. (2007). Bed forms created by simulated waves and currents in a large flume. *Journal of geophysical research*, V. 112, No. 18, 18pp.

- Ljutkevic, E.M. (1937). Geologiceskij ocerk i problem ugljenosnosti gory Piramidy ostrova Spicbergena. (Geological survey and problems of the coal fields of mount Pyramiden, Spitsbergen.) *Trudy Arktieeskogo Instituta Leningrad* V. 76, pp. 25-38.
- López-Blanco, M., Marzo, M., Piña J. (2000). Transgressive±regressive sequence hierarchy of foreland, fan-delta clastic wedges (Montserrat and Sant Llorenç del Munt, Middle Eocene, Ebro Basin, NE Spain). *Sedimentary Geology*, V. 138, pp 41-69
- Løseth, T.M., Steel, R.J. Crabaugh, J.P. & Schellpeper, M. (2006). Interplay between shoreline migration paths, architecture and pinchout distance for siliciclastic shoreline tongues: evidence from the rock record. *Sedimentology*, V. 54, No. 4, pp. 745-767.
- Major, H., & Nagy, J. (Cartographer), (1964). Adventdalen. *Geologisk kart*.
- Major, H., & Nagy, J. (1972). Geology of Adventdalen map area. Norsk Polarinstitutt Skrifter, 138, 1-58 (with 1: 100 000 geological sheet C9G).
- McKee & Weir, (1953). Terminology for stratification and cross-stratification in sedimentary rocks, *Geol, Soc, Amer, Bull*, 64, pp. 381-389.
- Mellere, D., Plink-Björklund, P., & Steel, R. (2002). Anatomy of shelf deltas at the edge of a prograding Eocene shelf margin, Spitsbergen. *Sedimentology*, V. 49, pp. 1181-1206.
- Midtkandal, I. & Nystuen, J.P. (2009). Depositional Architecture of a Low-gradient Ramp Shelf in an Epicontinental Sea: the Lower Cretaceous on Svalbard, *Basin Research*, pp. 1365-2117.
- Mulder, T., Syvitski, J. P. M., Migeon, S., Faugères, J. C. & Savoye, B. (2003). Marine hyperpycnal flows: initiation, behavior and related deposits. A review. *Marine and Petroleum Geology*, 20 (6-8), 861-882
- Myrow, P. M., & Southard, J. B. (1991). Combined-flow model for vertical stratification sequences in shallow marine storm-deposited beds. *Journal of Sedimentary Research*, V. 61, No. 2, pp. 202-210.
- Mørk, A., Knarud, R. & Worsley, D. (1982). Depositional and diagenetic environments of the Triassic and Lower Jurassic succession of Svalbard. In *Arctic Geology and Geophysics*. Ed. By A. F. Embry and H. R. Balkwill. Canadian Society of Petroleum Geologists, *Memoir* V. 8, pp. 371-398.
- Nagy, J., Kaminski, M.A. & Kuhnt, W. (2000). Agglutinated Foraminifera from Neritic to Bathyal Facies in the Paleogene of Spitsbergen and the Barents Sea. In: *Proceedings of the Fifth International Workshop on Agglutinated Foraminifera* (Eds M. B. Hart, M. A. Kaminski & C. W. Smart), pp. 333-361- Grzybowski Foundation Special Publication, 7.
- Nathorst, A. G. (1910). Beiträge zur Geologie der Bäreninsel, Spitzbergens und des König-Karl-Landes. *Bulletin Geologiska Institutionen Univeritetet i Uppsala*, 10 (1910-1911), pp. 261-416.
- Nemec, W. (1988). The shape of the rose. *Sedimentary Geology*, V. 59, pp. 149-152.
- Nichols, G. & Lüthje, C. (2008). Provenance and Flexural Basin Development: the Paleocene of the Central Tertiary Basin, Spitsbergen, *Basin Research*.
- Nøttvedt, A., Livbjerg, F., Midbøe, P.S., & Rasmussen, E. (1992). Hydrocarbon potential of the Central Spitsbergen Basin. *NPF Special Publication*, 2, pp. 333-361.
- Nøttvedt, A. & Kreisa, R.D. (1987). Model for the combined-flow origin of hummocky cross-stratification. *Geology*, 15, pp. 357-361.
- Olariu, C., Steel, R.J. & Petter, A.L. (2010). Delta-front hyperpycnal bed geometry and implications for reservoir modeling: Cretaceous Panther Tongue delta, Book Cliffs, Utah. *AAPG Bulletin*. V. 94, No. 6, pp. 819-845.
- Olsen, H.A. (2008). Sedimentology and Paleogeography of the Battfjellet Fm, Southern Van Mijenfjorden, Svalbard. University of Bergen, Bergen.
- Orvin, A. (1940). Outline of the geological history of Spitsbergen. *Skrifter om Svalbard og Ishavet*, V. 78, pp. (reprint 1969; 1961-1957).

- Parker, J.R. (1967). The Jurassic and Cretaceous sequence in Spitsbergen. *Geol. Mag.*, V. 104 No. 5, pp. 488-505.
- Peach, H.J. (1999). The Tertiary and Cretaceous of Spitsbergen and North-Greenland: Its Alpine Signature. (1999). *Polarforschung*, 69, pp. 107-115.
- Pedocchi, F. & García, M.H. (2009). Ripple morphology under oscillatory flow: 1. Prediction. *Journal of geophysical research*, V. 114, 16 pp.
- Petter, A.L. & Steel, R.J. (2006). Hyperpycnal flow variability and slope organization on an Eocene shelf margin, Central basin, Spitsbergen. *AAPG Bulletin*, V. 90, No. 10, pp. 1451-1472.
- Plink-Björklund, P., Mellere, D., & Steel, R. (2001). Turbidite variability and architecture of sand-prone, deep-water slopes: Eocene clinofolds in the central basin, Spitsbergen. *Journal of Sedimentary Research*, V.71, No. 6, pp. 895-912.
- Plink-Björklund, P.P. & Steel, R.J. (2002). Sea-level fall below the shelf edge, without basin-floor fans. *Geology*, v. 30, no. 2, pp. 115–118
- Plink-Björklund, P.P. & Steel, R.J. (2003). Initiation of turbidity currents: outcrop evidence for Eocene hyperpycnal flow turbidites. *Sedimentary Geology*, V. 165, pp. 29-52.
- Plink-Björklund, P. & Steel, R.J. (2004). Initiation of turbidity currents: outcrop evidence for Eocene hyperpycnal flow turbidites. *Sedimentary Geology*, 165 (2004), pp. 29-52.
- Prélat, A., Hodgson, D.M., Flint, S.S. (2009). Evolution, architecture and hierarchy of distributary deep-water deposits: a high-resolution outcrop investigation from the Permian Karoo Basin, South Africa. *Sedimentology*, V. 56, pp. 2132-2154
- Reading, H.G. (1996). *Sedimentary environments: processes, facies and stratigraphy* (3 ed.): Blackwell Publishing company.
- Reinecks, H.-E. (1963). *Sedimentgefüge im Bereich der Stüdlichen Nordsee: Abhandlungebder Sanckenbergischen Naturforschenden Gesellschaft, Stuttgart, 138p.*
- Riis, F., Lundschie, B.A., Høy, T., Mørk, A., & Mørk, M.B.E. (2008). Evolution of the Triassic shelf in the northern Barents Sea region. *Polar Research*, V. 27, No. 3, 318-338.
- Roep, T.B., Beets, D.J., Dronkert, H. & Pagnier, H. (1979). A Prograding Coastal Sequence of Wave-Built Structures of Messinian Age, Sorbas, Almeria, Spain. *Sedimentary Geology*, V. 22, pp. 135-163.
- Roux, J.P. & Elgueta, S. (1996). Paralic parasequences associated with Eocene sea-level oscillations in an active margin setting: Trihuco Formation of the Arauco Basin, Chile. *Sedimentary Geology*, V. 110, pp. 257-276.
- Skarpeid, S.S. (2010). *Facies Architecture and Paleogeography of the Battfjellet Formation, Rypefjellet, Spitsbergen. University of Bergen. 113pp.*
- Smith, D.G. (1991). Lacustrine Deltas. In *Canadian Landform Examples – 22. The Canadian Geographer* 35, no 3. Canadian Association of Geographers.
- Sonu, C.J. & van Beek, J.L. (1971). Systematic beach changes in the Outer Banks, North Carolina. *J. Geol.*, 74, 416-425.
- Steel, R.J. (1977). Observations on some Cretaceous and Tertiary sandstone bodies in Nordensköld Land, Svalbard. *Norsk Polarinstitutt Årbok 1976*, pp. 43-68.
- Steel, R.J., Dalland, A., Kalgraff, K., & Larsen, V. (1981). The central Tertiary basin of Spitsbergen - sedimentary developmentsof sheared-margin basin. *Geology of the North Atlantic Borderland*, V. 7, pp. 647-664.
- Steel, R.J., & Worsley, D. (1984). Svalbard's post-Caledonian strata – an atlas of sedimentational patterns and paleogeographic evolution. *Norwegian Petroleum Society (Graham & Trotman) (Petroleum Geology of the North European Margin)*,





















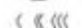




- pp. 109-135.
- Steel, R., Gjelberg, J. G., Helland-Hansen, W., Kleinspehn, K., Nøttvedt, A., & Rye-Larsen, M. (1985). The Tertiary strike-slip basin and orogenic belt of Spitsbergen. *SEPM Special Publication*, 37.
- Steel, R., Mellere, D., Plink-Björklund, P., Crabaugh, J., Deibert, J., Loeseth, T., Shellpeper, M., 2000. Deltas v rivers on the shelfedge: their relative contributions to the growth of shelf-margins and basin-floor fans (Barremian and Eocene, Spitsbergen). *GCSSEPM Foundation 20th Annual Research Conference Special Publication, CD. GCSSEPM*, pp. 981– 1009.
- Stene, S. A. K. (2009). Facies and architecture of the Battfjellet Formation, northern Nathorst Land, Spitsbergen. Bergen, [S.A.K. Stene]: University of Bergen. 104pp.
- Taylor, A.M. & Golding, R. (1993). Description and analysis of bioturbation and ichnofabric. *Journal of the Geological Society*, London, 150, pp. 141-148.
- Uroza, C.A. & Steel, R.J. (2008). A highstand shelf-margin delta system from the Eocene of West Spitsbergen, Norway. *Sedimentary Geology*, V. 203, No. 3-4, pp. 229-245.
- Van Wagoner, J.C., Mitchum, R.M., Campion, K.M. and Rahmanian, V.D. (1990) Siliciclastic Sequence Stratigraphy in Well Logs, Cores, and Outcrops: Concepts for High Resolution Correlation of Time and Facies. *AAPG Meth. Explor. Ser.*, 7, 55.
- Walker, R.G. (1978). Deep-Water Sandstone Facies and Ancient Submarine Fans: Models for Exploration for Stratigraphic Traps. *AAPG Bulletin*, 62.
- Worsley, D., Aga, O.J. (1984). The Geological History of Svalbard. Evolution of an arctic archipelago. *Det norske stats oljeselskap a.s 120pp*.
- Worsley, D. (2008). The post-Caledonian development of Svalbard and the western Barents Sea. *Polar Research*, V. 27, No. 3, pp. 298-317.
- Worsley, D., Aga, O.J., Dalland, A., Elverhøi, A. and Thon, A. (1986). The geological history of Svalbard, evolution of an arctic archipelago, 122. Statoil, Aske Trykkeri, Stavanger.
- Zavala, C., Ponce, J. J., Arcuri, M., Drittanti, D., Freije, H. & Asensio, M. (2006). Ancient Lacustrine Hyperpynites: A Depositional Model from a Case Study in the Rayoso Formation (Cretaceous) of West-Central Argentina. *Journal of Sedimentary Research*, V. 76, No. 1

Appendix 1: Lithostratigraphical logs:

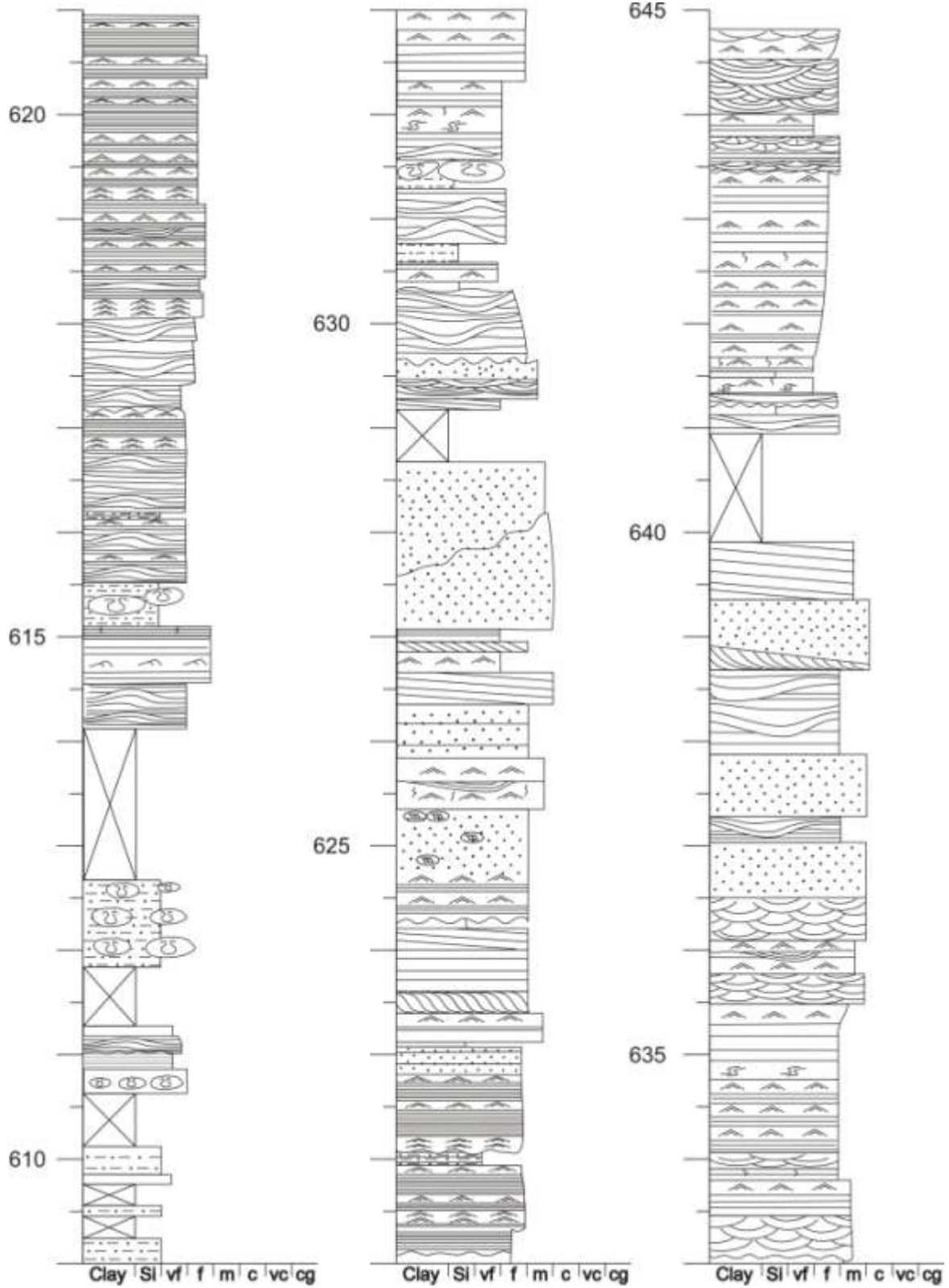
Order of appearance of the logged sections:

L1R1
L2S1
L3S2
L4S3
L5T1
L6T2
L7S4
L8R2
L9M1
L10M2
L11S5
L12T3
L13R3
L14M3
L15M4
L16T4
L17T5
L18R4
L19R5
L20S6
L21T6
L22T7

Legend:

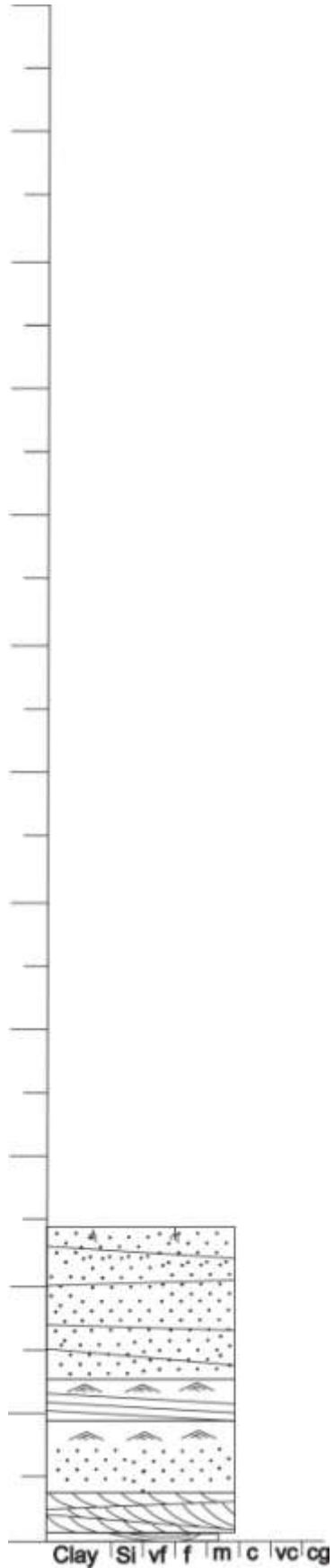
	Sandstone/massive appearance		Isolated trough		Rootlets
	Silty mudstone		Symmetrical small ripple		Fossilized plant fragments
	Siltstone		Combined flow ripple		<i>Teichichnus</i>
	Shale		Asymmetrical small ripple		<i>Ophiomorpha</i>
	Low angle stratification		Undifferentiated ripple		<i>Skolithos</i>
	Tabular cross-stratification		Load cast/ball and pillow		
	Trough cross-stratification		Soft sediment deformation		
	Plane parallel lamination		Bioturbation		
	Swaley cross-stratification		Siderite clast		
	Hummocky cross-stratification		Organic fragments		

The logs are presented in a 1:50 scale. Height in meters above sea level is provided every 5 meters.



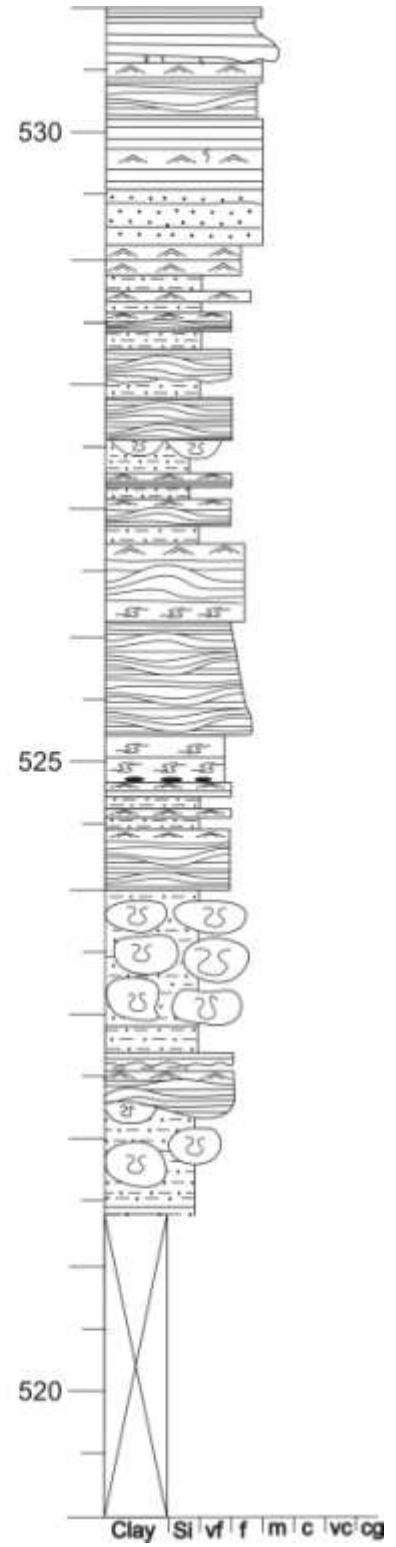
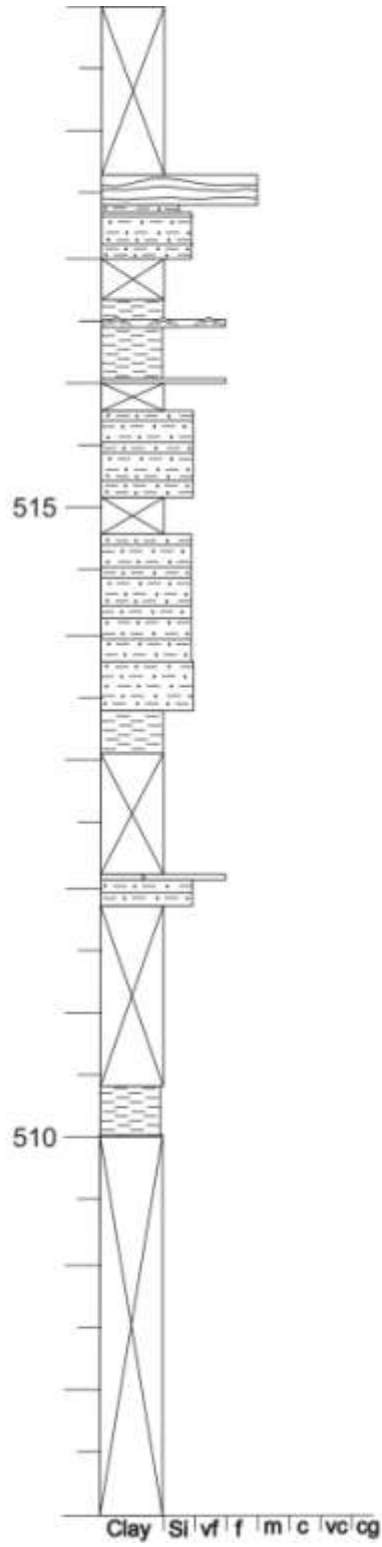
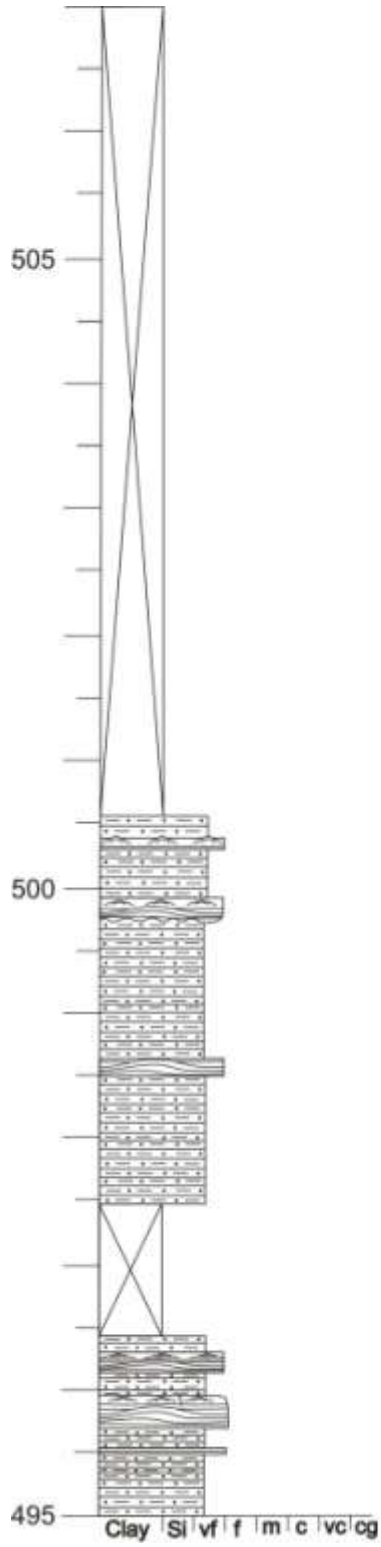
L1R1 2/2

Ringdalsfjellet



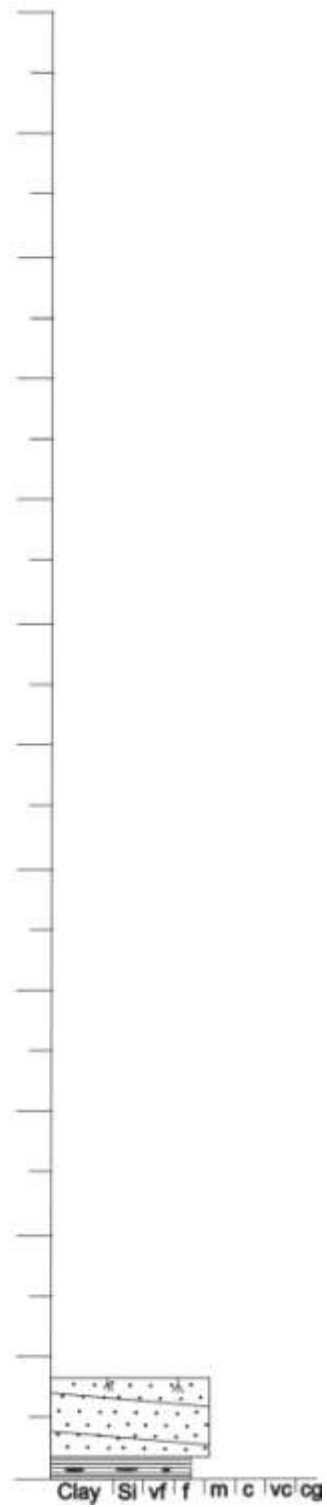
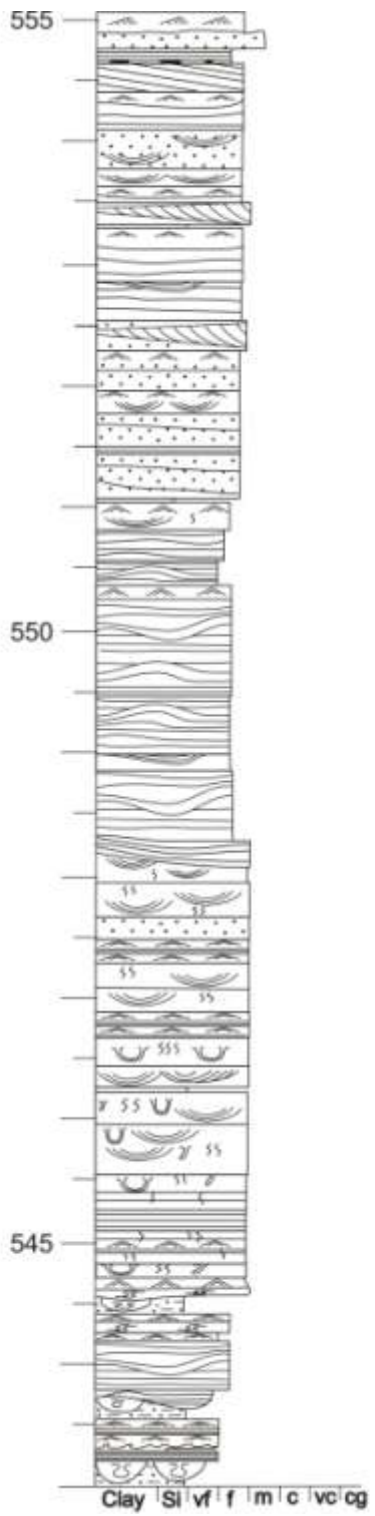
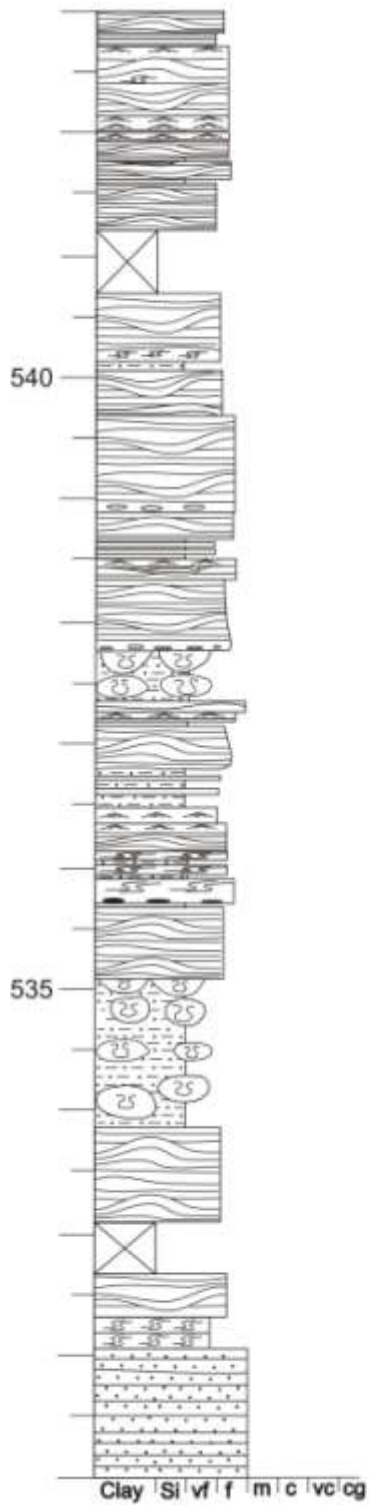
L2S2 1/2

Sandsteinsfjellet



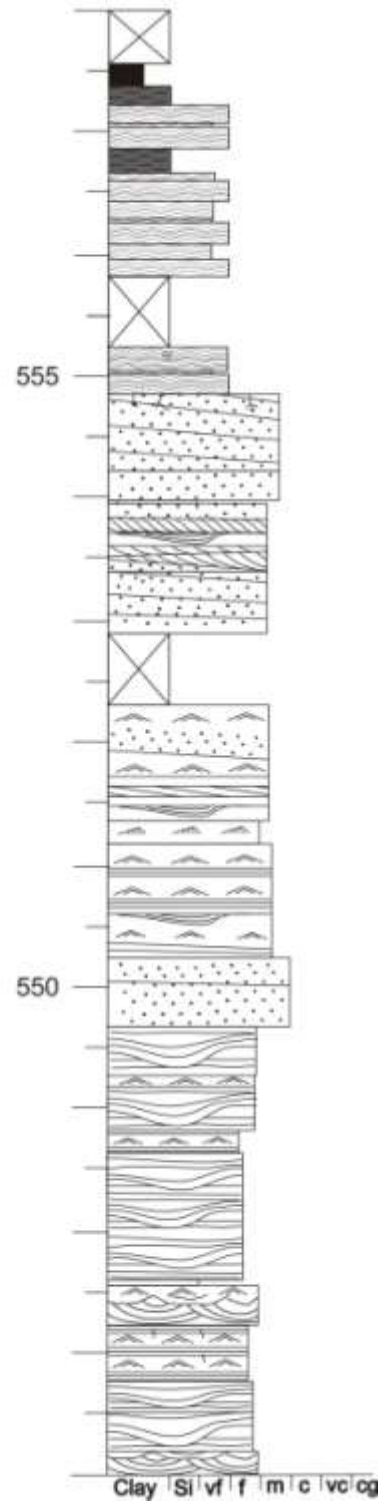
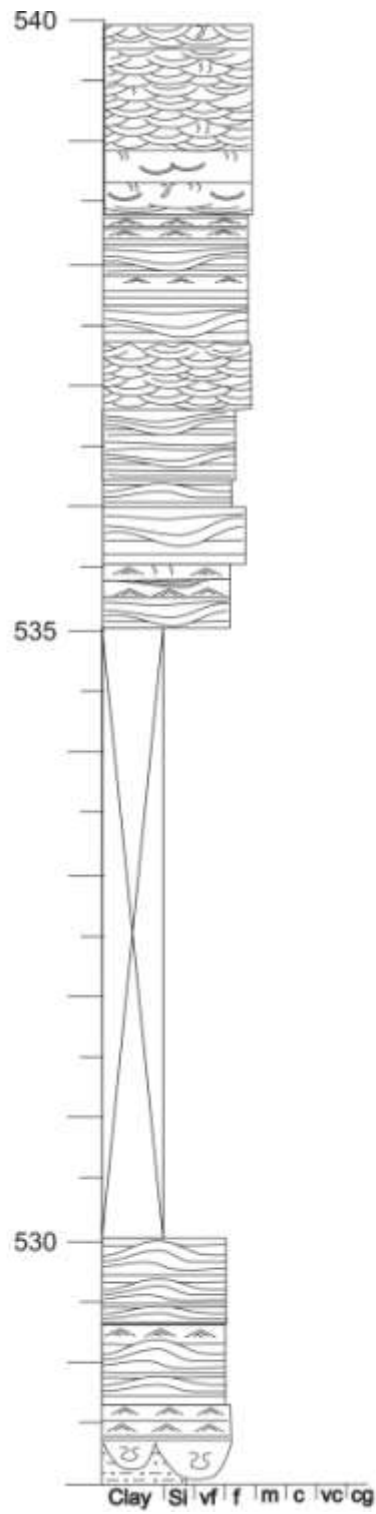
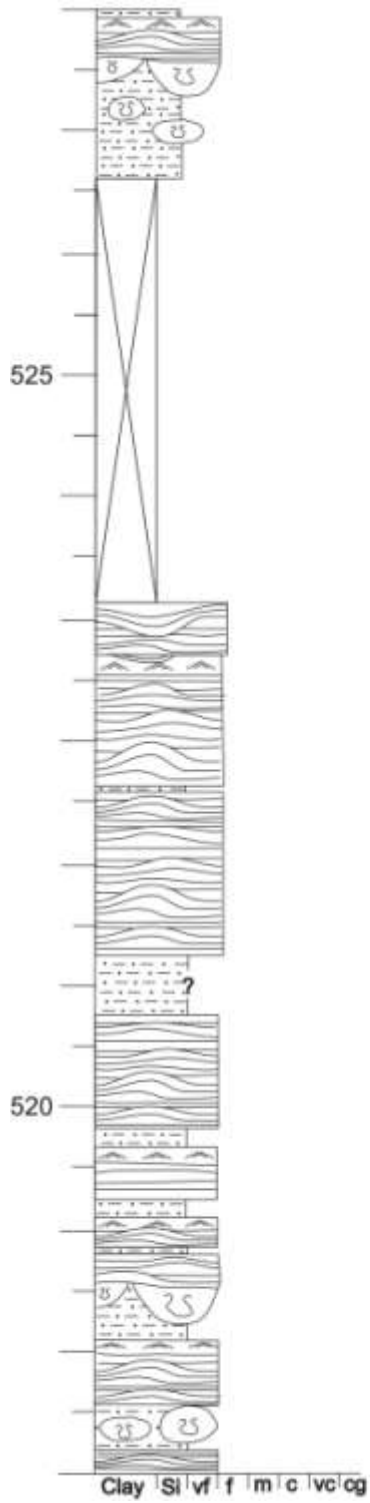
L2S2 2/2

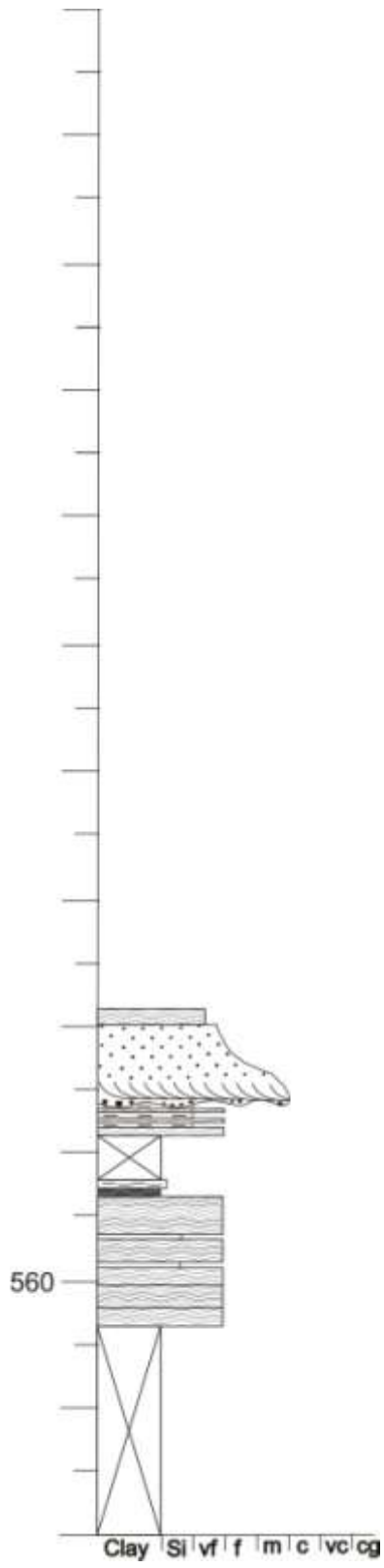
Sandsteinsfjellet



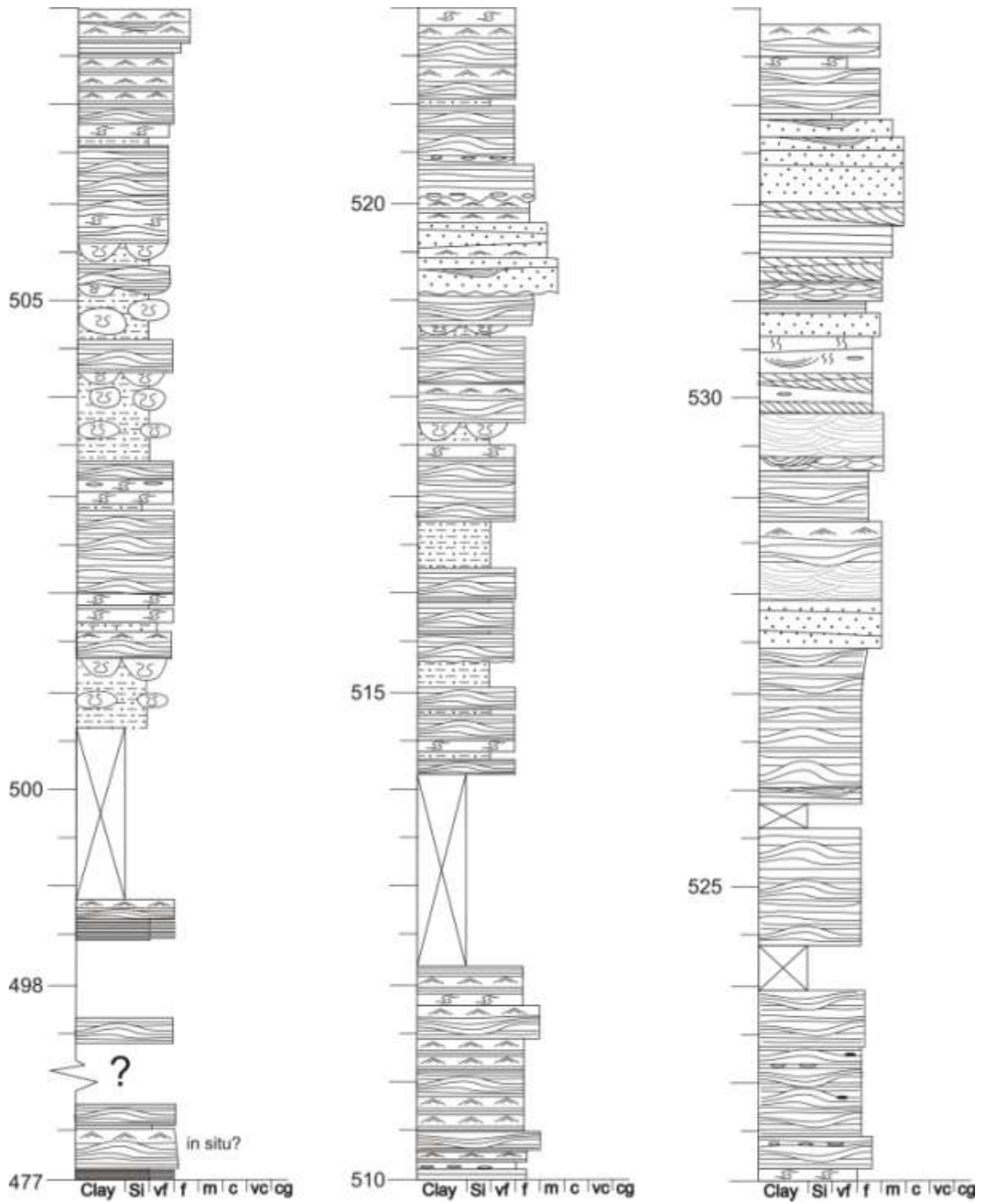
L3S2 1/2

Sandsteinsfjellet

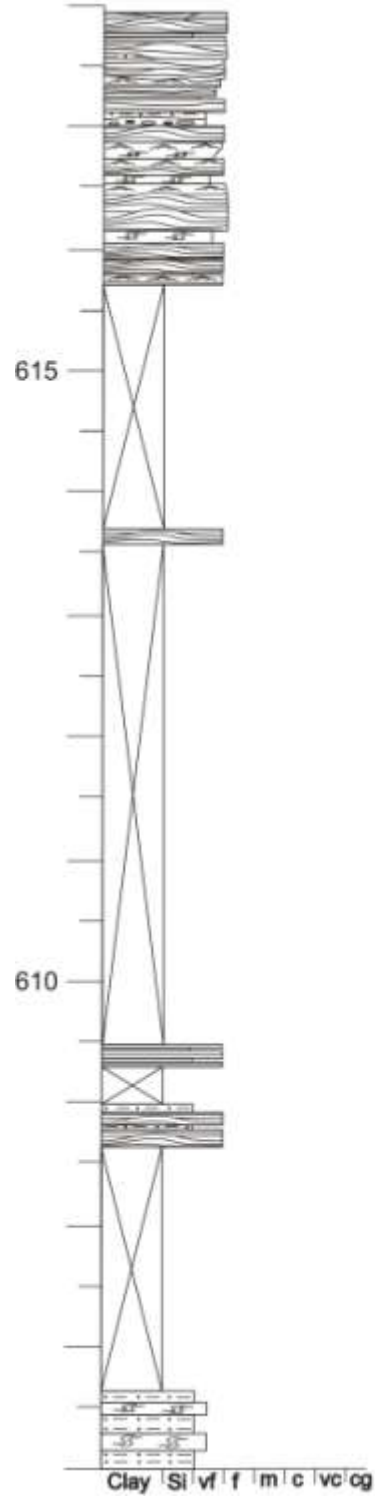




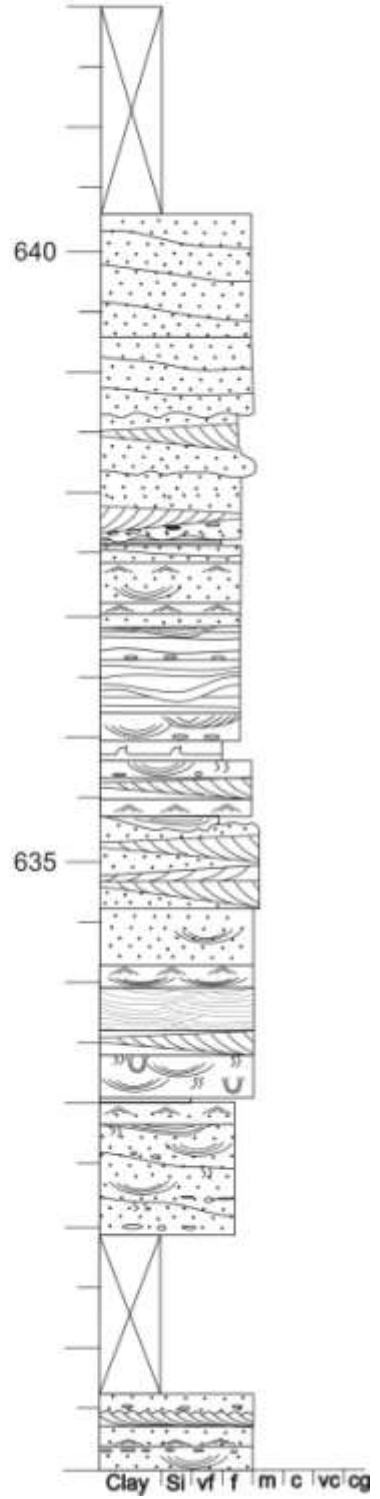
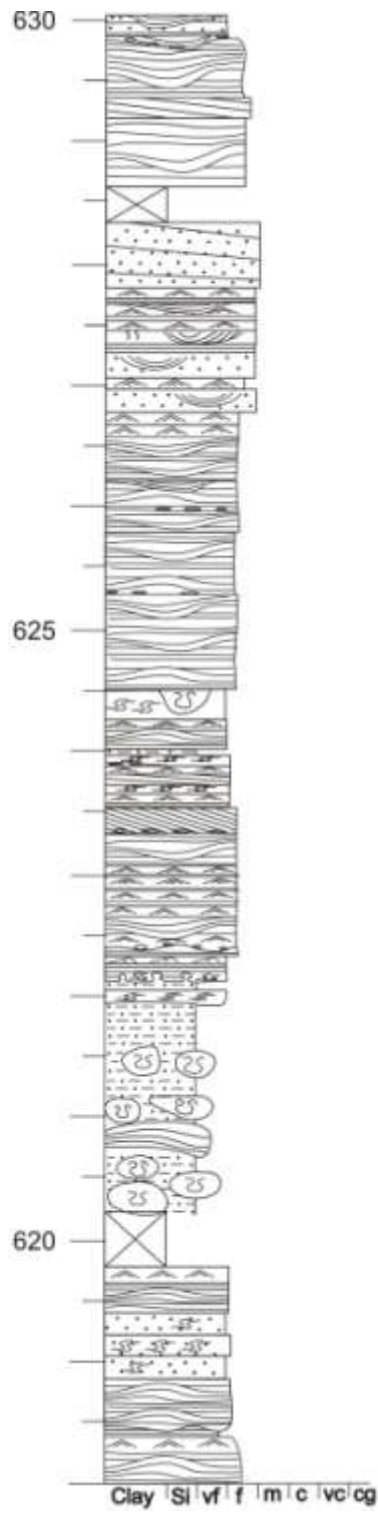
Sandsteinsfjellet



LST1 1/2

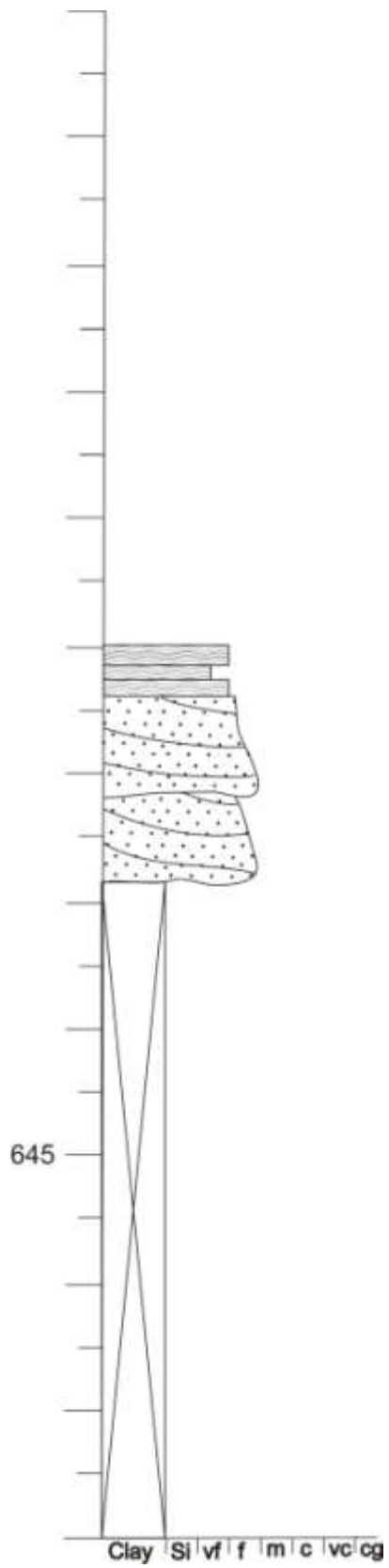


Tillbergsfjellet



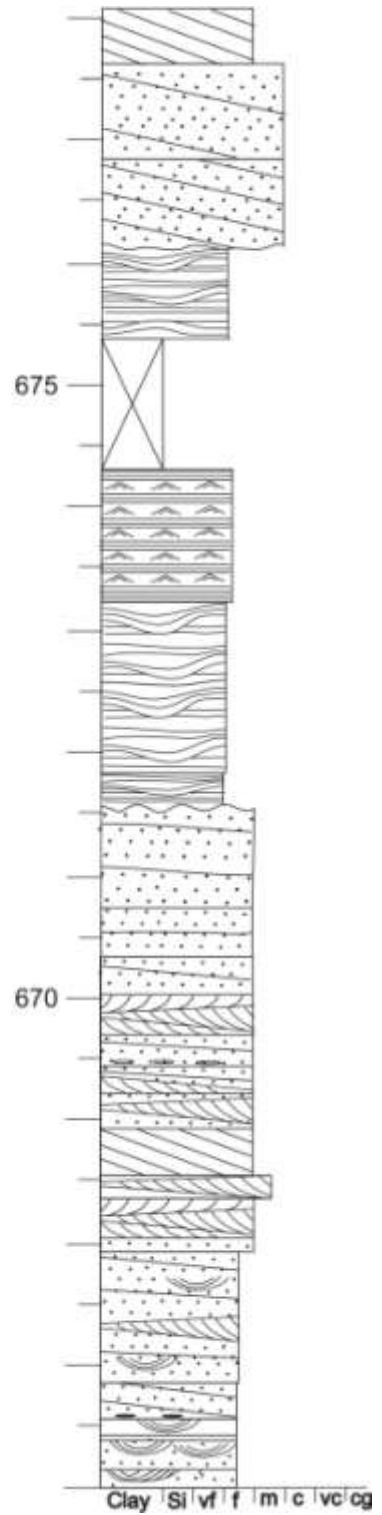
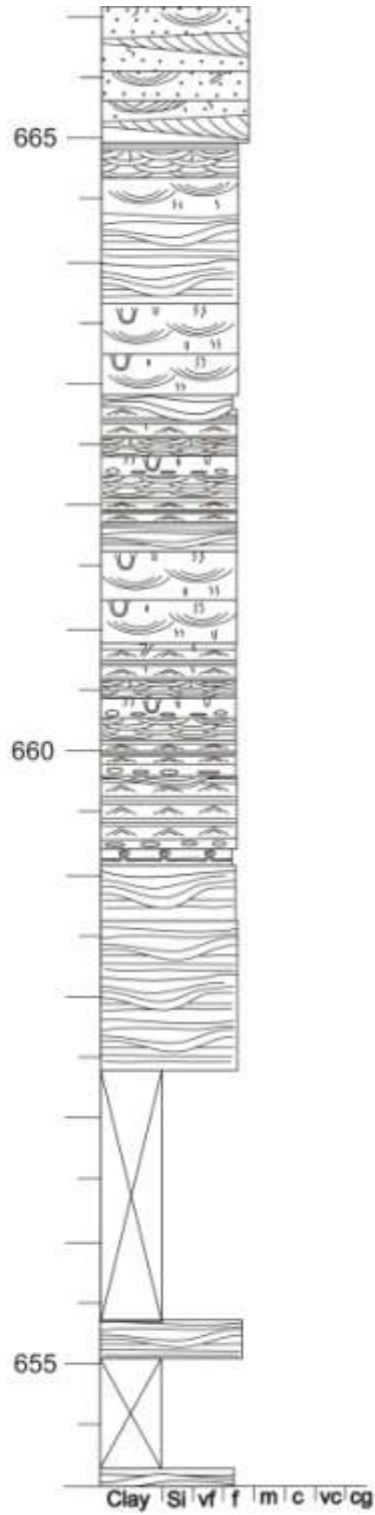
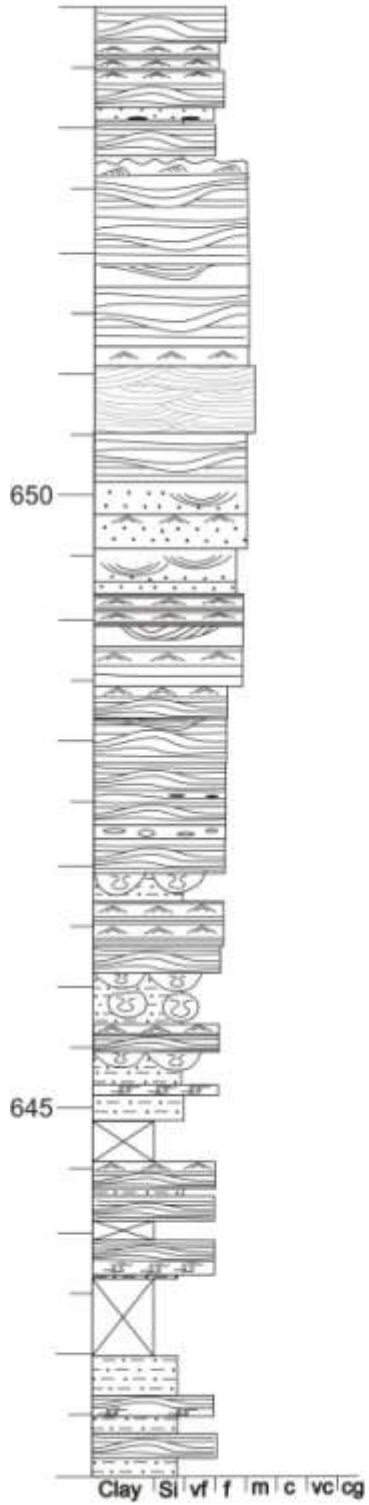
L5T1 2/2

Tillbergsfjellet

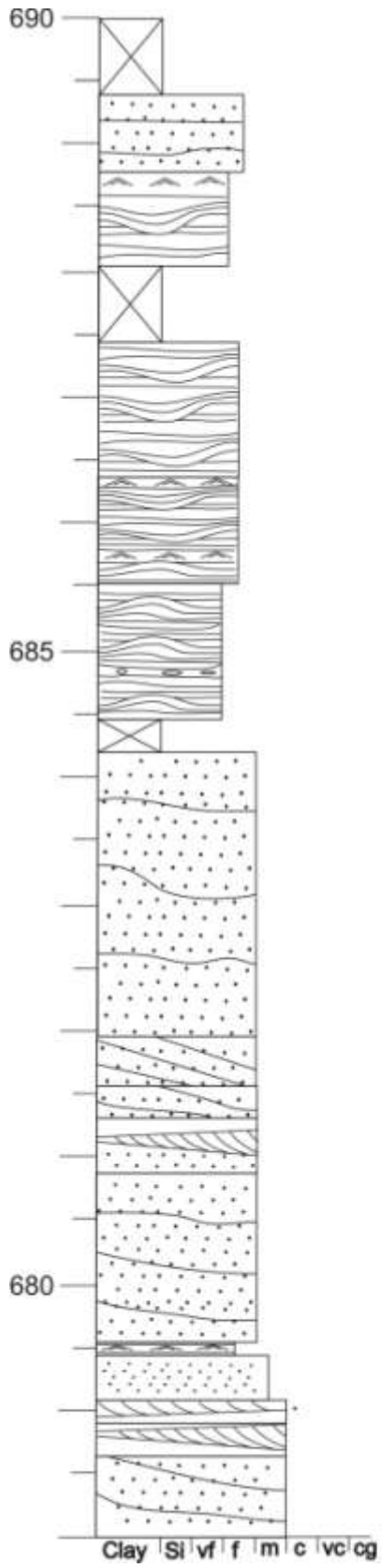


L6T2 1/2

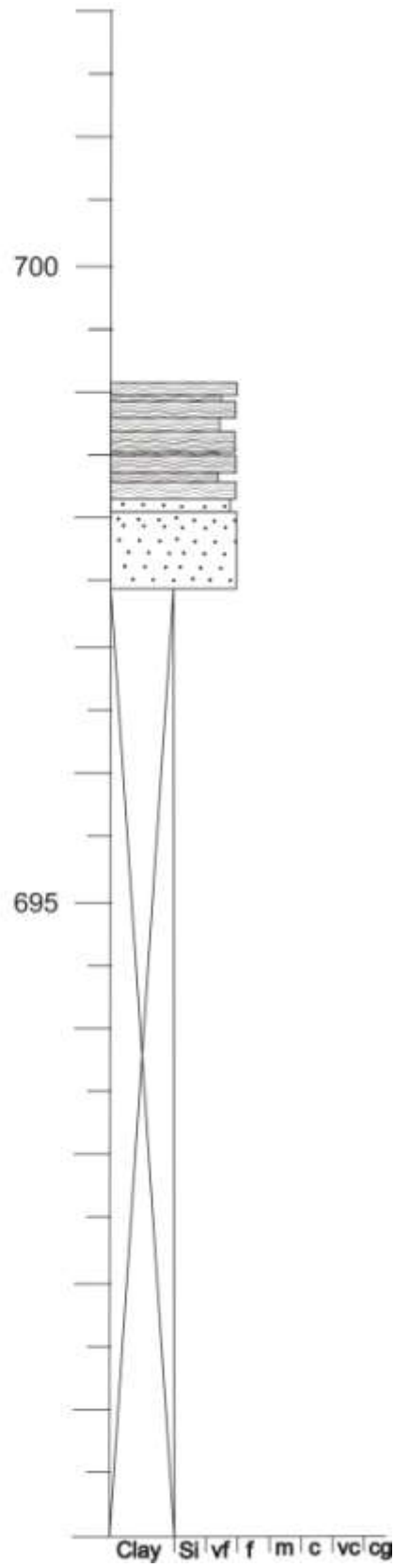
Tillbergsfjellet



L6T2 2/2

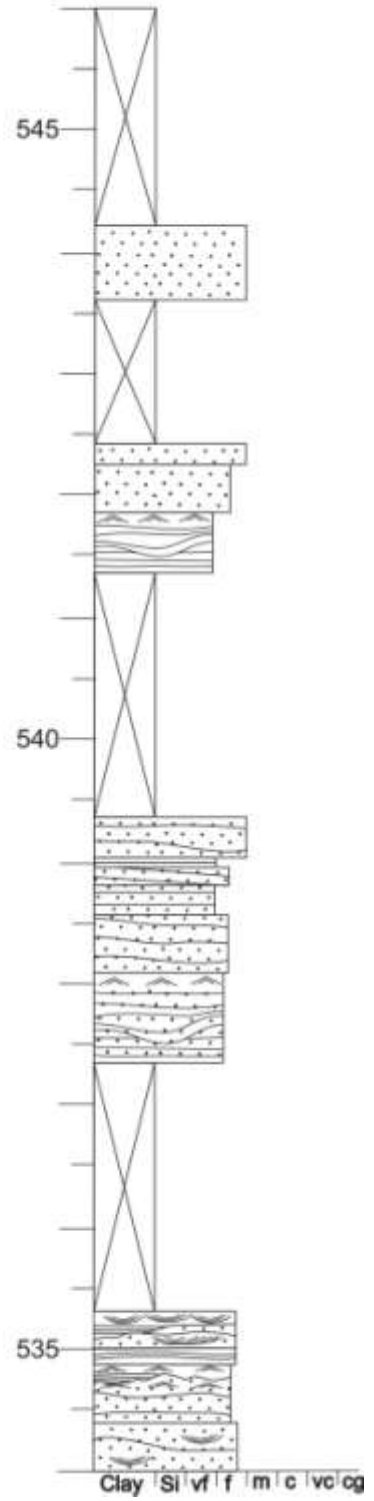
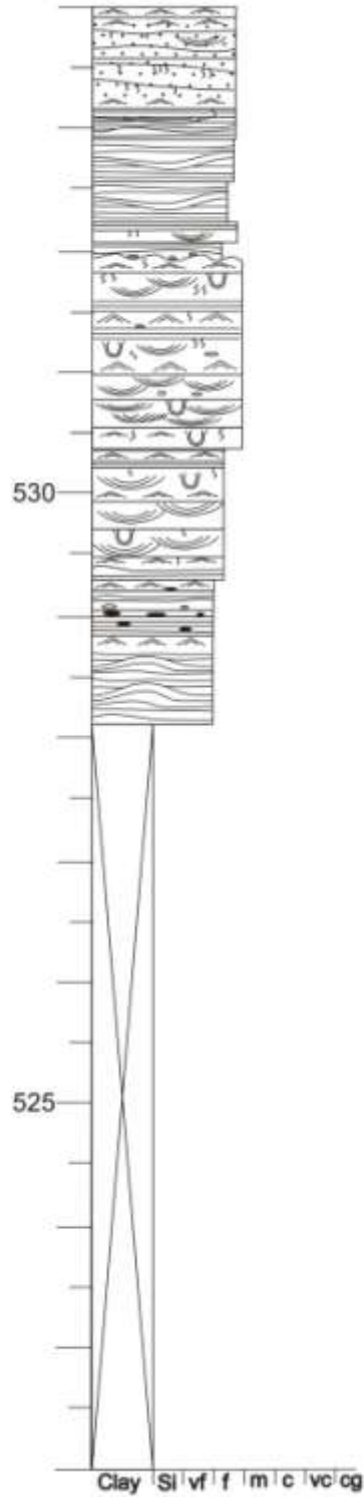
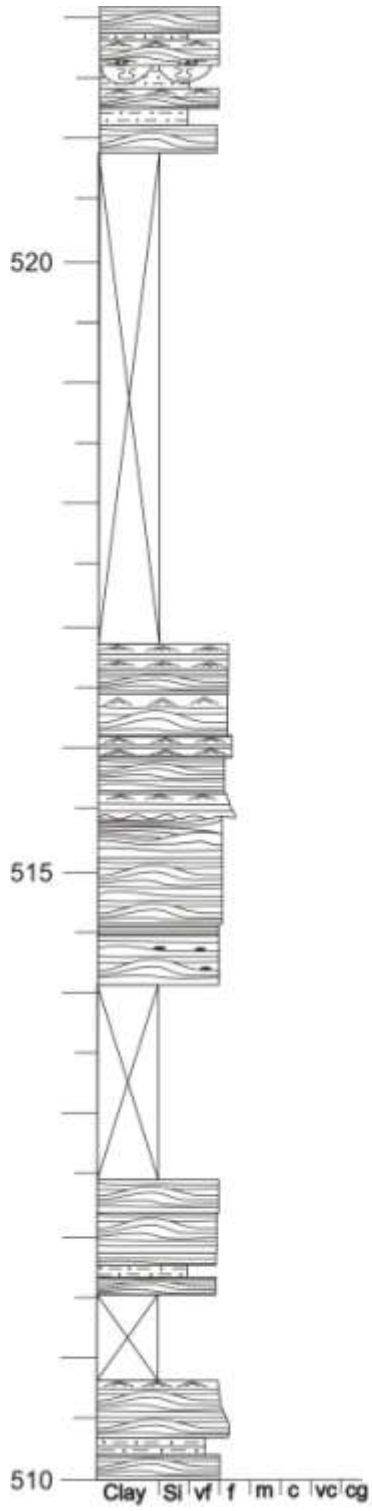


Tillbergsfjellet



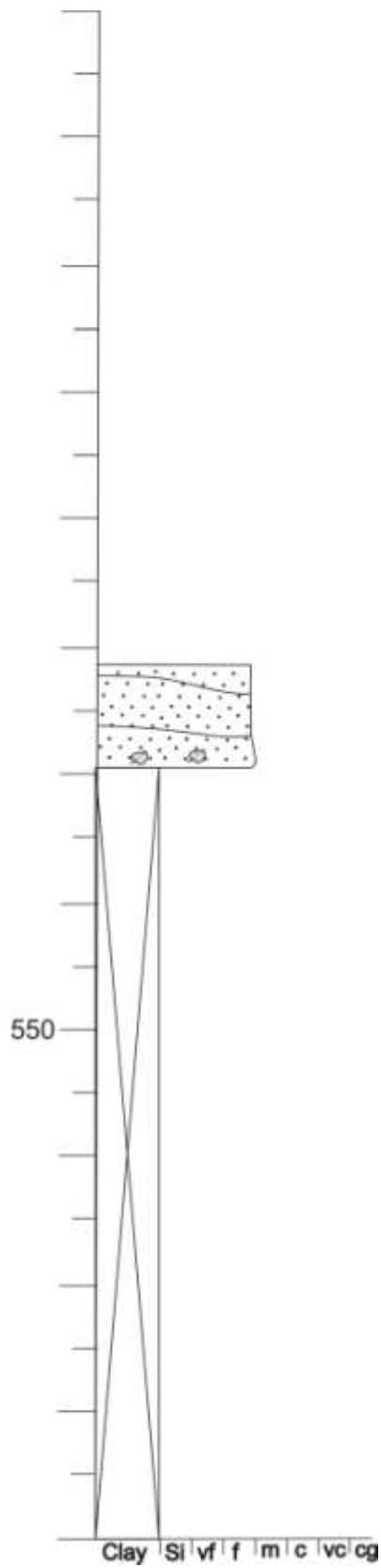
L7S4 1/2

Sandsteinsfjellet



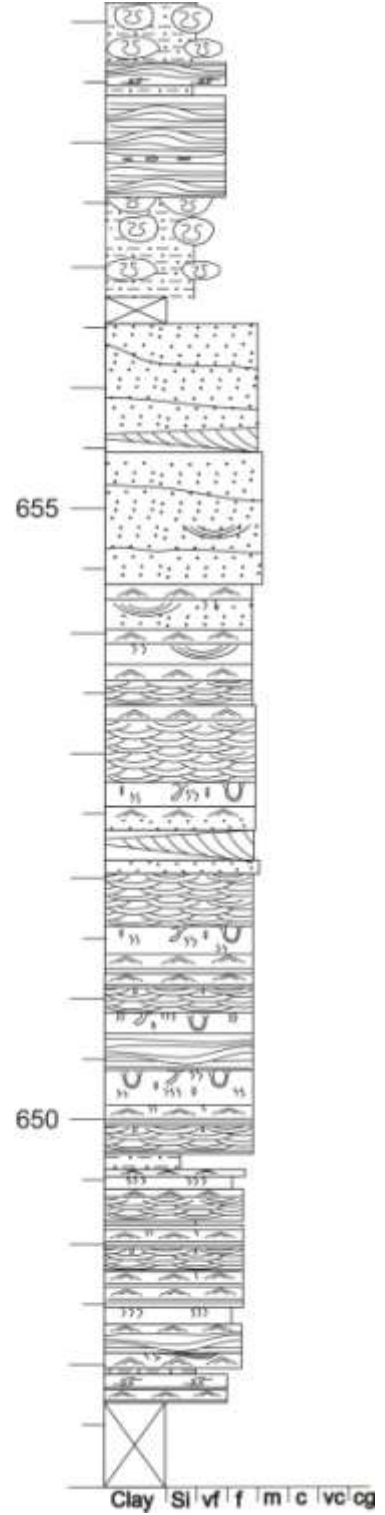
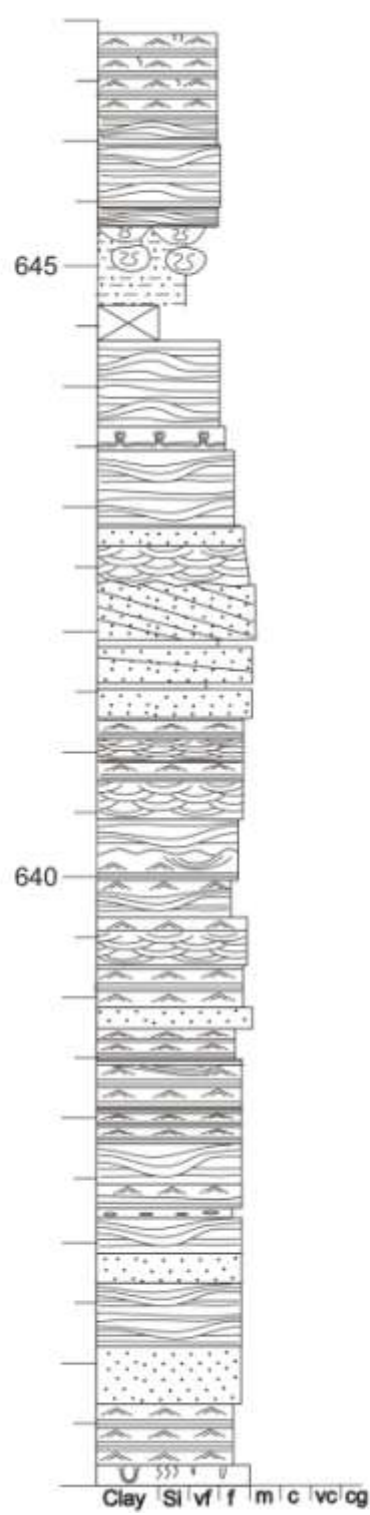
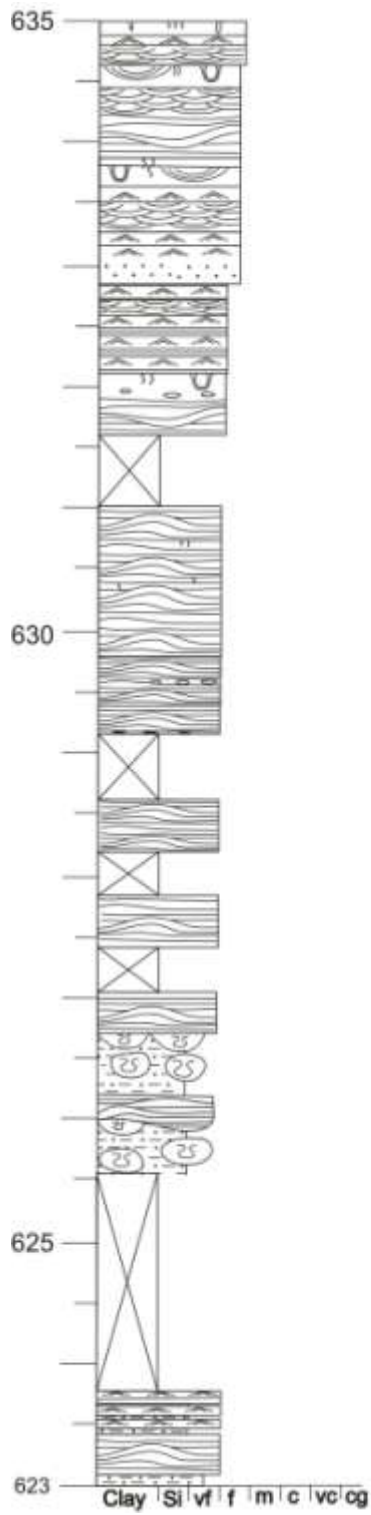
L7S4 2/2

Sandsteinsfjellet



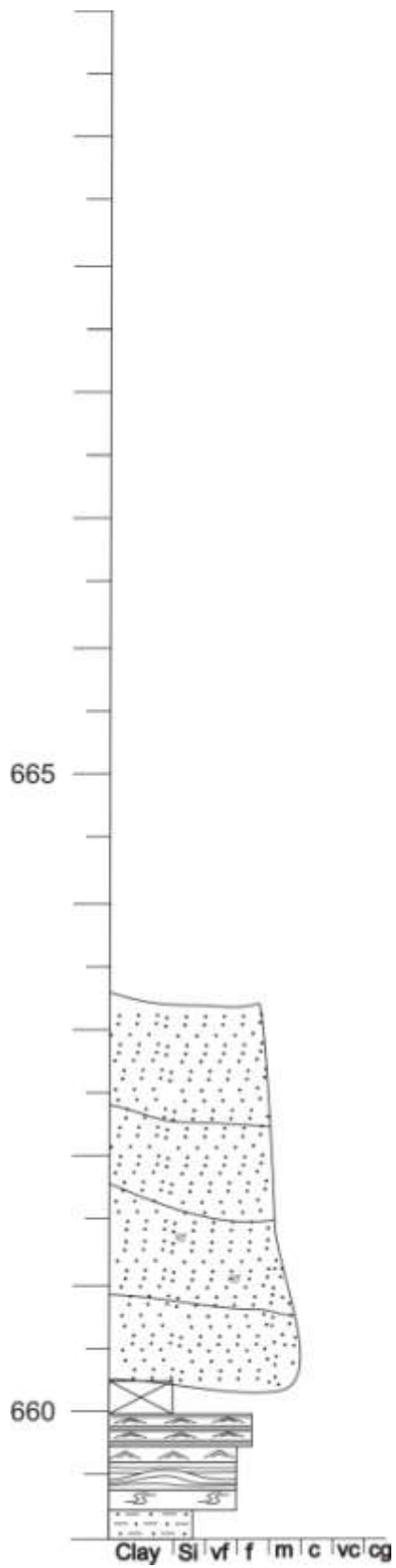
L8R2 1/2

Ringdalsfjellet



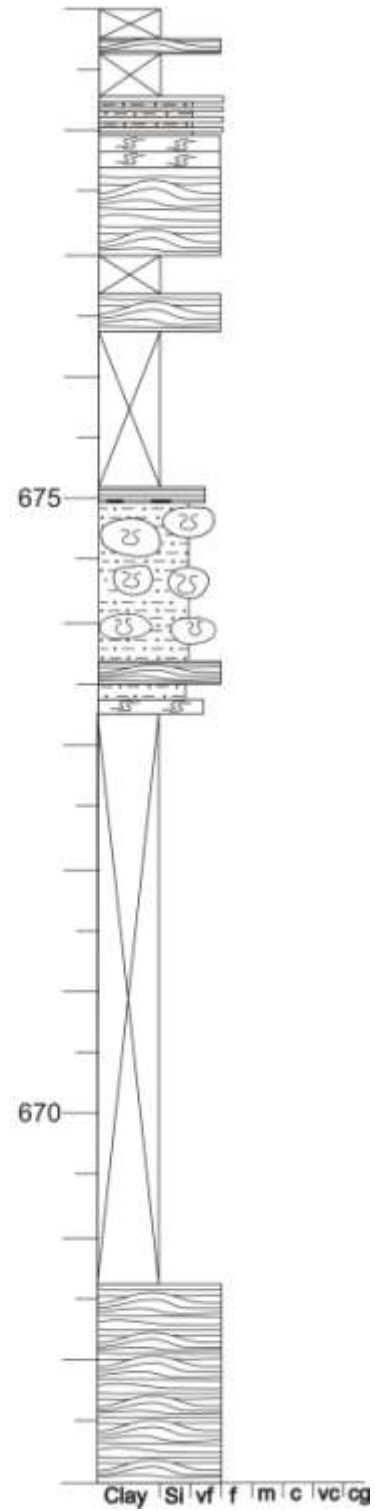
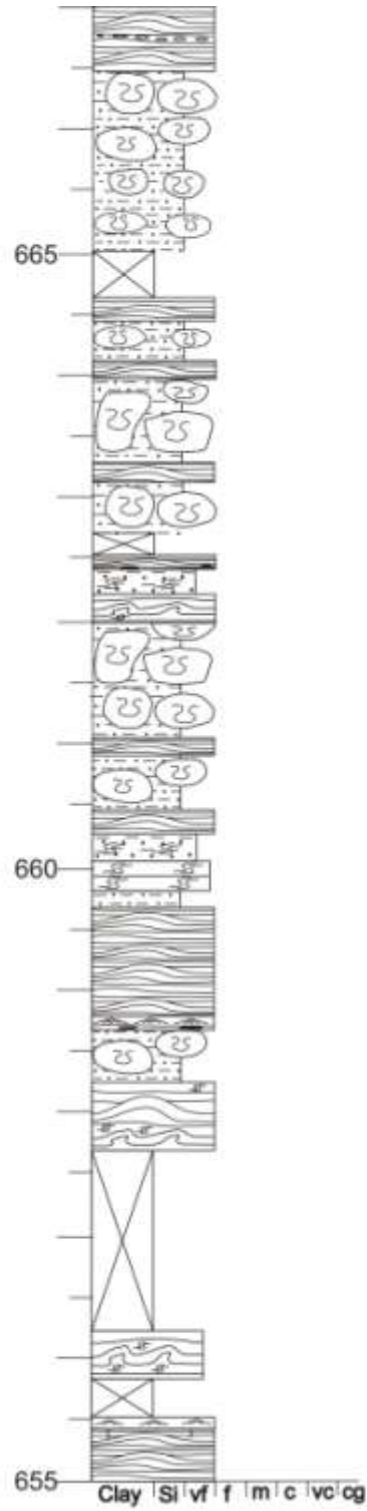
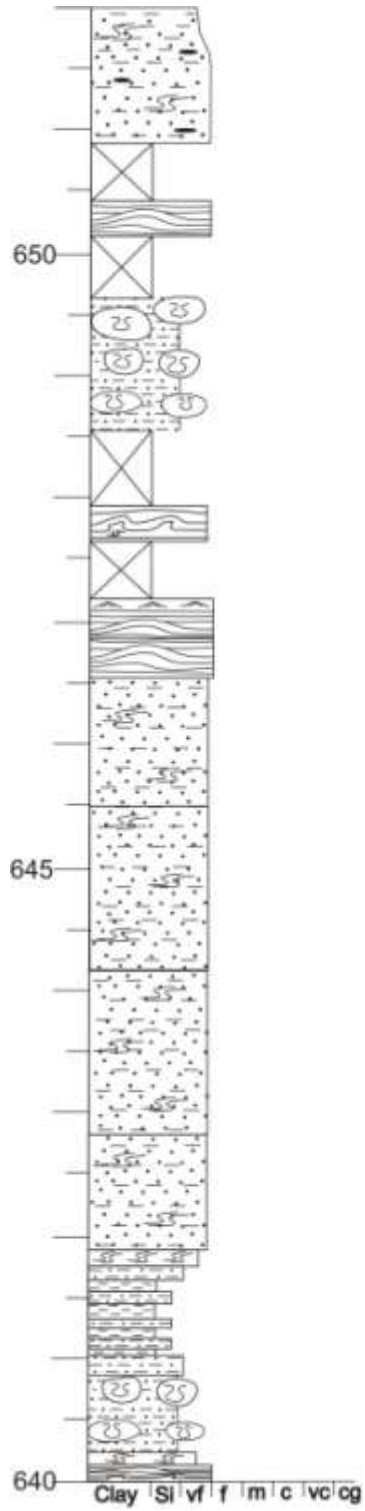
L8R2 2/2

Ringdalsfjellet



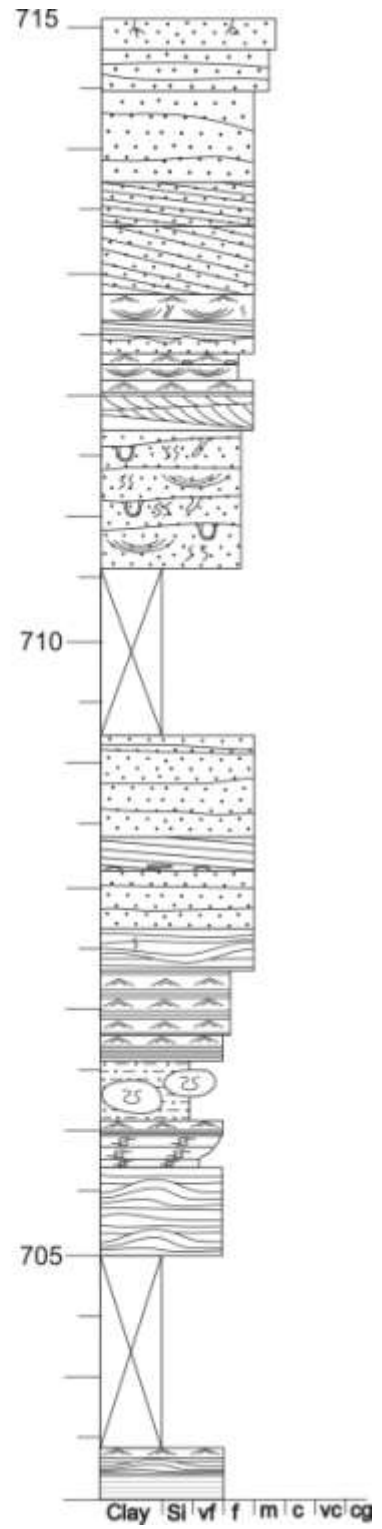
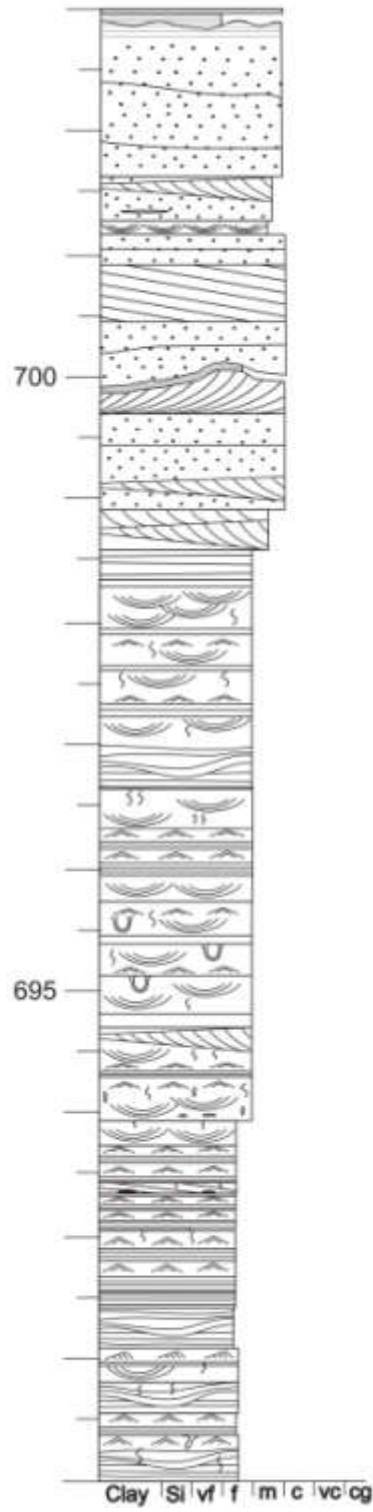
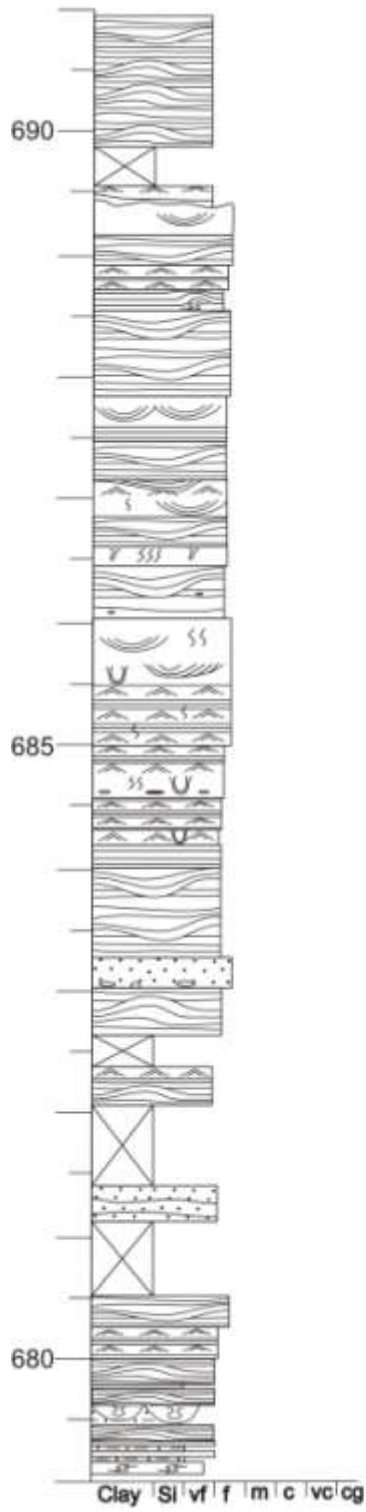
L9M1 1/3

Mefjellet



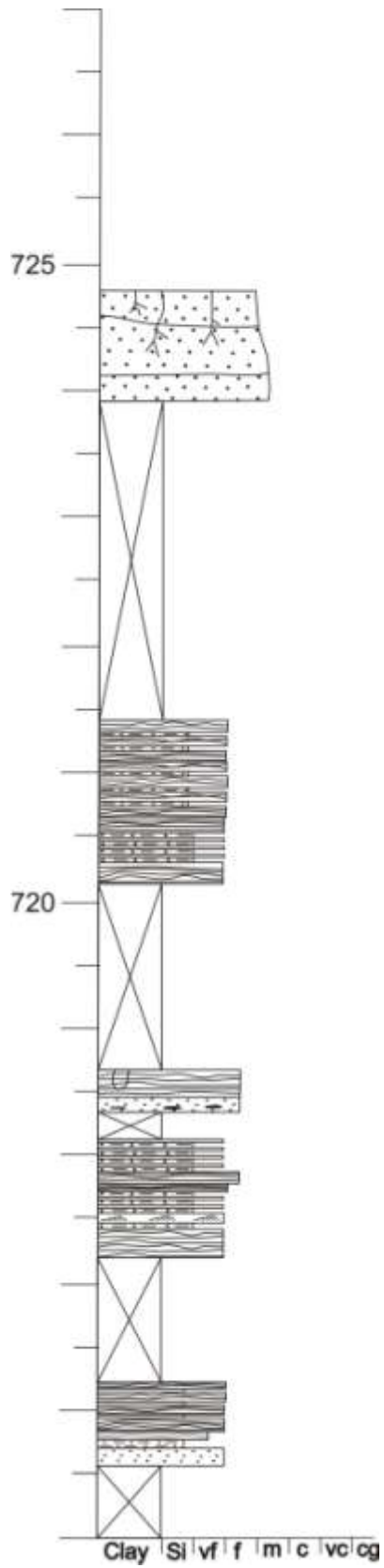
L9M1 2/3

Mefjellet



L9M1 3/3

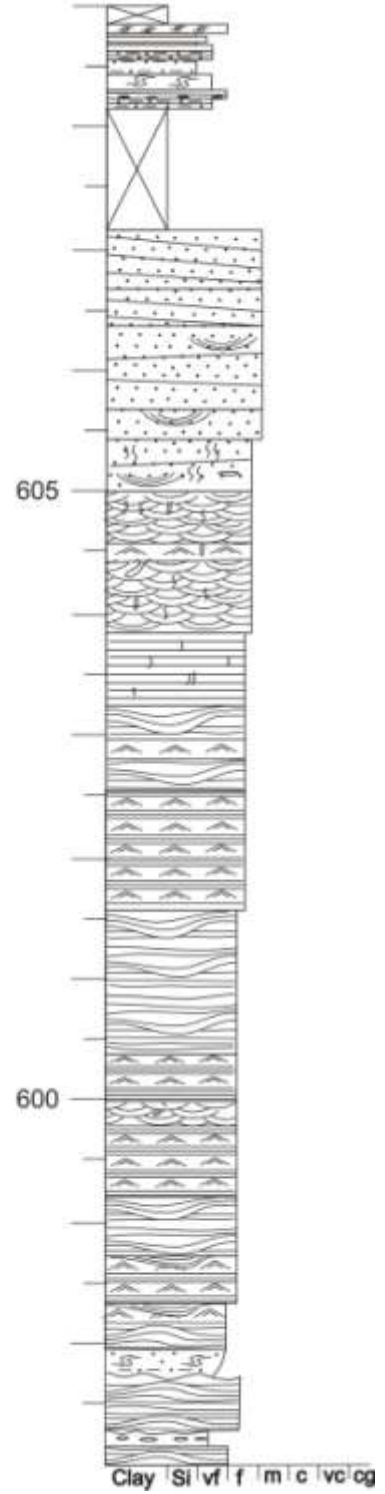
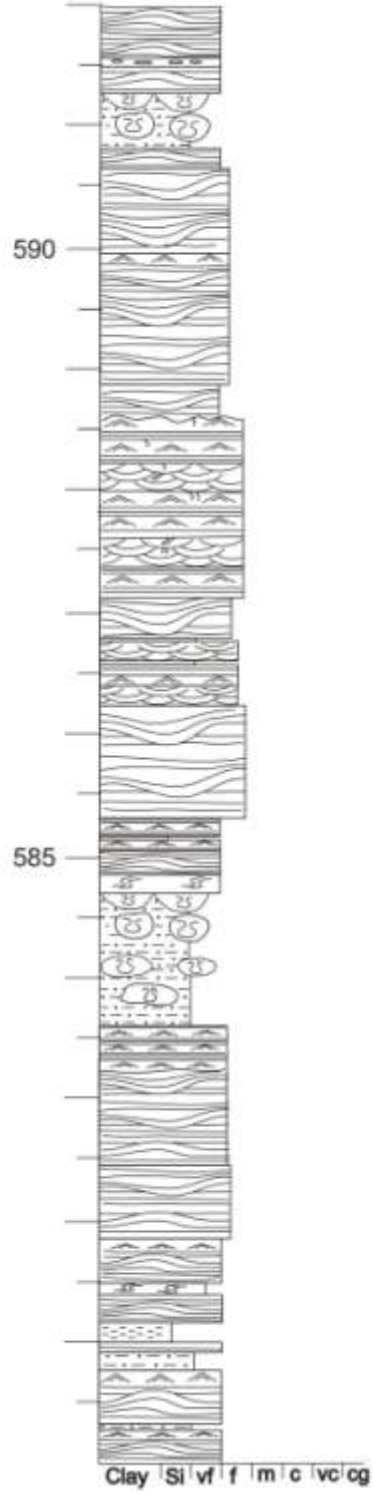
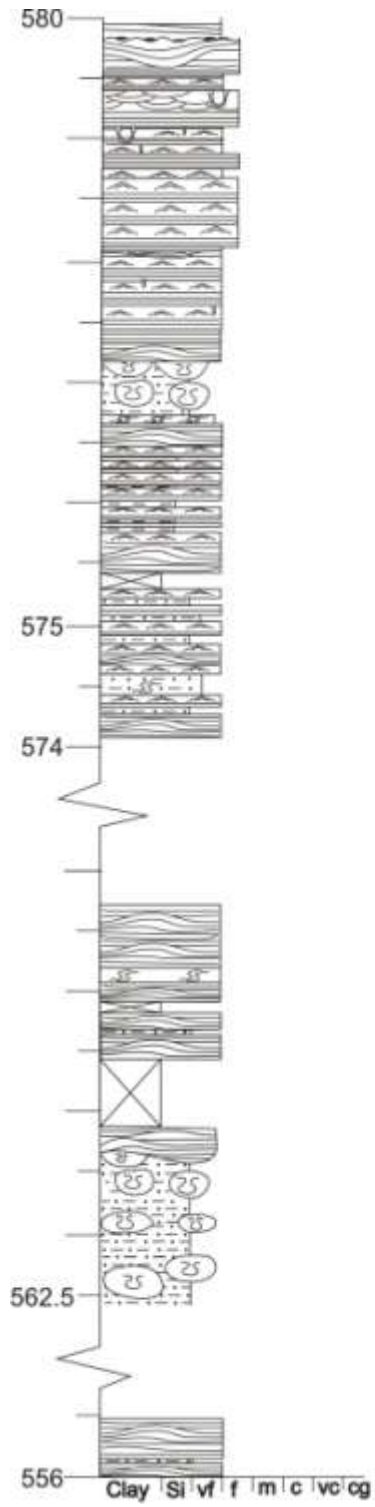
Mefjellet



L10M2

1/2

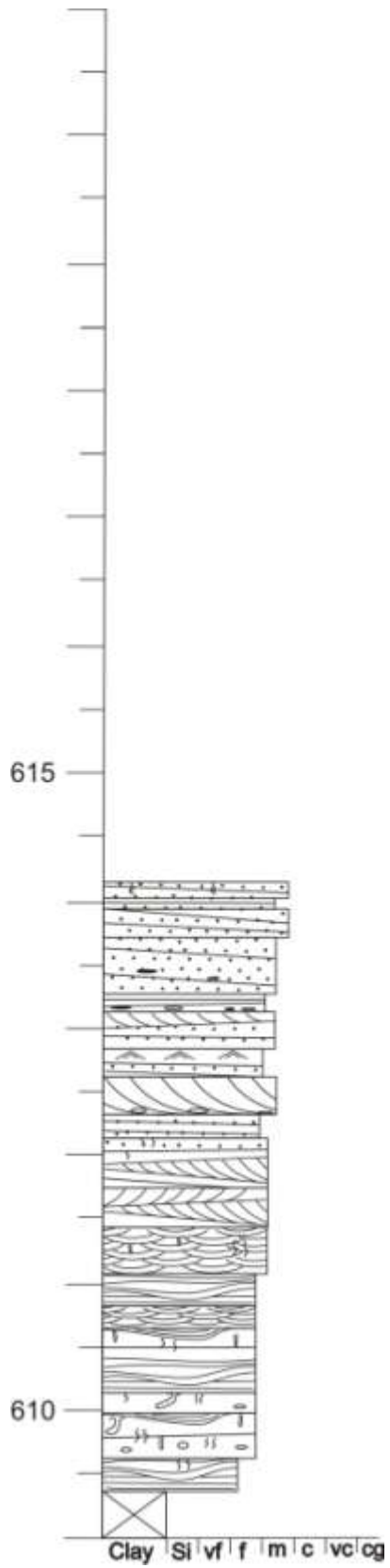
Mefjellet



L10M2

2/2

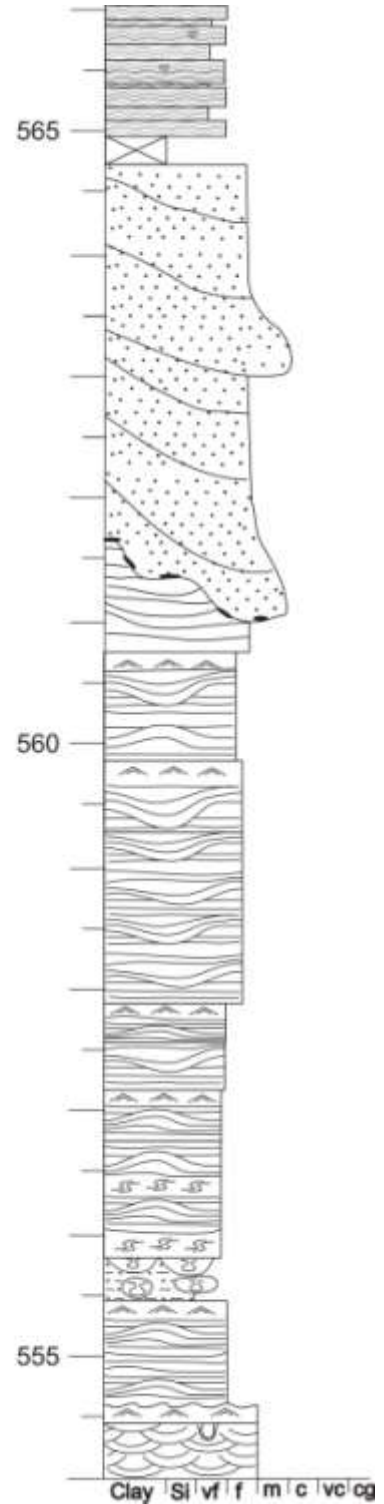
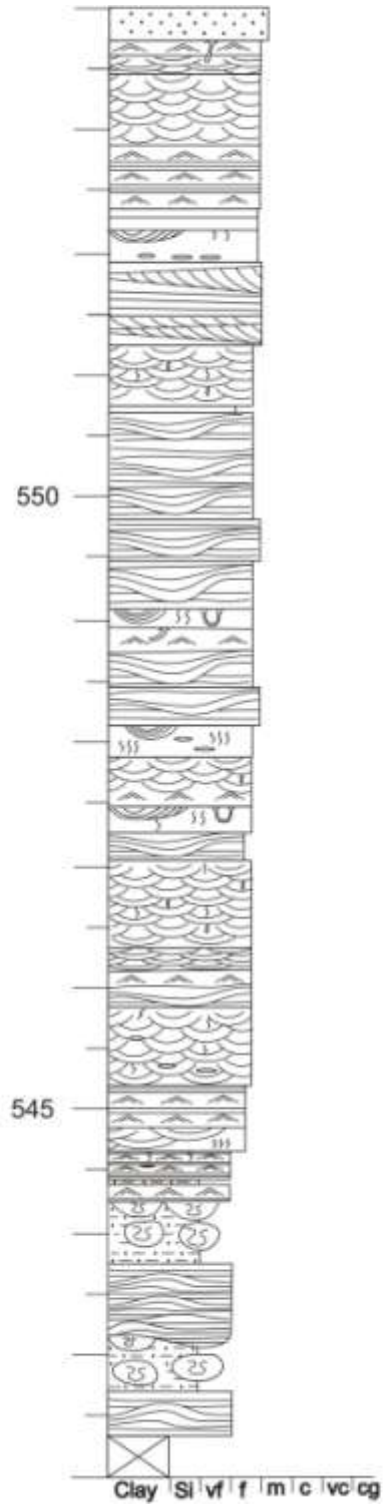
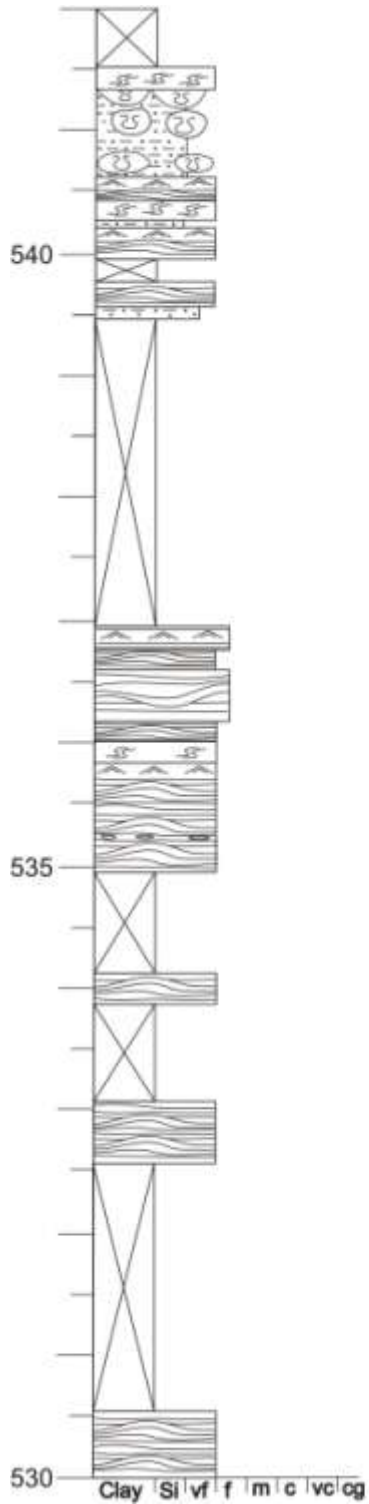
Mefjellet



L11S5

1/1

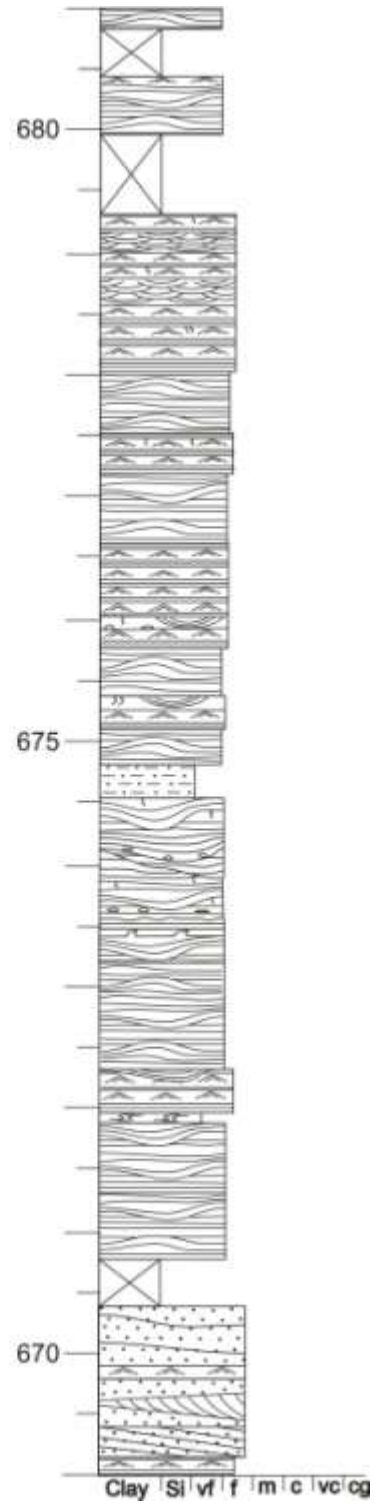
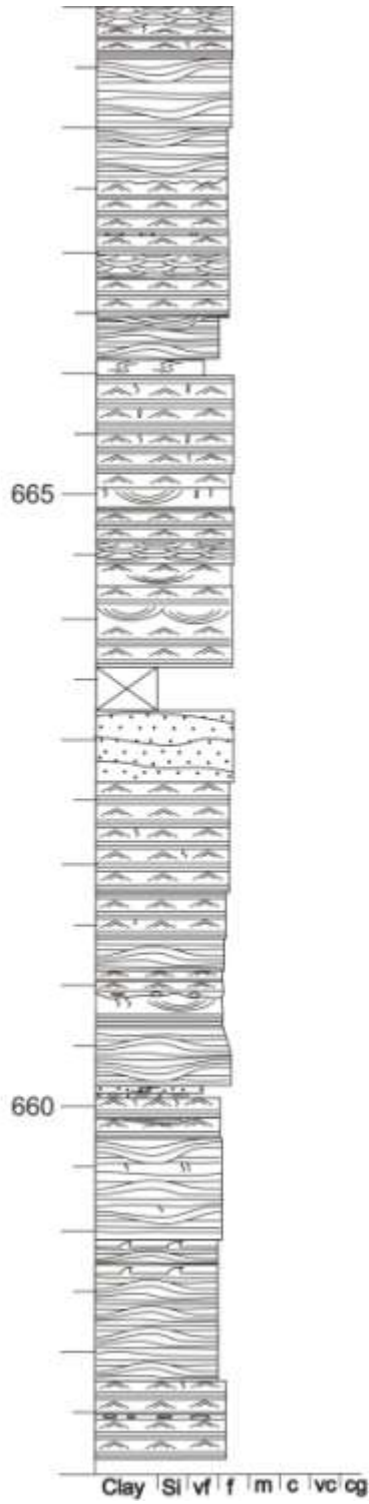
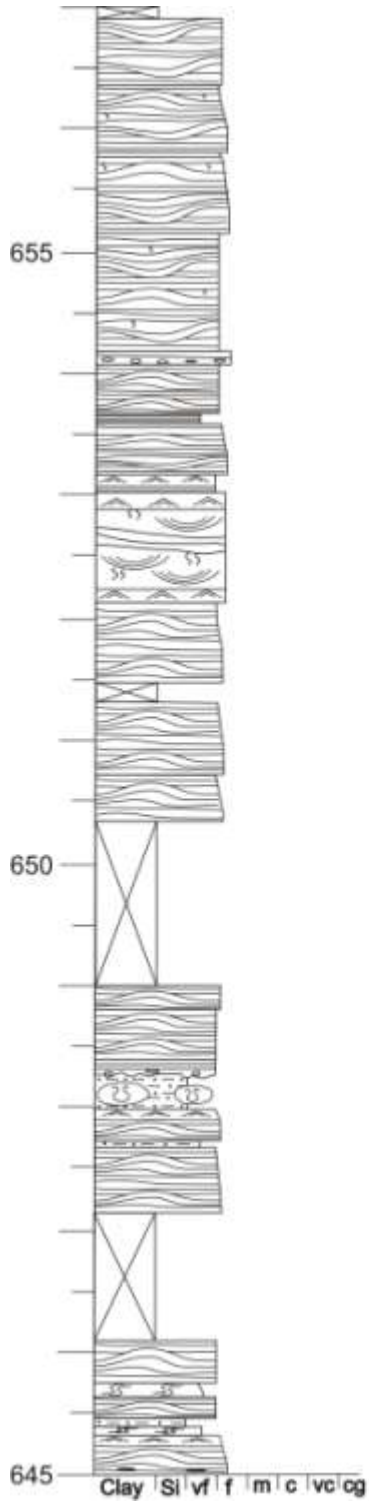
Sandsteinsfjellet



L12T3

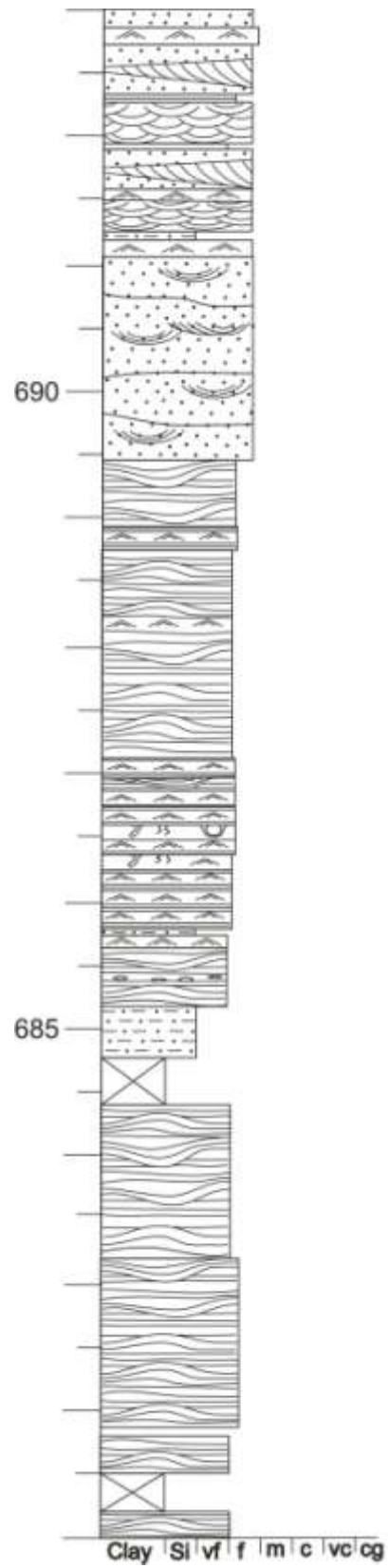
1/2

Tillbergsfjellet

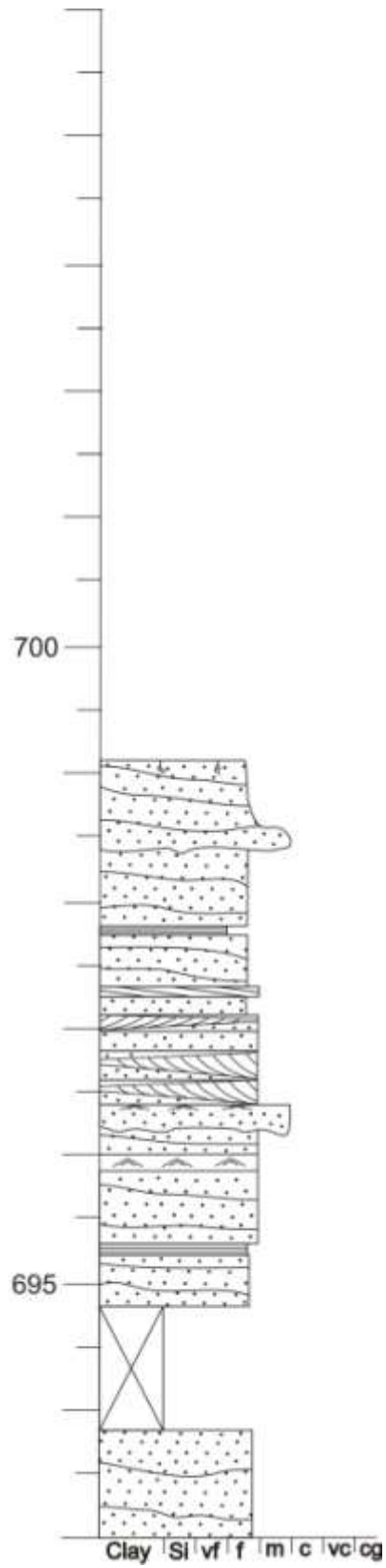


L12T3

2/2



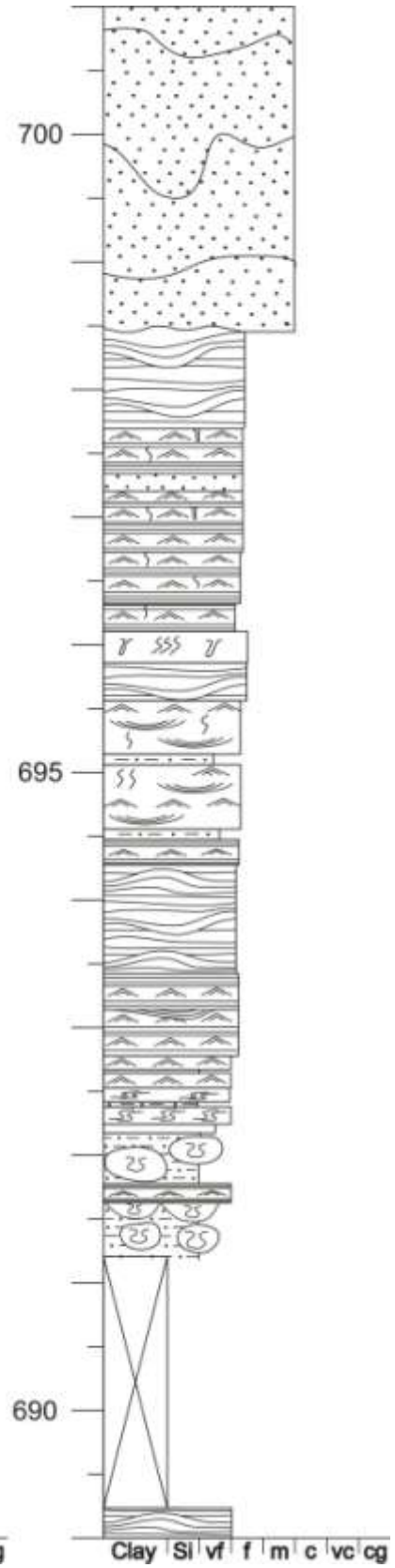
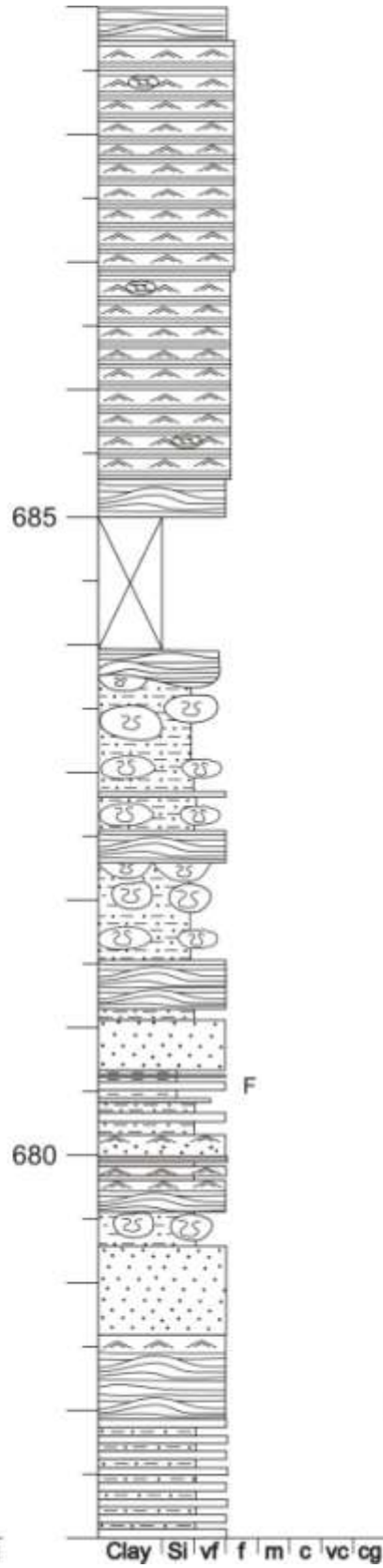
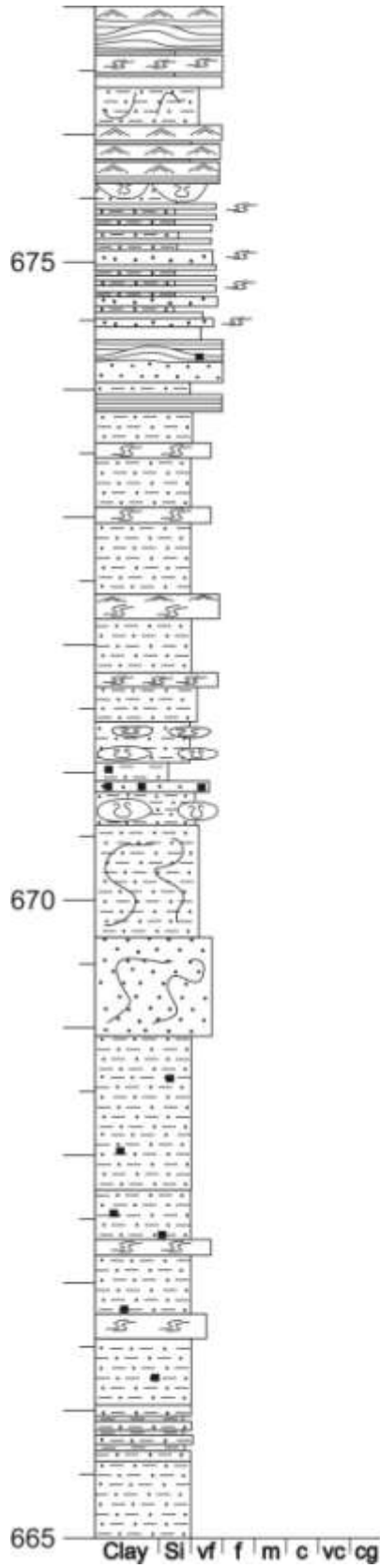
Tillbergsfjellet



L13R3

1/2

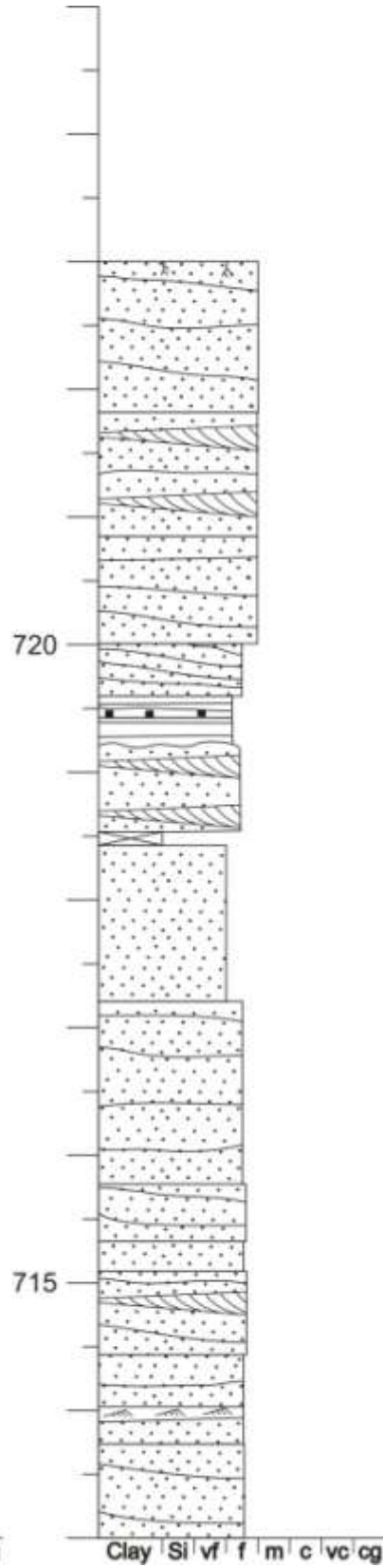
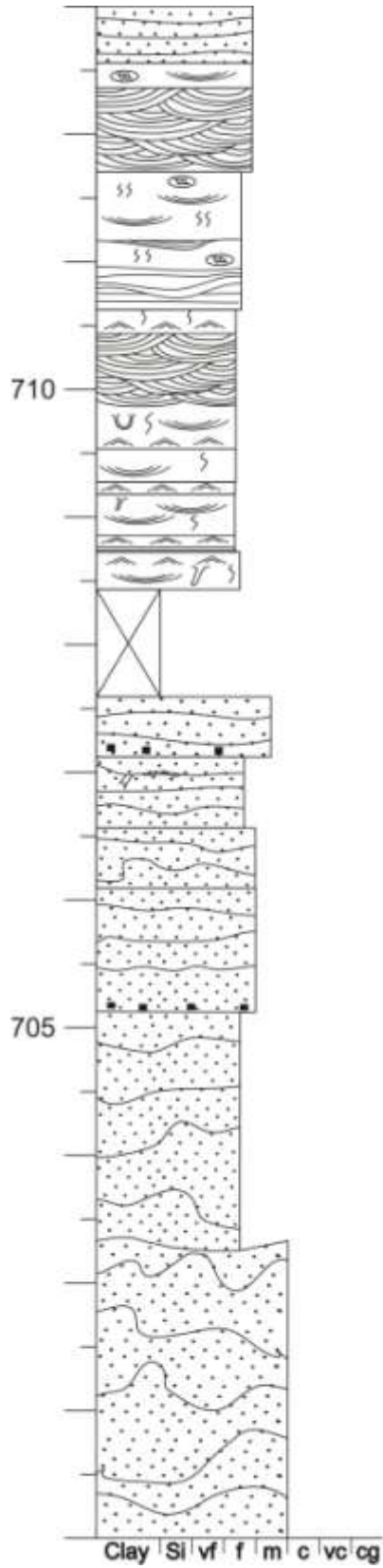
Ringdalsfjellet



L13R3

2/2

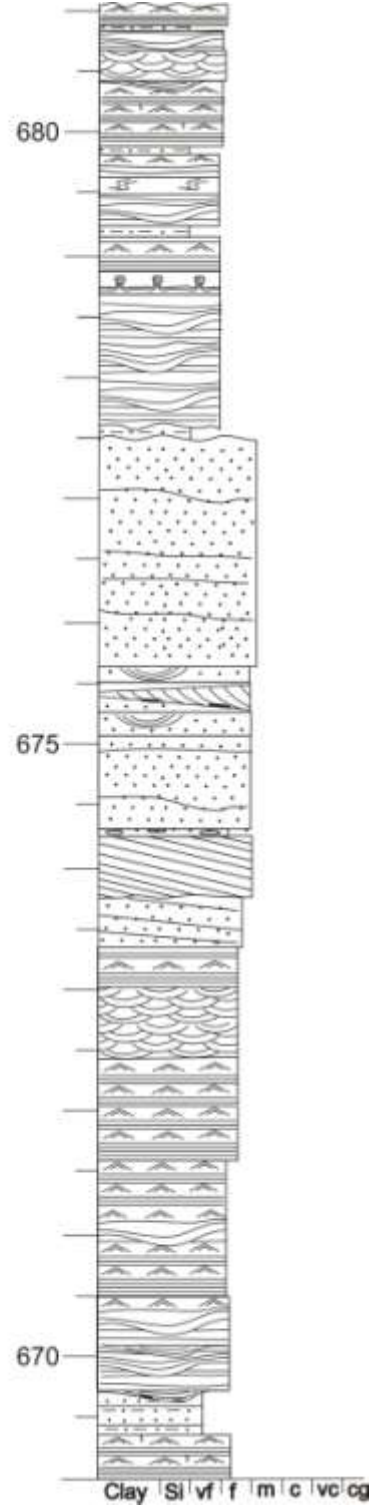
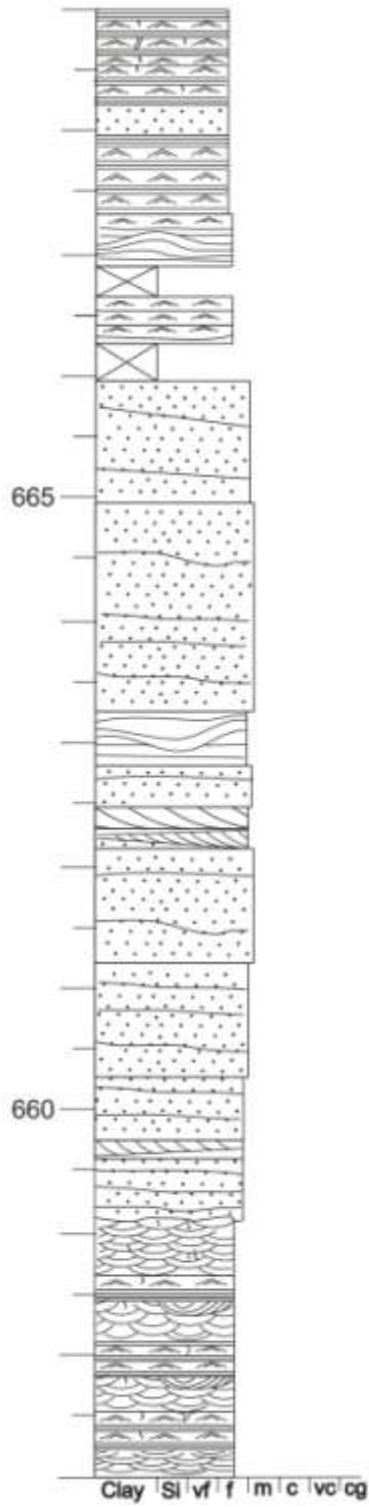
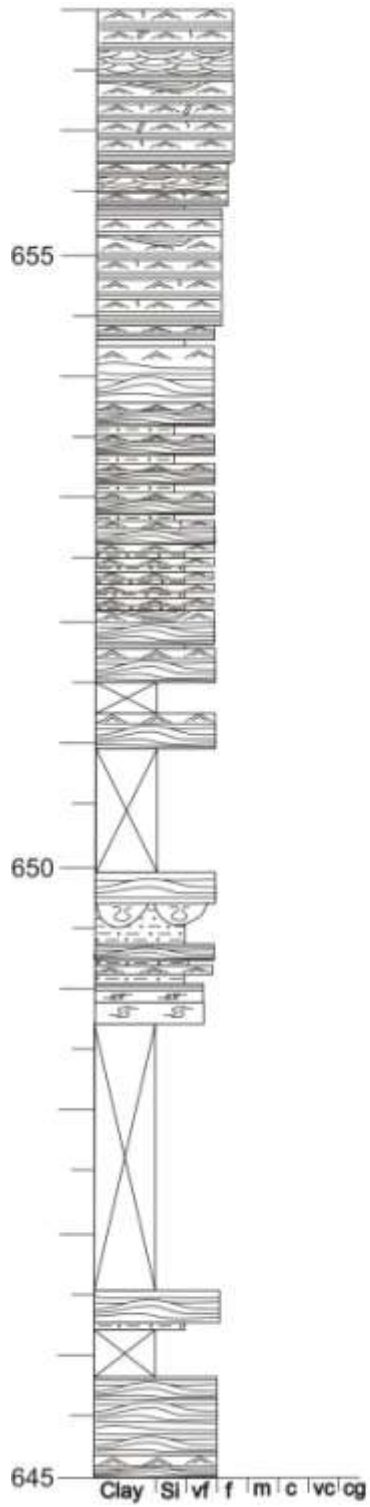
Ringdalsfjellet



L14M3

1/2

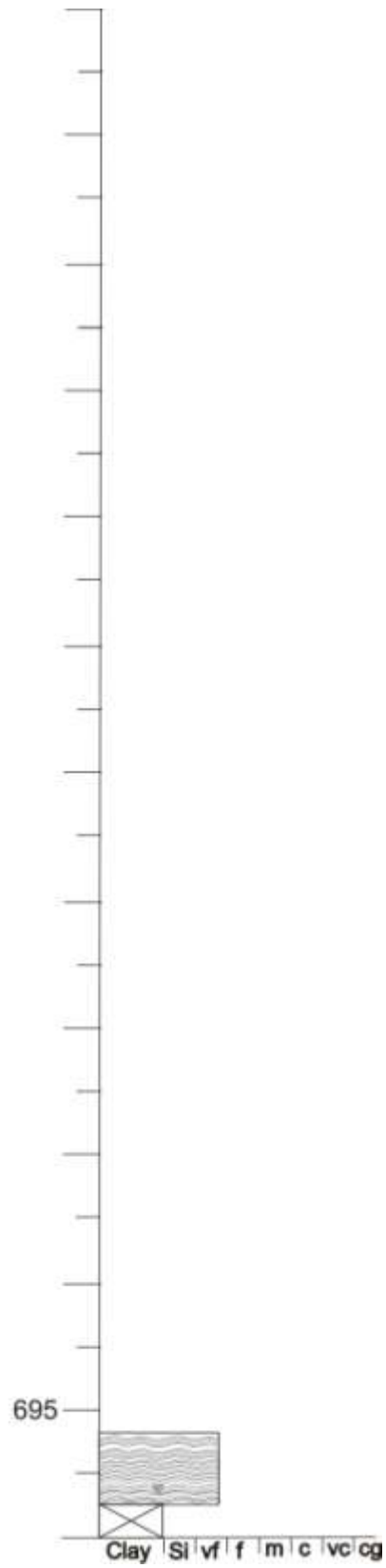
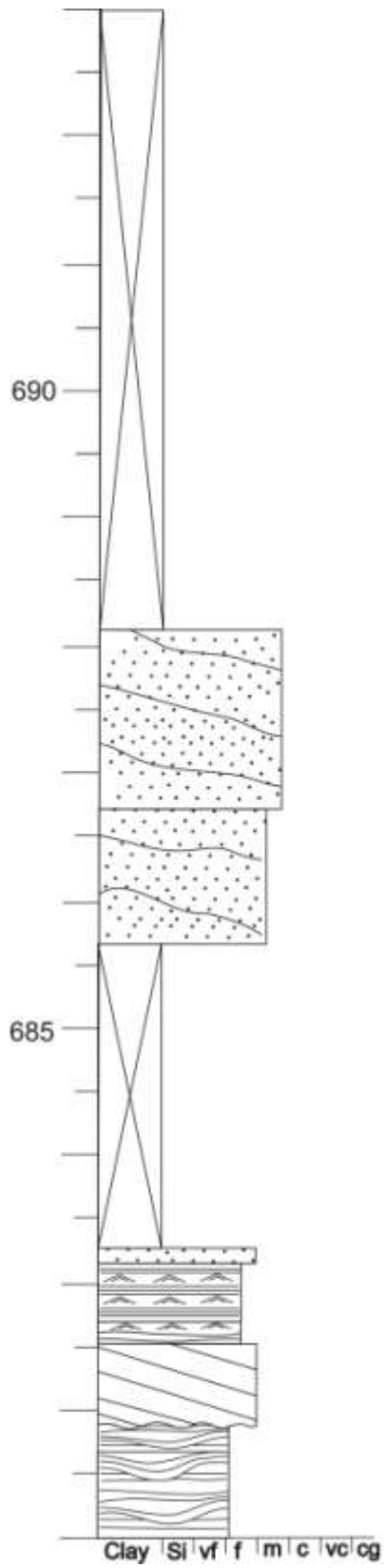
Mefjellet



L14M3

2/2

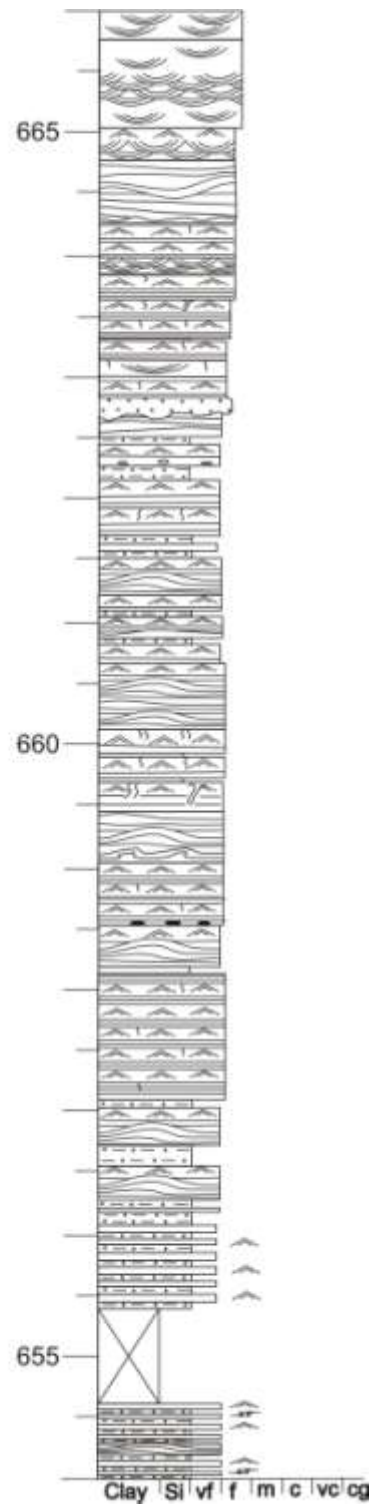
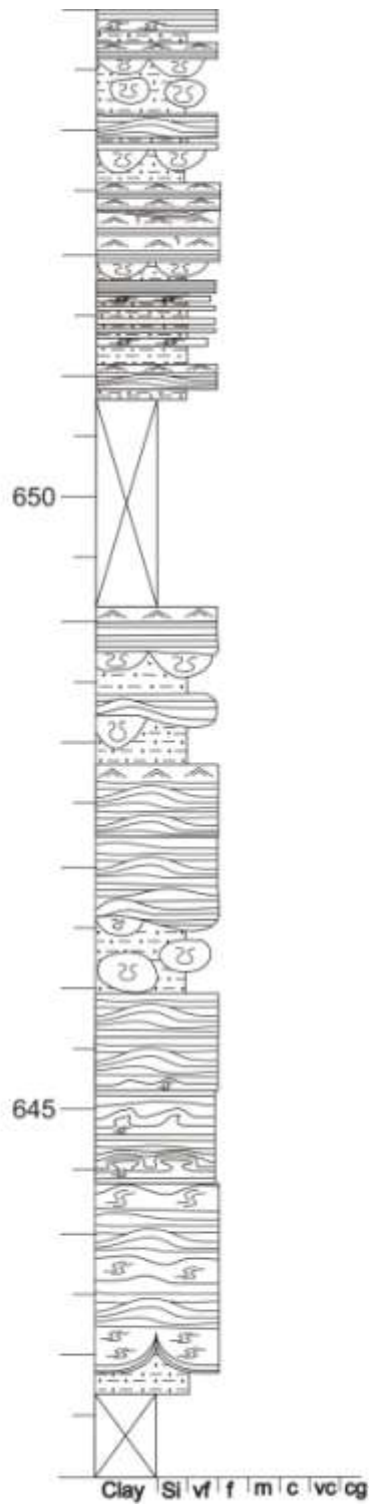
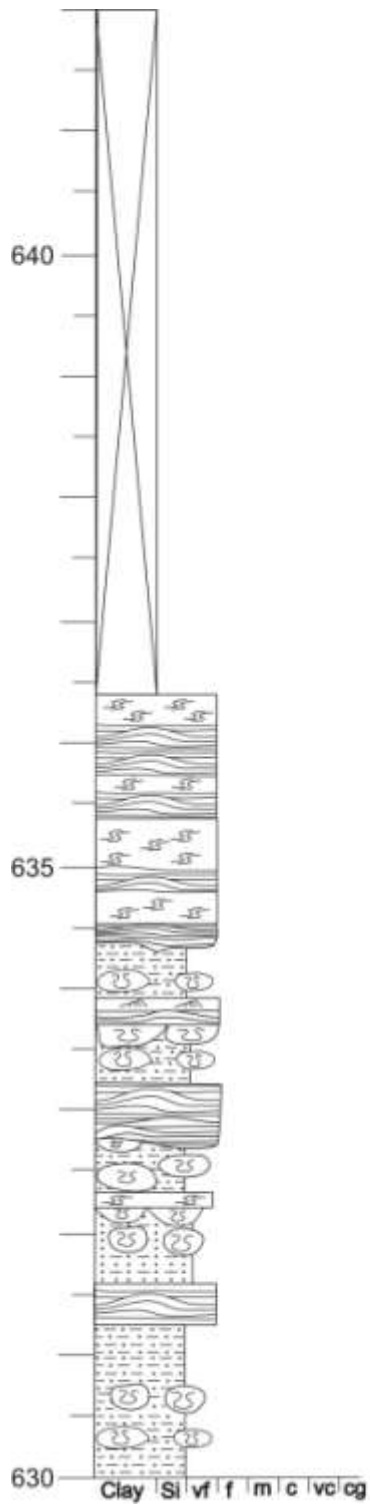
Mefjellet



L15M4

1/2

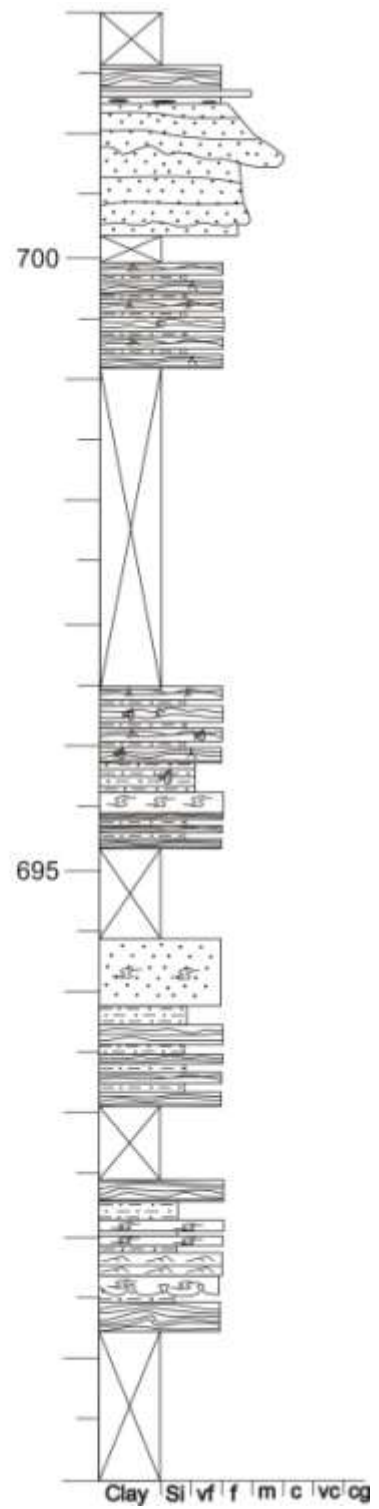
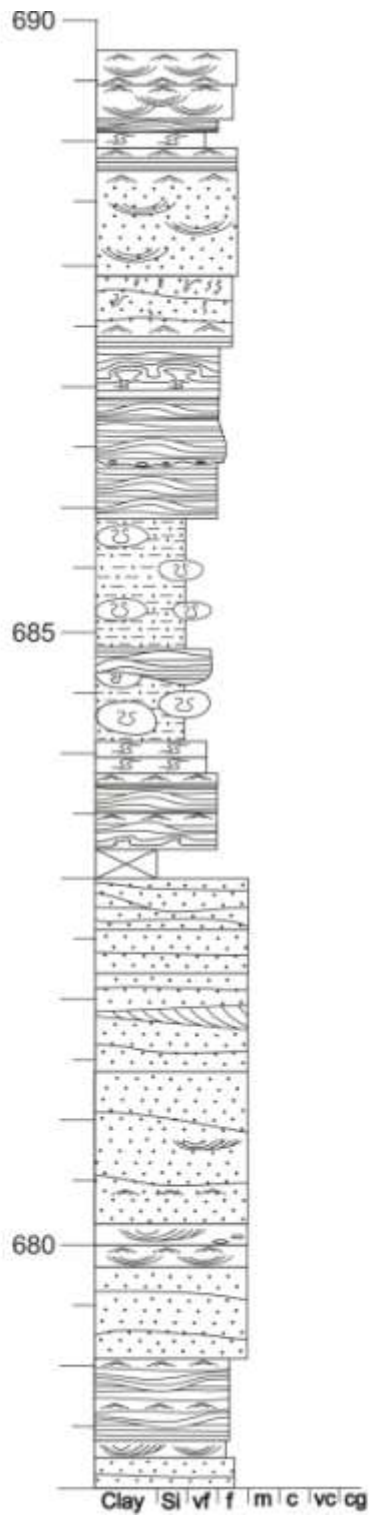
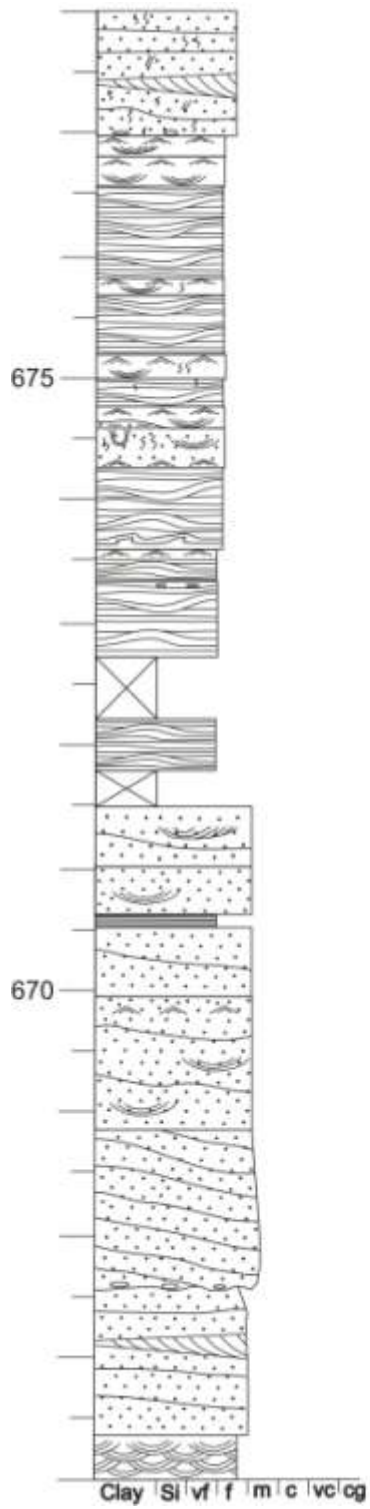
Mefjellet



L15M4

2/2

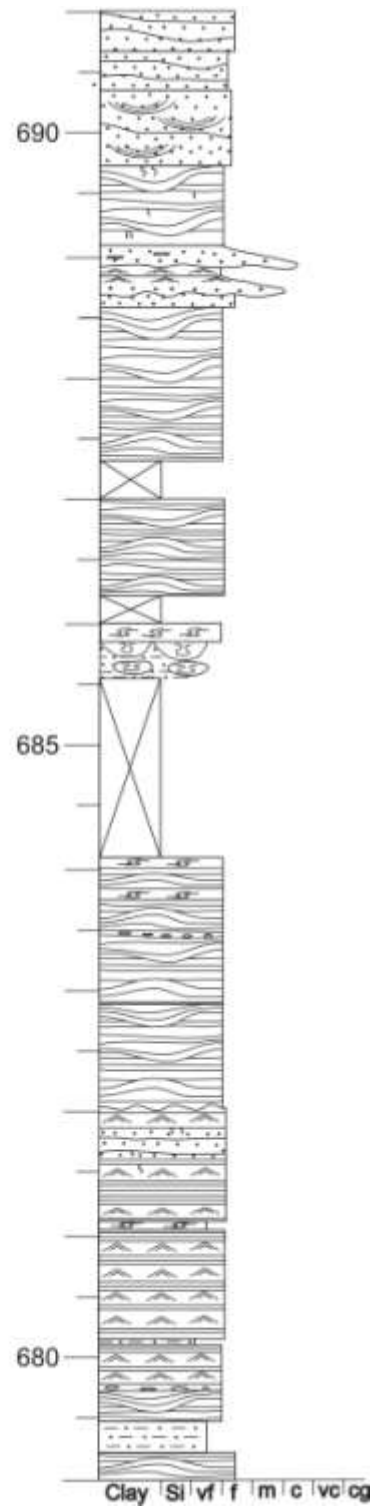
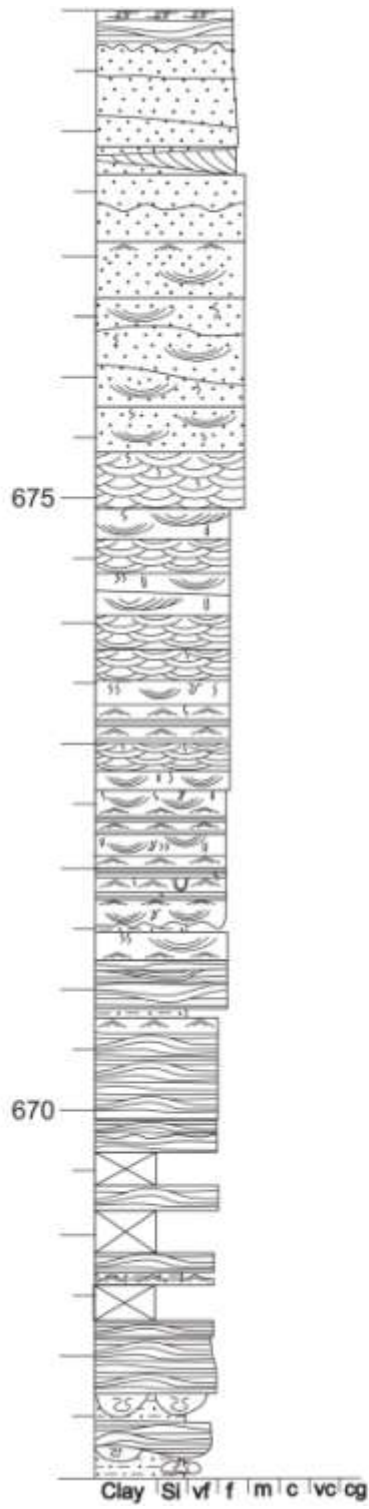
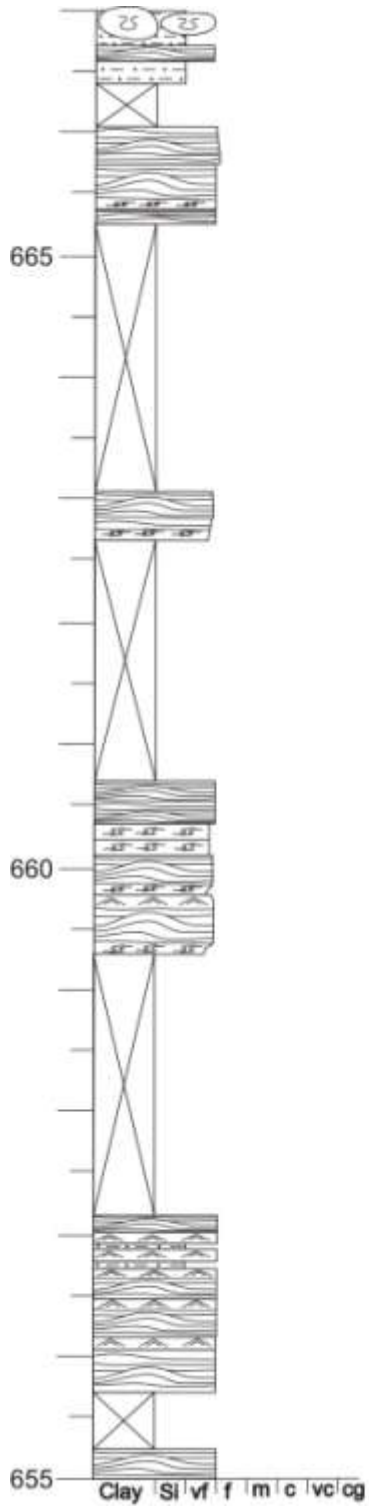
Mefjellet



L16T4

1/2

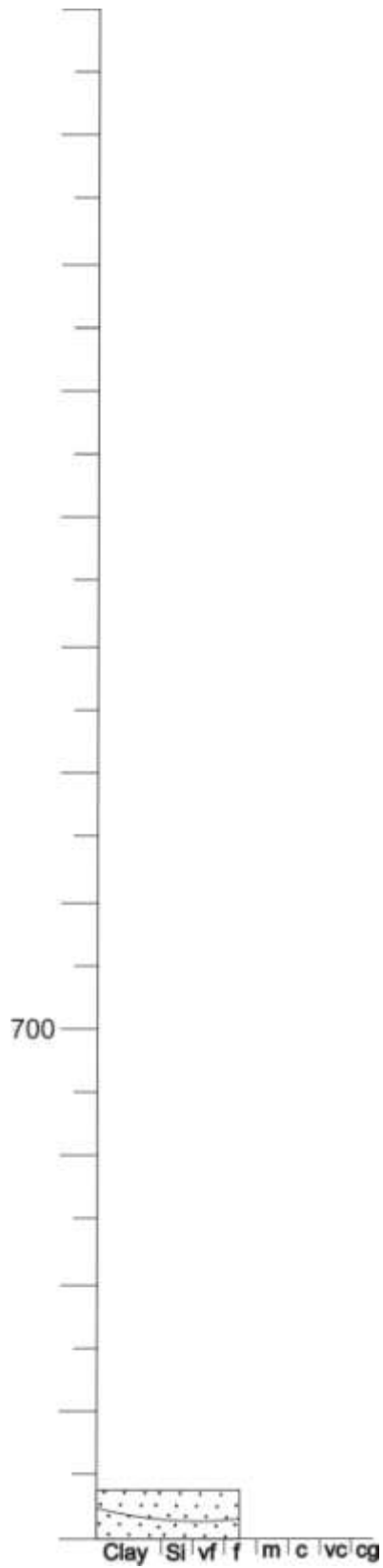
Tillbergsfjellet



L16T4

2/2

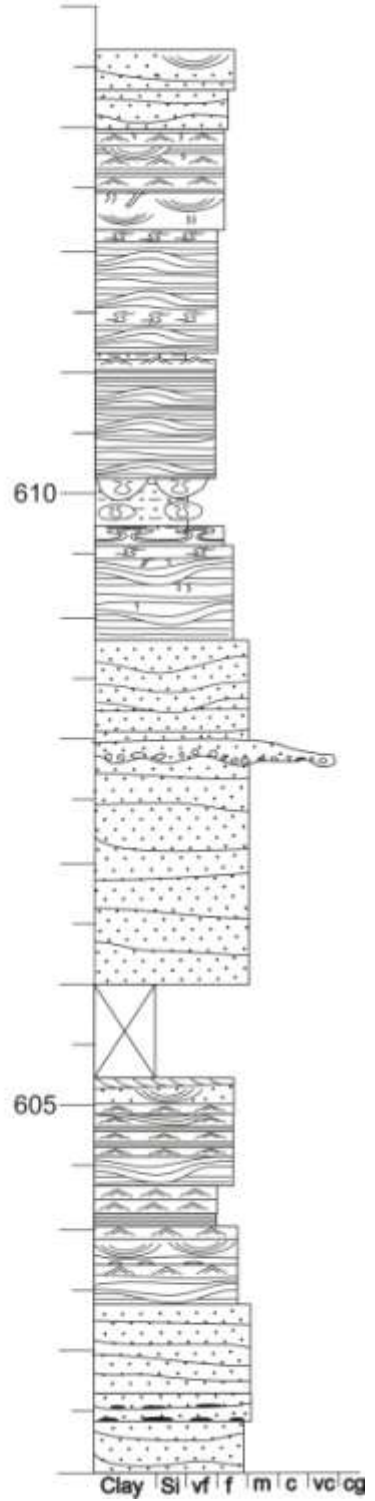
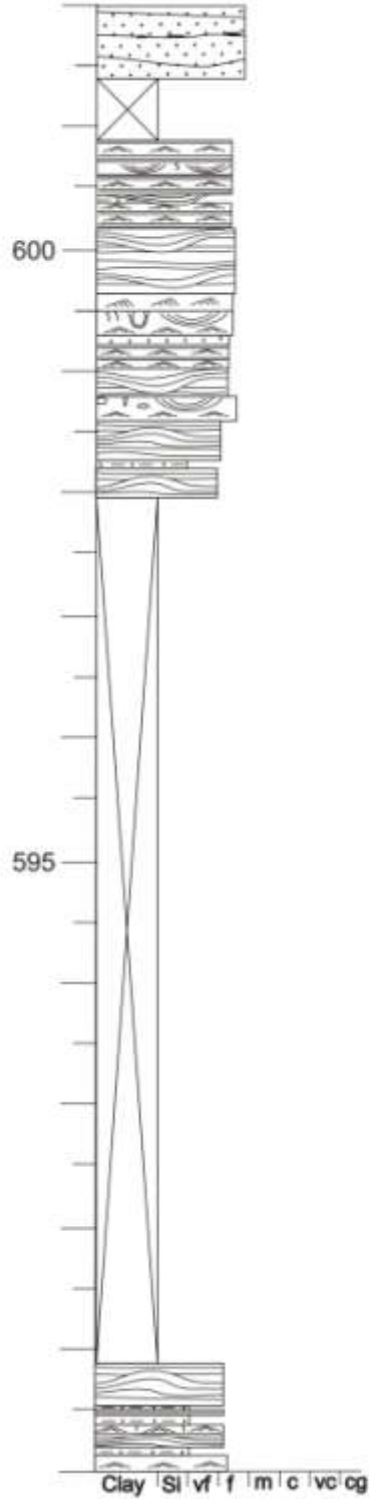
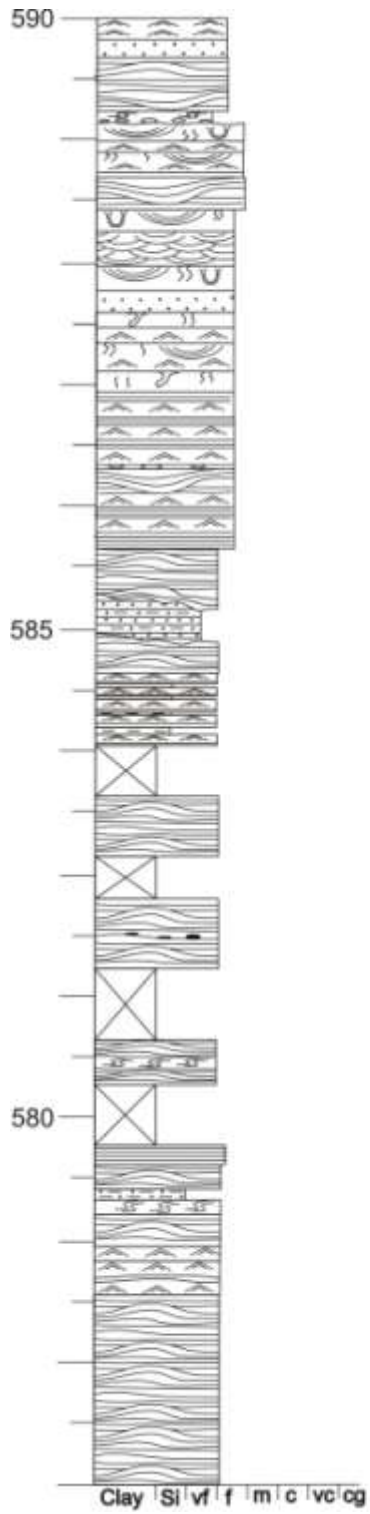
Tillbergsfjellet



L17T5

1/1

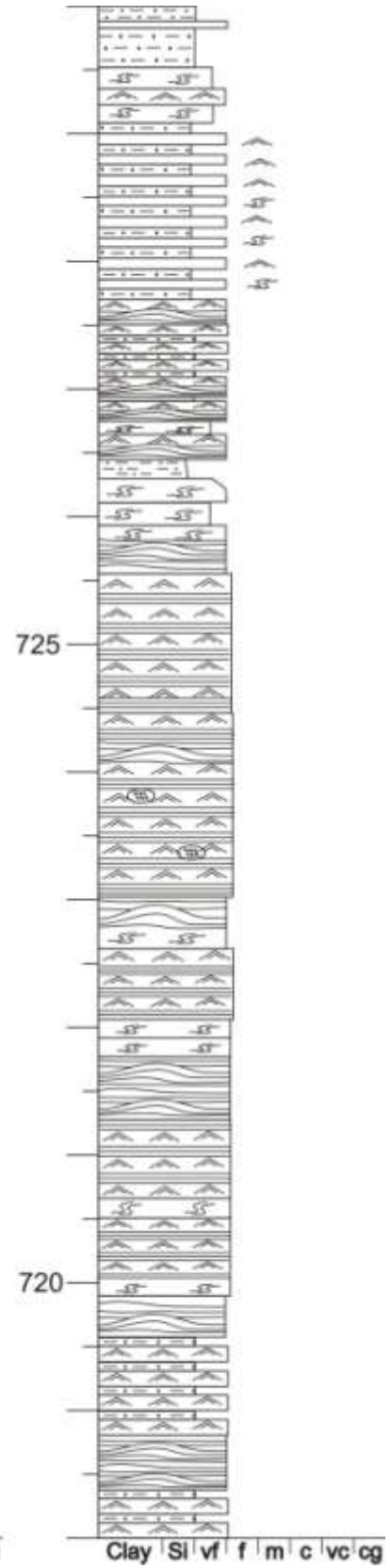
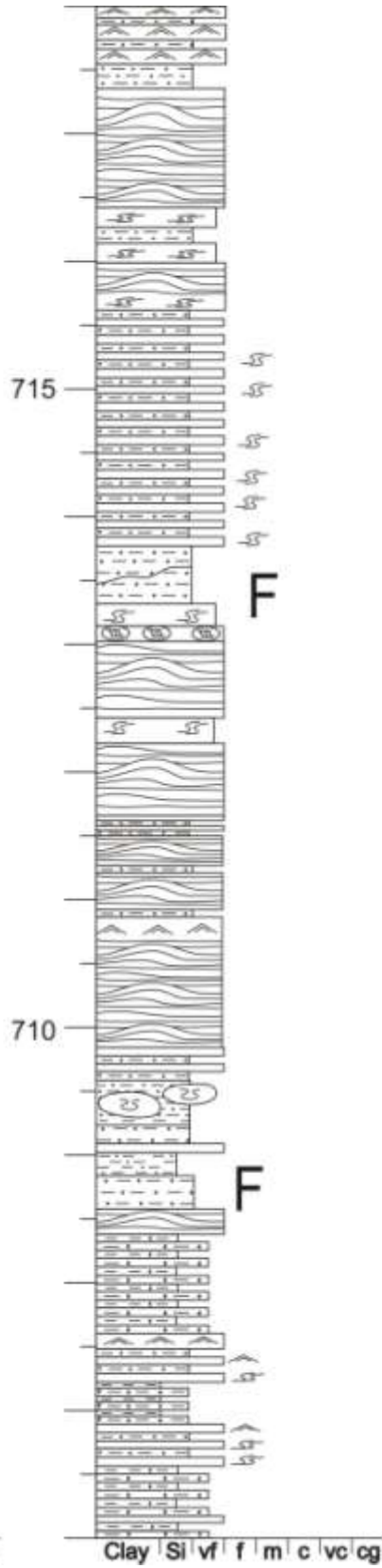
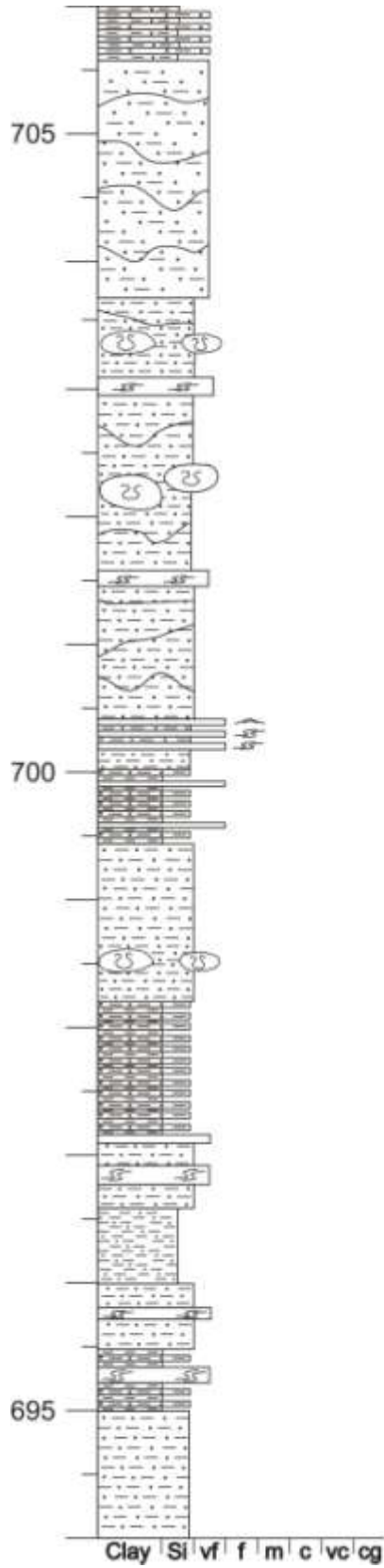
Tillbergsfjellet



L18R4

1/2

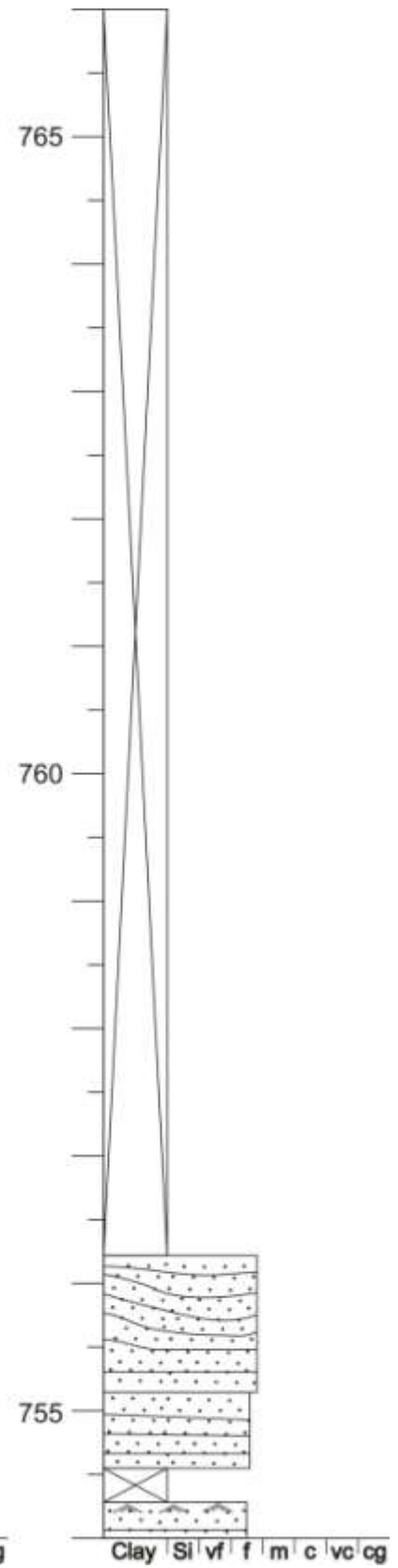
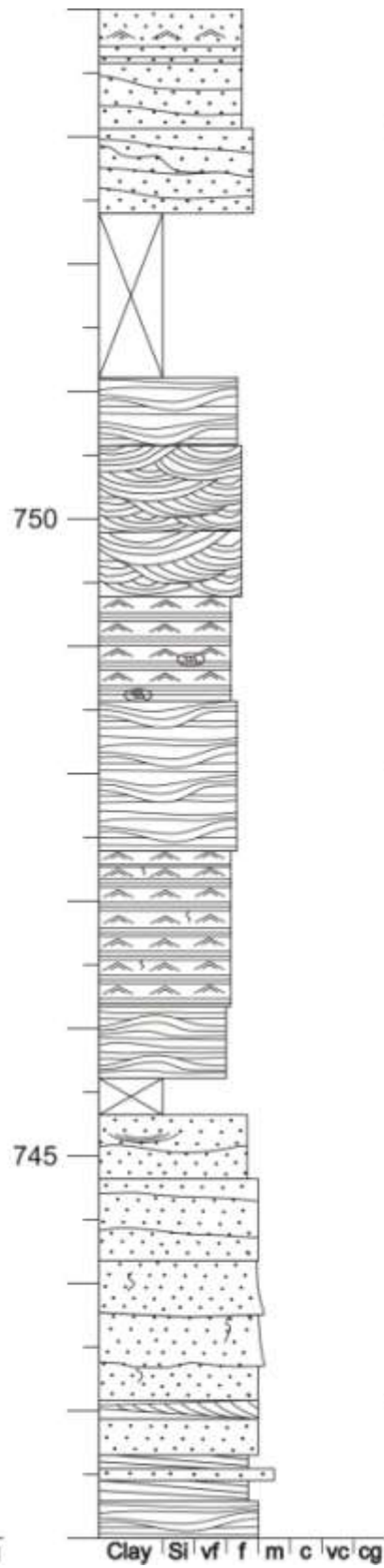
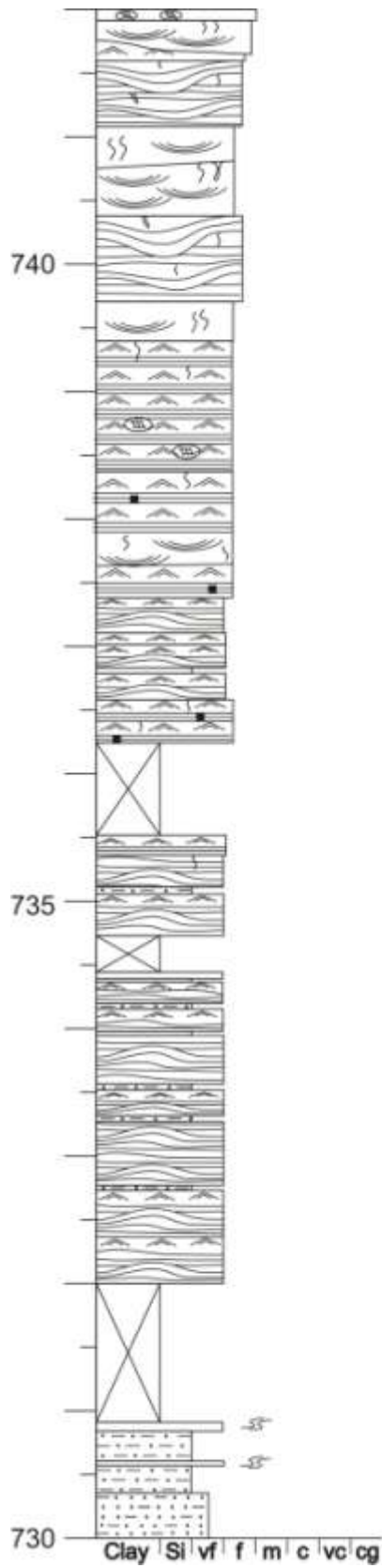
Ringdalsfjellet



L18R4

2/2

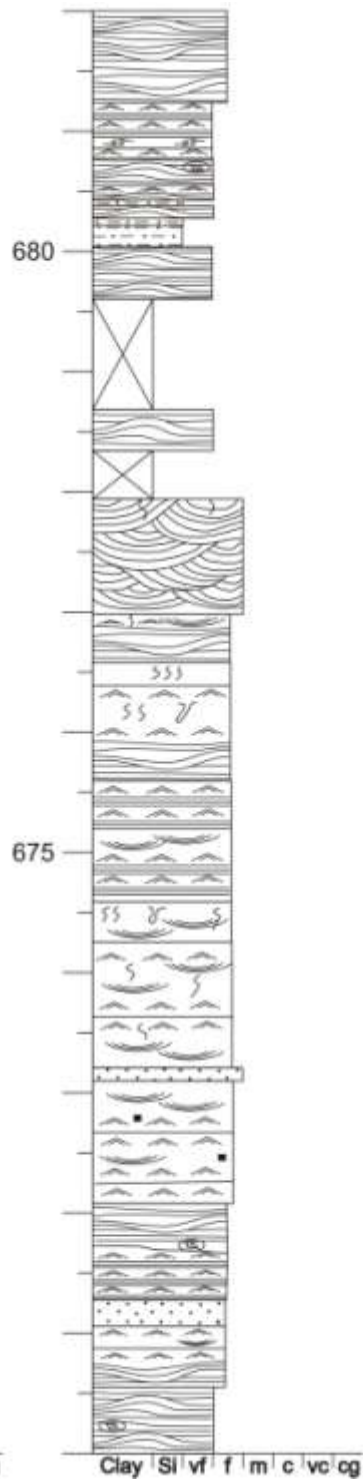
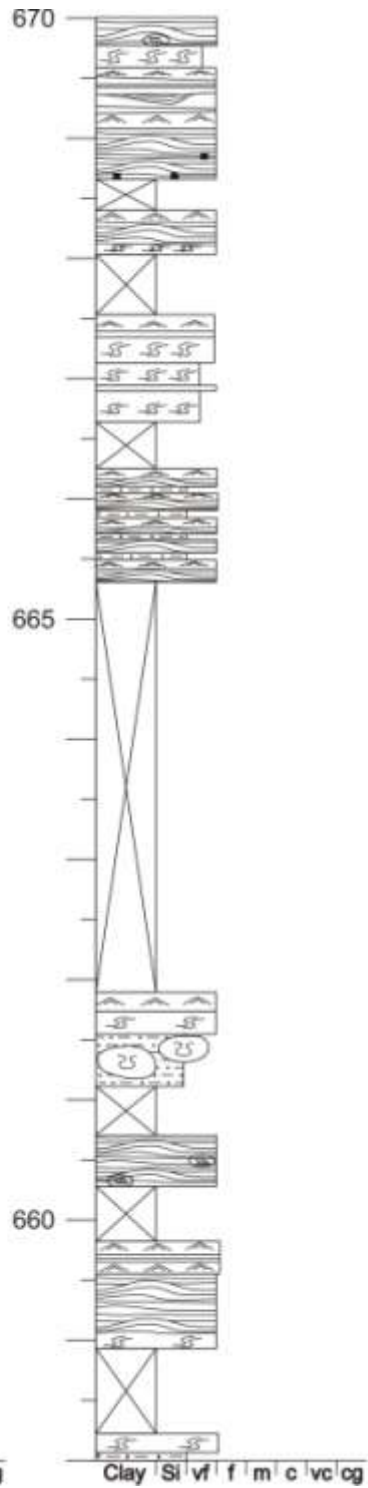
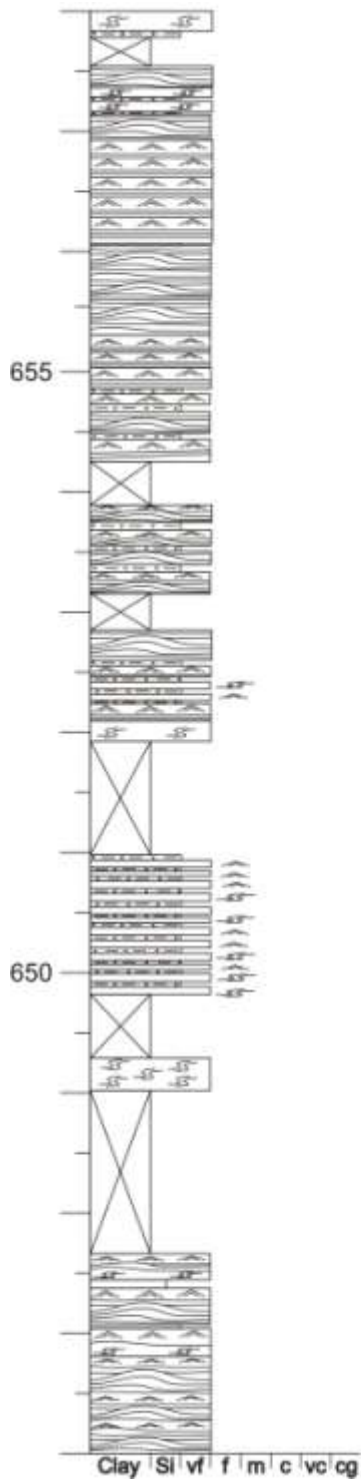
Ringdalsfjellet



L19R5

1/2

Ringdalsfjellet

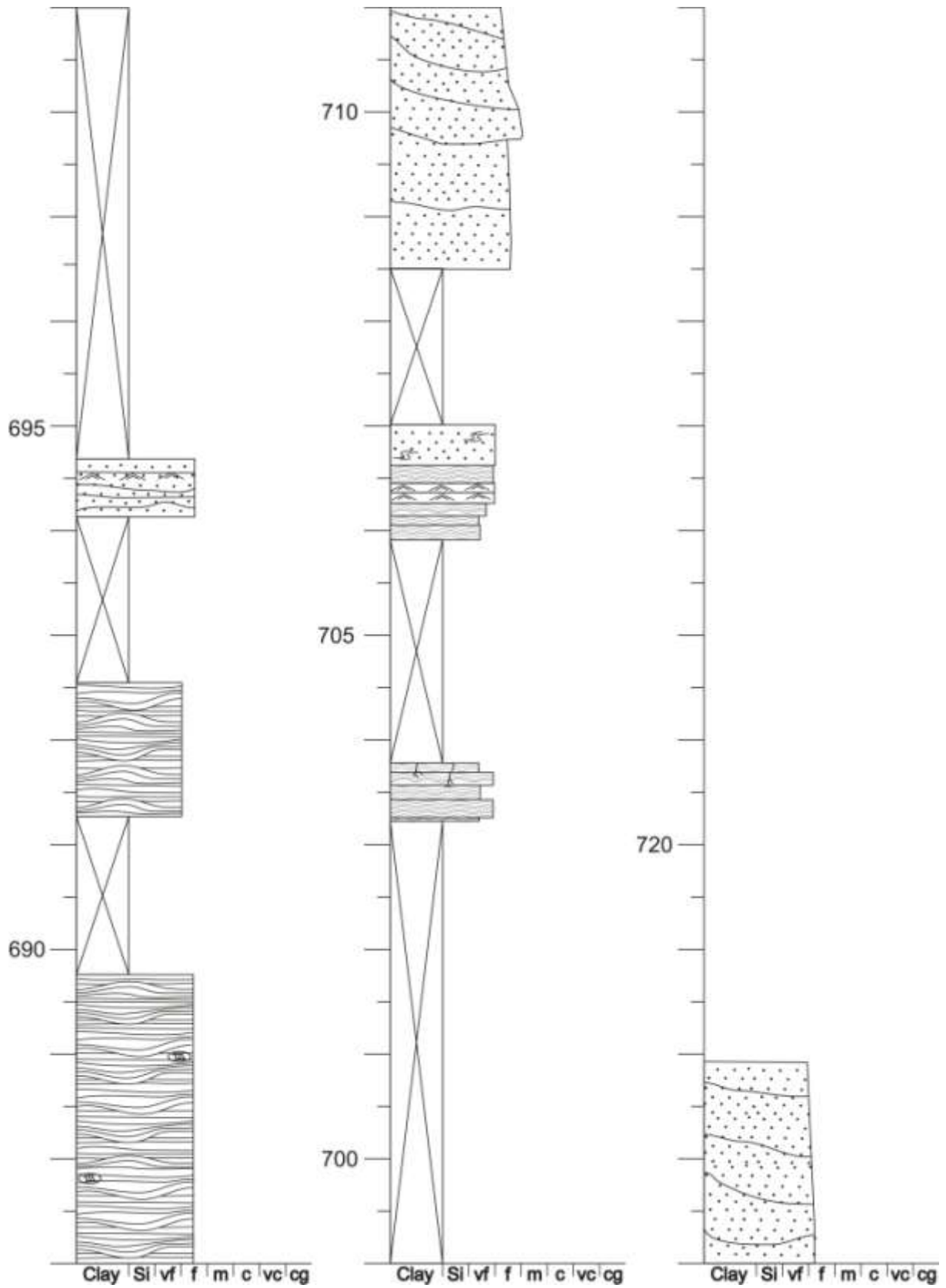


685

L19R5

2/2

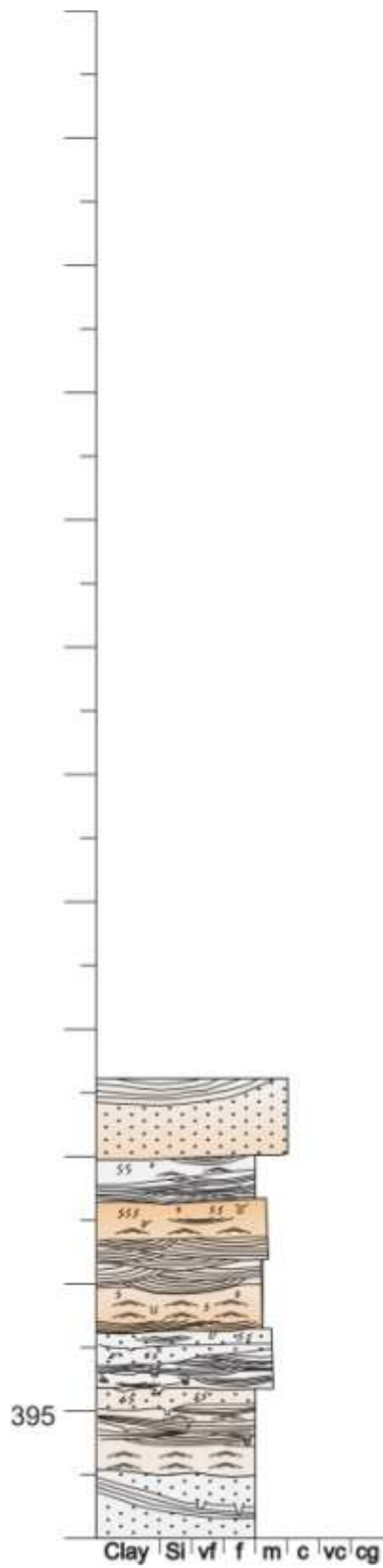
Ringdalsfjellet



L20S6

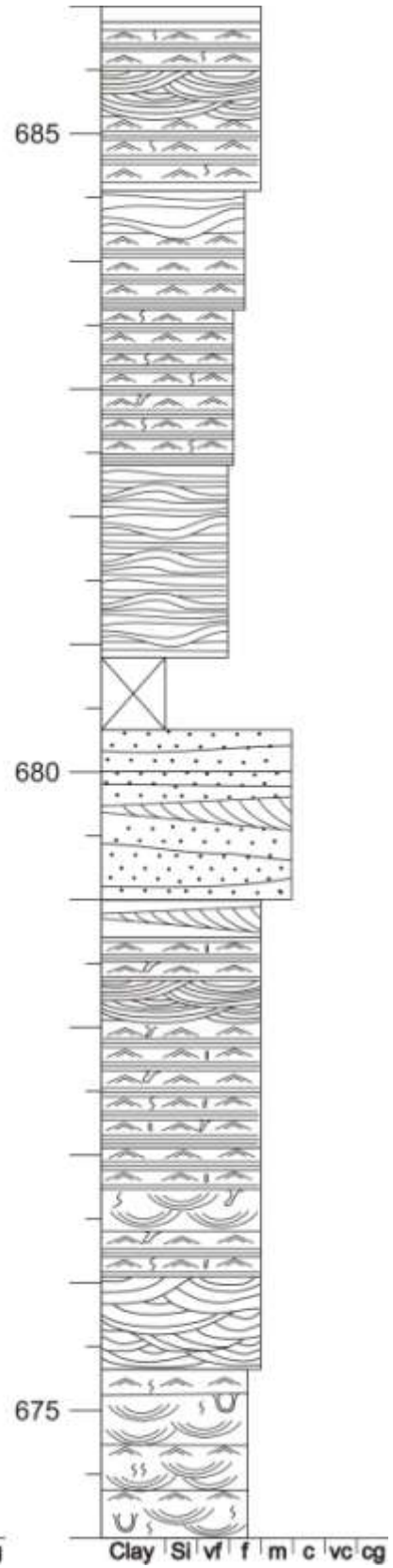
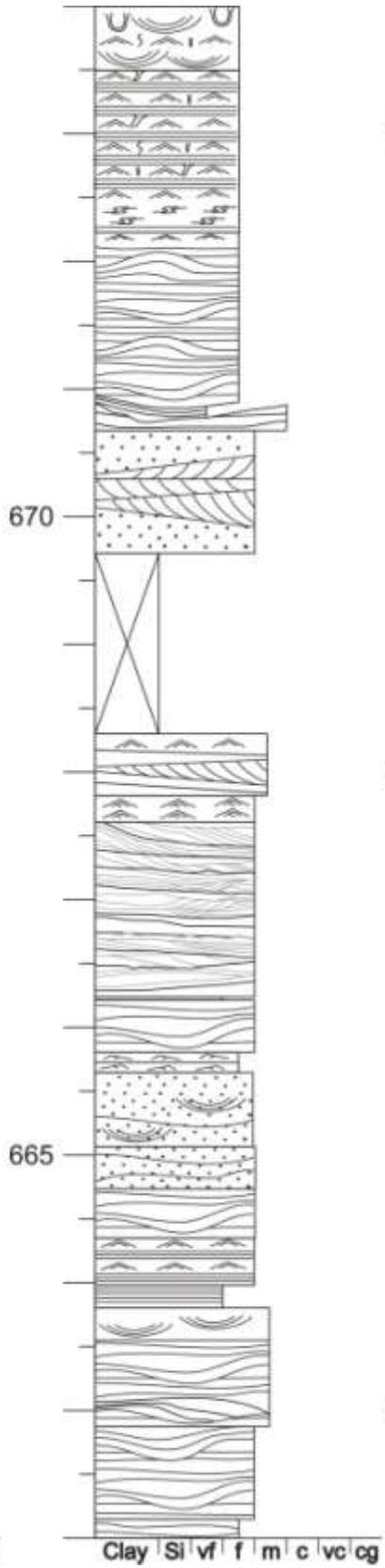
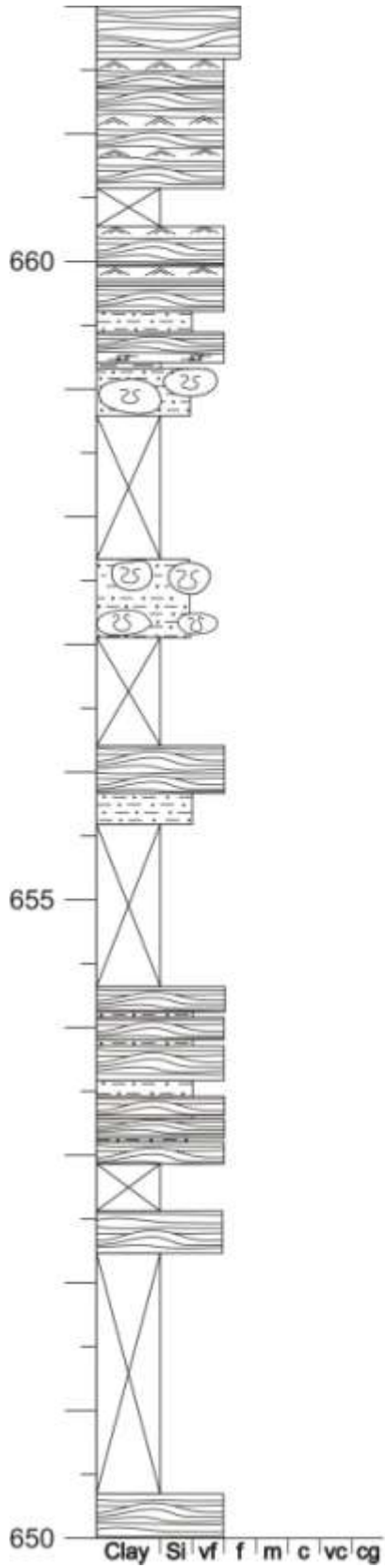
1/1

Sandsteinsfjellet



L21T6 1/2

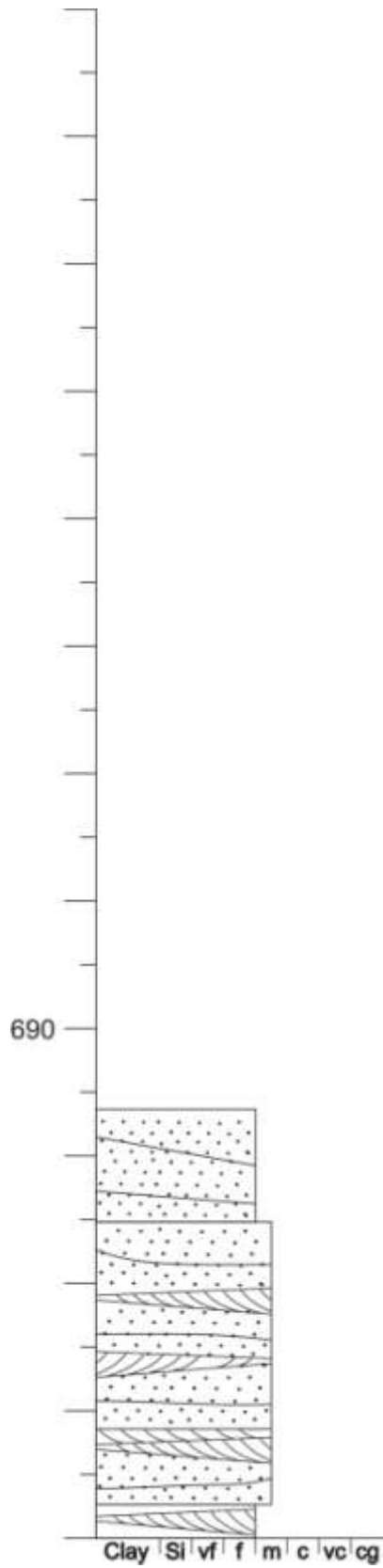
Tillbergsfjellet



L21T6

2/2

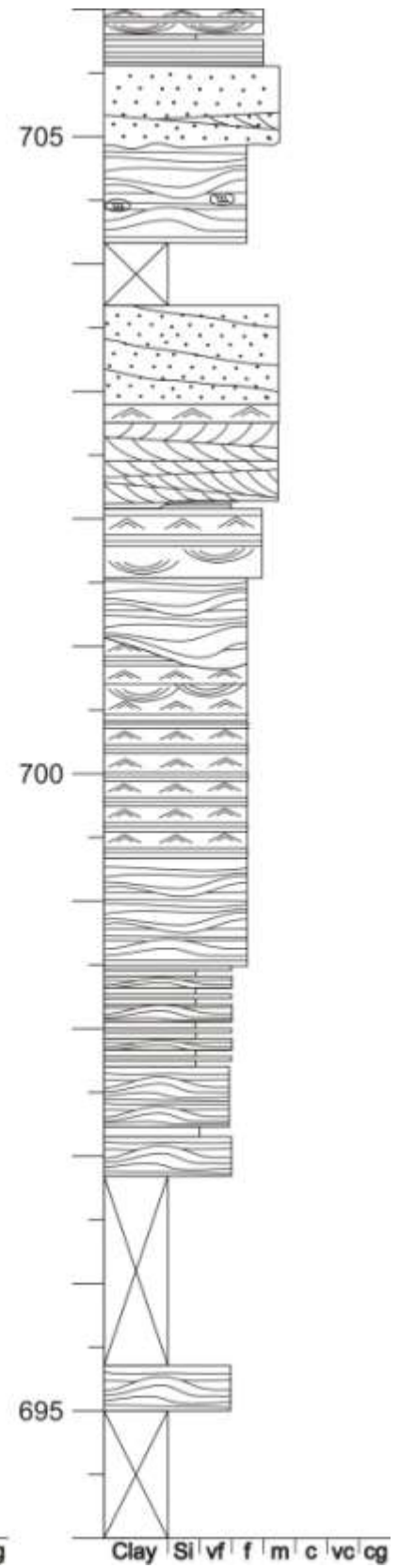
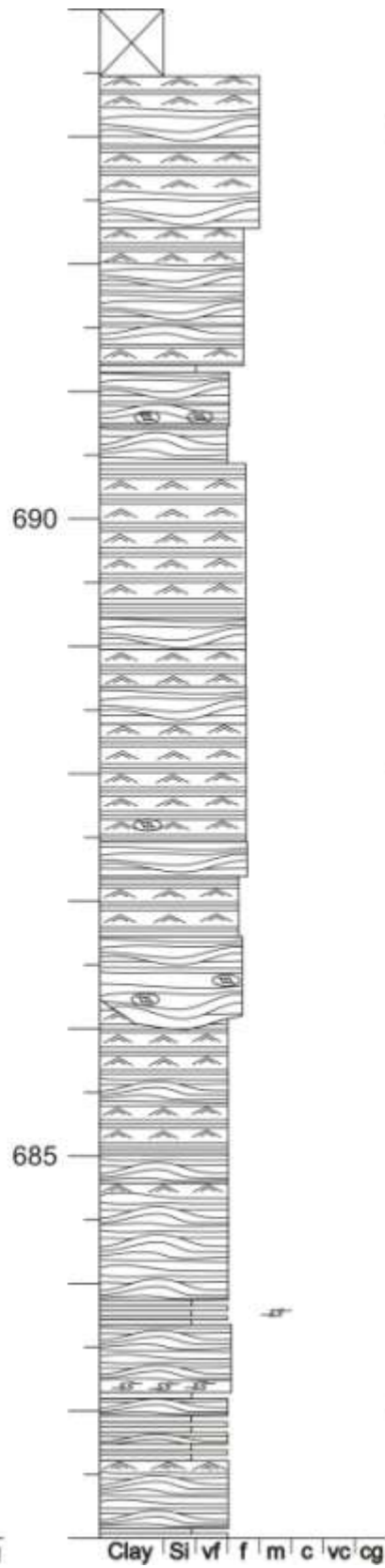
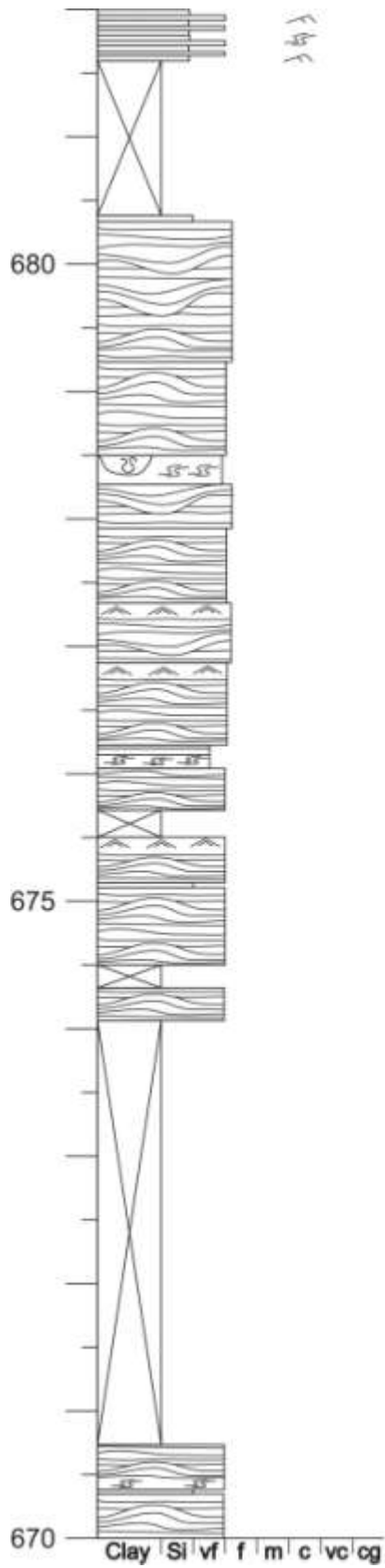
Tillbergsfjellet



L22T7

1/2

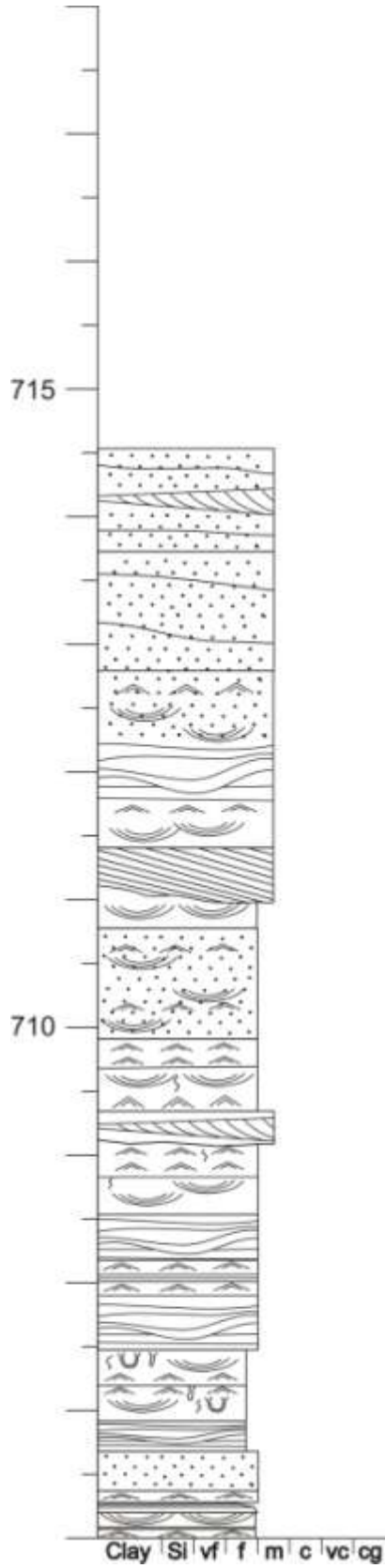
Tillbergsfjellet



L22T7

2/2

Tillbergsfjellet



Appendix 2: Paleocurrent data

Profile:	FA2:		FA3:		FA4:		FA5/FA6:	
	Current:	Crest:	Current:	Crest:	Current:	Crest:	Current:	Crest:
L1R1.:	154	355 350		22		360 8 355	234 150 315	322
L2S1.:	135 135	32 28 20	135	23 347 36		2 9	45 135 278 34	346 357
L3S2.:		12 337 345	90 120	334 19			127 45	291
L4S3.:		11					130 58 315 10	350
L5T1.:	91	345 331					50 292 220 330 30 210 173 28	346
L6T2.:		355					67 120 242 220 251 360 336 270 12 322 21 220	
L7S4.:		315		360				
L8R2.:					12 171	341 7	151 243 259 146	346

Profile:	FA2:		FA3:		FA4:		FA5/FA6:	
	Current:	Crest:	Current:	Crest:	Current:	Crest:	Current:	Crest:
L9M1.:		2		32		346	212 307 254 343 356 307 296 253 342	
L10M2.:		356		8	42	336 334 9 352 347 355	135 289 38	354
L11S5.:		349		343	359	328 322 347 326	169 233 94	
L12T3.:		15				338	224 330 104 26 283 257 115 200	15
L13R3.:		59 22 18				354 350	17 39	
L14M3.:		13				36	266 335 31 9 330	
L15M4.:		339 347		5 7 23		32 5 17 6 359	286 257 90 286 200 270 229 45	

Profile:	FA2:		FA3:		FA4:		FA5/FA6:	
	Current:	Crest:	Current:	Crest:	Current:	Crest:	Current:	Crest:
L16T4.:							76 315	
L17T5.:						11 16		
L18R4.:		1		360 339 350			345 327 135	
L19M5.:		349 17 21		33 11	135			
L20S6.:	Not in situ							
L21T6.:				31		346	171 121 267 147	337 351
L22T7.:				38			140	

Appendix 3: The mountains of the study area



Mefjellet



Sandsteinsfjellet



Ringdalsfjellet



Tillbergsfjellet